NITROGEN IMPLANTATION OF TOOL STEELS AND ENGINEERING COATINGS

JOSE IGNACIO OÑATE

Doctor of Philosophy

THE UNIVERSITY OF ASTON IN BIRMINGHAM

November 1987

The University of Aston in Birmingham

Title: Nitrogen implantation of tool steels and engineering coatings
Author: José Ignacio Oñate
Degree: Doctor of Philosophy
Date: November 1987

SUMMARY

Ion implantation modifies the surface composition and properties of materials by bombardment with high energy ions. The low temperature of the process ensures the avoidance of distortion and degradation of the surface or bulk mechanical properties of components.

In the present work nitrogen ion implantation at 90 keV and doses above 10^{17} ions/cm^2 has been carried out on AISI M2, D2 and 420 steels and engineering coatings such as hard chromium, electroless Ni-P and a brush plated Co-W alloy.

Evaluation of wear and frictional properties of these materials was performed with a lubricated Falex wear test at high loads up to 900 N and a dry pin-on-disc apparatus at loads up to 40 N. It was found that nitrogen implantation reduced the wear of AISI 420 stainless steel by a factor of 2.5 under high load lubricated conditions and by a factor of 5.5 in low load dry testing. Lower but significant reductions in wear were achieved for AISI M2 and D2 steels. Wear resistance of coating materials was improved by up to 4 times in lubricated wear of hard Cr coatings implanted at the optimum dose but lower improvements were obtained for the Co-W alloy coating. However, hardened electroless Ni-P coatings showed no enhancement in wear properties. The benefits obtained in wear behaviour for the above materials were generally accompanied by a significant decrease in the running-in friction.

Nitrogen implantation hardened the surface of steels and Cr and Co-W coatings. An ultra-microhardness technique showed that the true hardness of implanted layers was greater than the values obtained by conventional micro-hardness methods, which often result in penetration below the implanted depth. Scanning electron microscopy revealed that implantation reduced the ploughing effect during wear and a change in wear mechanism from an abrasive-adhesive type to a mild oxidative mode was evident.

Retention of nitrogen after implantation was studied by Nuclear Reaction Analysis and Auger Electron Spectroscopy. It was shown that maximum nitrogen retention occurs in hard Cr coatings and AISI 420 stainless steel, which explains the improvements obtained in wear resistance and hardness. X-ray photoelectron spectroscopy on these materials revealed that nitrogen is almost entirely bound to Cr, forming chromium nitrides.

It was concluded that nitrogen implantation at 90 keV and doses above 3×10^{17} ions/cm^2 produced the most significant improvements in mechanical properties in materials containing nitride formers by precipitation strengthening, improving the load bearing capacity of the surface and changing the wear mechanism from adhesive-abrasive to oxidative.

Keywords: Nitrogen ion implantation, tool steels, coatings, friction, wear resistance

DEDICATION

To my dear parents and beloved Maribel, continuous sources of encouragement

Attempt the end, and never stand to doubt,
nothing's so hard but search will find out.
Robert Herrick, *Seek and find*.

Nothing is so difficult but that it may be found by seeking
(Nil tam difficile est quin quærendo investigari possiet)
Terence, *Heauton Timorumenos,* l. 675 (Act IV, sc.2).

ACKNOWLEDGEMENTS

The author is very much indebted to the Basque Government's Department of Education whose financial contribution is gratefully acknowledged.

I also wish to express my gratitude to Dr JK Dennis, my supervisor, for his valuable guidance and help.

My thanks are also extended to Tech-Ni-Plant Ltd, especially Ms S Hamilton and Mr G Cooper for carrying out the nitrogen implantation treatments, encouragement and the many stimulating discussions about the research.

Further, I acknowledge the assistance given with the Spectroscopy work by Dr JL Sullivan, Mr A Tabbot and Ms T Choudhury from Applied Physics (Aston University) and, finally, my gratitude is extended to Dr L Earwalker (Birmingham University) and Dr HM Pollock (Lancaster University) for the Nuclear Reaction Analysis and ultra-microhardness work respectively.

List of Contents

Page

Title Page 1
Thesis Summary 2
Dedication 3
Acknowledgements 4
List of Contents 5
List of Tables 8
List of Figures 10

1 Introduction 20

2 Principles of ion implantation 23
2.1 Introduction 23
2.2 Description of the ion implantation process 24
2.3 Ion bombardment processes 27
2.3.1 Penetration range of ions in solids 29
- Energy loss processes 29
- Ion range distributions 30
- Channelling effects 33
- Penetration anomalies 35
2.3.2 Radiation damage 36
- Factors influencing damage 36
- Distribution of radiation damage 38
- Interaction of defects 39
2.3.3 Sputtering during implantation 40
- Limit of composition 41
- Preferential sputtering 42
2.4 Metallurgy of ion implantation into metals 42

Page

3 Effects of nitrogen implantation on surface mechanical properties 45
3.1 An introduction to friction 45
3.2 Wear mechanisms 48
3.2.1 Abrasive wear 49
3.2.2 Adhesive wear 52
3.2.3 Fatigue wear 55
3.2.4 Corrosive wear 57
3.2.5 Other categories of wear 58
3.3 Nitrogen ion-implantation effects on surface hardness 59
3.4 Effects of nitrogen implantation on friction 66
3.5 Nitrogen ion-implantation effects on wear resistance 68
3.6 Wear mechanisms on implanted surfaces 75

4 Experimental procedure 105
4.1 Materials 105
4.1.1 Steels 105
4.1.2 Coating systems 108
4.1.2.1 Electroless nickel-phosphorus alloy 108
Preplating sequence for the substrate material 109
4.1.2.2 Hard chromium 110
4.1.2.3 Cobalt-tungsten alloy coating 111
4.2 Nitrogen implantation 113
4.3 Microhardness testing 117
4.4 Friction and wear testing 118
4.4.1 "Falex" lubricated wear 118
4.4.2 Pin on disc dry wear testing 121
4.5 Electron microscopy 124
4.6 Surface analysis 125
4.6.1 Auger Electron Spectroscopy (AES) 125
- Physical principles 125
- Experimental details 126
4.6.2 X-ray photoelectron spectroscopy 127
- Experimental details 128
4.7 Nuclear Reaction Analysis (NRA) 129
- Experimental details 129
4.8 X-ray diffractometry 130

Page

5 Results 133
5.1 Surface hardness 133
5.1.1 Conventional (Vickers) microhardness testing 133
- Steels 133
- Coatings 135
5.1.2 Ultra-low load hardness testing 136
5.2 Wear testing 139
5.2.1 Lubricated "Falex" friction and wear 139
5.2.1.1 Steel materials 139
5.2.1.2 Coatings 149
5.2.2 Unlubricated "pin-on-disc" wear testing 159
5.3 Examination of worn surfaces 163
5.3.1 Profilometry 163
5.3.2 Scanning electron microscopy work 167
5.3.2.1 Steel materials 167
- Lubricated "Falex" wear 167
- Pin-on-disc dry testing 168
5.3.2.2 Coating materials 168
5.4 Surface analysis 180
5.4.1 Auger Electron Spectroscopy (AES) 180
5.4.1.1 Steels 180
5.4.1.2 Hard chromium electrodeposits 180
5.4.2 X-ray photoelectron spectroscopy 189
5.4.2.1 Steels 189
5.4.2.2 Coatings 189
5.5 Nuclear reaction analysis 203
5.6 Transmission electron microscopy 205
5.7 X-ray diffraction analysis 207

6 Discussion of results 211
6.1 Tool steels 211
- Wear resistance 219
6.2 Coatings 233
6.2.1 Electroless Ni-P coatings 233
6.2.2 Brush plated coatings 234
6.2.3 Hard chromium coatings 236

7 Conclusions and recommendations for further work 249
7.1 Conclusions 249
7.2 Recommendations for further work 251

8 List of references 254

List of Tables

Page

Table 1 Some areas of application of ion implantation into metal and its alloys 25

Table 2 Advantages and limitations of ion implantation as a surface treatment 25

Table 3 Characteristic features of mild and severe wear 53

Table 4 Effects of nitrogen implantation on surface hardness of steels and coatings 79-82

Table 5 Phases formed by nitrogen implantation 83-88

Table 6 Effects of nitrogen implantation on friction 89-92

Table 7 Effects of nitrogen implantation on wear resistance 93-102

Table 8 Improvements in wear lifetime of tools and components obtained by nitrogen implantation 103

Table 9 Steel compositions 105

Table 10 Heat treatment procedure 107

Table 11 Composition of activators for the precleaning sequence in Co-W brush plating 112

Table 12 Falex wear testing materials 122

Table 13 Relative hardness index for nitrogen implanted tool steel (Vickers, 5g load) 133

Table 14 Relative hardness index for nitrogen implanted coatings (Vickers, 5g load) 135

Table 15 Lubricated Falex wear testing results for AISI M2 high speed steel 900 N load, AISI M2 V-blocks 140

Page

Table 16 Lubricated Falex wear testing results for AISI D2 cold work tool steel 900 N load, AISI M2 V-blocks 141

Table 17 Lubricated Falex wear testing results for AISI 420 stainless steel 900 N load, AISI 420 V-blocks 142

Table 18 Falex wear test results for steels. Wear rate in g x 10^{-6}/min Operating cond.: 900 N load, lubricated, 140 min. wear time 149

Table 19 Lubricated Falex wear testing results for hard chromium coating (Type II), 710 N load, AISI 52100 steel V-blocks 150

Table 20 Lubricated Falex wear testing results for hardened electroless Ni-P coating, 710 N load, AISI 52100 steel V-blocks 151

Table 21 Falex wear test results for hard chromium (Type II coating) Operating cond.: 710 N load, lubricated, 90 min. wear time 152

Table 22 Falex wear test results for Co-1.5% W coatings. Oper. cond.: 710 N load, lubricated, 90 minutes wear time 152

Table 23 Unlubricated pin-on-disc wear results of AISI M2 steel. 159

Table 24 Unlubricated pin-on-disc wear results of AISI D2 and 420 steels 160

Table 25 Nuclear analysis data of tool steels 203

Table 26 Core-level binding for peaks fitted to Fe and Cr $2p_{3/2}$ spectra from untreated AISI 420 steel. 216

Table 27 Core-level binding energies for peaks fitted to Fe and Cr $2p_{3/2}$ and N 1s spectra from N^+ implanted AISI 420 steel. 217

Table 28 Reported binding energies (in eV) of Cr $2p_{3/2}$, Fe $2p_{3/2}$ and N 1s electron levels in stainless steel substrates and reference compounds. 218

Table 29 Core-level binding energies for untreated hard chromium coatings. 239

Table 30 Core-level binding energies for N^+ implanted hard Cr coatings. 240/241

List of Figures

Page

Figure 1 Schematic representation of the ion implantation process. Ions penetrate the surface, forming an approximate Gaussian depth profile. 24

Figure 2 Basic ion beam modification processes of materials. (A) Implantation of ions; (B) Radiation damage, (C) Sputtering and (D) Atomic mixing (Ref. 4). 28

Figure 3 The variation of nuclear and electronic stopping powers with ion velocity. 29

Figure 4 Schematic diagram showing the ion range parameters, R_p, R_T, ΔR_p and ΔR_l use to characterize the distribution of ions. 31

Figure 5 The projected range (R_p) and range straggling (ΔR_p) as a function of implantation energy for nitrogen in iron. 32

Figure 6 Theoretical range distributions of nitrogen ions in iron. 32

Figure 7 Typical range profiles for implanted ions in crystalline materials (Ref 22). 34

Figure 8 View down the <110> axial channel in a diamond structure crystal showing the spiral path followed by a typical channelling particle. After Brandt (23). 34

Figure 9 Schematic representations of radiation damage formation for (A) light ion ($M_1 < M_2$) and (B) heavy ion ($M_1 > M_2$). 37

Figure 10 Implanted nitrogen and target atom displacement distributions for N^+ implantation into Fe at 100 keV and 10^{17} ions/cm^2. After Dearnaley(32). 39

Figure 11 Schematic diagram of the main lubrication regimes. The friction coefficient is shown as a function of the speed-load-viscosity parameter. 47

Figure 12 Diagram showing factors which affect friction between solids. 49

Page

Figure 13 Schematic representation of the two most general abrasive wear mechanisms. 50

Figure 14 Relative wear resistance of metals as a function of hardness(70). 50

Figure 15 Schematic representation of the classical adhesion wear mechanism. 52

Figure 16 Transition wear behaviour of different steels. Welsh(82). 54

Figure 17 Effect of sliding speed on transition loads, for 0.52% C steel. Welsh(82). 54

Figure 18 Schematic representation of the various stages involved in the formation of delamination wear sheets, after Suh(86,87). 56

Figure 19 Schematic representation of a mild wear mechanism resulting from the repeated formation and removal of a surface oxide film. 58

Figure 20 Plot of surface stresses as a function of dose for nitrogen impl. En 40B steel. Implantation energy: 200 keV. Hartley(123). 63

Figure 21 Octahedral interstices in bcc and fcc iron. 63

Figure 22 Dose-Transformation-Temperature (DTT) diagram for nitrogen implantation in iron(108, 132). 65

Figure 23 Change in the coefficient of friction μ with sliding distance for untreated, plasma nitrided and nitrogen implanted Fe systems. Shepard and Suh(155) 67

Figure 24 Wear parameter as a function of applied load in a pin-on-disc test(2) 69

Figure 25 Volumetric wear parameter for a steel pin in contact with an implanted nitriding steel as a function of load. After Dearnaley and Hartley(170). 69

Figure 26 Relative change in wear resistance for AISI 420 steel. Iwaki et al(110). 72

Page

Figure 27 Ball on disc wear results for electroplated Cr. Oliver et al(101). Implantation: 90 keV, 3.5×10^{17} ions/cm^2. 74

Figure 28 Schematic representation of the evolution of model surfaces during wear(209). 78

Figure 29 Nominal dimensions in mm of wear testing samples.
(A) Specimens for pin-on-disc wear testing, Scale 1:1.
(B) Specimens for lubricated Falex wear testing, Scale 2:1. 106

Figure 30 Schematic representation of anode-cathode arrangement for Cr plating. 111

Figure 31 Type 222 HSDE implantation machine. 115

Figure 32 Z-101 implantation system. 115

Figure 33 Schematic diagram of the ion implantation process. 116

Figure 34 Individual depth-load run, showing loading and unloading curves. 117

Figure 35 Schematic diagram of Falex lubricant machine and testing components.
(a) Schematic diagram of Falex lubricant tester showing its main components.
(b) Expanded view of V-blocks and pin arrangement. 119

Figure 36 Calibration curve for Falex wear testing. 3000 lbs load gauge. 120

Figure 37 Schematic diagram of the pin-on-disc wear machine. 123

Figure 38 Schematic illustration of the generation of an Auger electron by electron bombardment. 126

Figure 39 Schematic illustration of the production of a 1s photoelectron by X-ray bombardment. 128

Figure 40 Variation of surface hardness of tool steels with nitrogen dose. Vickers, 5g load. 134

Page

Figure 41 Effect of varying load on microhardness of electroless Ni-P coatings. 134

Figure 42 Effect of nitrogen implantation on hardness of hard Cr coating. Vickers, 5g load. 137

Figure 43 Indentation depth ∂ against square root of load for AISI 420 steel. 137

Figure 44 Normalized hardness as a function of depth for AISI 420 steel. 138

Figure 45 Normalized hardness as a function of depth for electroless Ni-P coatings. 138

Figure 46 Falex wear results of AISI M2 high speed steel. 143

Figure 47 Falex wear results of AISI D2 cold work tool steel. 144

Figure 48 Falex wear results of AISI 420 martensitic stainless steel. 145

Figure 49 Wear reduction factors for AISI M2, D2 and 420 tool steels. Oper. cond.: Lubricated Falex testing. 900 N load, 290 rpm. 146

Figure 50 Falex wear results of AISI M2, D2 and 420 steels. Like-on-like material lubricated testing. 900 N load. 147

Figure 51 Variation of friction coefficient as a function of nitrogen dose for AISI D2 steel. 148

Figure 52 Friction curves for AISI 420 martensitic stainless steel. 148

Figure 53 Lubricated Falex wear results of hard Cr coatings. (Type II, 1050 $HV_{0.1}$) 153

Figure 54 Lubricated Falex wear results of hard Cr coatings. (Type I, 700 $HV_{0.1}$) 154

Figure 55 Lubricated Falex wear results of hardened electroless Ni-P coatings 155

Figure 56 Lubricated Falex wear results of Hard Cr (Type II) and Co-W coatings. Oper. cond.: 710 N load, AISI 52100 steel V-blocks. 156

Page

Figure 57 Lubricated Falex wear results of high efficiency hard Cr (Type III) coatings. Oper. cond.: 710 N load, AISI 52100 steel V-blocks. 157

Figure 58 Friction curves of hard Cr (Type II) and Co-W coatings. 158

Figure 59 Unlubricated pin-on-disc wear of AISI D2 and 420 steels. Oper. cond: 9.81 N load, 0.5 m/s sliding speed. 161

Figure 60 The effect of load on the gravimetric wear rate of AISI M2 steel. 162

Figure 61 Unlubricated pin-on-disc running-in friction of AISI 420 steel. Oper. cond.: 9.81 N load, 0.5 m/s slid. speed. AISI 420 steel disc 162

Figure 62 Prolifometer traces of worn steel surfaces after approximately 140 minutes lubricated Falex wear testing at 900 N load. Implantation carried out at optimum nitrogen dose 164

Figure 63 Prolifometer traces of hard Cr (Type I coating, 700 $HV_{0.1}$) after 60 minutes lubricated Falex wear testing at 710 N load. 165

Figure 64 Profilometer traces of hard Cr (Type II, 1050 $HV_{0.1}$) and Co-1.5%W coatings after 90 min. lubricated Falex wear testing at 710 N load. 166

Figure 65 Scanning micrographs of surfaces of AISI M2 and D2 steels after 90 min. Falex wear testing (A) Untreated AISI M2 (B) N^+ implanted AISI M2 (C) Untreated AISI D2 (D) N^+implanted AISI D2. 170

Figure 66 Debris generated during lubricated Falex wear of (A) Untreated AISI M2 steel and (B) N^+ implanted AISI M2 steel. (dose: 5×10^{17} ions/cm^2) 171

Figure 67 A,B. Scanning micrographs of worn surfaces after Falex testing of AISI 420 steel,(A) exhibiting severe scuffing and (B) adhesive wear. Debris generated is shown in C. (D): showing worn surface of N^+ implanted AISI 420 (4×10^{17} ions/cm^2). 172

Figure 68 Scanning micrographs of worn surfaces of AISI D2 steel after pin-on-disc dry wear testing (A) Untreated AISI D2 (B) N^+ implanted AISI D2. 173

Page

Figure 69 Scanning micrographs of surfaces of AISI 420 steel. (A) Unworn surface; (B) Untreated AISI 420 after about 4 hours dry pin-on-disc wear testing, and (C) N^+ implanted AISI 420 (dose: 3×10^{17}ions/cm^2) after same wear conditions. 174

Figure 70 Debris generated during dry pin-on-disc wear of (A) Untreated AISI 420 steel and (B) N^+ implanted AISI 420 steel. Testing conditions: 9.81 N load, 0.5 m/s sliding speed. Like on like material testing. 175

Figure 71 Scanning micrographs of chromium (Type I, 700 $HV_{0.1}$) coatings.
(A) Worn area from untreated Cr after 30 min Falex wear.
(B) Worn area of N^+ implanted Cr after similar period.
(C) Unworn area of untreated Cr showing cracking.
(D) Cracking on unworn surface of N^+ implanted Cr.
(nitrogen dose: 4×10^{17} ions/cm^2) 176

Figure 72 Scanning micrographs showing worn areas of hard Cr coatings (Type II, 1050 $HV_{0.1}$). (A) Unimplanted, illustrating a particle of chromium about to be detached. (B) N^+ implanted hard Cr (5×10^{17} ions/cm^2) and (C) Microcracking in the wear track of an untreated deposit. 177

Figure 73 Scanning micrographs of hardened electroless Ni-P coatings. (A) Unworn unimplanted specimen; (B) area of unimplanted coating after 95 min. Falex wear and (C) Worn area of N^+ implanted Ni-P coating after a similar Falex testing period. 178

Figure 74 Scanning micrographs of Co-1.5%W coatings.
(A) Unworn surface, to show the nodular structure of the deposit.
(B) Worn area of untreated coating after 90 min Falex testing.
(C) Worn area of N^+ implanted coating after 90 min. Falex wear. 179

Figure 75 Typical Auger derivative spectra of AISI 420 steel implanted at 4×10^{17} nitrogen ions/cm^2 (90 keV, 6 μA/cm^2). 182

Figure 76 Depth concentration profiles of AISI M2 steel implanted at 4×10^{17} nitrogen ions/cm^2. Sputtering rate: 3 nm/min. 183

Page

Figure 77 Depth concentration profiles of AISI D2 steel implanted at 3×10^{17} nitrogen ions/cm^2. Sputtering rate: 3nm/min. 183

Figure 78 Depth concentration profiles of AISI D2 steel implanted at 4×10^{17} nitrogen ions/cm^2. Sputtering rate: 3nm/min. 184

Figure 79 Depth concentration profiles of AISI 420 steel implanted at 3×10^{17} nitrogen ions/cm^2. Sputtering rate: 3nm/min. 184

Figure 80 Depth concentration profiles of AISI 420 steel implanted at 4×10^{17} nitrogen ions/cm^2. Sputtering rate: 3nm/min. 185

Figure 81 Depth concentration profiles of AISI 420 steel implanted at 5×10^{17} nitrogen ions/cm^2. Sputtering rate: 3nm/min. 185

Figure 82 Characteristic Auger derivative spectra of hard Cr coating implanted at 5×10^{17} nitrogen ions/cm^2. 186

Figure 83 Depth concentration profiles of untreated hard Cr coating. Sputtering rate: ~ 3 nm/min. 187

Figure 84 Depth concentration profiles of hard Cr coating implanted at 2×10^{17} nitrogen ions/cm^2. Sputtering rate: ~ 3nm/min. 187

Figure 85 Depth concentration profiles of hard Cr coating implanted at 5×10^{17} nitrogen ions/cm^2. Sputtering rate: ~ 3 nm/min. 188

Figure 86 Auger analysis of worn hard chromium coating implanted at 5×10^{17} ions/cm^2. 188

Figure 87 Fe 2p XPS spectra from untreated AISI 420 steel after: (A) 10 min., (B) 20 min. and (C) 40 min. sputtering time. 191

Figure 88 Cr 2p XPS spectra from untreated AISI 420 steel after: (A) 10 min., (B) 20 min. and (C) 40 min. sputtering time. 192

Figure 89 Fe 2p XPS spectra from impl. AISI 420 steel (4×10^{17} ions/cm^2) after (A) 6 min., (B) 22 min and (C) 50 min sputtering time. 193

Page

Figure 90 Cr 2p XPS spectra from impl. AISI 420 steel ($4x10^{17}$ions/cm^2) after (A) 6 min., (B) 22 min. and (C) 50 min. sputtering time. 194

Figure 91 N 1s XPS spectra from impl. AISI 420 steel ($4x10^{17}$ions/cm^2) after (A) 6 min., (B) 22 min. and (C) 50 min. sputtering time. 195

Figure 92 Cr 2p XPS spectra from untreated hard Cr coating (A) at the surface and (B) after 30 min. sputtering time. 196

Figure 93 O 1s XPS spectra from untreated hard Cr coating (A) at the surface and (B) after 30 min. sputtering time 197

Figure 94 Cr 2p XPS spectra from impl. hard Cr coating ($2x10^{17}$ ions/cm^2) (A) at the surface and (B) after 30 min. sputtering time. 198

Figure 95 N 1s XPS spectra from impl. hard Cr coating ($2x10^{17}$ ions/cm^2) (A) at the surface and (B) after 30 min. sputtering time. 199

Figure 96 Cr 2p XPS spectra from impl. hard Cr coating ($5x10^{17}$ ions/cm^2) (A) at the surface and (B) after 30 min. sputtering time. 200

Figure 97 O 1s XPS spectra from impl. hard Cr coating ($5x10^{17}$ ions/cm^2) (A) at the surface and (B) after 30 min. sputtering time. 201

Figure 98 N 1s XPS spectrum from impl. hard Cr coating ($5x10^{17}$ ions/cm^2) after 30 min. sputtering time. 202

Figure 99 Nuclear reaction analysis spectra obtained from tool steels implanted at 4 x 10^{17} nitrogen ions/cm^2. (A) AISI M2 high speed steel, (B) AISI D2 cold work tool steel and (C) AISI 420 martensitic stainless steel. 204

Figure 100 Bright field TEM image of hard chromium coatings.
A) Type I coating (700 $HV_{0.1}$). Unimplanted.
B) Type I coating (700 $HV_{0.1}$). Implanted at 4 x 10^{17} ions/cm^2.
C) Type II coating (1050 $HV_{0.1}$). Implanted at 4 x 10^{17} ions/cm^2. 206

Figure 101 X-ray diffraction patterns of as-plated electroless Ni-P coatings. A) As-plated coating. B) Implanted at 6 x 10^{17} ions/cm^2. 208

Page

Figure 102 X-ray diffraction patterns of hardened Ni-P coatings.
A) Hardened coating. B) Implanted at 6×10^{17} ions/cm^2. 209

Figure 103 Nitrogen concentration profiles of AISI M2, D2 and 420 steels
implanted at 4×10^{17} ions/cm^2. 214

Figure 104 Scanning electron micrograph of AISI M2 high speed steel showing
a microstructure consisting of carbides in a martensitic matrix.
2% Nital etch. 214

Figure 105 Nitrogen concentration profiles of impl. AISI D2 and 420 steels. 220

Figure 106 A) Worn surface of untreated AISI 420 steel, after pin-on-disc
testing, showing adhesive wear. B) EDX analysis of adhered debris 227

Figure 107 A) Characteristic oxidised worn surface of implanted AISI 420
steel (3×10^{17} ions/cm^2) after pin-on-disc testing. B) To show
spalling-off of a thicker oxide film. 231

Figure 108 Schematic diagram of wear evolution of N^+ implanted and
unimplanted steel surfaces. 232

Figure 109 Nitrogen concentration profiles from Auger analysis of implanted
hard chromium coatings. 237

Figure 110 Relative hardness index and wear reduction factors of implanted
hard chromium coatings as a function of nitrogen dose. 243

Figure 111 C 1s spectra from the surface of untreated and implanted
chromium coatings. 244

Figure 112 Lubricated Falex wear results of hard Cr coatings (Types II and III)
Implantation dose: 5×10^{17} nitrogen ions/cm^2.
Oper. cond.: 710 N load. AISI 52100 steel V-blocks. 247

CHAPTER 1

INTRODUCTION

1 INTRODUCTION

Limitations in the performance of a material can often result in a major obstacle to the achievement of a new technological advance. In most modern engineering processes, materials scientists and engineers endeavour to develop materials capable of withstanding arduous environmental conditions without undue deterioration in chemical or mechanical properties. A number of material properties including wear, friction, fatigue and corrosion are regarded as "surface sensitive" properties, since the few tens of atomic layers can determine the behaviour of the material. It is in this context that surface engineering has become an important research and development field aimed at improving the properties of materials so that they are capable of meeting the demanding requirements of numerous technological developments.

Many techniques are now available to provide functional coatings and surface treatments for engineering applications. Ion implantation has emerged in the last decade as a new method for modifying the surface-sensitive physical properties of materials and it is now well accepted that this technique can have a significant effect on the near surface properties of metals. In particular much evidence has accumulated over the past few years to demonstrate the improvements in wear resistance possible by nitrogen implantation of mainly ferrous materials. However, despite this substantial data on the tribological behaviour of nitrogen implanted materials, the chemical and physical changes and the persistence of the improved wear behaviour at greater depths than the treatment range are not understood completely.

Additionally, the wide spectrum of material substrates and implantation conditions that have been used do not often make possible a meaningful comparison between results obtained in different studies. To apply this treatment more efficiently on an industrial scale, research has to be directed towards a systematic wear testing of selected materials to assess the effectiveness of nitrogen implantation. The effect of nitrogen implantation is related to the alloy composition of the material and therefore an investigation of the range of optimum implantation conditions for each particular material is of practical interest. Moreover, to determine the mechanisms by which the implanted nitrogen affects the mechanical performance it is necessary to understand the microstructure of the implanted layers.

Aims

The objective of the present research was first to study the effects of nitrogen implantation upon the surface mechanical properties, mainly friction and wear, of tool steels and wear resistant coatings (electroless nickel-phosphorus, cobalt-tungsten and hard chromium) and, secondly, to seek the optimum implantation conditions for each particular material.

Nitrogen was chosen as the specie for ion implantation because it combines the economic advantages of a gaseous ion source with its efficacy to harden metal lattices. Three different steels were used in the present study, their designations correspond to AISI M2 high speed steel, AISI D2 cold work tool and die steel and AISI 420 martensitic stainless steel. These steel materials were selected due to their widespread use in cutting, forming and plastics moulding applications where nitrogen implantation can increase tool life.

Implantation was carried out at doses ranging from 2×10^{17} to 7×10^{17} ions/cm^2 and current densities from 1.3 to 6 μA/cm^2 which were chosen according to sample dimensions to avoid excessive target heating due to the energy of the beam. The nitrogen implanted layer was characterized by Auger Electron and X-ray Spectroscopy to determine the nitrogen concentration profiles and to investigate the chemical effects produced by the implantation which affect the microstructure of the modified layer. Conventional microhardness tests and an ultra-shallow depth indentation technique were used to determine the hardness effects produced by the treatment. Additionally, tribological tests were carried out under lubricated or dry conditions to examine the behaviour of the implanted layer under high or low load situations respectively. Worn surfaces were subsequently examined by Scanning Electron Microscopy to determine any changes in wear behaviour, ie. from abrasive or adhesive to mild oxidative wear, that might occur as a result of the implantation.

CHAPTER 2

PRINCIPLES OF ION IMPLANTATION

2 PRINCIPLES OF ION IMPLANTATION

2.1 Introduction

The breakthrough of ion implantation as a method to alter material properties can be considered to originate from the middle of the 1960's, when several nuclear research centres, including AERE Harwell and Oak Ridge National laboratory, took an interest in what was then considered as an emerging technology for the micro-electronics industry. By now, implantation is an indispensable step in the fabrication process of integrated circuits and its use is growing steadily in this field due to the potential advantages that this technique offers, such as greater doping accuracy, controllability over doping uniformity and accurate location of junction depth, in comparison with other semiconductor doping methods.

During the last two decades the strong technological driving force within the semiconductor industry has led to research into fundamental ion bombardment processes and on the effects of ion beams upon mechanical, optical and corrosion properties of metals.

Ion doses required to obtain significant effects in metals generally are two to three orders of magnitude greater than those used in microelectronic devices and, aided by the development of high beam intensity implanters with versatile ion sources, the first systematic investigation of the field of ion implantation in metals began at Harwell in about 1970.

These early studies demonstrated that ion implantation could bring about beneficial improvements in wear, friction, hardness and lubrication properties of steels and other metals(1-3). Encouraged by Harwell's work more research groups have extended the available data on ion implantation effects to many more metal substrates and implanted species. Table 1 lists improvements achieved by implantation in mechanical and other properties such as corrosion and superconductivity(4). Since the purpose of this work is the study of the effects of nitrogen implantation on tribological properties, only these will be reviewed in subsequent sections with the emphasis placed on the mechanical effects of the nitrogen bombardment on metal lattices.

2.2 Description of the Ion Implantation Process

During the process of ion implantation, atoms or molecules of the desired specie(s) are ionized, accelerated in an electrostatic field and directed with a high energy towards the surface to be treated. The accelerated energy can be between a few thousand electron volts (keV) and several million electron volts (MeV), depending on the penetration required, but normally lies between 50 to 200 keV for commercial implanters dedicated to metals processing. The vacuum chamber is evacuated to about 10^{-6} torr to minimize scattering or neutralization of the beam.

The ions reach the surface of the parts with high energy and penetrate it, coming to rest at a controlled depth following a near Gaussian distribution, once they have lost their energy mainly by electronic excitation and elastic collisions with the host atoms (see Figure 1).

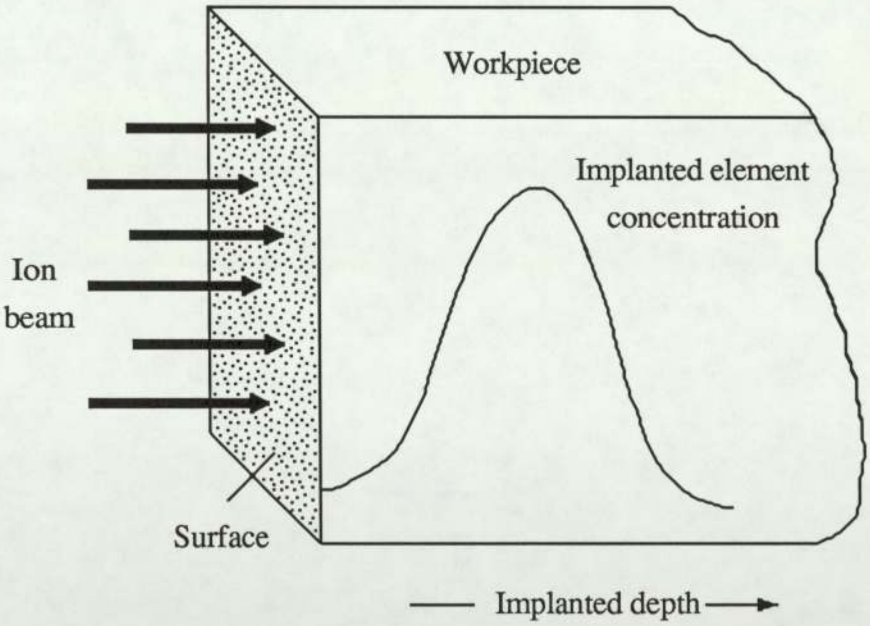

Fig. 1: Schematic representation of the ion implantation process. Ions penetrate the surface, forming an approximate Gaussian depth profile.

Ion implantation offers a number of technological advantages when compared to alternative surface treatments, such as coating or thermochemical processes, indicated in Table 2.

Table 1 - Some areas of application of ion implantation into metals and its alloys

Application and Property Changes	References
Mechanical properties	
* Fatigue resistance	Vardiman (5), Hubler (6)
* Hardness, wear and friction	Hirvonen et al(7), Hartley(2,8), Herman (9)
* Lubrication	
* Adhesion	Ingram (10)
Surface chemistry	
* Atmospheric oxidation	Dearnaley (11)
* Aqueous corrosion	Ashworth et al (12)
* Catalysis, electrochemistry	Wolf (13)
Superconductivity	Meyer (14)
Magnetic properties	North (15)

Table 2 - Advantages and limitations of ion implantation as a surface treatment

Advantages

1. Versatile treatment, as regards ion species and substrate materials.
2. Low temperature process.
3. Negligible dimensional changes.
4. No degradation of surface finish.
5. No sacrifice of bulk properties.
6. No adhesion problems, since there is no sharp interface.
7. Solid solubility limit of implanted species can be exceeded.
8. A fine dispersion of precipitates can be created. Optimum wear behaviour.
9. Clean vacuum process.
10. Minimum masking costs. Ability to treat selective areas.
11. Highly reproducible and controllable process.

Limitations

1. "Line-of-sight" process. Manipulation under vacuum necessary.
2. Shallow penetration.
3. Relatively expensive equipment and processing costs.

Ion implantation is a versatile process, as regards ion species and substrates that can be treated, since a variety of ion species can be implanted with the same basic equipment. For research purposes, or when metallic ions are implanted, which are extracted from a multi-component plasma, mass analysis of the ion beam is necessary, but when gaseous elements are used analysis is generally not required.

Implantation is a low temperature process, penetration of the ions is ruled mainly by their energy, and elevated temperatures are not required as in the case of diffusional treatments; hence, dimensional changes are negligible and there is no degradation of the surface finish or any sacrifice of bulk properties of the workpiece. Ion implantation must, therefore, be applied to finished components so that surface and bulk properties can be independently optimized.

One of the features of the implantation process is its non-equilibrium nature, which allows the introduction of species into a material, irrespective of solid solubility rules and constraints in thermal diffusion coefficients. Nonetheless, there is a maximum of concentration achievable due to sputtering, which is the kinetic ejection of surface atoms as a result of collisional energy transfers, and this limits the proportion of foreign atoms which can be incorporated into the matrix to usually below 50%. No build-up can be produced as a result of the treatment and, hence there is no possibility of forming a coating. The depth profile of the ions follows an approximate Gaussian distribution, as Figure 1 depicts, without sharp interfaces between the implanted surface layer and the substrate, eliminating the possibility of adhesion problems.

Ion implantation is a clean vacuum process without waste disposal problems. It is also controllable and can be monitored continuously by measurement of the ion beam current.

The technique does have several drawbacks which can limit its application. A basic limitation of implantation is that of being a line-of-sight process, without any significant "throwing power", and therefore manipulation under vacuum is necessary to achieve uniform implantations over complicated surfaces. This problem is overcome with specially designed jigging systems that enable uniform treatment to be provided over the surface of complex components.

It is also a shallow treatment; ion penetration is limited by practical energy constraints and is rarely more than 0.5 μm for the actual commercial implanters. This limitation might render ion implantation useless as a technique for engineering applications, but as it will be discussed in subsequent sections, there are wear mechanisms on implanted surfaces that provide a long lasting improvement in many industrial processes.

2.3 Ion Bombardment Processes

The interaction of the ion beam leads to a near-surface modification of the target material. Figure 2 illustrates schematically the four main material modification processes caused by ion bombardment(4). First of all (Figure 2a), ion implantation introduces foreign atoms into a solid, creating a concentration profile of the implanted element and thus, altering the near-surface composition of the material and its physico-chemical properties. Distribution of the ions is a function of both, their energy and the stopping processes operating along their trajectories, which determine how individual ions slow down and where they finally come to rest.

Figure 2b shows that "hard" elastic collisions between ions and host atoms can displace many atoms from their original sites and, as a consequence, ion implantation can create considerable structural damage to the material; this effect becoming very important in the case of heavy ions.

Another significant ion bombardment induced process is that of sputtering (Figure 2c) or erosion of the surface due to ejection of substrate atoms as a result of nuclear collisions. Finally, the process of atomic mixing is also illustrated (Figure 2d), in which solid atoms can be transported into the substrate at depths within the collision cascade, and as a consequence an appreciable intermixing between a thin film and the substrate can be achieved.

All these bombardment processes can have a significant effect on the properties of a material and a further analysis will be presented below to aid the understanding of the mechanical property changes brought about by ion implantation.

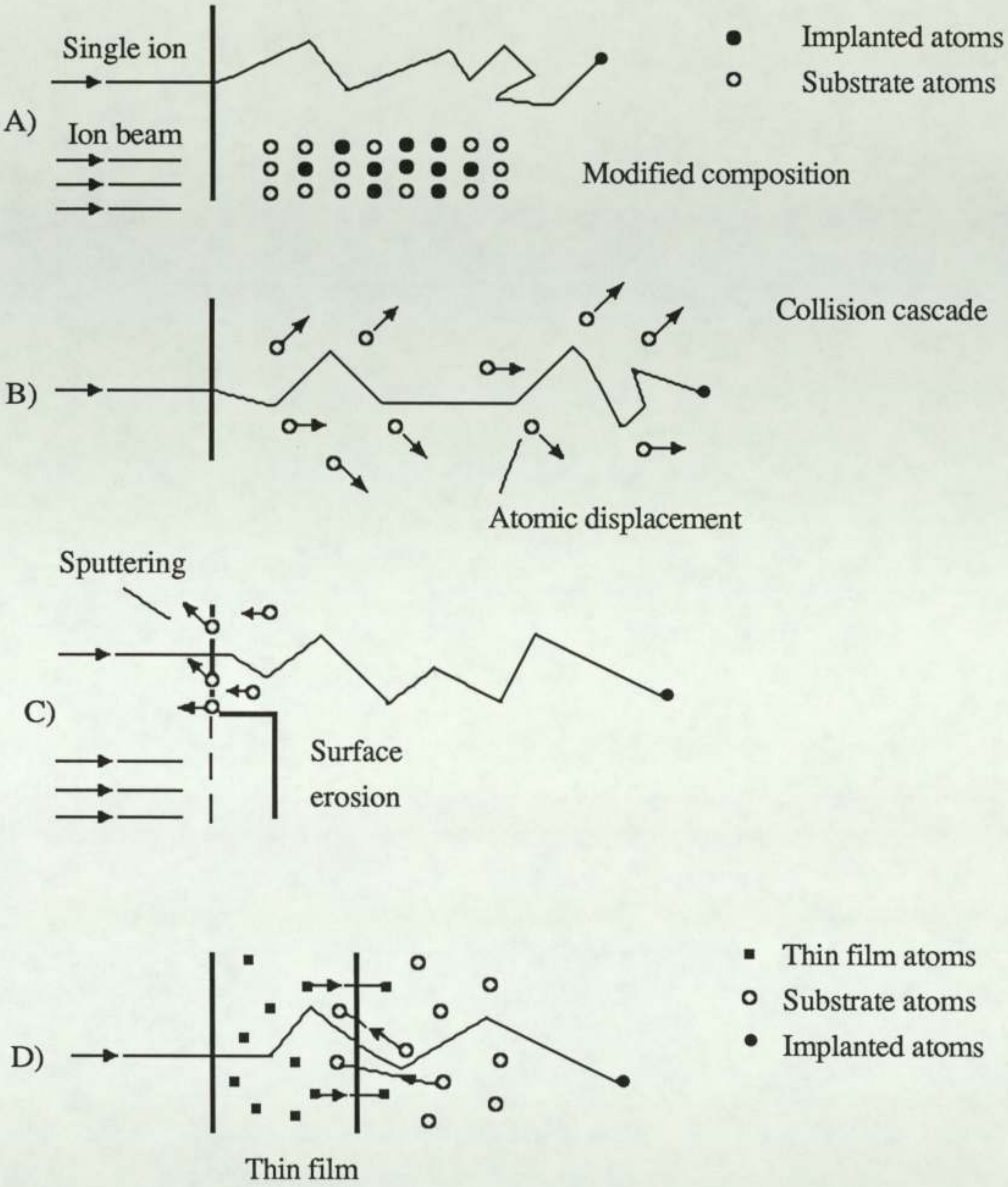

Fig.2: Basic ion beam modification processes of materials. A) Implantation of ions B) Radiation damage, C) Sputtering and D) Atomic mixing. (Ref. 4)

2.3.1 Penetration Range of Ions in Solids

- Energy Loss Processes

As an energetic ion penetrates a solid, it undergoes a series of binary collisions with the nuclei and electrons of the target atoms, losing energy at each encounter, until it comes to rest in approximately 10^{-13} seconds. The transfer of energy from the incident ion to the target material can be conveniently divided into two independent processes, namely nuclear collisions and electronic collisions, according to Lindhard and Scharff's model(16). The former process constitutes the elastic collisions between ion and lattice atoms, while the latter electronic component depicts the inelastic collisions occurring between the energetic ions and lattice electrons. In these collisions, smaller amounts of energy are usually transferred, but the large density of electrons and the high frequency of these encounters ensures a continuous energy loss of the incident ion. Which one of the two effects, nuclear or electronic, predominates depends upon the energy and mass of the ions, as well as upon the mass and atomic number of the target material. At the lower energy range the major contribution to energy loss is that of nuclear stopping(17); while at higher energies the effect of electronic collisions is predominant, as Figure 3 illustrates.

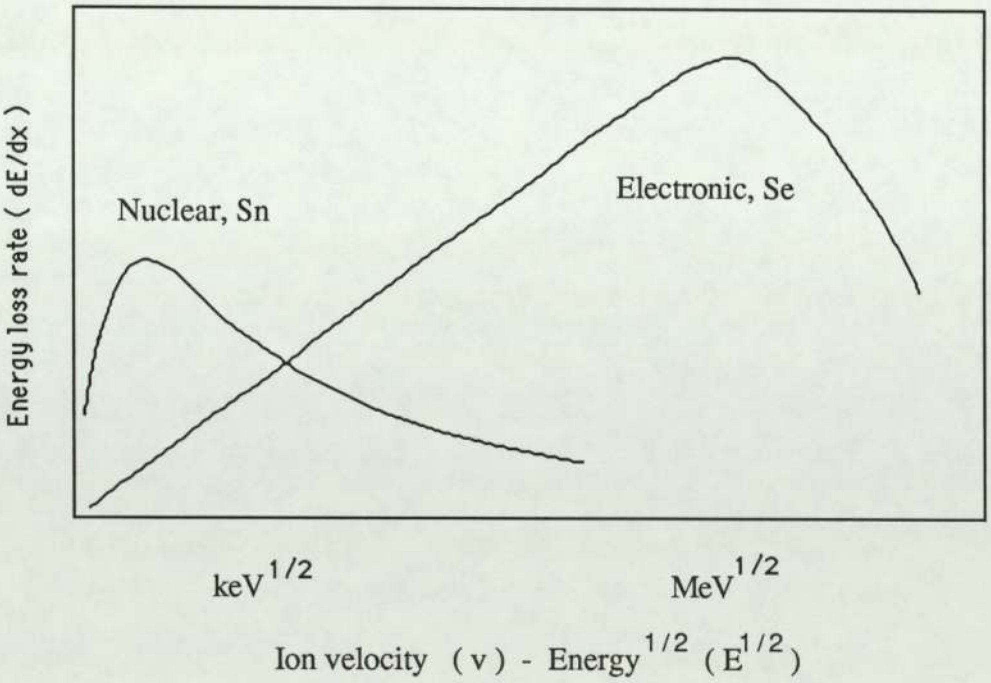

Fig. 3: The variation of nuclear and electronic stopping powers with ion velocity.

Assuming that both processes are independent of each other, the energy loss per distance unit can be expressed by the equation:

$$- dE / dx = N [Sn (E) + Se (E)] \qquad \text{..... 2.1}$$

where N is the number of target atoms per unit volume and Sn (E) and Se (E) are the nuclear and electronic stopping cross sections respectively. The general behaviour of both stopping powers is indicated schematically in Figure 3. At low ion energies (< 1 MeV), which are characteristic of ion implantation processes and in which nuclear energy loss dominates, the energy loss is shown to be proportional to the ion velocity (or $E^{1/2}$). At higher ion velocities, the ions are totally stripped of electrons during penetration and the energy-loss rate decreases as the projectile energy increases(18).

- Ion Range Distributions

The average total range of penetration R_T of an ion into an amorphous solid can be found by integrating the equation (2.1), knowing the values for the stopping cross sections, to give:

$$R_T = (1 / N) \int_o^E \{ d(E) / [Sn (E) + Se (E)] \} \qquad \text{..... 2.2}$$

where E is the incident energy(19).

The energy loss per collision and hence the total range will have a statistical spread of values, since energy is lost by the ion by successive discrete collisions with the target atoms and electrons. This leads to a near-Gaussian distribution of stopping distances, which can be evaluated using a Thomas-Fermi statistical model developed by Lindhard et al(18) and subsequently described as the "LSS" theory.

The stopping processes described above and the typical ion range parameters describing the distribution of implanted species are indicated in Figure 4. Since the ion will generally follow a path with many changes of direction, besides the total range R_T, it is also convenient to define a projected range R_p or distance travelled along the incident beam direction and the associated statistical spread or range straggling (standard deviation), both, parallel (ΔR_p) and perpendicular (ΔR_l) to the ion direction.

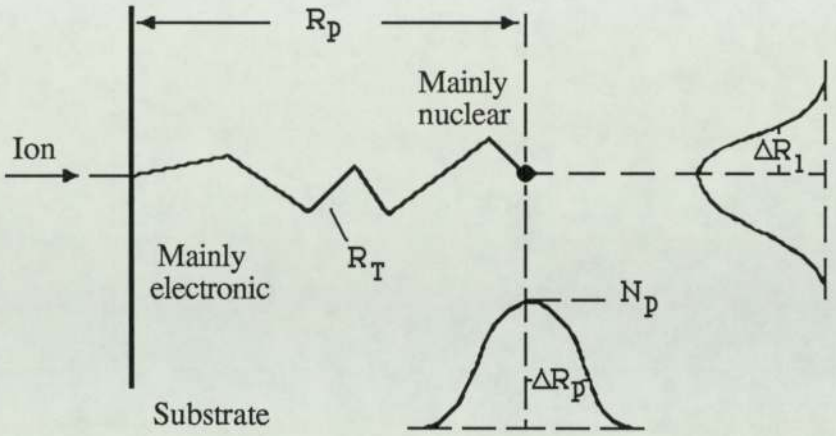

Fig.4: Schematic diagram showing the ion range parameters R_p , R_T ΔR_p and ΔR_1 used to characterise the distribution of ions.

The range R_P and the standard deviation ΔR_P are the parameters which are of practical interest and, based on the "LSS" theory, can be tabulated for various incident ion energies and ion-substrate combinations(20).

An example of the projected range for nitrogen ions in iron as a function of implantation energy can be seen in Figure 5, after Hirvonen(21).

The distribution of implanted ions, found to fit a Gaussian function for amorphous substances, is obtained from the average range R_p, the standard deviation ΔR_P, and the implanted dose N_D (ions per unit area), as follows:

$$N(x) = \frac{N_D}{\sqrt{2\pi} \cdot \Delta R_p} \exp \left\{ \frac{-(x - R_p)^2}{2 \cdot \Delta R_p^2} \right\} \qquad ..... 2.3$$

which has been calculated neglecting back-scattered ions. The error involved with this assumption may be considered to be minimal although it can be important for very low energy implantations.

The maximum concentration of implanted ions is:

$$N_{max} = \frac{N_D}{\sqrt{2\pi} \cdot \Delta R_p} \qquad ..... 2.4$$

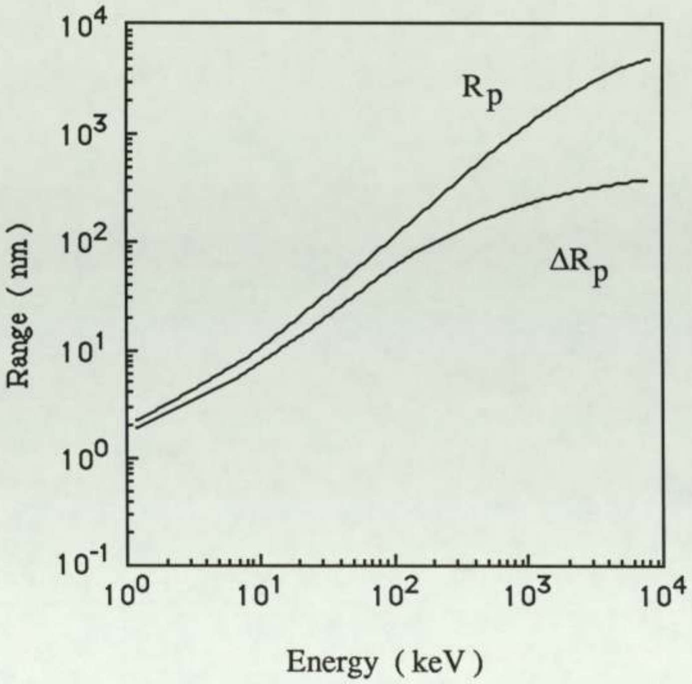

Fig.5: The projected range (R_p) and range straggling (ΔR_p) as a function of implantation energy for nitrogen in iron.

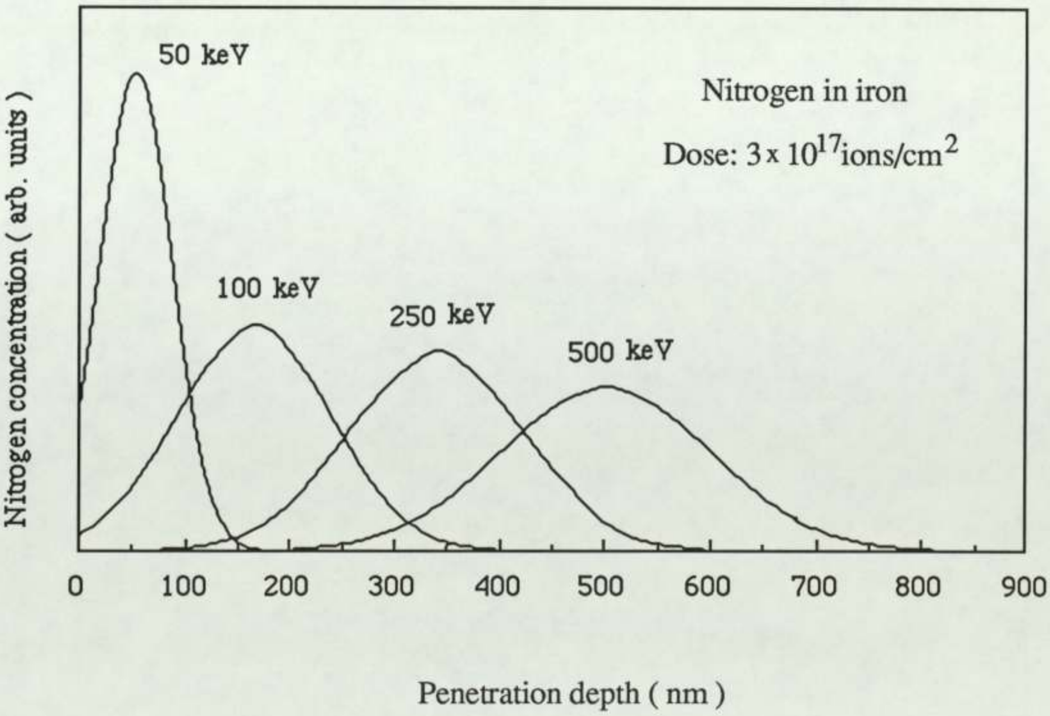

Fig. 6: Theoretical range distributions of nitrogen ions in iron.

Theoretical range profiles for ions at various implantation energies can be calculated by means of equation 2.3, providing that values for the range (R_P) and range straggling (ΔR_P) are known. Figure 6 presents concentration profiles for nitrogen ions in iron at different energies, the corresponding values of R_P and ΔR_P were obtained from Hirvonen(21), see Figure 5. It can be seen that with increasing energy and penetration depth the maximum concentration for a given dose decreases, because of the increasing range straggling.

Predicted depth distributions, such as those presented in Figure 6, are likely to be of limited accuracy due to limitations of the theory. While accuracy of the depth profile is of great importance to semiconductor applications, it may be of limited significance for metallurgical purposes. In practice, experimental methods are used to determine depth distributions of implanted ions, eg. Auger analysis combined with argon milling or nuclear reaction analysis.

- Channelling Effects

The energy loss and ion range considerations outlined above have been discussed in terms of amorphous targets. However, in practice, ion implantation is normally carried out on single or polycrystalline materials and, therefore, penetration of ions into an ordered lattice must be considered.

When single crystals are bombarded with ions along one of their major crystallographic directions or planes, the ions penetrate to greater distances in the crystal than those predicted by energy loss mechanisms in amorphous targets, and deviations from the theoretical Gaussian profile must be expected. Figure 7 illustrates schematically the channelling effect and its influence on the penetration of ions into the material(22). As shown, channelling can result in range distributions with deeply penetrating tails.

Within the so called channels (see Figure 8) there are practically no nuclear collisions and the energy loss is predominantly electronic. But if the ions are incident too close to the atom rows or with an angle which is not particularly well aligned with the axis, some nuclear collisions with the atom rows may lead to unstable trajectories and dechanelling occurs. These ions subsequently follow a random trajectory through the crystal and their behaviour is the same as for projectiles incident on amorphous materials.

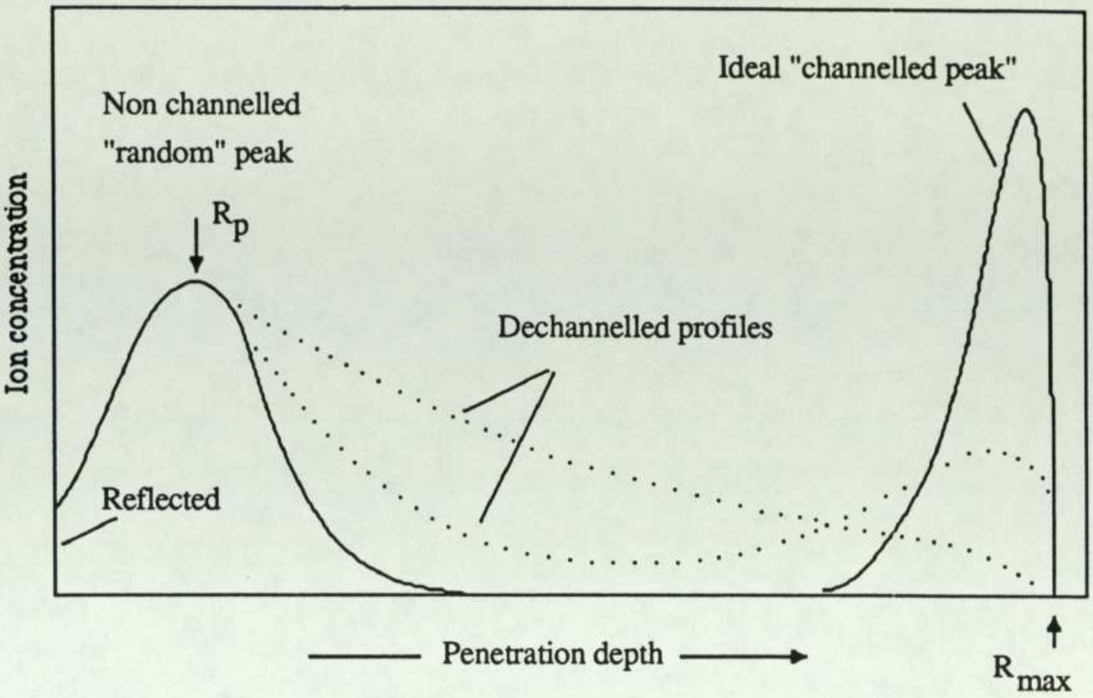

Fig. 7: Typical range profiles for implanted ions in crystalline materials. (Ref. 22)

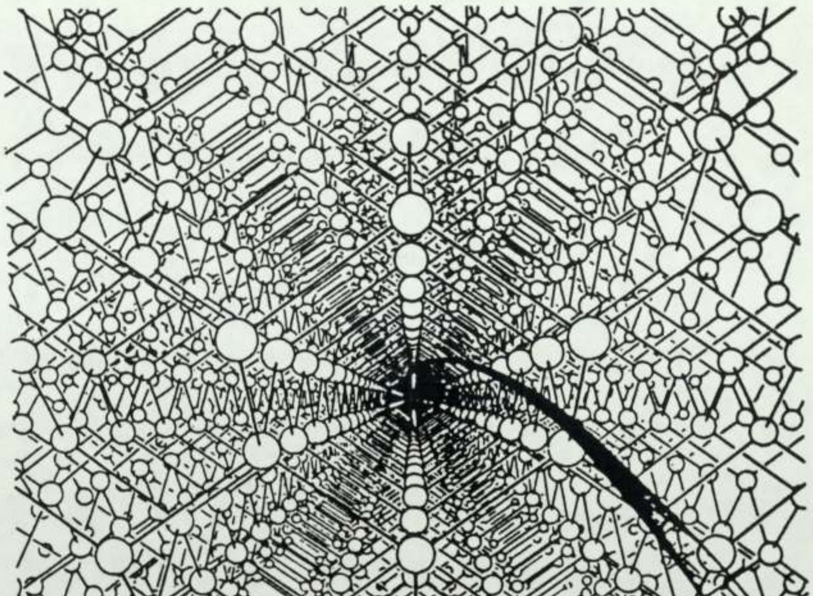

Fig. 8: View down the < 110 > axial channel in a diamond structure crystal showing the spiral path followed by a typical channelling particle. After Brandt [23].

Channelling is of some scientific application in producing deep implants but in most implantation studies, channelling effects are minimised or eliminated either by using a fine-grained polycrystalline target or by continuously rotating the material during implantation.

For non-semiconductor applications, the importance of channelling is reduced, since many implantation facilities use beams with an angular divergence greater than that required for channelling and if single crystals are treated, they can be orientated away from channelling directions. Furthermore, at very high doses, such as those used for modification of the properties of metals, implantation introduces disorder into the lattice and the channels can be destroyed. Comprehensive reviews of ion channelling processes, their mathematical models and implications have been carried out by Pathak(24) and Ryssel and Ruge(19).

- Penetration Anomalies

It has been shown that the ions follow a near Gaussian distribution in the case of amorphous targets and that some enhanced penetration can occur if the implantation is carried out along channelling directions in crystalline materials. There are other processes taking place during the implantation, such as sputtering and diffusion, that can also lead to a distortion of the predicted concentration profile.

The former is particularly important in the case of high dose implantation in metals, since it may limit the maximum amount of ions that can be introduced into the substrate and can produce significant surface topographical effects in the material(17,25). A separate section will be dedicated to the sputtering effect.

The second effect is that of diffusion, which can drive the ions further than their predicted range in the material. There are several types of diffusion which may operate with implanted species. The most common is that of "thermal diffusion" and can take place during the necessary annealing processes in semiconductors to eliminate the radiation damage or during the implantation itself. Metals are not normally annealed to remove the bombardment damage introduced by the implantation and thus, only diffusion during implantation will be of any significance.

The ion bombardment produces many vacancies and these can lead to diffusion of implanted species at relatively low temperatures. Interstitial diffusion, as in the case of light elements, can also play a significant role, since some of the implanted ions come to rest at irregular positions in the lattice and can diffuse quickly to interstitial lattice sites before combination with a vacancy. Another type of diffusion is that of "radiation-enhanced diffusion", which is produced by means of bombardment with high energy particles. This effect can be produced during the implantation through the energetic ions themselves, or after implantation by subsequent irradiation with non-doping particles, such as neutrons or protons. Defects, ideally vacancies, are produced by the bombardment increasing the diffusivity of the implanted species in the material.

2.3.2 Radiation Damage

During the implantation, nuclear collisions between the incident ions and atoms of the target material can impart sufficient energy to the target atoms to cause their displacement. These can themselves displace other atoms in the lattice, giving rise to what is referred to as a collision cascade.

The implanted ion may produce along its trajectory many of such displacement cascades, resulting in a high disorder within a confined volume around the ion path. This leads to an accumulation of vacancies and interstitial atoms (Frenkel defects) as well as to complex lattice defects along the ion trajectory (clusters).

- Factors Influencing Damage

The production of radiation damage and its distribution depends upon the energy and mass of the ions, mass of target atoms, temperature, implantation dose, dose rate and the channelling effect which may possibly occur. When ions are channelled in a single crystal, energy loss by nuclear collisions is much reduced; channelled ions do not suffer violent collisions with lattice atoms and, as a consequence, radiation damage is considerably reduced.

The formation of radiation damage for light and heavy ions is shown schematically in Figure 9. Heavy ions can transfer more energy to lattice atoms than lighter ones and therefore, for a given energy, their penetration into the target material is expected to be shallower.

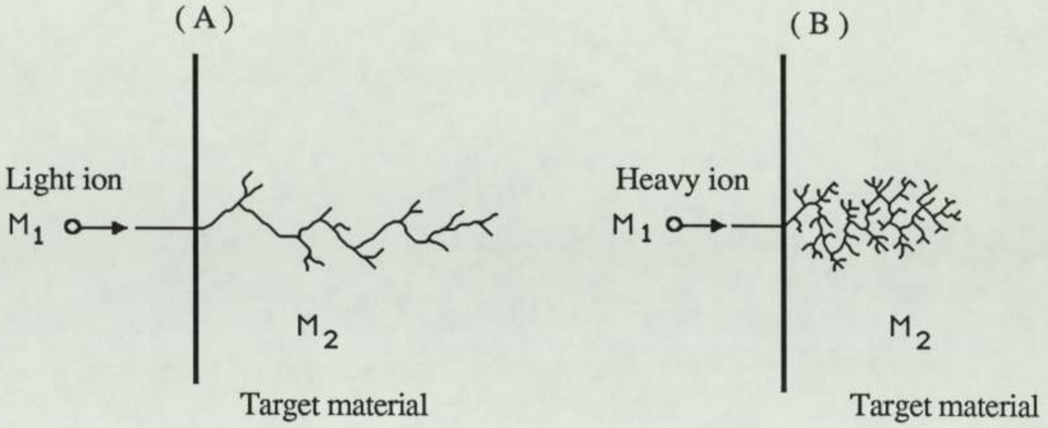

Fig.9: Schematic representation of radiation damage formation for A) light ion ($M_1 < M_2$) and B) heavy ion ($M_1 > M_2$)

At low implantation doses (eg. $\leq 10^{12}$ ions/cm^2) and with relatively light ions, simple defects are mainly obtained. There are individual damage regions around each ion track, with low probability of cascade overlapping. When the total dose increases significantly, the average separation between collision cascades becomes comparable to their dimensions and inter-cascade effects appear. If the implantation dose, and thus the concentration of radiation damage, is sufficiently high (eg. $\geq 10^{14}$ ions/cm^2), complete overlap of cascades with a uniform lateral distribution of damage occurs, more complex defects are developed and an amorphous layer can be formed, depending on the mass of ions and implantation temperature. This amorphous layer, in the case of semiconductors, is undesirable but the crystal lattice can be restored by a suitable heat treatment (annealing), and the implanted ions placed on electrically-active lattice sites.

Contrary to semiconductors, implantation in metals does not normally bring about amorphization of the surface layer, even after prolonged bombardment at low temperatures. The higher mobility of bombardment-induced point defects in metals, and the non-directionality of bonding preclude the production of amorphous metal phases, except in some special alloy systems(26). Therefore, annealing after implantation is not normally carried out in metal systems unless aiming at diffusion of implant species, precipitation or modification of metastable phases.

When implantation is carried out at a high dose rate or current density, some of the radiation damage can be annealed "in-situ", providing the sample is heated by the ion bombardment. If the material is not heated, higher defect concentrations are normally obtained with an increasing dose rate.

- Distribution of Radiation Damage

Calculations of deposited energy distributions as a function of depth can be obtained by means of the "LSS" theory(18). Winterbon et al(27) have developed analytical methods to obtain the distribution of energy transferred to the solid by nuclear interactions or energy loss $\nu(E)$, and tables providing collision cascade parameters can be found in the literature(20). Damage profiles obtained by these methods are closely related in shape to the corresponding distribution of ions. Alternatively, the deposited energy distribution can be obtained by means of Monte Carlo techniques(28), by simulating individual collision cascades and then averaging the results of a great number of cascades(29).

By knowing the above deposited energy distribution and the collision cascade dimensions, it is also possible to calculate the number and distribution of displaced atoms. The usual procedure is that of Kinchin and Pease(30), and assumes that only those recoils with an energy greater than E_d become displaced, where E_d is the threshold displacement energy determined from high energy electron bombardment. The number of displacements produced per ion, $N_d(E)$, is given by the equation(31) :

$$N_d(E) = 0.42\,\nu(E) / E_d \qquad \text{.....}\ 2.5$$

An example of such a distribution can be seen in Figure 10, after Dearnaley(32). Since ions require a certain energy for radiation damage production, the maximum of radiation damage distributions is always closer to the surface than the maximum of the implanted ions distribution, as Figure 10 illustrates for nitrogen ions.

When ion implantation is carried out in metals, recombination of defects can take place within the collision cascade even at low temperature; "in situ" annealing can also occur during the implantation. Consequently, defect levels can be much smaller than those predicted by theoretical models.

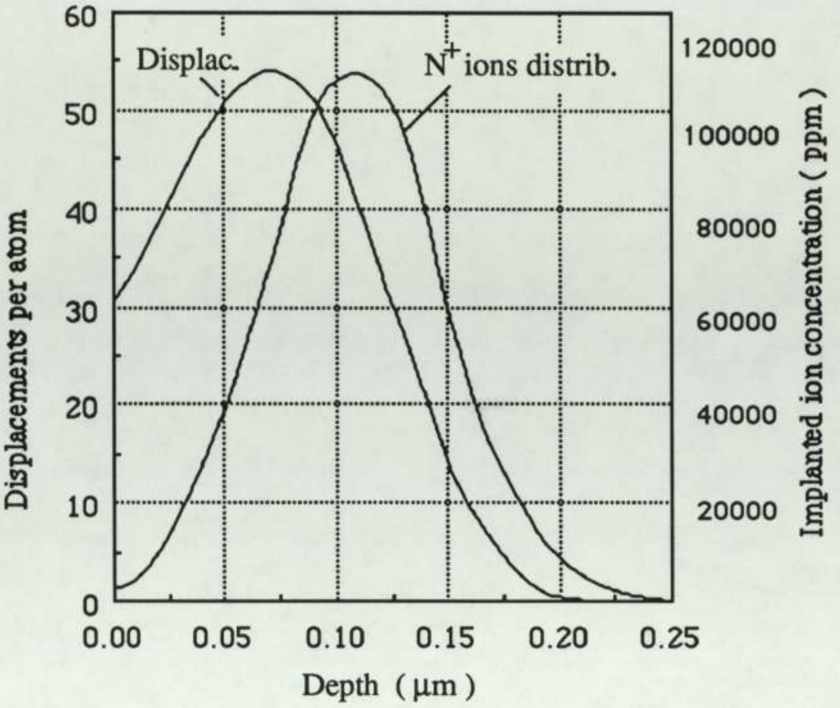

Fig.10: Implanted nitrogen and target atom displacement distributions for N^+ implantation into Fe at 100 keV and 10^{17} ions / cm^2. Dearnaley (32)

- Interaction of Defects

It has been shown that collisions between ions and lattice atoms can cause displacement of atoms from substitutional to interstitial sites. As a result, vacancies (atoms missing from normal lattice positions) and interstitials (atoms residing in non-normal lattice positions) are produced in a restricted region.

Vacancies tend to migrate due to localized stresses created in the lattice, in such a direction as to reduce the stored energy of the system, and this may be achieved by vacancy aggregation, the aggregate having smaller surface to volume ratio than many isolated vacancies. Vacancies interact also with other lattice defects like interstitials, dislocations, surfaces and solutes. The interaction vacancy-interstitial governs the Frenkel pair recombination, while the combination with dislocations and surfaces influences the vacancy annihilation. The interaction with solutes governs the solute or impurity diffusion and its relationship to the self-diffusion of the solvent atoms. Complex interactions of vacancies, vacancy clusters and solutes with dislocations cause such phenomena as dislocation pinning(33) or pipe diffusion. The classic dislocation pinning mechanism was proposed by Cottrell(34). He showed that impurity atoms differing in size from the host atoms of a lattice are attracted to a dislocation line. This attraction force exists because the strain field of a dislocation can be partially cancelled by the strain field of the impurity atoms, which arise from their misfit in the lattice and, therefore, the total elastic strain energy is reduced.

The excess of impurity atoms near a dislocation line is referred to as an impurity cloud. This "Cottrell" impurity cloud pins the dislocation to it, making dislocation motion difficult. In the case of steels and for implantation of light interstitial atoms, such as carbon or nitrogen, this effect can bring about improved resistance to fatigue and wear as discussed by Dearnaley(35) and other workers(36).

2.3.3 **Sputtering during implantation**

Hartley(37) has established that in order to obtain good tribological properties, the dose of implanted light ions (eg. carbon, nitrogen) has to be about 2 x 10^{17}ions/cm^2 . However, at such high doses used to achieve concentrations of implanted species greater than 10 at.% sputtering becomes a problem, limiting the maximum concentration of solute that can be obtained by implantation.

Sputtering is the process by which atoms are kinetically ejected from the target surface as a result of energy transfers from the incident ion to the substrate material(38). This effect can be especially perceptible in cases of heavy ions and high implantation doses, and may erode the surface sufficiently to distort the depth distribution of ions, eventually leading to a maximum concentration of implanted atoms at the surface.

This maximum is achieved when the concentration of solute at the surface is such that each implanted ion causes the atom of the same element to be sputtered, and further net addition of the element by implantation ceases.

The most important parameter in dealing with this topic is the sputtering yield, which can be defined as the number of ejected target atoms per incident ion. Based on the linear cascade theory(31,39), the sputtering yield "S" can be calculated approximately from the equation:

$$S = 0.042\, \alpha\, S_n / E_b \qquad ..... \ 2.6$$

for ions at normal incidence and amorphous elemental substrates; where E_b is the surface binding energy, α is a function of the mass ratio M_2/M_1 for target (M_2) and ion (M_1) and S_n is the nuclear stopping cross section at the incident ion energy.

Usually, theoretical and measured sputtering yields agree well, except in those cases in which displacement collisions are few and well separated (eg. for light ions) and when the energy deposition density is very high, as in the case of heavy ions on high mass target materials. Moreover, the above model does not apply for implantation at non-normal angles. The sputtering rate increases with deviations in incidence angle from the normal, with the exception of glancing angles, according to an inverse cosine distribution(38).

- **Limit of composition**

Sputtering limits the concentration of implanted elements which can be obtained in the material during high dose implantation. By ignoring precipitation processes occurring during implantation and assuming that implanted species are distributed uniformly in depth, the steady state maximum implant concentration ratio can be written as(40):

$$N_1 / N_m = r / (S - 1) \qquad ..... \; 2.7$$

where N_1 and N_m are the concentration of implanted species and atoms of target material, respectively; "S" is the sputtering yield of matrix atoms and "r" is the preferential sputtering factor or ratio of sputtering coefficient of matrix atoms to that of implanted atoms on the surface. This factor is usually taken to be unity for implantations into elemental targets.

This relationship, indicated by equation 2.7, has been found to apply for many systems(41). However, there are other processes that can modify the distribution of implanted species during high dose implantation, such as radiation-induced migration, impurity segregation and precipitation and also preferential sputtering and surface topographical changes occasioned by prolonged bombardment.

- Preferential sputtering

When multi-element materials are implanted, the main features of the sputtering phenomenon apply in the same way, but with additional complications since the various elemental constituents may not be sputtered at the same rate. Discrepancies in sputtering yield arise from differences in energy distribution in the collision cascade, ejection probabilities or binding energies between elements. This is known as preferential sputtering of one specie over the other and can result in a surface composition which differs considerably from the stoichiometric bulk composition of the material. Reviews of preferential sputtering can be found in the literature(41). When this effect occurs it appears to lead to a build up of the heavier target component(40) and depletion of lighter elements. This bears some significance in the interpretation of compositional profiling techniques, such as Auger spectroscopy (AES), which rely on ion etching as a method of surface layers removal during analysis.

2.4 Metallurgy of Ion Implantation into Metals

One of the main features of ion implantation is that of being a non-equilibrium process in which it is possible to introduce elements into a material to concentration levels exceeding their solid solubilities. As a result, implantation into metals at room temperature and at low and high concentrations has produced both equilibrium and metastable phases.

Metastable systems, either crystalline or amorphous, produced by the athermal process of ion implantation have been studied by Poate and Cullis(42). At low implantation doses, metastable dilute alloys can be formed and with a greater range of solubilities in those systems regarded by equilibrium considerations as immiscible or with limited solubility(42,43). Possible explanations for the observed greater solubility have been discussed by Poate and Cullis(42) in terms of (a) interactions of implanted elements with bombardment induced defects and (b) replacement collisions, in which the implanted ions may stop at substitutional sites from which they cannot escape.

As the implanted dose is increased to give concentrations of above ~1 at. %, the formation of supersaturated solid solutions has been observed in several metals(44). In addition, ion implantation has been shown to induce structural phase changes and to form alloys and compounds(45,46). In general, new compositions and structures not found in equilibrium phase conditions may be quite readily formed by implantation.

Equilibrium phases have also been obtained by ion implantation and have been the object of several studies(47). Temperature bears some importance in the formation of equilibrium phases during implantation. If implantation is carried out at low temperature, only diffusionless phase transitions are to be expected when the appropriate concentrations are reached, unless appreciable radiation enhanced diffusion occurs due to the bombardment.

When implantation is carried out at a sufficiently high temperature, the implanted impurities will become mobile and may agglomerate to form precipitates of new phases. Further heating during the implantation can lead first to growth of the precipitates and finally to their dissolution by migration of implanted atoms into the substrate(47). In the case of implantation of light interstitial elements (eg. carbon, nitrogen), these become mobile even at low temperatures. Adding to this mobility, defects created by the collision cascades of implanted atoms can result in an enhancement in their diffusion (by the creation of excess vacancies and interstitials). This migration aids the formation of precipitates. Furthermore, the displacement damage that accompanies the implantation can provide a high density of nucleation sites for precipitation to occur. This is corroborated by the fact that the density of small precipitates is much higher in implanted systems than that found in precipitated systems formed by conventional metallurgical treatments(47,48).

This high density and small size of precipitates is one of the special features of ion implantation systems and brings about beneficial surface hardening effects due to the fine dispersion of precipitates. Parameters that influence the size distribution of precipitates are the implantation dose, the dose rate and the temperature during implantation. Kant et al(49) found that the mean precipitates size increased and the number density decreased with increasing dose, increasing temperature and decreasing dose rate. Subsequent dissolution of the precipitated layer into the sample substrate will take place upon continued heating at temperatures where implanted atoms are mobile.

CHAPTER 3

EFFECTS OF NITROGEN IMPLANTATION ON SURFACE MECHANICAL PROPERTIES

3 EFFECTS OF NITROGEN IMPLANTATION ON SURFACE MECHANICAL PROPERTIES.

The last decade has seen the advent of ion implantation as a technique for improving the wear resistance and frictional characteristics of metal surfaces. Among all the species implanted, the most investigated and commercially utilized for enhancement of mechanical properties has been nitrogen(35,50); although increasing numbers of applications are reported for titanium and/or carbon implantations(51,52). Nitrogen is generally the preferred element due to the economic advantages of a gaseous ion source without the need for magnetic analysis or separation of the beam, and to the efficacy that this interstitial element possesses for hardening metal lattices.

Encouraged by preliminary studies at Harwell(2), there has been a great number of experiments with implantation into a variety of substrates that have provided conflicting results, probably caused by different implantation conditions and the complexity of the wear process.

In this section, first a brief introduction to wear and friction mechanisms will be presented, secondly, a detailed survey of the effects of nitrogen implantation on surface mechanical properties of steel substrates and coatings will be provided. Emphasis will be placed on hardness, friction and wear resistance improvements, which account for the majority of the research work carried out with the implantation process.

3.1 An Introduction to Friction

Historically, the first studies of friction were those of Leonardo da Vinci in the Sixteenth Century and the French physicist Amontons in 1699(53). These early investigations led to two findings about the friction force which became accepted as "laws of friction". These are: (i) the friction force is proportional to the normal load applied to the sliding contact and (ii) the friction force is independent of the (apparent) area of contact.

The above concepts are still considered as valid, however, the present knowledge of surface topography and area of contact has modified the interpretation of the relationship between contact area and surface geometry.

Real surfaces are typically irregular and when brought into contact will initially touch at asperity tips. The true area of contact is, hence, not determined by macroscopic dimensions of the surfaces, but by the microtopography of the surface, material properties and the force applied.

Bowden and Tabor(54) measured the real area of contact under sliding conditions. Studies of the relation between load and contact led them to conclude that elastic deformation of the asperities resulted in the contact area A being proportional to the two-thirds power of the load W ($A \propto W^{2/3}$). At sufficiently high stress levels, plastic deformation of asperities takes place and the contact area is directly proportional to the load ($A \propto W$)(55)

According to Bowden and Tabor's plastic deformation and cold welding hypothesis of friction, the friction force is in part due to the force required to break the junctions formed at contacting asperities between the sliding surfaces(54,56). The coefficient of friction can then be expressed as:

$$\mu = \tau / \sigma_y \qquad .....3.1$$

where τ is the shear strength of the junction and σ_y is the yield stress.

Archard(57,58) presented an elastic hypothesis of friction. In his work, the frictional force between sliding surfaces is associated with the energy required to deform the real area of contact elastically. Both hypothesis, plastic and elastic, can be considered to be relevant in explaining frictional behaviour of sliding couples. Under severe wear conditions, plastic deformation can be expected to be the dominant mechanism, but under a mild wear situation Archard's elastic deformation theory seems to be more applicable(59). Contemporary to the work of Bowden and Tabor, Kragelsky's research(60) set up the basis for a molecular-mechanical theory of friction. This theory was based upon the dual nature, deformational and molecular, of the friction force. Friction is, therefore, determined by the overcoming of intermolecular interaction forces between contacting surfaces and by the ploughing action of the asperities on the rough surfaces.

The presence of reaction layers or contamination films may modify the magnitude of the frictional force and this provides the basis for the concept of lubrication and surface treatments for protection.

The role of a lubricant is (i) to prevent interacting surfaces from coming into direct contact; (ii) to provide an easily sheared interfacial film, and (iii) to carry away any heat generated in lubricated contacts.

Lubrication by liquids comprises three main regimes, namely hydrodynamic, elastohydrodynamic and boundary, which are shown schematically in Figure 11. In this diagram(61) the coefficient of friction is presented as a function of a dimensionless parameter involving the viscosity of the lubricant, the sliding speed of the moving surfaces and the load at the interface.

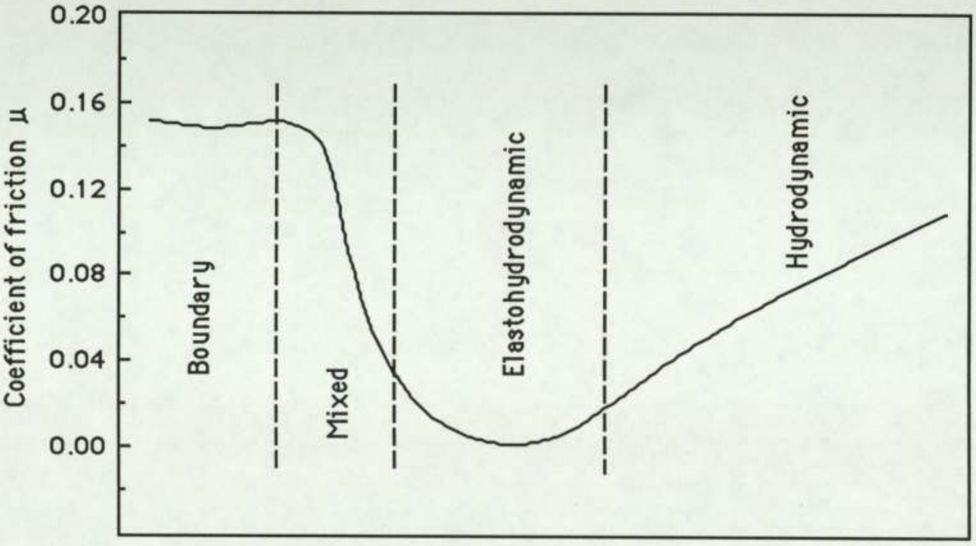

Viscosity x speed / load (Z x N / P)

Fig.11: Schematic diagram of the main lubrication regimes. The friction coeff. is shown as a function of the speed-load-viscosity parameter.

In the hydrodynamic regime, a film of lubricant is formed which is greater in thickness than the combined surface roughness. The surfaces are therefore separated, mutual contact prevented and wear damage minimized(62). Friction originates from the shearing of the lubricant film and involves the intermolecular interaction between the lubricant molecules.

Within elastohydrodynamic conditions, the oil film thickness between surfaces is reduced to the height of the surface roughness and contact of asperities through the oil film becomes a possibility. Deformation of both surfaces may occur, accompanied by formation of a thin oil film in the closest contacts(63).

In both regimes, hydrodynamic and elastohydrodynamic, wear generally is the consequence of the cyclic stresses applied to the surfaces, i.e. a fatigue wear mechanism.

Under more extreme conditions, the lubricant film can become thin enough to permit direct contact between surfaces, this is known as boundary lubrication. In this regime, any separation of surfaces depends upon molecules adhered to them, rather than a continuous oil film. Under these conditions, additives are normally used to provide protection of rubbing surfaces, the two main types are antiwear and extreme pressure (EP) additives(64). Friction between boundary lubricated surfaces arises from adhesion between asperities, shearing of the lubricant film and ploughing, the latter providing the major contribution to friction(65).

When certain conditions are encountered, eg. high temperature, low pressure or reactive atmospheres, liquid lubricants may not be suitable and solid lubrication has to be considered. The function of the solid lubricant is similar to that of liquids, ie. separation of surfaces and provision of a shear film. Examples of such lubricants are graphite and molybdenum disulphide.

3.2 Wear Mechanisms

It is generally agreed that wear can be defined as the progressive loss of material from the operating surface of a body as a result of relative motion occurring at the interface.

Wear is a complex, multi-stage process which can involve many variables, some of them uncontrollable. It is not, therefore, an intrinsic material property, but a characteristic of the engineering system. These factors, either internal or external, which can affect the frictional and wear behaviour between materials, are represented in Figure 12, after Kragelsky et al(67).

Wear processes are normally subdivided for simplification purposes into four main categories; namely abrasive, adhesive, fatigue and corrosive wear. Abrasive and adhesive wear are the most important and can account for up to 65% of the total wear encountered in industrial situations(68). Despite this subdivision, in practical wear environments it is quite common to find more than one type of wear process acting simultaneously. For example, debris generated through an adhesive wear mechanism can become entrapped between sliding surfaces and cause further wear by abrasion. Furthermore, the dominant mode is determined by several factors such as those indicated in Figure 12, which may change during operation as the system slips from one operating regime to another.

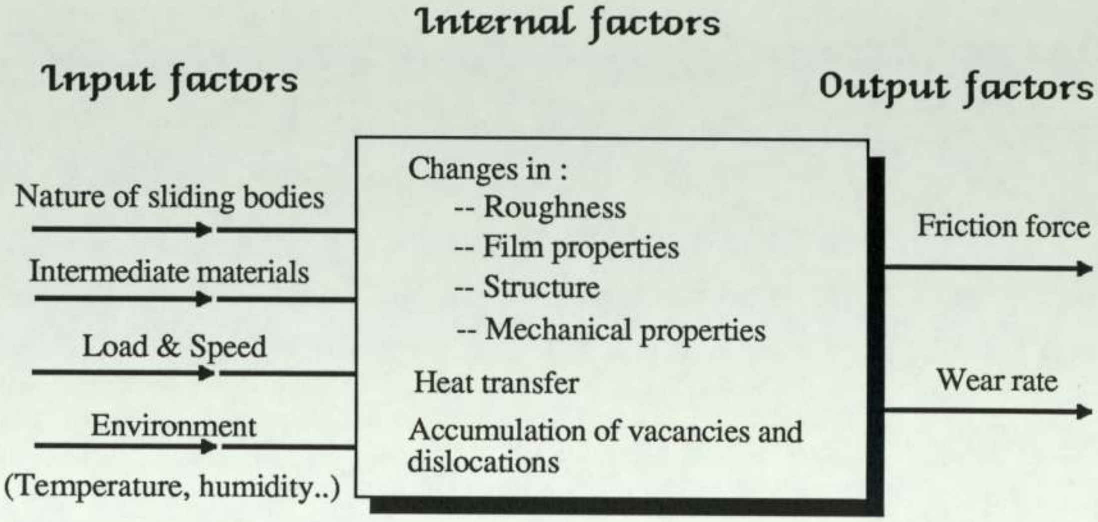

Fig.12: Diagram showing factors which affect friction between solids.

3.2.1 **Abrasive Wear**

This type of wear can be defined as the removal or displacement of material from one surface by the harder asperities of the counterface material or by harder loose particles(69). These hard asperities or particles indent the surface and, depending on the properties of the material, loading characteristics and type of motion, may remove material by mechanisms such as cutting, ploughing, chipping or fatigue cracking (Figure 13).

Moore(69) reports that for abrasive wear by multiple-particle contact, particle loading, geometry and attack angle are important parameters; each one having a significant influence on both the mechanism of material removal and the wear rate. Material removal can also be explained by two mechanisms; one in which plastic deformation is the predominant role and the other in which fracture with limited plastic deformation is dominant. Additionally, corrosion or environmental effects may also assist material removal.

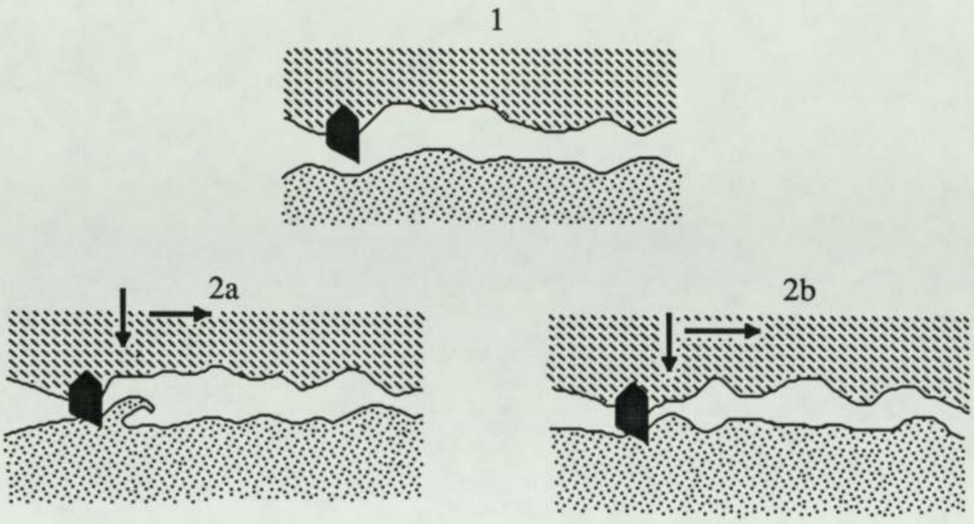

Chip formation

Ploughing

Fig.13: Schematic representation of the two most general abrasive wear mechanisms.

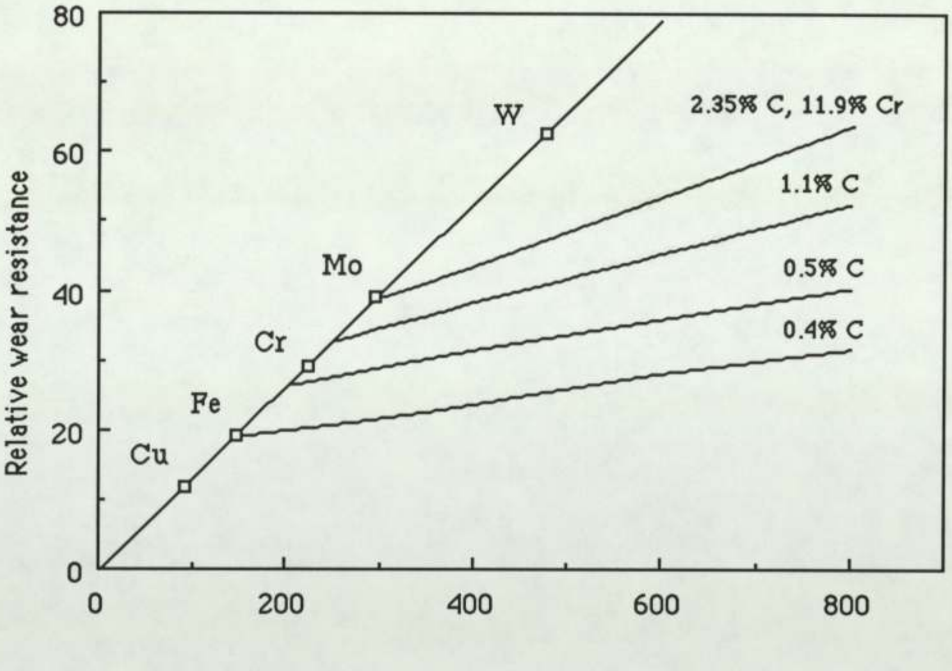

Fig.14: Relative wear resistance of metals as a function of hardness[(70)].

"Hard abrasion" is a term employed to characterize the situation in which the abrasive particles are much harder than the surface being worn. In this case, a simple relationship between wear resistance and hardness seems to take place(70). Commercially pure metals tend to show proportionality between abrasion resistance and hardness, whereas hardened steels depart from this relation and wear more rapidly than a pure metal of comparable hardness, as Figure 14 illustrates(70).

The microstructure of a material has an influence on the deformation and fracture behaviour leading to debris generation, and this can explain the discrepancies observed between hardness and abrasion resistance. Microstructural factors and the mechanics of the abrasive system lead to ploughing, cutting, or spalling modes of debris formation. Ploughing effects dominate in pure metals, cutting in hardened steels, while spalling is the preferential mode of debris generation in ceramics(71,72).

For steels, carbon content and the presence of carbides greatly influence their wear performance. The work of Popov(73) showed that both the volume and composition of carbides are important in determining the extent of abrasion and, usually there is an optimum carbide concentration beyond which no significant improvement occurs. Alloy addition effects on the wear resistance of steels are complex since they can affect matrix strain hardening, grain size, carbide precipitation and austenite stability(74).

For industrial applications, it is normal practice to select materials that have comparable hardness to the abrasive media at which they are exposed in service, in this case a "soft abrasion" takes place. The work of Richardson(75) pointed out that, in this category of abrasion, the ratio "K" of the hardness of the surface resisting wear to that of the abrasive must be greater than 0.5 if any improvement in wear performance is to be achieved. However, increasing "K" above 1·3 did not provide any further significant improvement. As a general rule(76,77) resistance to abrasion increases with hardness but microstructural factors or material properties, as indicated above, have a role to play. If hardness becomes too great, brittle failure may be initiated which can accelerate material degradation. Therefore, for a given wear severity, an optimum fracture toughness exists where abrasion resistance is a maximum.

3.2.2 Adhesive Wear

When two metal surfaces slide against each other under an applied load, the pressure between contacting asperities can be high enough to cause their plastic deformation and cold welding. Eventually, the junctions or welds formed fracture, usually resulting in metal transfer from one surface to the other, thus giving rise to the concept of adhesive wear (see Figure 15).

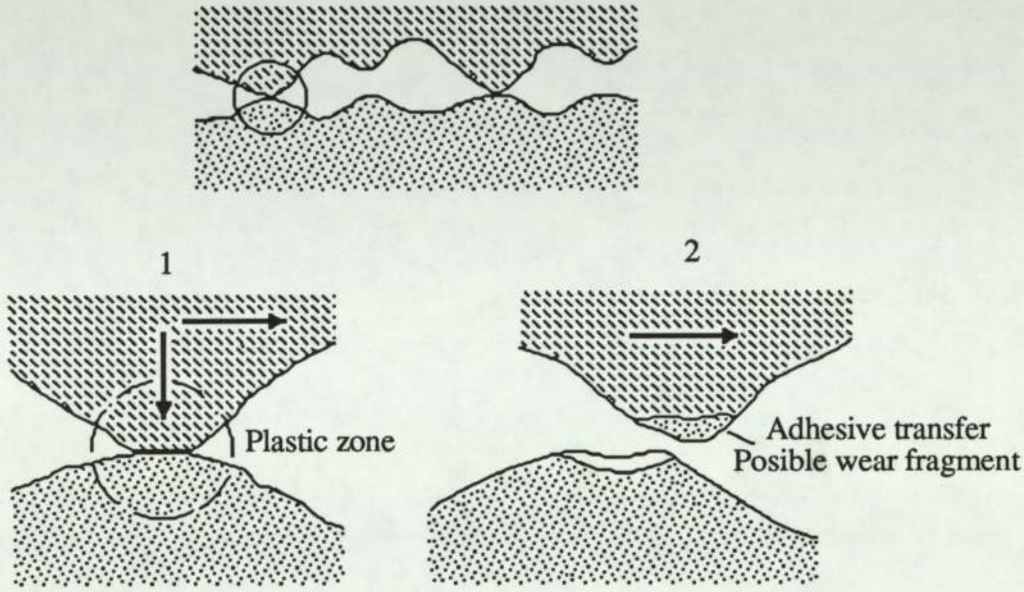

Fig.15: Schematic representation of the classical adhesion wear mechanism.

Explanation of this mode of adhesion lies in the capability of surface atoms to form bonds with other atomic planes placed in close proximity. It is expected, therefore, that adhesion would be favoured by clean surfaces, non-oxidizing conditions and by chemical and structural similarities between the rubbing surfaces. Rabinowicz(78) has related the adhesion occurring between pure metals to their mutual solubility and provided a comprehensive chart, showing friction and wear combinations for a variety of metals in accordance with their metallurgical compatibility(73).

The wear volume can be expressed by Archard's equation(80):

$$W = K D P / P_m \qquad .....3.2$$

where "K" is a constant and can be interpreted as the probability of producing on average a wear particle at each asperity encounter. "D" is the sliding distance, "P" is the applied load and "P_m" the flow stress of the wearing surface.

Although most of the current wear theories accept Archard's interpretation of the "K" factor, its usefulness is limited since it may not be constant for a given material and may change with applied load, sliding speed and temperature(81).

The work of Welsh(82) indicates that a slight change in load or speed can lead to very significant alterations of the K factor and, hence, the wear volume due to a transition from a mild to a severe type of wear. The characteristics of these wear regimes, as described by Quinn(59) are indicated in Table 3.

Table 3 - Characteristic features of mild and severe wear

Feature	Mild Wear	Severe Wear
Type of contact	Oxide film (high contact resistance)	Metallic (low contact resistance)
Surface topography	Relatively smooth	Deeply torn, rough
Wear debris	Small oxide (or oxidized) particles	Large, metallic particles

Welsh(82) was one of the first to examine systematically the origin of both wear regimes, and the sharp transitions T_1 and T_2 which can occur between these, as Figure 16 illustrates. Below T_1, wear takes place by the removal of oxide debris from an oxidized surface supported by a strong substrate. Above the transition load T_1, in the severe wear regime, plastic deformation of the substrate occurs due to higher near surface temperatures; the protective surface oxide is no longer supported, metallic debris is produced and the wear rate increases. At T_2, the surface temperature becomes high enough for phase hardening to produce a hard "white layer" structure which prevents surface deformation and helps to establish an oxidized surface again(84).

Transitions from mild to severe wear can be suppressed if the steel is sufficiently hard. The low "oxidative" wear regime can therefore be extended over the

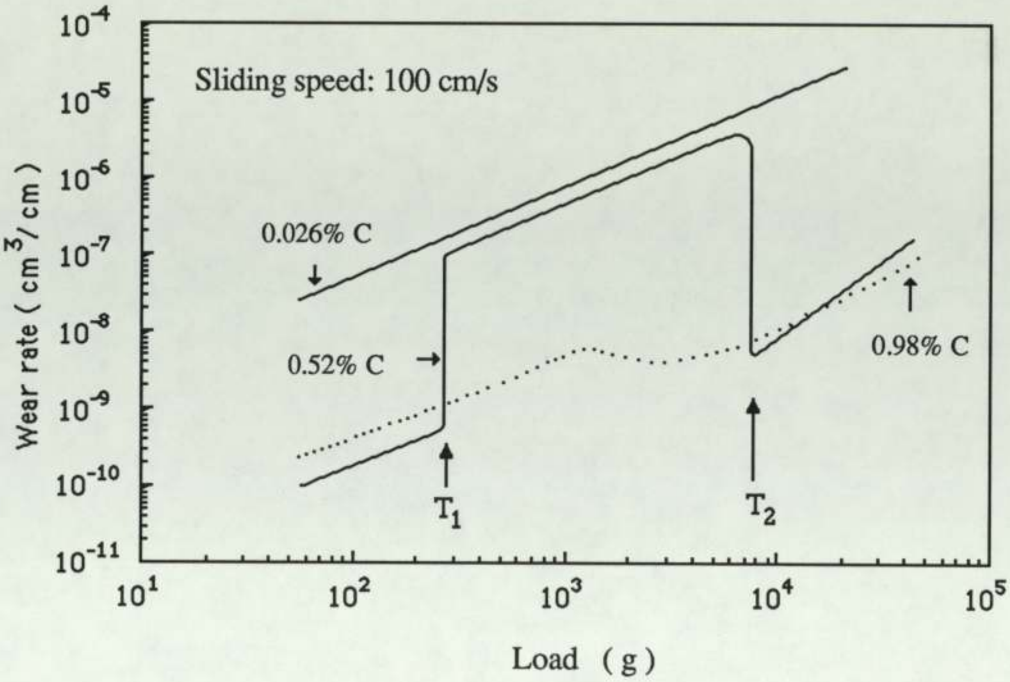

Fig.16: Transition wear behaviour of different steels. Welsh(82)

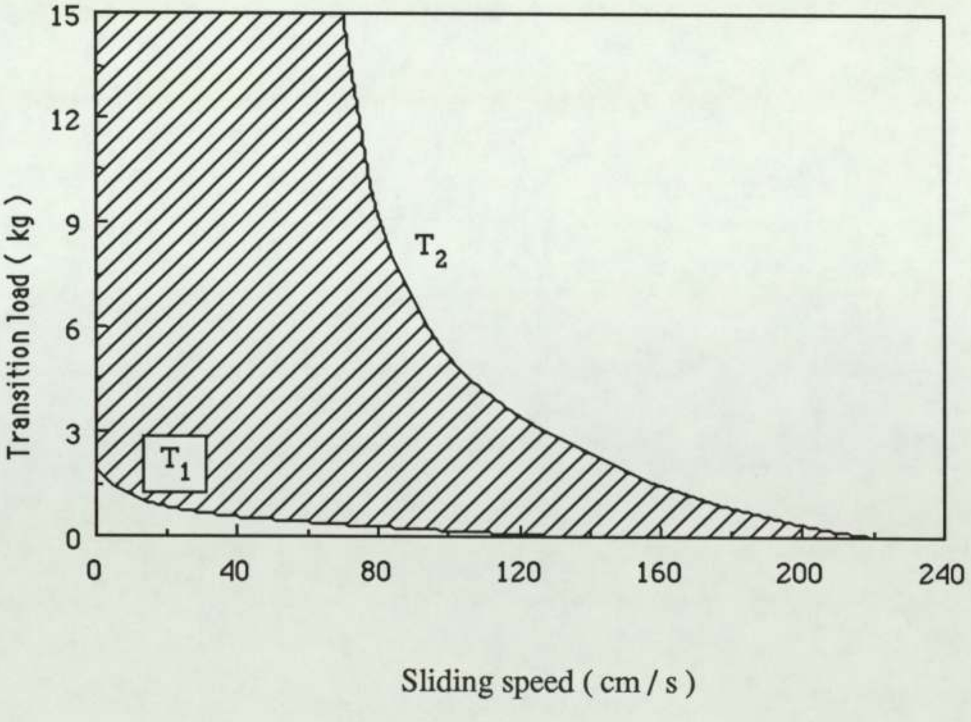

Fig.17: Effect of sliding speed on transition loads, for 0.52% C steel. Welsh(82)

whole load range, as Figure 16 depicts. This figure is based upon a constant sliding speed, however, sliding velocity can affect wear rates and transition loads. Figure 17 illustrates the change of transition loads with speed(82). Both, the effect of load and speed on the transition loads from one wear regime to another are of considerable importance for the design engineer.

3.2.3 **Fatigue Wear**

Fatigue wear can be described as the result of the cyclic variation of stress in the surface layers of a solid. The basis for this type of wear mechanism is the accumulation of damage or lattice defects as a consequence of the applied stress. Features of the damaged layer that have been reported include(85): plastic deformation, hardening or softening, increase in dislocation density, selective diffusion of certain constituents, phase transformation or formation of unusual intermetallic compounds, and eventual initiation and propagation of cracks. All of these features may not always be present in the subsurface layer or contribute to failure wear by fracture.

Contact fatigue can occur by two different forms, either sliding or rolling fatigue, depending upon the kind of frictional movement involved. The latter type of fatigue, rolling contact, can be defined as the observable cumulative effects from repetitive rolling over a given surface, a typical case being that of radial ball bearings. In these components, the inner ring can fail by fatigue cracking or spalling, the cracks propagating at the depth under the ball track where Hertzian shear stresses are near maximum.

An example of sliding fatigue wear is that of metal cutting tools, which often exhibit stress distributions giving rise to series of fatigue cracks normal to the cutting direction, eventually leading to material loss. During cyclic metal-to-metal sliding other effects such as temperature cycling may be superimposed on the stress variation and contact fatigue can also have a thermo-mechanical character.

An important mechanism that arises from the idea of cyclic stresses during wear is the delamination theory of wear developed by Suh(86,87). This model is based upon the formation of a shear crack at some distance below the near surface, whose growth leads to subsequent delamination of the plastically deformed surface layer, generating plate-like wear particles (see Figure 18). These particles differ in shape to those produced by deformation and fracture of asperities, which are small, and those originated by ploughing or abrasion, which tend to be long.

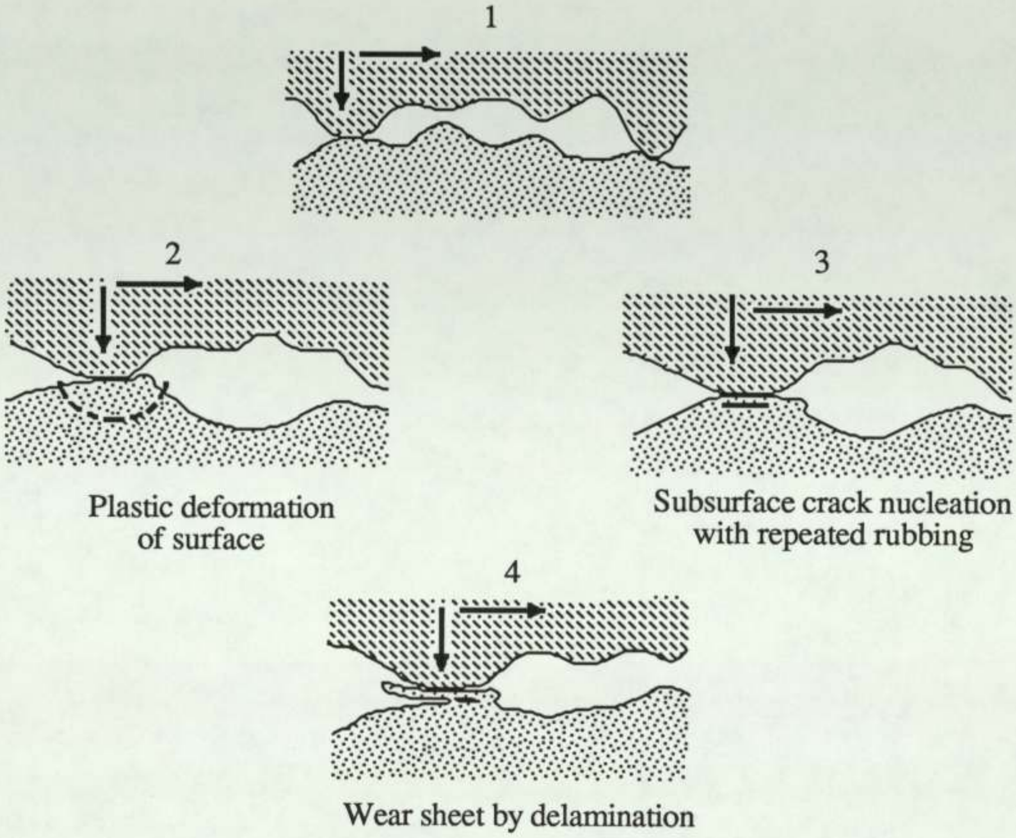

Fig.18: Schematic representation of the various stages involved in the formation of delamination wear sheets, after Suh (86,87)

The rate of delamination wear is determined by microstructural factors, such as density and type of inclusions or dispersed phases. Hard single phase materials or structures with coherent second phase precipitates will resist this kind of wear; on the contrary, if the material contains incoherent particles, inclusions or porosity, delamination is likely to occur.

The delamination mechanism is supported by a model of sliding wear based upon the concept of surface dislocations(88). During wear, a dislocation cell structure is created in the plastically deformed surface layer, giving rise to shear crack initiation at the interface between this surface layer and the inner undeformed layer. These cracks then grow causing delamination to occur. The rate of work hardening is a very important parameter, since it affects the degree of deformation, this being low for materials that work harden rapidly.

3.2.4 Corrosive Wear

This wear mechanism is caused by the simultaneous occurrence of a chemical reaction and one or more of the mechanical wear processes described above. In some cases, the reaction layer may serve as a lubricant and have a protective action, in other circumstances the chemical reaction may accelerate the wear processes.

Many variables can participate in tribological chemical reactions, making the study of corrosively worn surfaces difficult. However, one type of mechanism, such as oxidation, is repeatedly encountered in rubbing surfaces and has been analysed in detail.

Oxidative wear is observed when the sliding surfaces are subjected to the action of atmospheric air or oxygen contained in a lubricant, and the oxides formed on the surfaces undergo wear.

Oxide films on rubbing surfaces provide a protective action that depends on the relation between hardness of the base metal and that of the oxide. Films of hardness approximating to that of the substrate will give the maximum load-carrying capacity, while oxide films with high hardness values would be ruptured easily(67).

According to Tao(89), oxidative wear processes can be divided into three stages: diffusion of oxygen to the metal surface, growth of the oxide film and rupture of the film during sliding. The time required for rupture of the oxide film depending on its strength of adhesion to the substrate and the acting stresses. In the initial stages, the oxide film is hard and protects the base metal by lowering the friction and protecting the underlying layers against mechanical damage. The oxide film continues to grow, but upon reaching a critical thickness it breaks up at the metal-oxide boundary due to frictional forces, forming wear particles and exposing the metal to a new oxidation process (see Figure 19). Quinn(90) has also presented an oxidational theory of wear, which is generally accepted in cases involving mild wear.

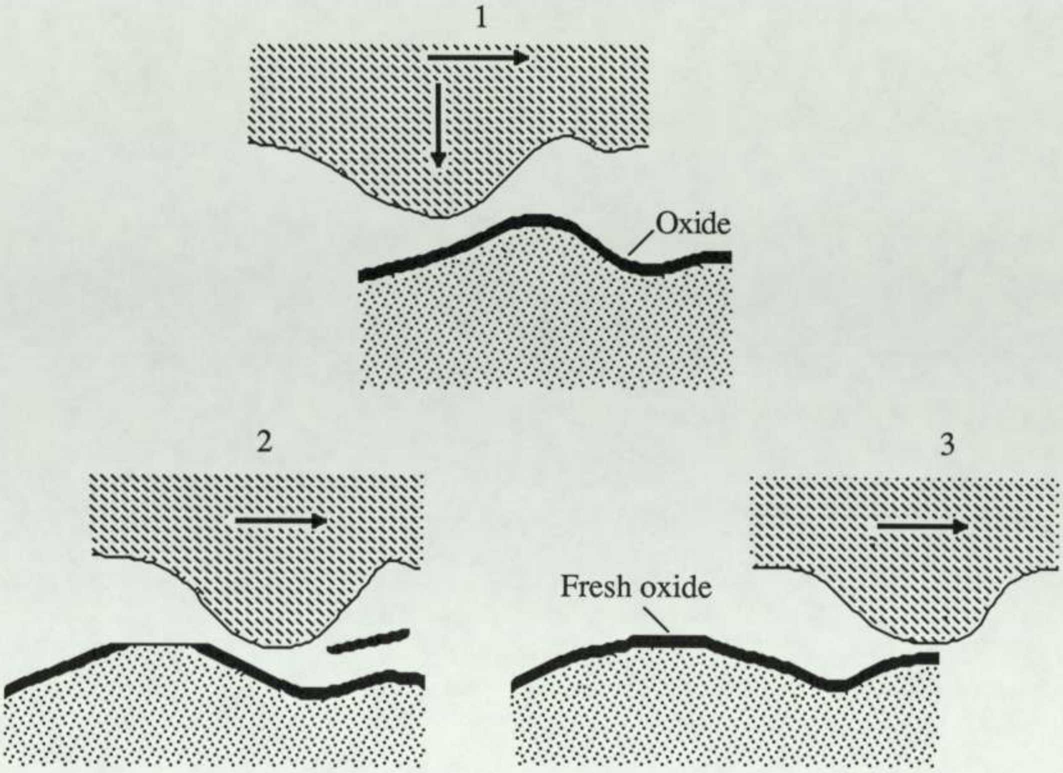

Fig.19: Schematic representation of a mild wear mechanism resulting from the repeated formation and removal of a surface oxide film.

3.2.5 Other Categories of Wear

So far only the major mechanisms of wear have been outlined. Other types of wear that can occur in specific situations or environments are fretting, erosive wear and cavitation erosion. Fretting wear is a term used specifically to describe wear phenomena occurring when two contacting surfaces undergo very small amplitude oscillatory or vibrational slip. It is characterized by the production of a finely oxidized debris which often flows out of the contact area. An accepted theory of fretting is that adhesive wear produces very small loose particles which become oxidized and, as they are trapped between the oscillating surfaces, cause abrasive wear at a higher rate; although wear might also be caused by surface fatigue combined with oxidation of the surface.

Erosion is a generic term covering a number of forms of wear which can occur whenever a surface is exposed to a moving fluid which may or may not contain solid particles. In general, however, the term "erosive wear" is used when solid particles are encountered and "fluid" or "cavitation erosion" when the wear is caused by the impact of the fluid alone.

Wear caused by impact of solid particles is similar to abrasion. Most theoretical studies of the subject have been based on the idea that impinging particles cut the surface as they strike at glancing angles. In cavitation erosion the damage arises from the collapse of bubbles formed by cavitation of a liquid and the following impact that the surface is subjected to by liquid.

3.3 Nitrogen Ion-Implantation Effects on Surface Hardness

Repeatedly, references have been made in the literature to hardness changes caused by nitrogen ion implantation usually linked with a wear reduction phenomenon. Dearnaley(91) reports that in each main category of wear (ie. adhesive, abrasive and corrosive-oxidative) the microhardness of the surface is clearly related to wear rate, and hence measurement of this parameter can be a useful indication of wear resistance. However, this information should be considered cautiously since an increase in the hardness of a metal might modify the deformation characteristics, promoting crack nucleation and thus wear by a fracture process.

Material hardness is a parameter which can be readily quantified. Static measurements are usually made by impressing a pyramidal diamond indentor into the surface of the sample under a fixed load, measuring the diagonal length of the indentation with a microscope and finally converting this to a Knoop or Vickers microhardness scale. This is calculated from the applied force and the surface area of the impression as load per unit area, kg/mm^2, and is generally related to the yield strength of the material.

Two different methods are used to determine the hardness in surface treated components, making the indentation either on the surface or a cross-section. Generally, the latter procedure is used to provide a more reliable hardness value; but it is obvious that microhardness values cannot be determined for implanted surfaces on cross-sections as it is usually feasible with coatings or thermo-chemically treated surfaces.

Low loads in the range 1 to 25 g are normally used for implanted surfaces. However, this sort of testing is limited by the fact that even under these low loads, the indentor penetrates beyond the depth of the implanted layer, which is unlikely to exceed 1 μm, with a distribution peak at 0.1 to 0.2 μm below the surface, for the energies commercially used. Thus the microhardness results describe not only properties of the implanted layer but also those of the underlying bulk material. The effects of implantation on hardness would be best observed at shallow indentation depths when the deformation volume contains a significant proportion of the implanted material. Nevertheless, conventional hardness measurements have been carried out on implanted surfaces and significant improvements have been obtained. Table 4 summarizes some of the experimental results dealing with surface hardness changes after nitrogen implantation. These show that not only implantation dose and energy are significant in achieving improvements in surface hardness, but also the dose rate(92) since bombardment induced heating effects can cause enhanced diffusion of implanted species, structural transformations(93) or softening of the substrate(96),

To overcome the problem of deep penetration with conventional microhardness testers a specialised instrument capable of making ultra-shallow indentations wholly in the implanted layer was devised by Pethica(99). It was shown(100) that for doses of 3.5×10^{17} nitrogen ions/cm^2 at an energy of 45 keV and 5 μA/cm^2 current density, the atomic concentrations of the implanted specie could reach a maximum value from 30 to 50 at % just below the surface (50 to 100nm) for materials such as Ti, hard chromium and iron. The hardness observed at this depth would be almost entirely due to any hardening effect within the implanted region.

Using a similar procedure, Oliver et al(101,102) reported improvements in hardness ranging from 20 to 30% for stainless steels and hard chromium electroplate; but no significant hardness increase was observed for the bearing steel AISI 52100. This is in agreement with other published work(103).

A similar ultra-low load (3 mN) penetration hardness tester has been reported elsewhere in the literature(104,105). Penetration depth of the indentor at a submicron scale was also measured as a function of the applied load. Using this technique, work by Newey et al(104) showed a remarkable increase in hardness at a dose of 10^{17} N_2^+/cm^2 (300 keV energy) for an iron specimen, but at higher doses the increase in hardness was less significant. Since iron foils were implanted it seems reasonable to argue that bombardment-enhanced diffusion could have occurred and that the hardness was not sampled at the point of maximum nitrogen concentration for each particular dose.

The increase in surface hardness after ion implantation is generally considered to be due to a number of possible mechanisms including:

(a) radiation-induced damage effects

(b) residual stresses

(c) solid-solution hardening, eg. by interstitial nitrogen or carbon, and

(d) precipitation (second-phase) strengthening.

One of the earliest irradiation-induced mechanical property changes reported was that of neutron-irradiation hardening, and it is now well understood on the basis of dislocation pinning(117). However, these irradiation hardening studies were carried out at high temperatures to investigate structural transformations in reactor materials subjected to high neutron fluxes. Ion implantation is normally carried out at low temperatures and therefore structural transformation of the bulk material dose not occur. Implantation of inert species, such as argon, into steel has produced widely differing hardening results. Gabovich et al(92) observed no improvement in hardness which is in contrast to the work of Pavlov et al(118) who reported hardening effects for 40 keV Ar^+ ions and doses up to 9×10^{17} ions/cm^2. The latter implantation was carried out at room temperature with a low current density. Un-annealed damage effects may well have extended beyond the mean projected range of the ions, which could thus explain the observed hardness discrepancies(3). It still remains to be established to what extent bombardment damage is responsible for the improvement in hardness for elements such as nitrogen, carbon or boron, which can contribute to variations in yield strength by other mechanisms, eg. compound formation.

It is known that hardness is dependent on the state of stress in the material(119). Ion implantation can produce a great number of defects and introduce an excess quantity of atoms which can stabilize as intermetallic compounds. Providing the implantation is carried out at low temperature, the mobility of defects created by radiation damage is low, hence complete recovery of the substrate does not take place, leading to volume changes. Aggregation of damage may cause macroscopic density changes and if the substrate material constrains this deformation a residual surface stress will be created.

Eernisse(120) has shown by a cantilever beam technique that implantation produces a large amount of stress within the surface layer of the material. The same device was used by Robic et al(121) to measure the residual stress for a number of metal-ion combinations and to evaluate its influence on hardness and wear. It was concluded that although surface hardness can be increased by ion implantation no hardness correlation exists with the induced stress. However, as stated by Hutchings(122), this conclusion does not take into account the complexity of the stress profile and accurate hardness measurements would have to be taken at penetration depths equal to the depth of peak stress, using specialized apparatus such as those mentioned earlier(99,104).

Further surface stress measurements have been carried out in other work on steel substrates, using high dose Ar^+ and N^+ implantation(123). Both ions were found to introduce surface compressive stresses over the implanted region, which might be in excess of the yield stress of the material. See for example Figure 20 for nitrogen implantation on a nitriding steel. Such residual stress effects would be expected to occur appreciably for many alloys subjected to nitrogen implantation since the nitrogen (with atomic radius 0.07 nm) has the tendency to be situated at octahedral interstices(36,124) (with radii 0.049 to 0.062 nm for most alloys of commercial interest). Figure 21 shows the octahedral interstitial positions in bcc and fcc iron(83). High dose implantation of light ions, eg. nitrogen or carbon, would also create local stresses owing to the difference in molar volume of any intermetallic compounds formed, ie. nitrides or carbides(122).

The role of residual stresses in hardening metal surfaces remains controversial, and may be considered as a minor part of the total hardening effect after ion implantation. Solid solution hardening is a well reported strengthening method in metals and it is understood in terms of the interactions between solute atoms and dislocations(125). An increase in yield stress is produced by elements in solid solution. This is most marked when the individual solute elements produce elastic distortions in the host lattice which are markedly asymmetric. For example,

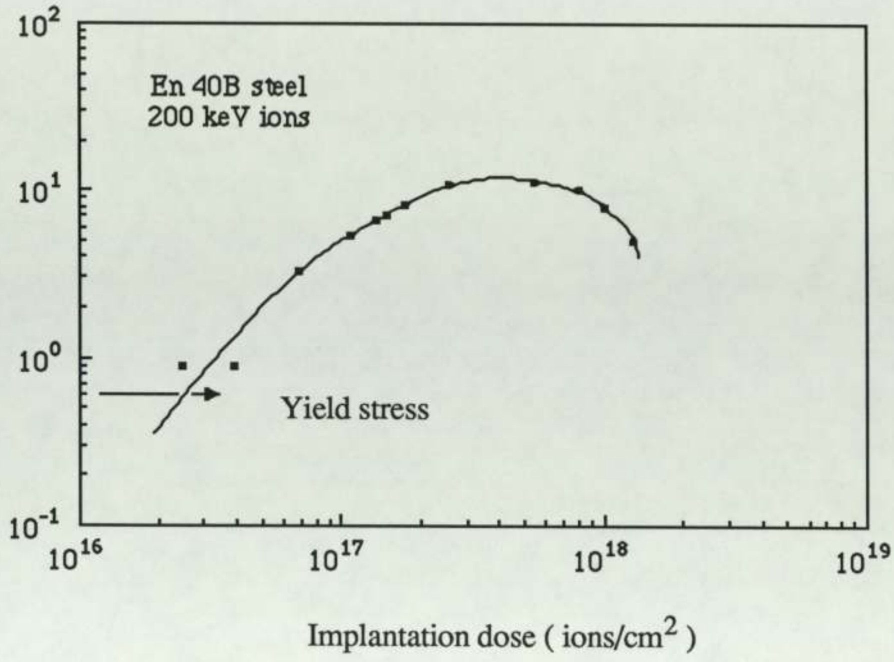

Fig.20: Plot of surface stresses as a function of dose for nitrogen implanted En 40B steel. Implantation energy: 200 keV. Hartley (123)

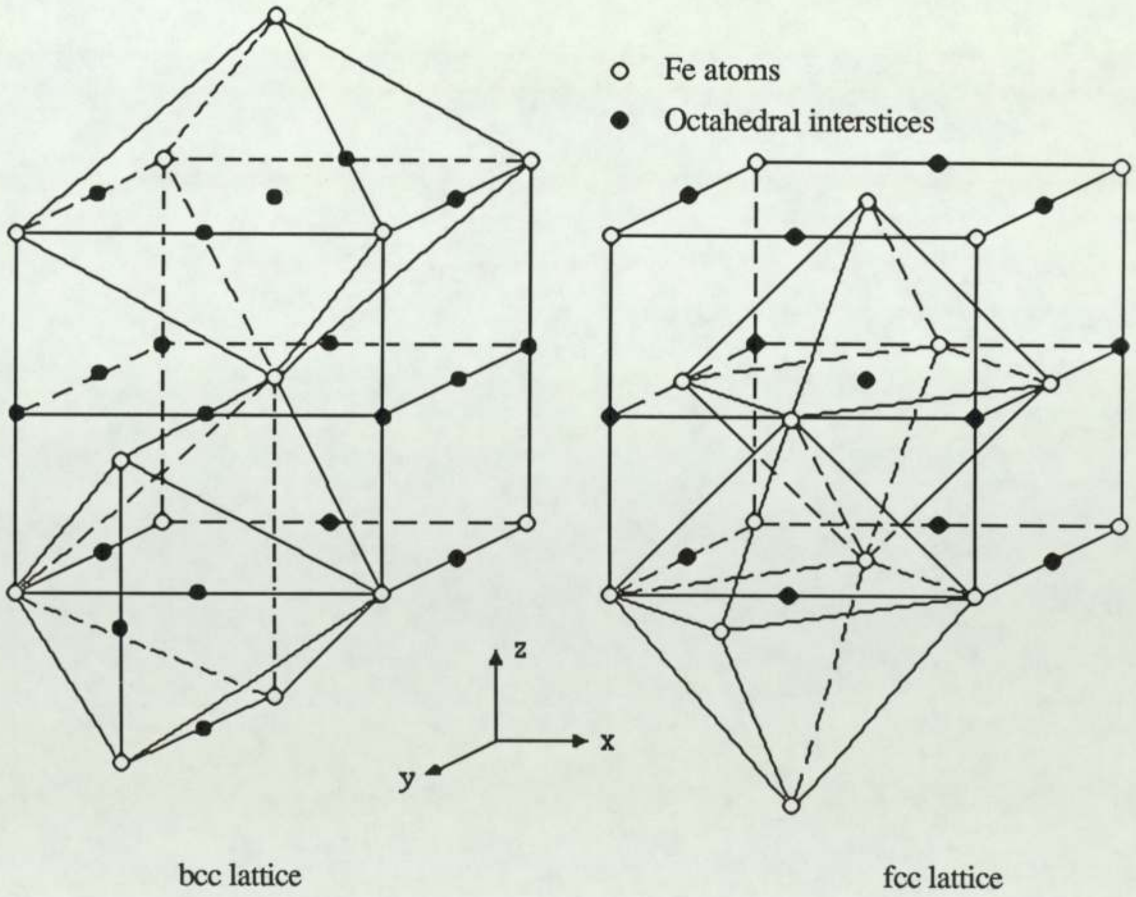

Fig.21: Octahedral interstices in bcc and fcc iron.

substitutional atoms in cubic crystals produce spherically symmetric distortions and hence weak solution hardening, and interstitial atoms in body-centred cubic metals produce a tetragonal distortion and therefore very strong solution hardening effects, eg. carbon in martensite.

Implantation of interstitial elements, nitrogen or carbon, is expected to provide solid solution strengthening. The extent of any solution hardening will depend on the substrate material and the already available strengthening mechanisms in the host lattice and their interaction with the implantation effects. In the case of ferrous materials, it is difficult to separate solid solution phenomena from other contributions to martensite strength and especially to distinguish clearly between solution and precipitation hardening.

The presence of nitrides and phase changes by nitrogen implantation, which can account for the observed hardness and wear resistance improvement, have been shown to occur by a number of surface analytical techniques. Table 5 lists some of the precipitation effects produced by nitrogen implantation.

One of the earliest studies of nitrogen implantation induced precipitation was by Bykov et al(126). Using Mössbauer spectroscopy on iron foils they found the presence of hcp precipitates at doses above 5 x 10^{16} ions/cm^2. The formation of iron nitrides for nitrogen doses in excess of 10^{17} ions/cm^2 was also shown by the work of Longworth and Hartley(127). These results have been confirmed using other techniques, such as electron diffraction analysis(128). Rauschembach and co-workers(129-131) provided a more systematic study of the nitrides and phase changes that occurred when iron foils were implanted at doses of 10^{16} to 10^{18} N^+ ions/cm^2. From this investigation it was possible to produce a dose-transformation-temperature diagram (DTT diagram)(108,132) for the Fe-N implantation system. Figure 22 depicts such a diagram, showing the iron-nitride phases that could be formed depending on the temperature and implantation dose. A similar diagram, constructed from experimental data of boron implanted iron has also been reported in the literature(132,133). These diagrams, nonetheless, describe the states far away from thermodynamic equilibrium for each system, and should not therefore be correlated with conventional phase diagrams. Ion implantation is regarded as a non-equilibrium process and a metastable condition may persist. Additionally, the diagram depicted in

Figure 22 was obtained at an implantation energy of 50 keV. Higher energies for a given dose and beam current density would lead to deeper penetration of the ions and lower peak nitrogen concentrations. This could affect the phases formed by the implantation.

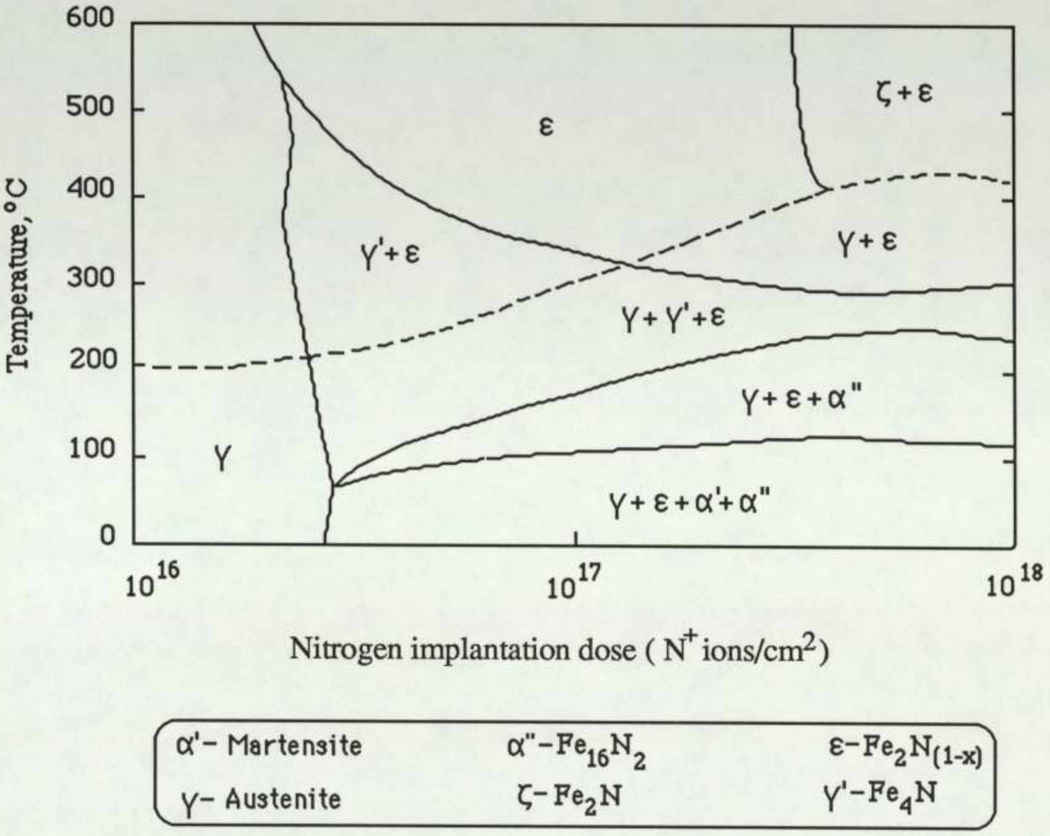

Fig.22: DTT diagram for nitrogen implantation in iron.(108,132)

Extensive work has also been carried out on stainless steels(141-152) in an attempt to investigate the chemical effects of the implantation and their relationship with tribological behaviour. These studies have shown that chromium acts as a nitrogen trap, allowing nitrogen to be retained at higher concentrations that in any other steel(147). Both, chromium and iron nitrides are formed(148,149), but at lower doses it seems that chromium precipitates are formed in preference to iron nitrides(142,145,147). The contribution of iron compounds becomes more important as the dose increases.

To summarize, the effects of nitrogen implantation on hardness can be explained in terms of bombardment induced effects, residual stresses, solid solution strengthening and precipitation hardening. It would be difficult to attribute any one of these effects as accounting for the hardness enhancement, since they are all interrelated. However, it would appear that the latter two mechanisms play the major role in hardening metal lattices following nitrogen implantation.

3.4 Effects of Nitrogen Implantation on Friction

Friction was one of the first mechanical properties to be analysed following ion implantation. The early work by Hartley et al(1) showed that implantation of various metallic and non-metallic ions into a 1% Ni-Cr steel could bring about considerable reduction (up to 60%) in the friction coefficient. Inert gas implantation did not improve the frictional characteristics, which therefore suggests that implantation damage or possible contaminants (carbon, oxygen) introduced during the process are not the main cause of friction reduction.

Hartley(3,154) discussed friction effects in terms of the yield stress of deformed material at metallic junctions formed during sliding. He assumed that the dominant effect of the implanted species was to lower the shear strength of the implanted layer by promoting oxide film formation, leading to a friction reduction.

Shepard and Suh(155) report that if ion implantation creates a hard surface alloy, it will decrease the ploughing component of friction under lubrication conditions, which in turn will reduce the friction coefficient. Figure 23 shows the change in friction coefficient for nitrogen implanted and plasma nitrided iron specimens. The steady-state friction is reduced considerably after implantation (μ=0.07) and is even lower than the friction value for the plasma nitrided sample (μ=0.1), when compared with the unimplanted value (μ=0.122).

Dearnaley(156) considers that the coefficient of friction may be reduced by ion implantation due to two effects, firstly the junctions formed between the two sliding surfaces will be more brittle, due to a decreasing dislocation movement. These junctions will therefore break off resulting in a smoother, burnished surface. Secondly, an oxide film is more likely to be retained under these circumstances. The presence of the oxide reduces metal to metal adhesion at the interface.

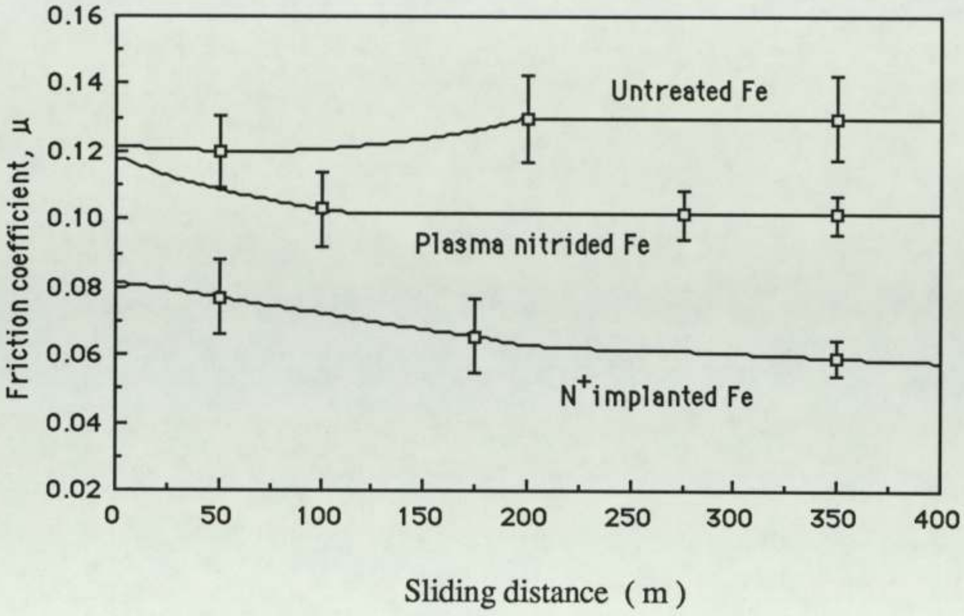

Fig.23: Change in the coefficient of friction μ with sliding distance for untreated, plasma nitrided and nitrogen implanted Fe systems. Shepard and Suh.(155)

Important friction improvements have been achieved by titanium and carbon implantation in austenitic and martensitic steel structures(51), reported to be due to the formation of an amorphous surface layer.

A summary of frictional changes brought about by implantation for all metal-ion combinations is not intended in this study, the reader is therefore referred to several reviews on the subject(8,35,157). Since this work is concerned primarily with the tribological effects of nitrogen implantation, only these will be reviewed.

Table 6 summarizes the effects of nitrogen implantation upon frictional characteristics of essentially steel substrates. As a general trend, it appears that nitrogen implantation does not produce any significant change in the friction coefficient for carbon, bearing or tool steels. Despite this observation, in some cases a considerable wear improvement has been reported(159).

Friction was reduced by up to 45% after high dose nitrogen implantation into a 316 austenitic stainless steel(98) and similar results have been reported for grade AISI 304 stainless steel(112,162). However, on the contrary, Dimigen et al(103) and other workers(164,165) failed to observe any frictional change on implanted austenitic stainless steels. Differing experimental conditions are likely to account for the discrepancies observed.

Hartley(8) reports that under the effects of the bombardment, an enhanced migration of impurity oxygen atoms inward and of iron atoms outwards from the substrate material leads to an Fe_2O_3-rich outer layer. The reduction on friction could therefore be due to oxide formation and chemical changes occurring on the surface. Chromium and iron nitrides have been observed in stainless steels following nitrogen implantation(103,142,144-146,148,153). Nitride precipitation can also account for the friction enhancement. Danroc et al(166) observed a substantial friction reduction for CrN films compared to electrodeposited chromium.

To summarize, friction is not always reduced by ion implantation. Frictional changes seem to be dependent upon the nature of ion and substrate material. Nitrogen implantation has been reported to improve the frictional behaviour of stainless steels but little benefits have been shown for other types of steels. A number of mechanisms could possibly explain the improvement in friction(154,156) and have been described above; however, there is generally a lack of a valid model for all ion-material combinations. The formation of a hard layer in steels, with enhanced friction properties appears to be related to surface alloying.

3.5 Nitrogen Ion-Implantation Effects on Wear Resistance

Hardness and friction are important properties to investigate after ion implantation. However, for the majority of engineering applications wear behaviour attracts the main interest since it is more useful for assessing the lifetime of a component. As a consequence, the effect of implantation on wear resistance has been studied more frequently than any other mechanical property. Table 7 shows the results of a review of wear investigations after nitrogen implantation on mainly ferrous based materials.

Early experiments, using a pin-on-disc wear tester, were those of the Harwell group(2,3,8,169). Mild and nitriding steels showed a remarkable reduction of the wear parameter under lubricant sliding after nitrogen implantation. Figures 24 and 25 show some of these results. In this experimental arrangement only the disc was implanted, taking the performance of the pin as an index for the effectiveness of the

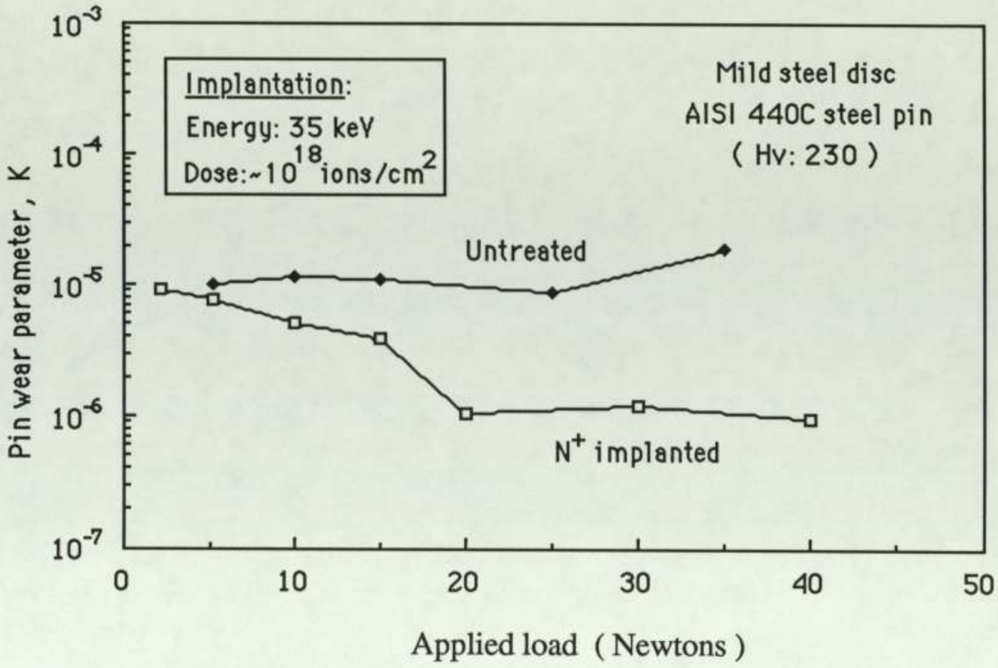

Fig.24: Wear parameter as a function of applied load in a pin-on-disc test.(2)

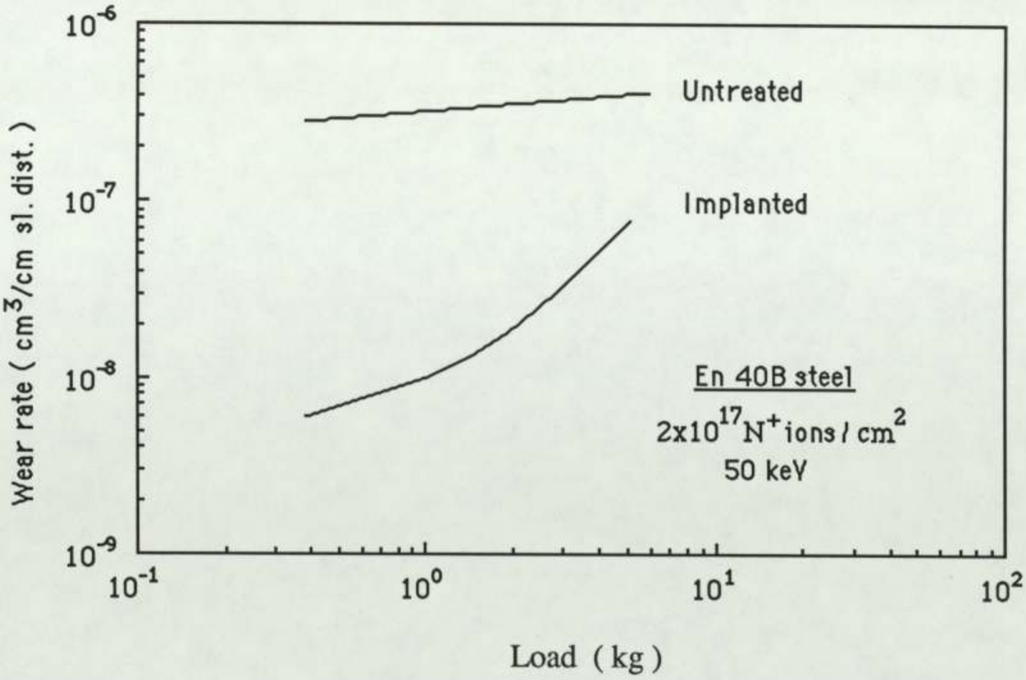

Fig.25: Volumetric wear parameter for a steel pin in contact with an implanted nitriding steel as a function of load. Dearnaley and Hartley.(170)

implantation. Although the wear rate is determined by the mutual interaction between two surfaces, the above approach can be doubted to provide the true effect of the implantation treatment. Measuring wear on implanted surfaces is a more realistic method and can be directly compared to industrial tooling situations.

A systematic investigation of the wear process has been hampered by the large variety of tests used in its study. The most common types of wear testing devices are those of pin-on-disc configuration, although other geometries such as cylinder-on-cylinder(7,171), ball-on-disc(7,103),pin-on-cylinder(97,158) and a vibratory abrasive technique(95,172,173) have also been utilized for implanted surfaces. The aim in all cases is to measure the total amount of wear over a fixed period of time as function of load and/or speed.

The general procedure with all these tests is to use low loads (usually up to 20 N) and/or low contact pressures under lubricated conditions. These conditions are more appropriate when investigating the mild wear performance of a shallow implanted layer. However, a more severe testing procedure has been used with the Falex friction and wear tester(159,175-179). The aim was to study the anti-scuffing properties of nitrogen implanted AISI 3135 steel under high loading conditions (890 N). Hale et al(175-179) reported a 12 to 16 improvement factor in wear resistance for a dose of 2.5 x 10^{17} ions/cm^2. The results of Hartley and Hirvonen(159) showed a lower, but still significant enhancement when the same material was tested. The discrepancy in the results can be attributed to differences in testing conditions, ie. choice of lubricant and implantation treatment.

Nitrogen implantation does not bring about the same effects in all materials, alloying elements and structure appearing to be a limited factor. It is generally agreed that implantation of nitrogen into pure iron and low to medium carbon or alloyed steels causes a significant decrease in the wear rate(3,8,103,106,107,155,159,172,176,180-184). The improvement in wear resistance varies depending upon implantation and test conditions, reaching factors of 10-15 enhancement.

Considerable work has been carried out on stainless steel substrates in an attempt to lessen the galling characteristics of these materials. Large reductions in wear after nitrogen implantation have been reported to occur under lubricated(7,101,112,162,164,185-187) or dry(98,103,150,152,188) wear testing conditions.

Dimigen and co-workers(103), using a ball-on-disc tester reported an increase of wear resistance for 304 and 321 austenitic stainless steels of up to three orders of magnitude under dry testing conditions. For such an improvement to occur, the nitrogen concentration had to be 10-15 at %, which corresponded to a nominal dose of 3 x 10^{17} nitrogen ions/cm^2 or more, at an ion energy of 100 keV. Below 2 x 10^{17} ions/cm^2 no wear reducing effects occurred. Other investigations(98,150,188,152) also indicated benefits under similar dry wear conditions.

Paradoxically, under lubricated conditions lower wear improvements were generally obtained, although not direct comparison can be made for different tests. Oliver et al(101) reported a 26 times decrease in the wear rate of AISI 304 stainless steel; in agreement with this other workers(7,112,162,164,185-187) also found significant improvements.

These wear results for austenitic steels have been explained in a variety of ways. Initially it was suggested that improvements were due to hardening of the surface by interstitial solid-solution or precipitation strengthening mechanisms. Chromium and iron nitrides have been found in austenitic stainless steels after nitrogen implantation(116,141,145,148,149). An alternative explanation(6,189) is that nitrogen stabilizes the austenite phase, preventing a strain-induced transformation to martensite. This would avoid the unfavourable situation of a very thin hard layer on a softer substrate, which could generate abrasive wear debris. This theory is supported by the observations of Cavalleri et al(152) using a glancing X-ray diffraction technique. On the contrary, Whitton et al(146) using a similar technique observed an ion-bombardment induced transformation of austenite to martensite for a single crystal austenitic stainless steel. Fayeulle et al(148) also reported formation of α'-martensite after nitrogen implantation on an electropolished stainless steel, thereby eliminating any remaining mechanically induced martensitic phase prior to implantation. The latter treatment was carried out at a high dose rate of 20 μA/cm^2; bombardment induced temperature increases within the implanted layer might have caused the martensitic transformation. Despite these research efforts, the mechanisms involved which are responsible for the wear behaviour in these steels are as yet not understood fully.

Improved wear behaviour has also been achieved by nitrogen implantation of martensitic stainless steels. Wear reductions up to 20 times were obtained by Dimigen et al(103) and similar results have been reported by Iwaki et al(110) and other workers(7,101,150,161).

In contrast, the work of Pope et al(160) and Yost and co-workers(144) showed no significant wear reduction when a bearing AISI 440C martensitic stainless steel was implanted with nitrogen. It has been suggested(6) that implantation of nitrogen or carbon would not contribute to any further strengthening of the martensite phase by interstitial solid solution effects. This seems to be the case in high carbon steels, but the above steels contain a high chromium content (12-18% Cr) and precipitation strengthening mechanisms are likely to be operative. This is in agreement with the reported chromium nitride precipitation in martensitic stainless steels(103). The apparent discrepancy in results can be explained by the fact that Pope's wear research was carried out at contact pressures in excess of the bulk yield strength of the material. Additionally, implantation was conducted at a fixed dosage. The work of Iwaki et al(110) has shown that implantation on a similar steel is dose dependent and reduced improvement is achieved above an optimum nitrogen dose, as indicated in Figure 26.

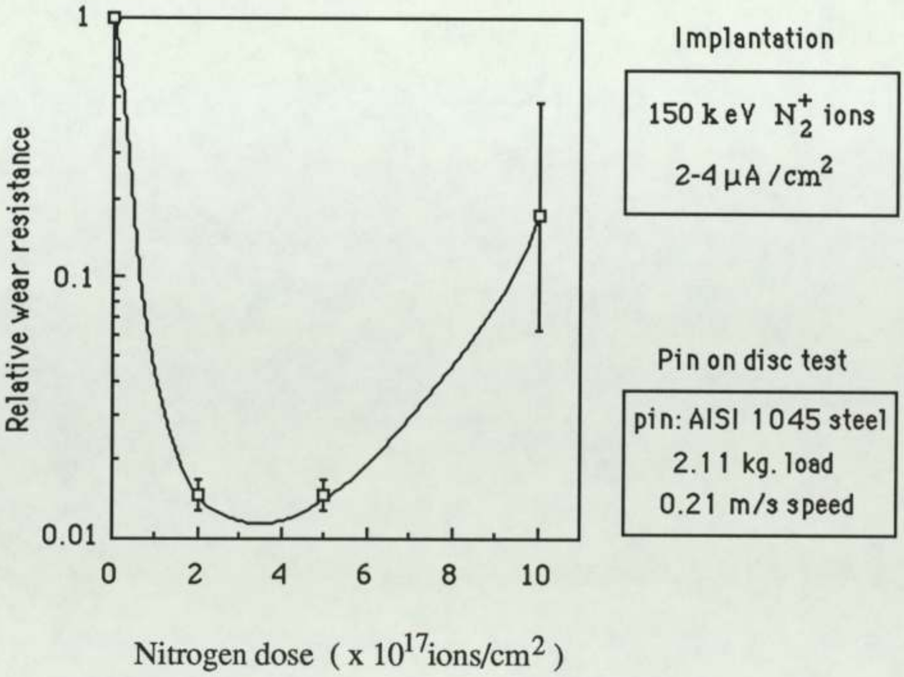

Fig.26: Relative change in wear resistance of AISI 420 steel. Iwaki et al.(110)

It has been reported(157,192) that nitrogen implantation has little effect on wear mechanisms or wear resistance of tool steels. This is based mainly on material studies of the bearing steel AISI 52100. It is generally agreed(101,103,150,157,172) that implantation of nitrogen does not cause any significant tribological improvement in this steel when fully hardened. The available hardening mechanisms (ie. solid solution hardening and dispersion strengthening) are already effective in this martensitic structure, and further improvement is unlikely to occur after nitrogen implantation(101). However, tool steels contain a wide range of alloying elements with a strong affinity for nitrogen and implantation could be expected to provide additional benefits to the martensitic structures.

Limited work has been conducted to date on implantation of these steels despite all the potential applications in tooling and engineering components. This has probably been caused by the less promising results on other martensitic steels (eg. AISI 52100) and the beneficial effects of other implant species, such as titanium(157). The most systematic study was that of Iwaki et al(110) who reported significant improvements in wear resistance for AISI D2, A2 and H13 tools steels. The optimum dose was 5 x 10^{17} ions/cm^2 for 150 keV N_2^+ ions, saturation occurred and no further decrease in wear was observed beyond this dose. Other investigations include those of Yu Kun(171), Daniels(185), Goode and Baumvol(187) and Wolf et al(193,194), who reported increased load bearing capacity and significant wear reductions for tool steels, including AISI M2, T8 and O1. Results of industrial trials with these steels have also been reviewed by Dearnaley(32) and Hirvonen(50), showing a life increase of the tool by 5 to 12 times for M2 high speed steel and up to 3 times for D2 steel, as Table 8 indicates.

Contrary to the above findings, Hirvonen(7) did not observe any benefit by implanting nitrogen in M42 steel at a dose of 10^{17} ions/cm^2 and 40 keV energy. Increasing doses and energies should be studied in this substrate before ruling out the implantation treatment.

Limited data is available on the effect of nitrogen implantation on wear resistant coatings. Ion implantation has been generally considered as an alternative surface treatment and this has limited its application as a duplex process.

The most studied coating has been electrodeposited chromium, due to its widespread use in engineering applications and the need to improve further its durability in cases involving severe abrasion, such as in the case of moulding of thermosetting plastics containing abrasive fillers(197,198). The work of Oliver et al(101) showed a remarkable 23 improvement factor in the wear rate of hard chromium, when implanted to a dose of 3.5 x 10^{17} nitrogen ions/cm^2 (90 keV) as Figure 27 shows. Watkins and Dearnaley(199) also found an improvement in the abrasive wear behaviour of this coating after nitrogen implantation and significant wear improvements have been reported recently elsewhere(168) when using a more severe testing procedure. As discussed earlier, the formation of chromium nitrides(46,122) can be expected to increase the load bearing capacity of the surface and the wear resistance. Hutchings(122) also suggests that inherent microcracks in the untreated hard chromium coating provide preferential sites for the nucleation of wear debris. Closure of these microcracks, owing to the volume expansion produced by the chromium nitrides, would thereby lead to the observed improvement in wear resistance. This is contradicted by the recent findings of Terashima et al(168) and the present author(200), who did not observe any evidence for preferential wear at microcracks and/or their closure as a result of the stresses induced by the implantation.

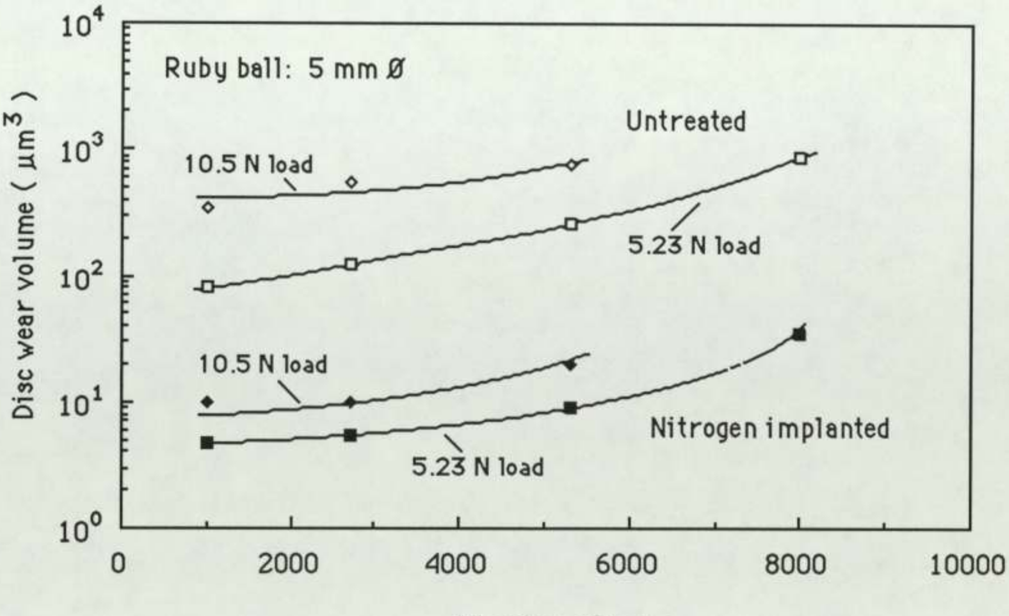

Fig.27: Ball on disc wear results of electroplated chromium. Oliver et al.(101)
Implantation: 90 keV, 3.5x10^{17}ions/cm^2

3.6 Wear Mechanisms on Implanted Surfaces

An extraordinary phenomenon which has been reported in implanted steel substrates is that of the persistence of the wear reduction to depths of metal removal exceeding the range of the nitrogen ions(35,98,174). Dearnaley(35) and Hartley(8) originally explained this effect in terms of the locking of dislocations by interstitial atoms forming "Cottrell" atmospheres. This model involves segregation of nitrogen atoms at dislocations created by plastic deformation of the asperities during wear and originates from the solid solution hardening mechanisms proposed by Cottrell et al(204). The implanted interstitials undergo diffusion along dislocations ahead of the wear interface at the temperatures generated locally by frictional heating; thus, hardening the lattice and improving its wear resistance.

The above model was supported by internal friction studies carried out by Herman et al(48) on nitrogen implanted AISI 1018 carbon steel. As a result of the implantation, the room temperature internal friction decreased by almost 70%, indicating that the implanted nitrogen restricted the movement of dislocations. Adding to the credence of a mobile interstitial model, Longworth and Hartley(127) used the Mössbauer technique to show that although γ'-Fe_4 N and ε-Fe_2N nitrides are formed after nitrogen implantation (depending on the dosage), these are thermally unstable. At temperatures as low as 220°C, nitrogen dissolved to form an interstitial solid solution similar to nitrogen martensite.

During sliding wear, temperatures well in excess of 220°C will occur at the contacting asperities. This temperature rise would therefore cause nitride destabilization and its decomposition to unbound nitrogen, free once again to entangle dislocations. Similar studies to those of Longworth and Hartley have been reported elsewhere in the literature(128,136,143). In these experiments Conversion Electron Mössbauer Spectroscopy has been combined with annealing treatments to investigate the evolution and/or decomposition of nitrides as a function of nitrogen dose and temperature for a range of steels.

The formation of new phases by ion implantation is probably one of the main reasons for the wear resistance improvements. Nitride formation in implanted materials has been discussed earlier and a review of the different studies has been presented in Table 5. Size and density of precipitates is very important for optimum improvement in wear properties. Room temperature implantation appears to produce micro-precipitates at much higher densities than would be obtained with conventional diffusional processes such as gas nitriding(48). It has been shown(205) that at the optimum implantation dose for a Fe-Cr alloy the size of the precipitates was of the order of 3-5 nm. Typical nitride sizes in conventionally nitrided surfaces can be 1 to 100 μm(206). This can explain the beneficial contribution of nitrogen implantation in steels which had already been nitrided(155,163); a dispersion of much smaller precipitates would be more effective in pinning dislocations during wear processes.

Several research groups have attempted to investigate the beneficial effects of the nitrogen beyond the initial depth range of the ions. Techniques such as Nuclear Reaction Analysis (NRA)(137,190,207) and Secondary Ion Mass Spectroscopy (SIMS)(198) have been used on deeply worn surfaces to detect any nitrogen remaining after wear. Results have been contradictory, although some(98,137,190) support the model described by the Harwell group(35,170) to explain the long lasting improvement, others have not detected any deep nitrogen migration during wear(95,184,208). It has to be taken into account that some of the techniques, such as NRA, have a relatively broad analysis beam and unworn areas close to the wear track might have provided the detected nitrogen. Additionally, it has been argued by Singer(192) that wear debris entrapped on the surface or plastic deformation in the wear scar could have apparently pushed the nitrogen to such depths. The latter seems to be the case in the work of Cui Fu-Zhai et al(98), in which annealed steels were tested. Furthermore, little attention was initially given to implantation conditions. High beam current densities with inadequate heat sinks for the workpieces could also have contributed to misleading results due to an enhanced diffusion of nitrogen, deeper than the predicted theoretical range.

More recent analyses of implanted systems(208,209) have failed to observe any nitrogen in-diffusion but, despite this, a lasting wear improvement was evident. Sommerer et al(209) have reported the persistence of enhanced wear behaviour to depths 10 times the implanted range, although no nitrogen could be detected below about twice the range. This effect is explained by the fact that nitrogen initiates the formation of a wear resistant layer which is able to propagate at or ahead of the wear front. TEM studies of fatigued specimens suggest that the dislocation substructure formed in some implanted materials differs from that in the unimplanted ones(210). Nitrogen implantation can, therefore, be regarded as the initiator but not the sustainer of good wear conditions(209). Dearnaley(91) explained this behaviour in terms of a modification of the strain-hardening processes in the surface and that, once 'run-in' has been completed, this effect may become self-propagating.

Other authors have also interpreted the benefits of the implantation as being due to a change in the wear mechanism(110). In addition to the reported change from adhesive to abrasive wear when a severe wear tester (Falex) was employed(176), Goode et al(182) and Pollock and co-workers(208) interpreted their results by the oxidative wear theory, suggesting that nitrogen stabilizes the oxide film. This strongly adherent film is maintained more tenaciously by the underlying hard implanted surface and thus plays a role in protecting the surface against further wear.

On the contrary, Hutchings et al(102) and Shepard and Suh(155) found no change in wear mechanism when iron was implanted with nitrogen. Both, unimplanted and treated surfaces showed a ductile-ploughing process; although implantation increased the strength of the surface and the abrasion resistance.

No universal model of wear seems to be operative in materials implanted with nitrogen. A schematic representation of the possible evolution of implanted surfaces can be seen in Figure 28 after Sommerer et al(209). Differences in wear behaviour will be observed depending on substrate material, implantation treatment and wear testing procedure; therefore, a good understanding of the complex tribological interactions for a particular system or application is required to apply the implantation process to a maximum advantage.

In conclusion, the benefits of ion implantation can be described to be due to a combination of the following mechanisms(192):

(i) production of a low friction surface by alteration of the surface chemistry
(ii) hardening of the surface, mainly by solid solution and precipitation strengthening
(iii) stabilization of the microstructure against deleterious work hardening effects
(iv) creation of large residual stresses, which combat fracture, and
(v) change in the wear mechanism, eg. from adhesive to oxidative wear.

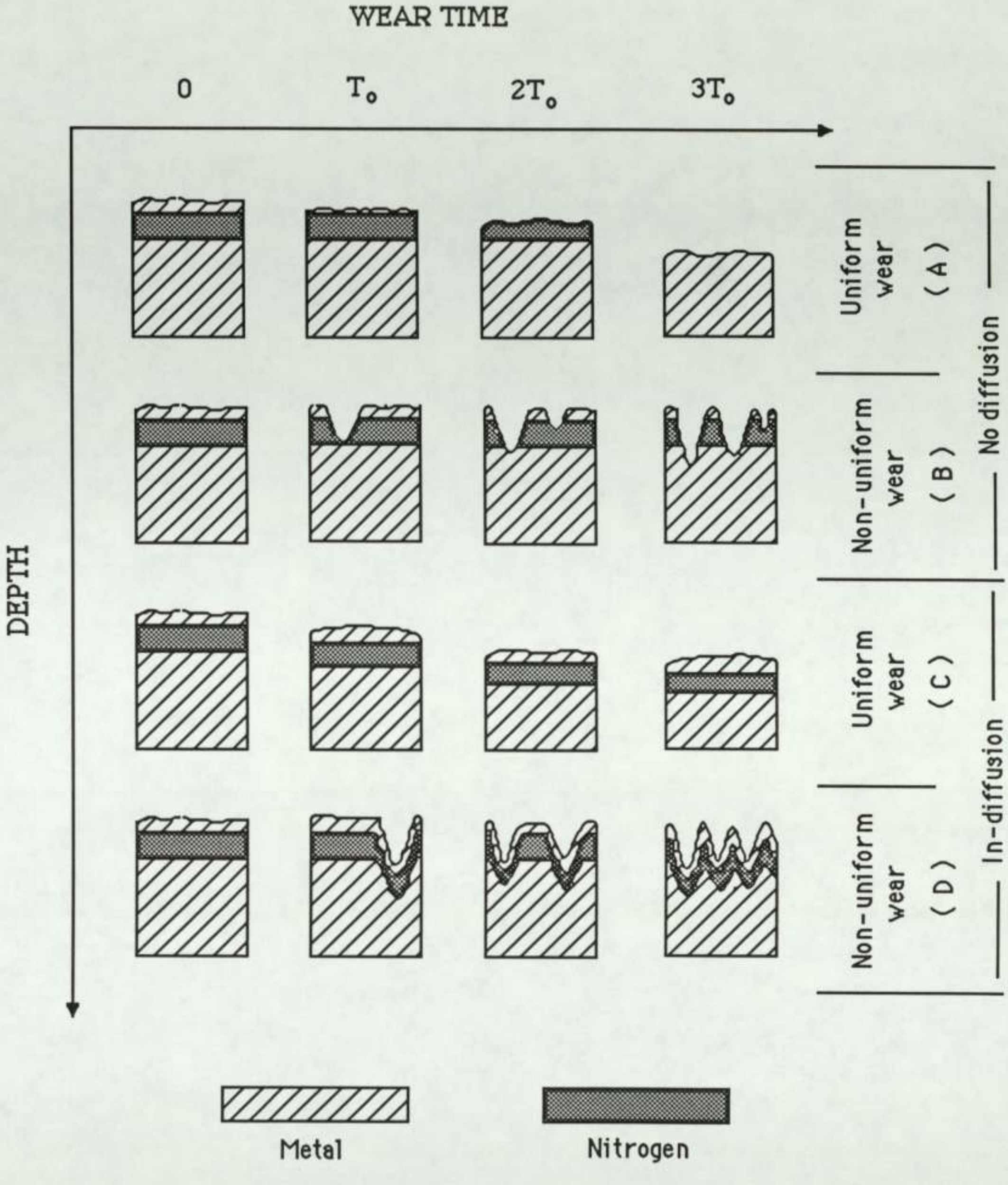

Fig.28: Schematic representation of the evolution of model surfaces during wear.(209)

Table 4 - Effects of nitrogen implantation on surface hardness of steels and coatings

Reference	Material	Implantation Parameters	Load	Hardness (kg/mm^2)			Remarks
				$H_{untr.}$	$H_{impl.}$		
	*Unhardened:	100 keV $N+$, $N^++N_2^+$	15g	137 (carbon s.)	N^+	$N^+ + N_2^+$	*No signific. diff. between
Fu-Zhai	- 0.2 C steel	$5x10^{17}$ ions/cm^2	(Hv)	179 (bearing s.)	176	192	N^+ and $N^++N_2^+$ implant.
et al (98)	- AISI 52100	dose rate:16; 35 $\mu A/cm^2$		164 (stainless s.)	243	240	*Up to 44% improvement
	*AISI 316				--	238	in 'soft' steels.
		150 keV N^+					*Mild steel:
Iwaki	* Mild steel	5 x 10^{16} ions/cm^2	1.5, 21g				x 2 increase (1.5g)
et al (97)			(Hv)				x1.4 increase (21g)
	* Tool steel	10^{17} ions/cm^2					*Tool steel: x2.5 increase.
	*UNI C85	105 keV $N^+ + N_2^+$					*Very high dose rate.
Ramous	high C steel	$3x10^{17}$ ions/cm^2	200 g	185 (annealed)	220		*Softening in quenched
et al (96)	(quenched, annealed)		(Hv)	960 (quenched)	410-600		sample due to tempering
		dose rate: 50,100,200 $\mu A/cm^2$					effect (~320-450°C)
		50 keV N^+	40g	875	1100		*x1.26 max. improvement.
Hohmuth	C100W1 steel	1-9 x 10^{17} ions/cm^2	(Hv)				(dose: 6 x 10^{17} ions/cm^2)
et al (108)							*Decrease at higher doses.
Gabovich	Steel	15 keV N^+	100g				*High improvement. Dose
et al (92)		(Temp.: 500-600°C)					rate dominant parameter.

Reference	Material	Implantation Parameters	Load	Hardness (kg/mm^2)		Remarks
				H_{untr}	H_{impl}	
Iwaki et al (110)	*D2, A2, H13 tool steels *A538 maraging *P21 steel *AISI 420 *17-4PH steel	150 keV N_2^+ 2-10 x 10^{17} ions/cm^2 dose rate: 2-4 μA/cm^2	5, 200g (Knoop)			*No improv at 200g load *AISI D2,420: max 20-30% incr at 5 x 10^{17} ions/cm^2 *H13: 50% increase. *P21, 17-4PH: 25% increase at the highest dose
Kothari et al (111)	AISI 304	30 keV N_2^+ 10^{17}, 10^{18} ions/cm^2 dose rate: 15-20 μA/cm^2	25g	355	395 (10^{17} ions/cm^2) 730 (10^{18} ions/cm^2)	*More than 100% improv. at the highest dose
Dimigen et al (103)	*AISI 52100 *AISI 4140H *AISI 416(soft) *AISI 321 *AISI 440B	100 keV N^+ 5 x 10^{17} N^+/cm^2 dose rate: 1.5-5 μA/cm^2	0.02N (Knoop)			*52100: 8% increase *4140H: 41% " *321: 56% " *440B: 65% " *416: 200% "
Oliver et al (101, 102)	*AISI 410 *AISI 304 *AISI 52100 *Cr coating *Armco Fe	90 keV N_2^+ 3.5 x 10^{17} ions/cm^2 dose rate: 5 μA/cm^2	<5mN (50nm depth)			*410 : x1.2 improvement *304 : x1.25 " *52100 : No improvement *Hard Cr: x1.3 improvement *Armco Fe:x1.8 "
Jones & Ferrante (106)	M50 steel	1.5 MeV N^+ 5 x 10^{17} ions/cm^2	? (Hv)	821	996	* Indent. penetration: 2-3 μm * 21% improvement

Reference	Material	Implantation Parameters	Load	Hardness (kg/mm^2)		Remarks
				H$_{untr}$	H$_{impl}$	
Kanaya et al (93)	SCM steel (Cr-Mo steel)	24 keV N^+ 10^{17} ions/cm^2 (1.5 mA, 15 min.)	1kg (Hv)	300	400	* x1.33 improvement *Dose rate might have caused transformation in structure.
Newey et al (104)	Fe	300 keV N_2^+ 1-6 x 10^{17} ions/cm^2 Room temp. implant.	< 10mN			*Best increase in hardness at lowest dose
Dienel (115)	*90 MnV8 steel *C100W1 steel	50 keV $N^+ + N_2^+$ 10^{17}-10^{18} ions/cm^2	40g	60 Rc 60 Rc		Max. 25% impr. for C100W1 steel at 6x10^{17} N^+/cm^2
Li et al (94)	*Fe, steels, *Non-ferrous alloys	100 kev N^+ 6 x 10^{16} 10^{18} ions cm^2	20g (Hv)			*80% hardness increase at the highest dose
Suri et al (112)	AISI 304	50 kev N^+ 10^{17} ions/cm^2	15g (Knoop)	296	632	114% improvement
Bolster & Singer (95)	*AISI 304 *Carbon steel	80 keV $N^+ + N_2^+$ 10^{17} ions/cm^2				*Improvement with an abrasive polishing technique
Tosto (107)	38NCD4 steel	30 keV $N^+ + N_2^+$ 2 x 10^{17} ions/cm^2 100 μA	15 g. (Hv)	360	600	67% improvement.

Reference	Material	Implantation Parameters	Load	Hardness (kg/mm^2) H_{untr}	H_{impl}	Remarks
Singh et al (113)	AISI 4145 steel	94 keV N^+ 2.8-6.5x10^{17} ions/cm^2 dose rate: 5 μA/cm^2	10, 20 and 40 g (Hv)	22Rc		*No significant improvement
Prabhawalkar et al (116)	AISI 304	30 keV N_2^+ 10^{17}, 10^{18} ions/cm^2 dose rate:15-20 μA/cm^2	25 g (Hv)	350	395 730	x 1.13 improv.(10^{17} ions/cm^2) x 2.09 improv.(10^{18} ions/cm^2)
Oliver et al (109)	AISI 304 (electropolished, mech. polished)	(A) 40 keV 10^{17} N^+/cm^2 (B) 90 keV 2.5 x 10^{17} N^+/cm^2	<5 mN			(A) Electropol. 50% improv. @40nm Mech pol: 10-20% impr. (B) Mech pol: 50-60% impr.
Dearnaley et al (114)	*NSOH tool steel *En 8 mild steel	50 keV nitrogen 7 x 10^{17} ions/cm^2	10 g. (Knoop)	Tool steel: 610 Mild steel: 210	730 310	*Tool steel: 20% improv. *Mild steel: 50% improv.
Madakson (167)	18W-4Cr-1V (bearing steel)	400 keV N_2^+ 10^{13}-10^{17} ions/cm^2	10 g.			x4 improv. at highest dose
Terashima et al (168)	*Electrodep.Cr *Pure Cr	90 keV (40% N^++60% N_2^+) 3 x 10^{17} ions/cm^2 3mA	*2-20 g. (Vickers) *Ultra-microhardness (0.03 g/min. loading rate)			*20% improv at lowest Vickers load (2g) *Penetrat. depth reduced by 3 at 0.1g load.

Table 5 - Phases formed by nitrogen implantation

Reference	Material	Implantation parameters	Technique	Phases observed
Ramous et al (96)	UNI C85 (High carbon steel, quenched, annealed)	105 keV N^+ 3×10^{17} ions/cm^2 dose rate: 50, 200 µA/cm^2	CEMS	*γ-Fe_4N, ε-Fe-N phase (not for 200 µA/cm^2). Note: larger contribution of compounds at 50 µA/cm^2 than at 200 µA/cm^2. *Heating effects due to high dose rate.
Dimigen et al (103)	AISI 4149 steel AISI 321 steel AISI 440B steel	100 keV N^+ 5×10^{17} ions/cm^2 dose rate: 1.5-5 µA/cm^2	XPS	*Cr-N or Fe-Cr-N finely dispersed precipitates. *Chromium almost entirely bound to nitrogen.
Hutchings(122)	Hard Cr coating	90 keV N^+ 3.5×10^{17} ions/cm^2 power dens.: 5 kW/m^2	TEM	*Cr_2N (fine grained, continuous layer) *$Cr_2 0_3$
Rauschenbach et al (129-132)	Iron films	30-60 keV N^+ 10^{16}-10^{18} ions/cm^2 dose rate: < 8 µA/cm^2	TEM	*$1\text{-}4 \times 10^{16}$ N^+/cm^2: γ-Fe-N (γ-austenite) *4×10^{16}-10^{18} N^+/cm^2: γ-austenite, α'-martensite, α''-$Fe_{16}N_2$, ε-Fe_2N_{1-x}. *4×10^{16}-10^{17} N^+/cm^2: ε-nitride (~ Fe_3N). *10^{18} N^+/cm^2: ε-nitride (Fe_2N).
Bykov et al (126)	Fe films	50 keV N^+ 0.1-5 $\times 10^{17}$ ions/cm^2 Impl. temp.< 50° C	CEMS TEM	*hcp precipitates.

Reference	Material	Implantation parameters	Technique	Phases observed
Barnavon et al(138)	AISI 1006	40 keV N^+ 10^{17} ions/cm^2 dose rate: 10 μA/cm^2	CEMS	* α' martensite, ε-nitrides, α"-$Fe_{16}N_2$
Carbucicchio et al (139)	38NCD4 steel (bainitic structure)	30 keV nitrogen ions 5 x 10^{16}, 10^{17} ions/cm^2 Impl.current: 53-210 μA	CEMS	*Austenite (10 at % N) *$Fe_{2+x}N$ $(0 \leq x < 0.3)$ *$Fe_{2+y}N$ $(0.3 \leq y \leq 2.7)$
Carbucicchio & Tosto (140)	38NCD4 steel (quenched, annealed)	30 keV N^+ 10^{16}-10^{18} ions/cm^2 dose rate: 210 μA/cm^2	SEM	*Austenite regions (high temperature implant.) *Fe_2N microprecip. of Fe-rich compounds. *Porosity
Singer & Murday (141)	AISI 304	80 keV N_2^+ 10^{16}-10^{18} ions/cm^2 dose rate: 1-15 μA/cm^2	XPS	*Nitrogen in nitrided state at all doses. *Above 2 x 10^{17} N^+/cm^2: Cr nitrides. *At 10^{18} N^+/cm^2: Cr + Fe nitrides.
Baron et al (142)	AISI 304 AISI 316	400 keV N^+ 1.2 x 10^{17}ions/cm^2	TEM	*CrN *TEM+AES: 2-8% solubility limit of nitrogen in AISI 304 and 316 stainless steels.
Yost et al (144)	AISI 304 AISI 15-5PH	50 keV N^+ 4 x 10^{17} ions/cm^2	TEM	*CrN. However, electron diffraction patterns 'indexed well' to $(Cr,Fe)_2N_{1-x}$ $(x = 0 - 0.5)$
Whitton et al (146)	Single crystal 70 Fe-17Cr-13 Ni austenitic st. steel	25-165 keV N^+ 2.5x10^{15}-1.5x10^{17} ions/cm^2 Room temperature implant.	GXRD	*Ion bombardment transformation of austenite to martensite. *Cr_2N (more likely to form than CrN). Fe_2N

Reference	Material	Implantation parameters	Technique	Phases observed
Cavalleri et al (152)	AISI 304	100 keV nitrogen 3 x 10^{17} ions/cm^2	GXRD	*Implantation inhibits austenite to martensite transformation (γ-stabilization).
Bone et al(145)	AISI 304	40 keV N^+ 10^{16}-10^{18} ions/cm^2	SIMS	*CrN, increases with dose. *Cr_2N, saturated at 2x10^{17} ions/cm^2.
Longworth & Hartley (127)	α-iron foils	100 keV N_2^+ 1-6 x 10^{17} ions/cm^2	CEMS	*Fe nitrides formed for doses > 10^{17} ions/cm^2 *First, formation of γ'-Fe_4N, followed by a phase close to Fe_2N composition.
Dos Santos et al (143)	AISI 1020 (low C) RCC tool steel AISI 304	100 keV N^+ 2-6 x 10^{17} ions/cm^2 Implantation temp.: < 70°C	CEMS	<u>AISI 1020</u>: Fe_3 (C,N) or Fe_3N. <u>Tool steel</u>: Fe-C-N martensite. <u>AISI 304</u>: ε or ζ -Fe_2N. *Fe_2N preferentially formed above 4x10^{17} Dose (ions/cm^2) 2x10^{17} 4x10^{17} 6x10^{17} 1020 42% 24% 24% Tool s. 5% 17% 20% (all %Fe2N) 304 24% 39% 54%.
Belii et al(46)	Cr, Mo and Ni films	60 keV N_2^+ 5x10^{15} - 5x10^{17} ions/cm^2 dose rate: 20 μA/cm^2	TEM	<u>Cr</u>: *10^{16} ions/cm^2: Cr_2N+ CrN *Increasing dose: CrN incr., Cr_2N decr. *4x10^{17} ions/cm^2: CrN only *No effect by annealing at 700° C <u>Mo</u>: *Mo_2N. Dissolution at 900° C <u>Ni</u>: *Ni_3N increases with increasing dose. *Ni_3N disappears by annealing at 500° C

Reference	Material	Implantation parameters	Technique	Phases observed
Drako & Gumanskij(128)	Fe film	60 keV N_2^+ 1-3x10^{17} ions/cm^2 Implant. temp: < 200° C	TEM	*Hexagonal ε-Fe N nitrides at 280Å depth. *Decomposition of nitrides at 600° C.
Jata & Starke (135)	AISI 4140	100 keV N^+ 2x10^{17} ions/cm^2	TEM	γ-Fe_4N nitrides.
Feller et al(150)	AISI 321	4x10^{17} N^+ ions/cm^2	SIMS	Most of the nitrogen in elemental state.
Marest et al(136)	AISI 52100 AISI 4142	40 keV N^+ 2x10^{17} ions/cm^2 dose rate: 10 μA/cm^2	CEMS	AISI 52100: ε-$Fe_{2+x}N$, Fe_4N *3h treatm. at 250° C: Fe_2N disappears, Fe_4N decreases slowly and dilute $Fe_{16}N_2$ appears. AISI 4142: ε-Fe_{2+x} N (Fe_2N, Fe_3N), γ'-Fe_4N
Terashima et al(168)	Electrodeposited Cr	90 keV (N^++ N_2^+) 3x10^{17} ions/cm^2 3mA beam current	AES + XPS	* Cr_2N and Cr_2O_3
Herman et al(48)	AISI 1018	150 keV N_2^+ 2x10^{17} ions/cm^2	TEM	*Fe_{16} N_2 precipitates at much higher density than those from conventional nitriding.
Prabhawalkar et al(116)	AISI 304	30 keV N_2^+ 10^{17} ions/cm^2 dose rate: 15-20 μA/cm^2	XPS	*Maximum N concentration at 30nm *Up to 20nm: Cr nitride, Fe_{2+x}, N and nitrogen bubbles *20-40 nm: mainly Fe_{2+x},N nitrides. *> 40nm: diffused N species and Fe_{2+x},N.

Reference	Material	Implantation parameters	Technique	Phases observed
Principi et al(134)	UNI C80 (quenched) Martens. high C steel	100 keV N^+ 2-8x10^{17} ions/cm^2	CEMS	*No changes below 2x10^{17} ions/cm^2. *ε-like carbonitrides at 4x10^{17} ions/cm^2. *Increase of precipitates with increasing dose.
Marest et al(137)	42CD4 steel	40 keV $^{15}N^+$ 10^{16}-6x10^{17} ions/cm^2 Dose rate: 10-20 $\mu A/cm^2$	CEMS	*At 2x10^{17} part of N bound as carbonitrides. * ε-Fe_2N,γ'-Fe_4N,ε-Fe_{2+x}(C,N) and dilute N * γ'-Fe_4N disappears after 50 nm wear, ε-Fe_2N and carbonitrides persist.
Fayeulle al (148)	AISI 304	40 keV N^+ 10^{16}-6x10^{17} ions/cm^2 Dose rate: 20 $\mu A/cm^2$	GXRD	*10^{17}: Broadening of γ austenite peaks. α'-martensite formation. *2x10^{17}: α'-martensite. γaustenite in very et small quantity. Nitrides: ζ-Fe_2N, Cr_2 (C,N) and (Cr, Fe)$_2N_{1-x}$, hexag. or orthorhombic. *6x10^{17}: α'-martensite, ε-Fe_2N nitrides.
Fayeulle et al(149)	AISI 304	40 keV N^+ 10^{17}-6x10^{17} ions/cm^2 Room temperature implantation	TEM	*10^{17}: γ-austenite, α'-martensite, orthorhombic nitride ζ-Fe_2N hexagonal nitride (Cr, Fe)$_2$ N_{1-x} and hexagonal ε-martensite *2x10^{17}: orthor. or hex. nitrides and α'-mart. *6x10^{17}: γ'-aust., α'-mart. and orthor. nitrides.

Reference	Material	Implantation parameters	Technique	Phases observed
Fayeulle et al(153)	Fe-Cr alloy (bcc)	40 keV N^+ 10^{16} - 6 x 10^{17} ions/cm^2. Room temperature implantation	TEM	*10^{16}: No nitrides. *10^{17}: (15% N) -Matrix: bct nitrogen martensite. fcc γ-Fe nitrogen solid solution. -Nitrides:ε-Fe_{2+x} N, $(Cr, Fe)_{2+x}N$, Cr_2 (C,N) *6x10^{17}: (35% N) Fe_3O_4, $(Cr, Fe)_{2+x}N$, Cr_2 (C,N) Not fcc or bct.
Principi et al(147)	X30 Cr 13 steel UNI 100Cr6 " UNI X10Cr17 "	100 keV $N_2^+ + N^+$ 1-7x10^{17} ions/cm^2 Dose rate: 20-140 µA/cm^2	NRA CEMS	*ρ = spectral area Fe-N / spectral area matrix. *ρ increases with nitrogen dose. *Threshold concentration of retained nitrogen increases with Cr content. *Cr-N bond more favoured than Fe-N.
Arnaud et al (151)	AISI 304L AISI 321	100 keV (100% N_2^+) 80 keV (40% N^+, 60% N_2^+) 4x10^{17} ions/cm^2		*CrN, ß-Cr_2N, ζ-Fe_2N, Ni_3N and ε-Fe_2N-Fe_3N *CrN localised in ≤ 100 Å layer *Cr_2N, $(Cr, Fe)_2 N_{1-x}$ appear in the underlayer

NB:
CEMS = Conversion Electron Mössbaiier Spectroscopy.
SIMS = Secondary Ion Mass Spectroscopy.
SEM = Scanning Electron Microscope.
XPS = X-Ray Photoelectron Spectroscopy.
TEM = Transmission Electron Microscopy.
GXRD = Glancing X-Ray Diffraction.
NRA = Nuclear Reaction Analysis.
AES = Auger Electron Spectroscopy.

Table 6 - Effects of nitrogen implantation on friction

Reference	Material	Implant. Param.	Tribotester	Load	Lubricant	Friction coeff.		Remarks
						$\mu_{unt.}$	$\mu_{imp.}$	
Hartley (8)	Mild steel	30 keV N^+ $3.2x10^{17}$ ions/cm^2	pin on disc	1.5 kg.	SAE 30 oil	0.15-0.35	0.075	Pin: 1.2 C steel (1mm Ø). 60 rpm
Fu-Zhai et al (98)	AISI 316	100 keV $N^+ + N_2^+$ 5 x 10^{17} ions/cm^2 dose rate: 35 μA/cm^2	pin on disc	4.7-10.7N	Kerosene	0.1-0.16	0.08-0.11	Up to 45% decrease. Pin: GCr6 steel (0.2mm point)
Iwaki et al (97)	Fe Mild steel Carbon steel	100, 150 keV 10^{15}-10^{17} N^+/cm^2	Bowden- Leben	50-250 g.				20-40% reduction Pin: carbon steel (2.7mm/s speed)
Dimigen et al (103)	AISI 52100 AISI 4140 AISI 416, 440B AISI 304, 321	100 keV N^+ 4-5 x 10^{17} ions/cm^2 dose rate: 1.5-5 μA/cm^2	Ball on disc	2.2N	--	No change in μ (within± 15%)		Ball: Co-WC or AISI 52100
Oliver et al (101,102)	Armco Fe AISI 5210 AISI 304 AISI 422 Hard Cr	90 keV $N^+ + N_2^+$ 3.5 x 10^{17} ions/cm^2 dose rate: 5 μA/cm^2	Ball on disc	0.98-10.5N	Ethanol	Fe: 0.20 52100: 0.19 304: 0.17-0.12 422: 0.18 Cr: 0.17	0.26 0.19 0.15 0.17 0.17	*No significant improvement Ball: ruby, 5mmØ

Reference	Material	Implant. Param.	Tribotester	Load	Lubricant	Friction coeff.		Remarks
						$\mu_{unt.}$	$\mu_{imp.}$	
Feller et al (150)	AISI 4140, 416 AISI 52100 AISI 304, 321	4 x 10^{17} N^+/cm^2	pin on disc	2.5 N (0.2N/mm^2)		Sometimes lower μ (at least during run-in wear)		
Hirano & Miyake (161)	SUS 440C (mart. stainless)	90 keV $N_2^+ + N^+$ 4 x 10^{17} ions/cm^2	Oscillatory machine (3 x 10^6 oscill. cycles)	29.4 N		Air: Inside torque red x 0.5 Outside torque red x 0.8 Vacuum: inside and outside torque reduced by 0.57		*Signif reduction in starting torque
Carosella et al (157)	AISI 52100	46 keV N^+ 190 keV Ti^+ 2.3x10^{17}ions/cm^2 dose rate: 50 μA/cm^2	Stick slip Pin on disc Ball-on-cylind.	9.8 N (0.57 GPa)	Hexadec.	Dry: 0.65 Lubr.: 0.16	N^+: 0.66 Ti^+: 0.32 N^+: 0.16 Ti^+: 0.18	N^+ impl. No significant change Ti^+ impl. Improv. in dry wear.
Bunshah et al (112)	AISI 304	50 keV N^+ 10^{17} ions/cm^2	pin on disc (440C steel pin)	0.4 kg	Kerosene	μ_S = 0.65 μ_D = 0.42 μ_L = 0.15	0.60 0.17 0.15	μ_S = static (dry) μ_D = dynamic μ_L = lubricated Up to 40% improv.
Shepard & Suh (155)	Fe	10^{17} N^+/cm^2 4.3-6.2 μA/cm^2	pin on disc	0.4 kg	Mineral oil	~ 0.12	0.065	85% reduction Pin material: Fe

Reference	Material	Implant. Param.	Tribotester	Load	Lubricant	Friction coeff.		Remarks
						$\mu_{unt.}$	$\mu_{imp.}$	
Kirk et al (162)	AISI 1018 AISI 304	120 keV N_2^+ 2-6.6x10^{17} ions/cm^2	pin on disc	(10-700 MPa)	SAE 30	<u>1018 steel</u>: 0.086 <u>304 steel</u>: 0.101	0.075 0.086	Pin: 440C steel
Ecer et al (163)	17-4PH Nitrided steel	100 keV N^+ 10^{17} ions/cm^2 dose rate: 5.5 μA/cm^2	cylinder on disc	163-273 Newtons	Chevron BRB-2-SR1 (stand. petroleum lubricant)			Improv. at low loads. Best results for nitrided and N^+ implanted.
Jones & Ferrante (106)	Fe	1.5 MeV N^+ 5, 500x10^{15} ions/cm^2 dose rate: 20 μA/cm^2	pin on disc	0.5 kg.	n-hexadecane and USP mineral oil	0.15	0.15	Disc: M50 steel (unimplanted)
Yost et al (144)	AISI 304 15-5 PH AISI 440C	50 keV 4x10^{17} ions/cm^2 dose rate: 7 μA/cm^2	pin on disc	12.3-100.3 gf	--			*440C: no reduction. *304: 15% reduction at low loads.
Hartley & Hirvonen(159)	*AISI 3135 *9130 steel (Carburized)	N^+ ions 4 x 10^{17} ions/cm^2	Falex	200 lb 700 lb	Hercolube A oil	(200 lb) 0.053	(200 lb) 0.067	*No reduction V-blocks: AISI 1137 steel.
Madakson(167)	18 W-4Cr-1V (bearing steel)	400 keV N_2^+ 10^{14}-10^{17} ions/cm^2	pin on disc	1 kg (0.57 MN/m^2)	White spirit			20±5% reduction for the highest dose.

Reference	Material	Implant. Param.	Tribotester	Load	Lubricant	Friction coeff. $\mu_{unt.}$	$\mu_{imp.}$	Remarks
Iwaki et al (158)	Low C steel	100 - 150 keV (32% N^+, 48% N_2^+, 20% NO^+) 2.5-100 x 10^{15} ions/cm^2 dose rate: 3 μA/cm^2	pin on cylinder	1 kg	--	0.35	0.53	Pin: 1045 steel
Pope et al (160)	AISI 440C	50 keV N^+ 4x10^{17} ions/cm^2 T < 373° K	pin on disc	0.2 - 1 kg	--			*Slight reduction for loads < 0.4 kg. (2320MPa) *No reduction for loads > 0.6 kg. Pin material: AISI 304 and 440C steels.
Fayeulle & Treheux(164)	AISI 304 (electropolished)	40 keV 0.1-6x10^{17} ions/cm^2 dose rate: 20 μA/cm^2	pin on cylinder	50 N (100 MPa)	Dodecan	No significant change (μ = 0.2)		Cylinder: 42CD4 steel (38 HRc)
Singer & Jeffries(165)	*Unhardened: AISI 1018 AISI M2 *AISI 304	N^+, Ti^+, & N^++Ti^+ <u>N</u>$^+$: 180 keV 4 x 10^{17} ions/cm^2 <u>Ti</u>$^+$: 50 keV 2 x 10^{17} ions/cm^2	Ball on disc (Hardened ball)		Dry or "Shell 2190 TEP"	<u>Dry:</u> AISI 304: AISI 1018: AISI M2: <u>Lubricated</u>:	 μ_{N^+} : μ_{Ti^+}: $\mu_{Ti^++N^+}$: μ_{N^+}: μ_{Ti^+}: μ_{N+}: μ_{Ti+}: No trends	 no difference. reduced x2. reduced x2. no difference. reduced increased reduced

Table 7 - Effects of nitrogen implantation on wear resistance

Reference	Materials	Implantation Param.	Tribotester	Load	Lubricant	Wear Improvement
Hartley (8)	Mild steel	30 keV N^+	pin on disc (60 rpm)	1.5 kg	SAE 30 oil (Kerosene)	x200 wear red. after N^+ implant. Pin: carbon steel, (1mm Ø)
Shepard & Suh (155)	Fe	10^{17} N^+ ions/cm^2 4.3 - 6.2 μA/cm^2	pin on disc (0.5-2m/min)	0.4 kg	Mineral oil	*No measurable wear after N^+ implantation
Fu-Zhai et al (98)	Carbon steel* AISI 52100* AISI 316 (*in soft condition)	100 keV N^+, N^++N_2^+ ions 5x10^{17}ions/cm^2	pin on disc (like on like test)	4.7, 7.7 and 10.7 N	--	AISI 52100: x15 max. wear red. Carbon steel: x10 max. wear red. AISI 316: x160 max. wear red.
Iwaki et al (97,158)	AISI 1045 steel	100, 150 keV (32% N^+, 48% N_2^+, 20% NO^+) 2.5-100 x 10^{15} ions/cm^2 dose rate: 3 μA/cm^2	pin on cylinder (105 mm/s)	1 kg	--	*Decrease in wear after nitrogen implantation Pin: AISI 1045 steel
Iwaki et al (110)	AISI D2, A2 AISI 420 AISI H13 AISI P21 AISI 17-4PH Maraging A538	150 keV N_2^+ 1-10 x 10^{17} ions/cm^2 dose rate: 2-4 μA/cm^2	pin on disc (105-210 mm/s) Pin: AISI 1045 (sphere 5mmØ)	0.71-2.11 kg	--	D2,A2: wear reduced (saturation above 5x10^{17} ions/cm^2) P21,17-4: small improvement at dose 10^{18} ions/cm^2 H13, Marag st: signific. wear red. as dose increas AISI 420: ~ x 40 max. wear red. at 2-5x10^{17} ions/cm^2

Reference	Materials	Implantation Param.	Tribotester	Load	Lubricant	Wear Improvement
Dimigen et al (103)	AISI 52100 AISI 4140H AISI 416 AISI 304 AISI 321 AISI 440B (hard.)	100 keV N^+ 4 - $5x10^{17}$ ions/cm^2 dose rate: 1.5 - 5 μA/cm^2	Oscillating ball on disc (Balls: Co-WC and AISI 52100)	2.2 N	--	AISI 52100: No improvement AISI 4140H: x1.5-3 wear red. AISI 416: x2 -20 wear red. AISI 304: x25-43 wear red. AISI 321: x100-230 wear red. AISI 440B: x3-20 wear red. *No wear red.for stainless steels below dose of $2x10^{17}$ N^+/cm^2
Yost et al(144)	AISI 304 15-5PH AISI 440C	50 keV N^+ $4x10^{17}$ ions/cm^2 dose rate: 7 μA/cm^2	Pin-on-disc (pin: 304,440C)	12.3 to 100.3 gf.		*Reduced wear at low loads *Vacuum heat treatment: no effect
Oliver et al (101,102)	Armco Fe AISI 52100 steel AISI 304 " AISI 410 " Hard Cr Plate	90 keV N^++N_2^+ $3.5x10^{17}$ ions/cm^2 dose rate: 5 μA/cm^2	Ball on disc (5.65cm/s) 5mm Ø ruby ball	0.98-10.5 N	Ethanol	Armco Fe: small wear red. for loads < 1N AISI 52100: No signif. change AISI 304: x 26 wear reduction AISI 410: x 4.5 wear reduction Hard Cr: x 23 wear reduction
Bolster & Singer (95)	AISI 304 steel SAE 1095	80 keV N_2^+ 1-$2x10^{17}$ ions/cm^2 dose rate:3-5μ A/c m^2	Vibratory polisher (abrasive tester)		Paraffin oil	AISI 304: Red. wear resistance possibly due to transformation hardening during wear Carbon steel: wear resist. improv.

Reference	Materials	Implantation Param.	Tribotester	Load	Lubricant	Wear Improvement
Feller et al (150)	AISI 52100 AISI 4140 H AISI 416, 304, 321	4×10^{17} ions/cm^2	pin on disc (0.5m/s)	2.5 N (0.2 N/mm^2)		*Significant lower wear rates for AISI 321, 304 and 416 stainless steels.
Carosella et al (157)	AISI 52100	75 keV N^+ 2×10^{17} ions/cm^2 dose rate: 50 μA/cm^2	Ball on cylinder (66 cm/s)	2 kg	Synthetic polyester	*No wear reduction for N^+ impl. *If Ti^+ or $Ti^+ + C^+$ implantation: x 5 wear reduction.
Bunshah & Suri (112)	AISI 304	50 keV N^+ 10^{17} ions/cm^2	pin on disc Pin: 440C steel	0.4 kg	Kerosene	*Reduced wear rate. *If dry sliding, beneficial effect of N^+ impl. only for short dist.
Ecer et al (163)	17-4PH steel Nitrided 17-4PH	100, 150 keV N^+ 1-8x10^{17} ions/cm^2 dose rate: 5.5-14.1 μA/cm^2	Cylinder on disc	229 N	Standard petroleum lubricant	*Wear reduced by low dose N^+ implantation. *Best results when nitrided+N^+ impl. (2 orders mag. wear red.)
Kirk et al (162)	AISI 1018 AISI 304	120 keV N_2^+ 2;4 x 10^{17} ions/cm^2 (AISI 1018) 3; 6.6.x 10^{17} ions/cm^2 (AISI 304)	pin on disc Pin: 440C steel	9.81 N	SAE 30	AISI 1018: No improvement. AISI 304: max. 50% wear red. Wear area not dependent on dose
Jones & Ferrante(106)	Iron (pin)	1.5 MeV N^+ 5×10^{15}, 5×10^{17} ions/cm^2	pin on disc (43-78mm/s) Disc: unimpl.M50	0.5 kg	n-hexadecane or USP mineral oil	*No difference for low doses *20-40% wear reduction for high dose implantation

Reference	Materials	Implantation Param.	Tribotester	Load	Lubricant	Wear Improvement
Singer et al (172)	AISI 52100 Carbon steel	80 keV N_2^+ 2 x 10 ions/cm^2 dose rate: 4 μA/cm^2	Vibratory polisher	--	Paraffin	AISI 52100: No improvement Carbon steel: increase in abrasive wear resist. after N^+ implantation
Hohmuth et al (191)	C 100W1 steel 90 MnV8 steel	30 - 60 keV N^+ 10^{16}-10^{18} ions/cm^2 dose rate: <10 μA/cm^2	Fixed ball on disc	20 MPa 0.1 MPa	n-dodecane --	*Lubricated: (20 MPa): wear red. between 10^{17} to 6x10^{17} ions/cm^2 Above 6x10^{17} increase in wear. *Dry sliding (0.1 MPa): wear red. with increasing dose. Above 10^{18} ions/cm^2 incr. in wear.
Varjoranta et al (181)	Mild steel	50 keV N^+ 10^{15}-10^{18} ions/cm^2 dose rate: 10 μA/cm^2	Reciprocal motion tester (1cm/s)	3 - 18 N	Kerosene	Wear reduction up to x60 times
Hirvonen et al (7)	AISI 304 AISI 52100 AISI M42 AISI 416	40 keV N^+ 10^{17} ions/cm^2 dose rate:~ 2 μA/cm^2	Crossed cylinder on cylinder (304, 416) Ball on disc (M42, 52100)	2 - 4 kg.	Polyester oil bath with wear particles	St. steels: N^+ implant. improves load bearing capacity. AISI 52100: x2 wear reduction. No improv if dry testing. M42: No improvement.
Yu Kun et al (171)	-AISI 52100, T8 -38 Cr Mo A1A (Nitriding steel) -18 Cr, 2Ni 4WA (Carb.alloy steel) -Low carbon steel -1Cr 19Ni 9Ti (aust.stainless steel)	100 keV $N^++N_2^+$ 0.625-7.5x10^{17} ions/cm^2 dose rate: 20, 40 μA/cm^2	Crossed cylinder on cylinder (1080rpm) Static cylinder: AISI 52100	0.5-8 kg	Kerosene (30^o C)	*Implant. increased load bearing capacity of hardened and tempered steels. *Annealed materials: highest. improvement for nitriding steel, lowest for tool steel

Reference	**Materials**	**Implantation Param.**	**Tribotester**	**Load**	**Lubricant**	**Wear Improvement**
Madakson (167)	18W-4Cr-1V (bearing steel)	400 keV N_2^+ 10^{14} to 10^{17} ions/cm^2	Pin on disc	1, 3 kg (0.57, 1.7MN/m^2)	White spirit	*Wear reduced by 2.4 at the lowest load. *No improvement at 3 kg load.
Lo Russo et al (190)	38 NCD 4 steel	30 keV $N^+ + N_2^+$ 2-80 x 10^{16} ions/cm^2 80 μA	Reciprocal motion (0.1 m/s)	2 kg	--	*Best effect for 2×10^{17} ions/cm^2. *Rider: cemented steel.
Hale et al (176)	SAE 3135 (Ni-Cr steel)	180 keV N_2^+ 2.5×10^{17} ions/cm^2 dose rate: 15 μA/cm^2	Falex lubricant tester (290rpm)	200 lbs (890 N)	Mild oil	*Wear rate reduced from 250 g/s to 20 g/s (x12.5 red.) after impl. *AISI 1137 steel V-blocks
Xie Zhong et al (195)	AISI M2 (annealed) AISI 52100 (annealed)	110 keV N^+ <u>M2</u>: 8×10^{17} ions/cm^2 <u>52100</u>: 2×10^{17} ions/cm^2				<u>M2</u>: <u>Unimp</u> <u>N^+ impl</u> Worn width: 1.5 mm 1.25 mm worn depth: 20 m 9 m <u>AISI 52100</u>: Worn width: 0.54 mm 0.34 mm Worn depth: 8 m 5 m
Hale et al (175)	SAE 3135 (Ni-Cr steel)	180 keV N_2^+ 2.5×10^{17} ions/cm^2	Falex tester (290 rpm)	200 lbs (890 N)	Peanut oil	*Wear rate reduced from 2.6 g/s to 0.18g/s (x14 impr) after impl. *AISI 1137 steel V-blocks
Fayeulle & Treheux (164)	AISI 304 steel	40 keV N^+ 10^{16}-6 x 10^{17} ions/cm^2 (electropolished)	Pin on cylinder dose rate: 20 μA/cm^2	50 N (100 MPa)	Dodecan	*About 3 times wear reduction for the best dose (2×10^{17} ions/cm^2).

Reference	Materials	Implantation Param.	Tribotester	Load	Lubricant	Wear Improvement
Goode & Baumvol(187)	AISI 304 NSOH tool steel (BS4569)	90 keV N^+ 4×10^{17} ions/cm^2 dose rate: 5; 25 µA/cm^2	pin on disc (60 cm/s)	25 N	White spirit	Small sliding dist.: x20 wear red. Longer distances: (a) AISI 304: best improv. at low dose rate (5 µA/cm^2) and high implant. temperature (330°C). (b) Tool steel: best improv at low dose rate (5 µA/cm^2) and low implantation temperature (46°C).
Fayeulle et al (173,174)	Z 200 C13 steel (2% C, 13% Cr) (60 Rc)	40 keV N^+ 1-4 x 10^{17} ions/cm^2	Vibratory polisher			*Max. nitrogen in-diffusion for 2×10^{17} ions/cm^2. No significant improvement for mild wear.
Hirvonen & Mayer (188)	AISI 304 steel (electropolished)	75 keV N_2^+ 4×10^{17} ions/cm^2	Ball on plate (fretting wear)	1.64 N		*Remarkable improvement. (Increase in load bearing capacity and reduction in adhesion)
Dienel (115)	90 MnV8 steel C100 W1 steel (60 Rc)	50 keV nitrogen 10^{17}-10^{18} ions/cm^2	Ball on disc (bearing ball) 1m/s speed	20 N 0.1 N	... n-dodecane ... dry	*C 100W1: signific. improvement up to 6×10^{17} ions/cm^2. *90 MnV8: signific.improvement up to 6×10^{17} ions/cm^2
Terashima et al (168)	Cr electrodeposits (40° C, 20 to 50A/dm^2)	90 keV (40% N^++ 60% N_2^+ ions) 3×10^{17} ions/cm^2 Beam current: 3mA	* Taber abrasion * Ohgoshi rapid wear test	... 1 kg .. 18.9 kg	-- Oil	*Abrasion tests: implant.reduced by 1/2 the wear volume. *Ohgoshi: reduced wear.

Reference	Materials	Implantation Param.	Tribotester	Load	Lubricant	Wear Improvement
Cavalleri et al (152)	AISI 304	100 keV N^+ $3x10^{17}$ ions/cm^2 dose rate: 30 μA/cm^2	Reciprocal motion (150 cycles/min)	5 N (M42 rider)		*More than x 2 wear reduction after 5000 cycles
Hirano et al (161)	SUS 440C (martens.stainless steel ball bearings)	90 keV $N_2^+ + N^+$ $4x10^{17}$ ions/cm^2	Small-angle oscillatory motion (fretting wear)	29.4 N		*Bearing life increased by 100. *Wear depth reduced from 8 to 1μm by implantation
Harding(180)	En 40B En 8, En 58B	50 keV, N^+ ions 2-$8x10^{17}$ ions/cm^2	Pin on disc (pin:stainless steel)	10 N	White spirit	*Very significant wear improvements.
Tosto (107)	38NC D4 steel (0.35C, 0.8Ni, 0.7Cr, 0.2Mo, 0.7Mn, 0.2 Si)	30 keV $N^+ + N_2^+$ $2x10^{17}$ ions/cm^2 100 μA	Reciprocal motion	Increments from 5 kg	Alcohol	*Implantation increased load bearing capacity by 40%.
Watkins & Dearnaley(199)	Hard Cr coating (15 μm)	150 keV N_2^+ $4x10^{17}$ ions/cm^2	Pin on disc (Tufnol pins 2mmØ)	20 N (0.65 Kg/mm^2)	Abrasive slurry	*Much improved durability.
Goode et al (182)	Fe	90 keV N_2^+ 7 - $120x10^{16}$ ions/cm^2 dose rate: 4.7 μA/cm^2	pin on disc (0.6m/s) Pin: Fe	25 N	White spirit	*Significant wear reduction even for $7x10^{16}$ ions/cm^2. *No dependence on N^+ dose
Pope et al (160)	AISI 440C	50 keV N^+ $4x10^{17}$ ions/cm^2 Implant. temp.:< 100° C	Pin on disc	0.2-1 kg		*Mean wear depth not signific. reduced by N^+ implantation.

Reference	Materials	Implantation Param.	Tribotester	Load	Lubricant	Wear Improvement
Hartley & Hirvonen(159)	AISI 3135	---	Falex tester	200 lbs (890 N)	Hercolube A (synthetic)	.x 3 red. in wear rate by N^+ impl. (From 3.09 to 0.96 μg/s)
Hartley (2,3,169)	Mild steel	35 keV N^+.... ~ 10^{18} ions/cm^2	...Pin on disc (300 rpm)	0.22 kg	White spirit	*Wear parameter reduced with increasing load
	Nitriding steel (En40B)	30 keV N^+.... 10^{16}-10^{18} ions/cm^2	...Pin on disc (300 rpm)	1.22 kg	White spirit	*x10 max. improv.in wear resist. if dose >$2x10^{17}$ ions/cm^2
		30 keV N^+.... $1.8x10^{18}$ ions/cm^2	...Pin on disc (1500 rpm)	1.50 kg	White spirit	*Wear perameter reduced with increasing distance
Daniels & Wilbur (185)	AISI 304 (19Rc) SAE 01 (30 Rc) AISI M2 (60 Rc)	60 keV N_2^+ $2x10^{17}$ N_2^+/cm^2 dose rate: 100 μA/cm^2	Ring on block (190rpm)	2220 to 2670 N	Gear oil 150	*SAE 01: 63% red. wear vol *AISI M2: 25% red. wear vol *AISI 304: load bearing capacity increased by 40
Pollock et al(184)	Bright mild steel	25 - 65 keV nitrogen 0.9 - $6x10^{17}$ ions/cm^2 dose rate: 20-25 μA/cm^2	Ball-on-disc (carbide ball 1cm Ø)	20 to 100g · (0.8 m/s)	Paraffin	*Wear reduced by 15 at 20g load
Zhao Jie et al (196)	*GCr15 bearing steel *QBe2 beryllium bronze *Recoil impl. on 300 Å Cr film	N^+ ions 120+70+30 keV $3x10^{17}$ ions/cm^2 Recoil impl.: 30, 70 keV $2x10^{17}$ ions/cm^2	Pin on disc (Pin: Be bronze) (640 rpm)	400 g 1200 g	Yes	*N^+ impl.: reduced adhesion of QBe2 beryllium bronze. *Recoil impl.: improved signific. wear resistance. *GCr15 steel: no wear red. but reduced adhesion in counterface.

Reference	Materials	Implantation Param.	Tribotester	Load	Lubricant	Wear Improvement
Singer & Jeffries (165)	Unhardened: --AISI 1018 --AISI M2 AISI 304	N^+, Ti^+ and $Ti^+ + N^+$ <u>N</u>$^+$: 180 keV $4x10^{17}$ions/cm^2 <u>Ti</u>$^+$: 50 keV $2x10^{17}$ ions/cm^2	Ball-on-disc (hardened ball)		Dry and "Shell 2190 TEP"	<u>Dry</u>: *N^+ impl.: delayed shearing and strengthened AISI 304 & 1018. No improvement for AISI M2· *Ti^+ impl.: delayed wear. *Ti^++ N^+ impl.: best results <u>Lubricated</u>: *N^+ impl: more effective than Ti^+ in AISI 304. No improv. for rest *Ti^++N^+ impl.: elimin. deformat.
Wolf et al (193,194)	AISI M2, D2 (AISI 5120 workpieces)	Nitrogen, 150 keV $6x10^{17}$-10^{18} ions/cm^2	<u>Cold forming:</u> (A) Backward can extrusion (B) Upsetting between flat parallel dies		Soap lubricant (Bonderlube 236)	(A) Wear reduced by 2-3. (B) Wear reduced by 20-25%. *Similar results to nitrocarburized punches but "cracking" eliminated by implantation.
Deutchman, Partyka(183)	*4140 steel (44 Rc) *Carburized 4140	40 keV nitrogen 1-$5x10^{17}$ atoms/cm^2 dose rate: 250 μA/cm^2	Pin on disc	10 psi		*4140 steel: x 4 wear reduction. *Carburized 4140: x 10 wear red.
Kustas et al (186)	AISI 303	93 keV $N^+ + N_2^+$ $3x10^{17}$ ions/cm^2 Dose rate: 10-15 μA/cm^2	Gear mechanism	Cont. stress: 76.2 klb/in	BRAYCO 899 (Teflon-containing lubr.)	*Post-impl. anneal: incr. in wear. *Wear reduced by 40% and dedendum spalling by 49%.

Reference	Materials	Implantation Param.	Tribotester	Load	Lubricant	Wear Improvement
Hale et al (177)	SAE 3135 steel (pins) AISI 1137 (V-blocks)	180 keV N_2^+ 2.5×10^{17} ions/cm^2 Dose rate: $\leq 15\ \mu A/cm^2$	Falex	200 lbs (890 N)	Yes	* x 16 wear reduction for pins. * Only 7 times wear improvement when implanted V-blocks used
Hale et al (178,179)	SAE 3135 (pins) AISI 1137(V-blocks)	180 keV N_2^+ 2.5×10^{17} ions/cm^2	Falex	200 lbs (890 N)	Duo-seal oil	*Pin wear reduced by 15. *Oxidizing treatment (315° C for 75 min): ~x 13 wear red.

Table 8 - Improvements in wear lifetime of tools and components obtained by nitrogen implantation

Application	Material	Result
Scoring and forming dies for Al cans (50)	D2	x3 life increase and reduced metal pick-up.
Finishing rolls for Cu rod (203)	H13	x8 life increase. Improved product.
Paper slitters (32)	1.6% Cr, 1% C steel	x2 cutting life.
Taps for phenolic resin and Thread-cutting dies (32)	M2	Up to x12 life increase. x2-5 life improvement.
Forming, press tools (32)	Tool steels	x10 steel pressings. Much reduced adhesive wear.
Progression tools (197)	M2, ASP 23	x6 life increase.
Fuel injectors and metering pump	Tool steel	x100 life, in engine tests.
Bakery knives (202)		x6 lifetime, preserved cutting edge.
Plastic calibrator die (183)	Nitrided H13	x2 life improvement.
Profile hot die for plastic extrusion (183)	P20	x4 life increase.
Injection screws and nozzles, sprue bushes, impression moulds, feed runner blocks, etc. for the moulding of filled plastics (197,201)	Tool steels	x4-6 life increase.
Spark-eroded tool finishes (197)	Tool steels	x4 life increase. Maintained surface.

CHAPTER 4

EXPERIMENTAL PROCEDURE

4 EXPERIMENTAL PROCEDURE

4.1 Materials

4.1.1 Steels

Three conventional steels were chosen to be nitrogen implanted for the experimental work. AISI M2 high speed steel, D2 cold work tool steel and 420, a martensitic stainless steel commonly used for plastic moulding tools. AISI H13 hot work tool steel was used as the substrate material underneath the coatings that will be described below. The chemical composition of these steels is indicated in Table 9.

Table 9 - Steels compositions

AISI	Typical analysis wt %						
Designation	C	Si	Mn	Cr	Mo	V	W
M2	0.87	-	-	4.2	5	1.9	6.4
D2	1.55	0.3	0.3	12	0.8	0.8	-
420	0.38	0.8	0.5	13.6	-	0.3	-
H13*	0.35	-	-	5.0	1.5	1.0	-

* Substrate material for coatings, not implanted

The materials were received in round bar form of varying diameters and in a soft annealed condition. After machining and grinding to the correct dimensions for wear (see Figure 29) and microhardness testing (12.5 mm Ø x 6 mm) the specimens were heat-treated to the required hardness as displayed in Table 10. Following heat treatment the specimens were surface ground and mechanically polished to a surface roughness of 0.18 - 0.36 μm CLA prior to nitrogen implantation.

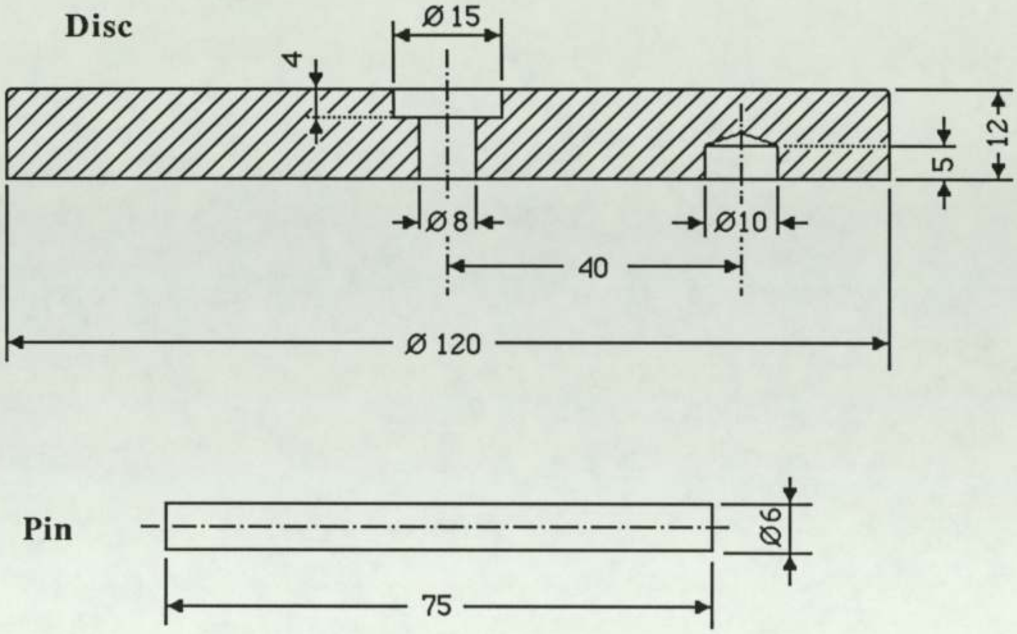

A) Specimens for pin-on-disc wear testing. Scale 1:1

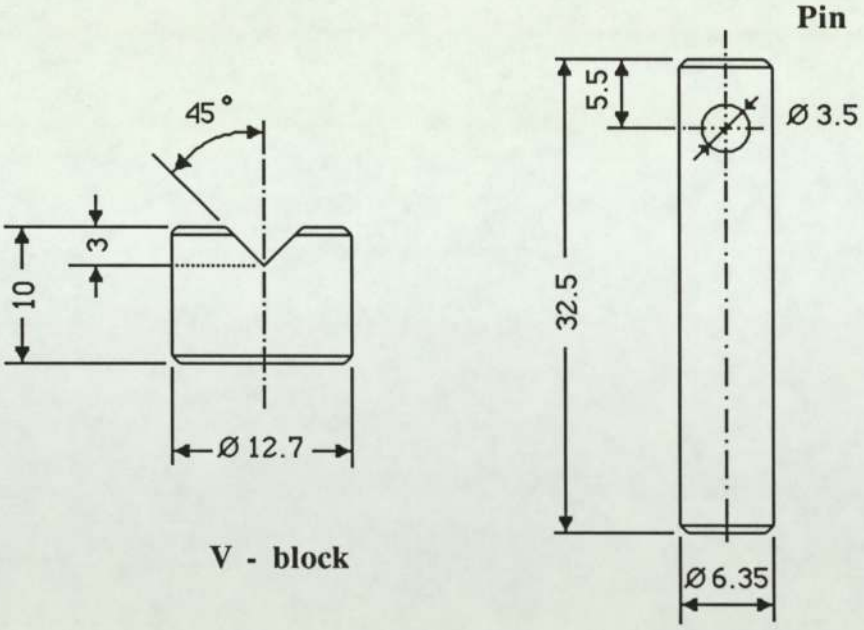

B) Specimens for lubricated Falex wear testing. Scale 2:1

Fig.29: Nominal dimensions in mm of wear testing samples.

Table 10: Heat Treatment Procedure

Steel (AISI code)	Heating	Quenching medium	Tempering	Hardness
M2	(Vacuum furnace) * Preheating steps: 450°C (20 mins) 850°C (20 mins) * Austenitizing 1180°C (5 mins)	(Vacuum furnace) Gas (Nitrogen)	(Air circul. furnace) 550° C (1 h) Twice	63 ± 1 HRc (850 ± 10 HV)
D2	(Vacuum furnace) * Preheating: 650°C (20 mins) * Austenitizing 1020°C (15-20 mins)	(Vacuum furnace) Gas (Nitrogen)	(Air circul. furnace) 350°C (1 h)	59 ± 1 HRc (680 ± 10 HV)
420	(Salt bath furnace) * Preheating: 600-850°C * Austenitizing: 1025°C (15-30 mins)	Oil	300°C (1h)	53 ± 1 HRc (600 HV)
H13	(Vacuum furnace) * Austenitizing: 1010°C	(Vacuun furnace) Gas (Nitrogen)	(Air circul. furnace) 550°C (1h)	52 ± 1 HRc (580 ± 10 HV)

4.1.2 Coating Systems

One of the aims of the present work was to investigate the influence of nitrogen implantation upon the mechanical properties of engineering coatings. Electroless nickel-phosphorus and hard chromium deposits were chosen due to their widespread use in engineering applications which require an increase in the life of parts subject to wear. Electrodeposited cobalt-tungsten was also investigated since this has shown promise as a wear resistant coating on hot and cold metal working tools.

4.1.2.1 Electroless Nickel - Phosphorus Alloy

This coating, known also as autocatalytic or chemical nickel, is deposited from an aqueous solution by a chemical reaction without the need of an externally applied current.

Its increasing use in engineering applications is mainly due to the uniform deposit thickness, ease of plating and good wear and corrosion properties.

The phosphorus content of the coating is primarily affected by the pH but is also related to temperature and solution composition, and is an important parameter that influences the structure and properties of the deposit.

As deposited, the coating structure is regarded as being amorphous(211,212) with a hardness of about 500 HV, but upon heat treatment the coating undergoes significant changes. A suitable heat treatment procedure produces Ni_3P precipitates inducing considerable second phase strengthening so that hardness values of 900 to 1000 HV are achieved.

In the present work "Nifoss 2000", a commercially available(213) acid solution for the electroless deposition of Ni-P alloys, was used. This solution contains nickel sulphate, sodium hypophosphite as the reducing agent and the requisite buffers, stabilizers, brighteners and wetting agents. The initial plating solution was prepared following the suppliers instructions, which are indicated below:

Base solution (Nifoss 2000)	.... 100 ml
Initial additive (Nifoss 2000)	.... 200 ml
Distilled water	.... 700 ml

One litre of solution was used per 0.5 to 1 dm^2 of surface to be plated.

Once the solution had been prepared, it was heated to and maintained at a temperature of 90° C, with a pH of 4.8 ± 0.1. The pH of the solution was checked at regular intervals during deposition with a pH-meter and adjusted when required using 50% NH_3 or 10% H_2SO_4 solutions.

-Preplating cleaning sequence for the substrate material

An appropriate cleaning procedure is very important if good adhesion of the coating to the substrate material is to be obtained. This sequence removes surface contaminants and prepares the surface for the plating process. The procedure used for all ferrous base materials was the following:

1. Ultrasonic degreasing with a suitable solvent.
2. Anodic cleaning in a proprietary hot alkaline solution (70°C) at a current density of 4 A/dm^2 for 4 minutes.
3. Water rinse.
4. Dip in a 50% HCl acid solution, 15-30 seconds.
5. Water rinse.
6. Anodic cleaning in a proprietary cyanide solution at a current density of 4 A/dm^2 for 2 minutes
7. Water rinse
8. Immediate transfer of the samples to the plating solution

Air agitation was used during the deposition process to ensure uniformity of the coating over the surface of the samples. A coating thickness of about 25 μm was applied for the wear test parts and coupons for hardness testing. This required an immersion time of about 75 minutes at the above operating conditions. Periodic additions of maintenance solutions were necessary to maintain a constant rate of deposition and uniformity of the deposit structure.

Following the plating process, the electroless Ni-P coated samples were heat-treated at 400°C for 1 hour, in order to obtain a maximum increase in hardness of the deposit and a corresponding improvement in wear resistance by dispersion strengthening of Ni_3P precipitates.

4.1.2.2 **Hard Chromium**

The hard chromium solution was prepared according to the following formulation:

Chromic acid ..... 225 to 250 g/l
Sulphuric acid ..... 2.25 to 2.50 g/l

which gave a chromic to sulphate ratio of 100:1. With ferrous base materials it is essential that after the pre-cleaning sequence (as for electroless Ni-P deposition) the parts to be chromium plated are electrolytically etched to ensure satisfactory adhesion. The samples were therefore etched anodically in a chromic acid solution similar to that used for hard chromium deposition, at 55°C by applying a voltage of 6 volts for 30 to 60 seconds. After etching, the samples were immediately transferred to the plating solution with the current already switched on. The plating conditions were as follows:

Cathode current density ..... 40 A/dm^2
Voltage ..... 5.5 to 7 volts
Bath temperature ..... 55°C
Anode ..... Alloy lead

To ensure maximum uniformity of the deposit in the case of the cylindrical Falex wear test samples, a special anode arrangement was devised, which can be seen in Figure 30.

Areas on which plating was not required were protected with stopping off lacquer. The deposition time was approximately 2 hours to achieve a thickness of about 30 μm on the samples. In addition to the procedure described above, samples were also plated using a commercial "Hychrome Hard Chrome" plating solution(213). Similar operative conditions were followed, but no attempt to obtain a uniform coating was made. The cylindrical test samples were subsequently centreless ground to a uniform thickness of about 35 μm and mechanically polished to a surface roughness of 0.4 μm (CLA) prior to implantation. Limited work was also carried out on a new "High Speed Mach 1 Hard Chromium" coating(213), the thickness applied to the wear test specimens was of approximately 30 μm but the deposit was much brighter (0.22 CLA) than the above chromium coatings and additional polishing was not necessary.

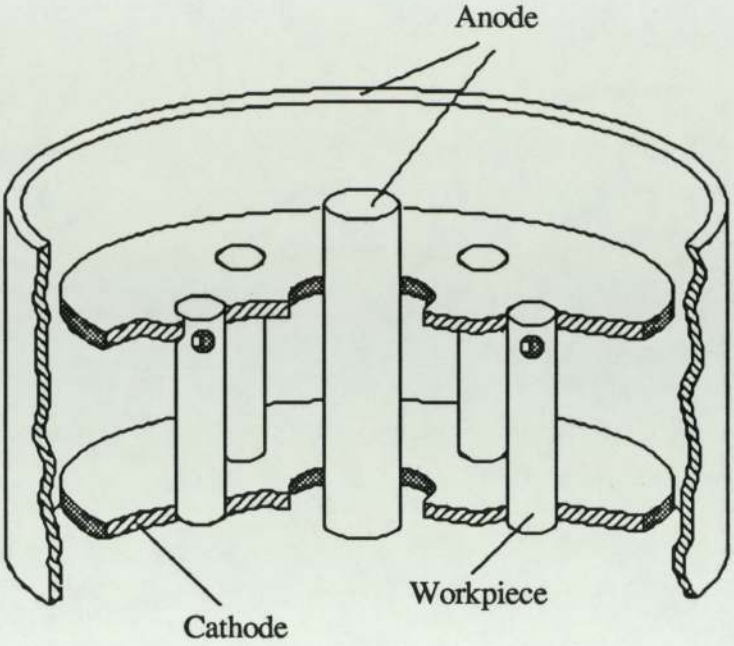

Fig.30: Schematic representation of anode-cathode arrangement for Cr plating.

4.1.2.3 **Cobalt - Tungsten Alloy Coating**

This coating was applied to the steel substrates by a technique known as brush or selective plating. In this electroplating method an absorbent pad is wrapped around an inert anode, soaked with electrolyte and rubbed over the surface to be coated.

A description of the technique, with its advantages and limitations as compared to conventional vat electroplating has been presented elsewhere(214). The particular coating was chosen due to its potential applications on cold working dies, as reported by Lodge et al(215,216).

The electrolyte used in the present study was based on previous work at Aston University(216) and formulated with simple inorganic salts of cobalt and tungsten with two different complexants and mineral acids to control pH. The composition was:

Co^{2+}	..... 2.0 M
W^{6+}	..... 0.2 M
Complexant A - Hydroxy-carboxylic or soluble salt	..... 0.7 M
Complexant B - Carboxylic acid or soluble salt	.....0.7 M

A commercial brush plating rectifier with reversing switch, safety cut out device and digital ampere hour meter was used for electrodeposition. The operating conditions were: pH 1.5 and 17 to 20 volts.

The plating stylus for brush plating consisted of an inert electrode (high density purified carbon) covered with a suitable absorbent material to hold the solution. The absorbent material was long fibre cotton wool covered with a mixed polypropylene-nylon felt bonded with acrylic resin. This technique provided a smooth surface finish to the coating, removing surface inequalities as they were formed(214).

To carry out either electrocleaning or plating, the stylus was dipped into the appropriate solutions and rubbed gently over the area to be coated. The solutions used in the pre-plating cleaning stage are indicated in Table 11.

Table 11 - Composition of activators for the precleaning sequence in Co-W brush plating

Activator	Composition
A	110 g/l Sodium chloride solution adjusted to pH 2.0 with dilute hydrochloric acid.
B	180 g/l Tartaric acid solution, adjusted to pH 5.0 with concentrated sodium hydroxide solution.
C	150 g/l Ammonium sulphate solution, adjusted to pH 2.0 with diluted sulphuric acid.

Previous to any brush plating the samples were thoroughly cleaned using the procedure described below:

1. Electroclean with a conventional alkaline cleaning solution. Stylus made cathodic with respect to the workpiece. 10-15 volts.
2 Water swill.
3. Etch with activator "A" until obtaining an even dark surface on the sample. Stylus cathodic. 8-15 volts.

4. Water swill.
5. Remove black smut by electrocleaning with activator "B", stylus still cathodic with respect to the workpiece, at 15-20 volts until an even light grey etched surface is visible.
6. Water swill.
7. Reverse current, ie. stylus is now anodic. Clean briefly the surface of the sample with activator "C" at 10-15 volts.

It is important at this stage not to swill with water but to leave the activator "C" on the surface before plating.

After the cleaning sequence the surface of the workpiece was well wetted with solution using the stylus before the external voltage was applied and deposition started. The voltage was then raised slowly to the operating value of 17-20 volts and the plating was carried out to the required ampere-hour measurement to provide a 25 μm thickness deposit.

To obtain a uniform deposit over the cylindrical wear test surface of the Falex specimens, these were rotated at about 70 rpm during the brush pre-cleaning and plating sequences.

4.2 Nitrogen Implantation

Two different implantation machines at Tech-Ni-Plant Ltd were used throughout the experimental work. One, a Type 222 model supplied by Hawker Siddeley Dynamics Eng Ltd, had a work chamber of nominal dimensions 610 mm cubed, a saddle field ion source, an ultra high vacuum system based on a diffusion pump and a high voltage supply with a maximum output of 100 kilovolts (see Figure 31). The second machine was a microprocessor controlled Zymet Z-101 implanter(217), where parts up to 200 mm in diameter and height can be treated. This implanter has similar voltage characteristics to the above model (see Figure 32).

All implantation treatments were carried out at ion energies of 90 to 95 keV and nitrogen doses from 2 to 7 x 10^{17} ions/cm^2. None of the implantation systems had magnetic analysis in order to separate the required N^+ ions from the rest of the output of the ion source. The beam consisted of a mixture of molecular and monoatomic species, being approximately 75% atomic nitrogen ions and 25% molecular nitrogen ions for the Hawker equipment, while the ratio was 60/40 respectively for the Zymet system.

Beam current densities were chosen so as to avoid excessive heating, the bulk temperature of the samples being kept below 150° C. Current densities therefore varied from 1.3 to 6 $\mu A/cm^2$ depending upon size of the workpieces and implantation dose.

The implantation procedure for the Zymet equipment was as follows: the samples already ultrasonically cleaned were mounted in a water cooled production tray with a low melting point metal eutectic bath, in order to provide a good thermal sink during the treatment. The pumping stage was then brought into operation and when at 10^{-6} torr the implantation process began by feeding a very small stream of nitrogen gas into the ion source.

Nitrogen ions are formed in the hot cathode arc discharge ion source, where the ionizing electrons are thermoionically emitted from a directly heated tungsten filament and accelerated to an arc potential of approximately 100 volts. These electrons initiate and sustain the discharge by ionizing molecules of a feed gas. The ions are extracted from the side of the arc chamber from a slit parallel to the filament, as depicted in Figure 33(218), focussed into a beam, and accelerated to an energy of approximately 90 keV towards the workpieces.

The samples were tilted if necessary at an angle in order to expose the working surface to the ions, and rotated to achieve a uniform implantation until the desired nitrogen dose was achieved. Typical treatment times varied from 4 to about 14 hours depending upon the rotation factor, nitrogen dose and beam current density applied.

Tech-Ni-Plant's ion implantation systems

Figure 31: Type 222 HSDE implantation machine

Figure 32: Z-101 implantation system

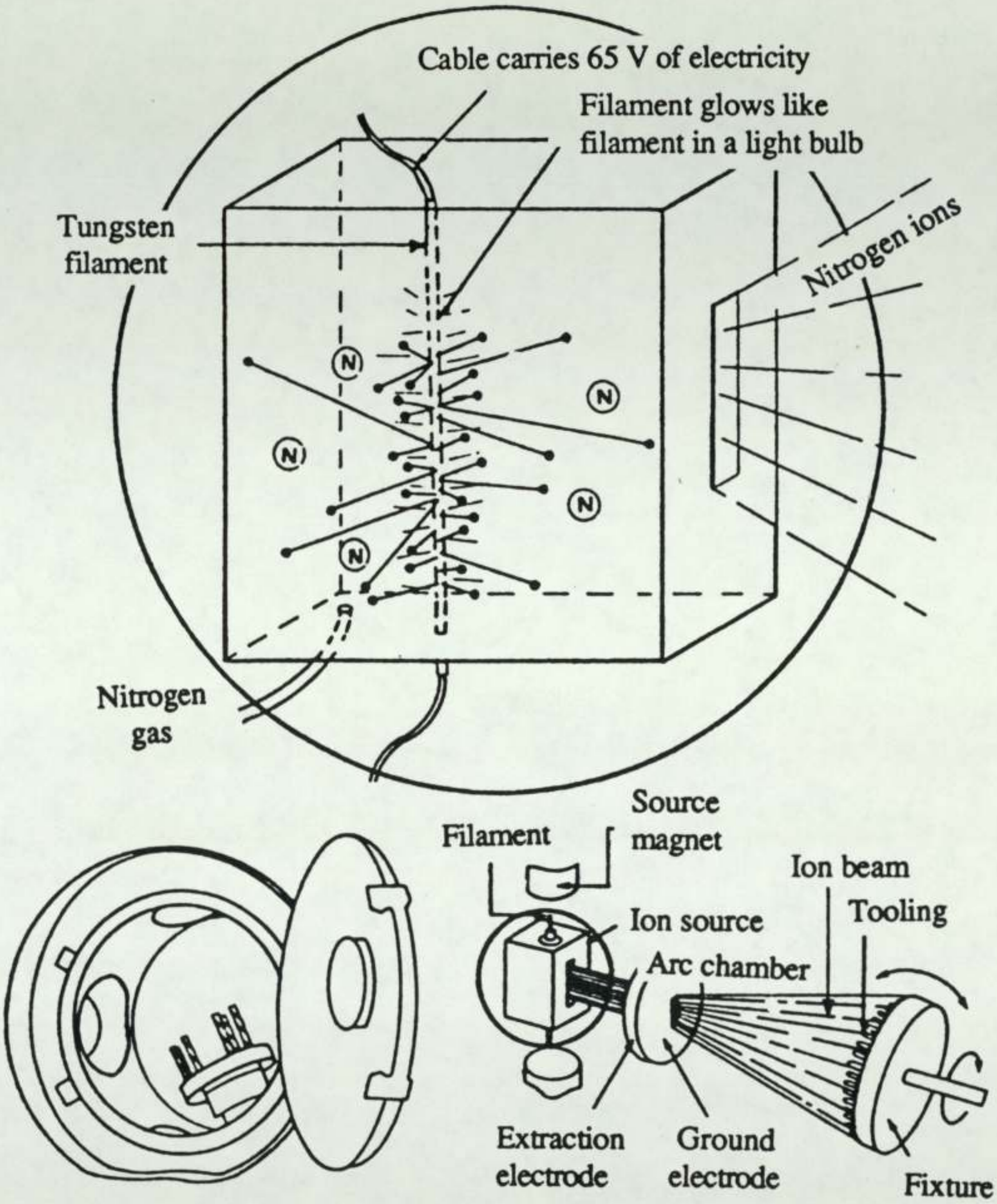

Figure 33: Schematic diagram of the ion implantation process.

4.3 Microhardness Testing

Surface hardness of the materials was evaluated before and after nitrogen implantation using a Vickers M-41 Photoplan Microscope. Very light loads of 49 to 98 mN (5 to 10 g) were used in order to limit penetration of the pyramidal indenter. This is necessary so that the hardness of the implanted layer can be calculated minimizing any contribution from the underlying bulk material.

As a comparison, samples of AISI 420 martensitic stainless steel and electroless nickel-phosphorus coating were also tested at Lancaster University using a special ultra-microhardness technique devised by Pollock and co-workers(104,105). This hardness tester uses very light loads up to approximately 9.8 mN (1 g), therefore limiting the penetration of the 90° trigonal indenter to a sub-micron scale within the implanted layer.

An individual run, with a loading rate of 0.07 mN/s, showing the characteristic loading and unloading curves can be seen in Figure 34.

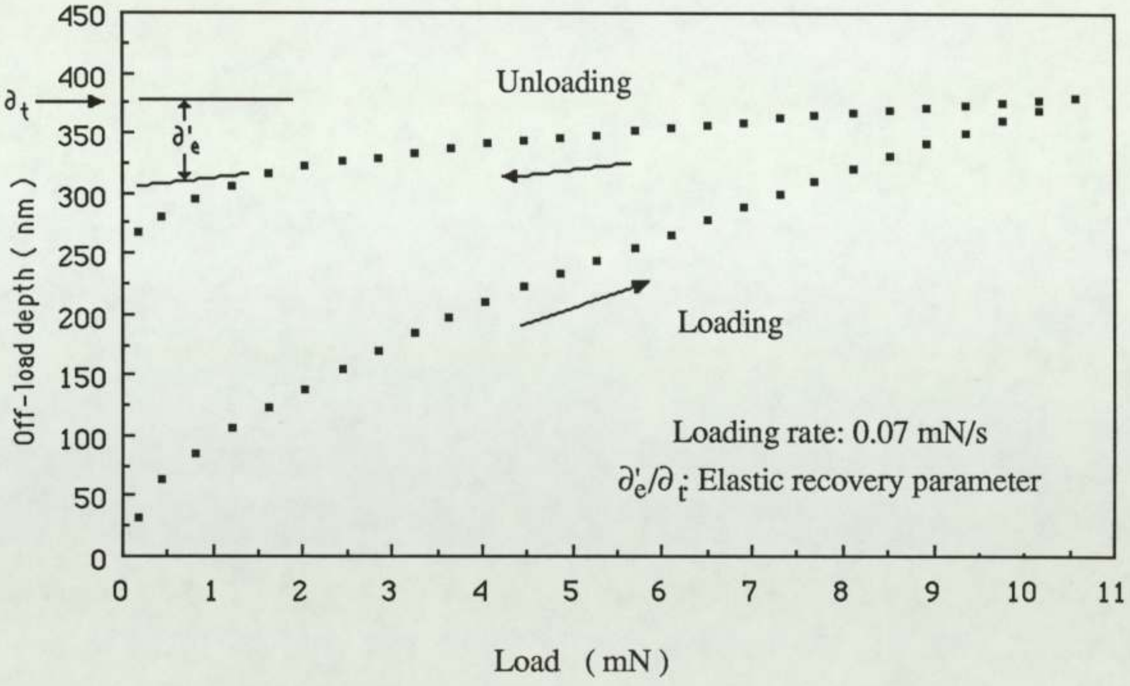

Fig.34: Individual depth-load run, showing loading and unloading curves.

4.4 Friction and Wear Testing

Friction and wear tests were carried out with two different machines. A Falex tester(219), under high loads (up to about 900 N) and lubricated conditions, and a pin-on-disc arrangement involving lower loads (9.81 to 49 N) and dry environment, were used for the experiments. A drawing of the specimens used in the wear testing can be seen in Figure 29.

4.4.1 "Falex" Lubricated Wear

The Falex wear and friction testing machine is normally used to evaluate the load-carrying capacity and lubricating effectiveness of various lubricants(220). However, it has been proved successful in assessing the wear performance of several coatings and materials in either lubricated or dry condition(221,222).

Figure 35 shows the testing machine, which rotates a cylindrical sample, loaded against two V-blocks, at 290 rpm. The load is applied to the V-blocks through a nut-cracker action lever-arm and spring gauge. The load is actuated by means of a ratchet wheel mechanism which squeezes the pin into the vertical grooves of the V-blocks. Wear takes place as the pin rotates under the applied load, causing a decrease in the pin diameter and the production of two vertical line wear scars in each V-block. The torque produced when the load is applied is recorded and related to the coefficient of friction by a formula that can be derived from the geometry of the test piece and V-blocks:

$$\mu = \frac{0.072 \text{ x Torque } (\text{N x m})}{\text{Load } (\text{N})} \qquad \text{..... } 4.1$$

Prior to testing, the loading system was calibrated, as indicated by ASTM D2625-69 designation, using a copper test coupon of known hardness (37.5 ± 1 BHN). Brinell-like indentations were made with a 10 mm diameter steel ball on the test coupon by applying gauge loads ranging from 900 to 2070 N. Indentation diameters in millimetres were then plotted on log-log paper against the gauge load at which they were made. The resultant line (see Figure 36) was then compared with the theoretical gauge line and hence, the true applied load could be calculated for the gauge load reading.

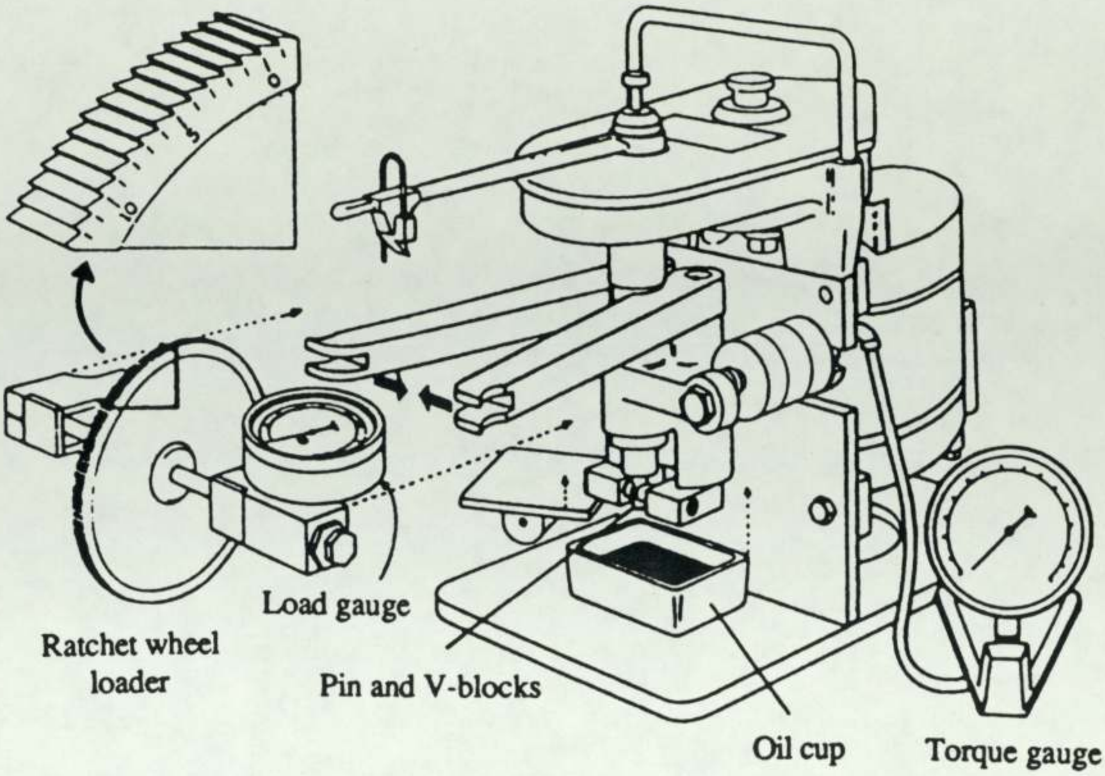

a) Schematic diagram of Falex lubricant tester showing its main components.

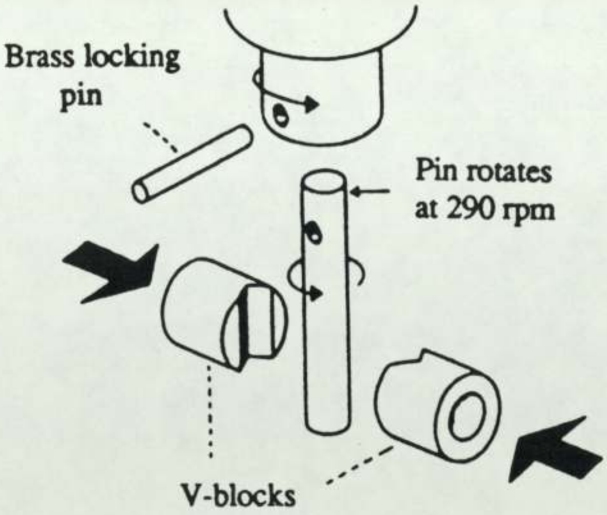

b) Expanded view of V-blocks and pin arrangement.

Fig.35: Schematic diagram of Falex lubricant machine and testing components.

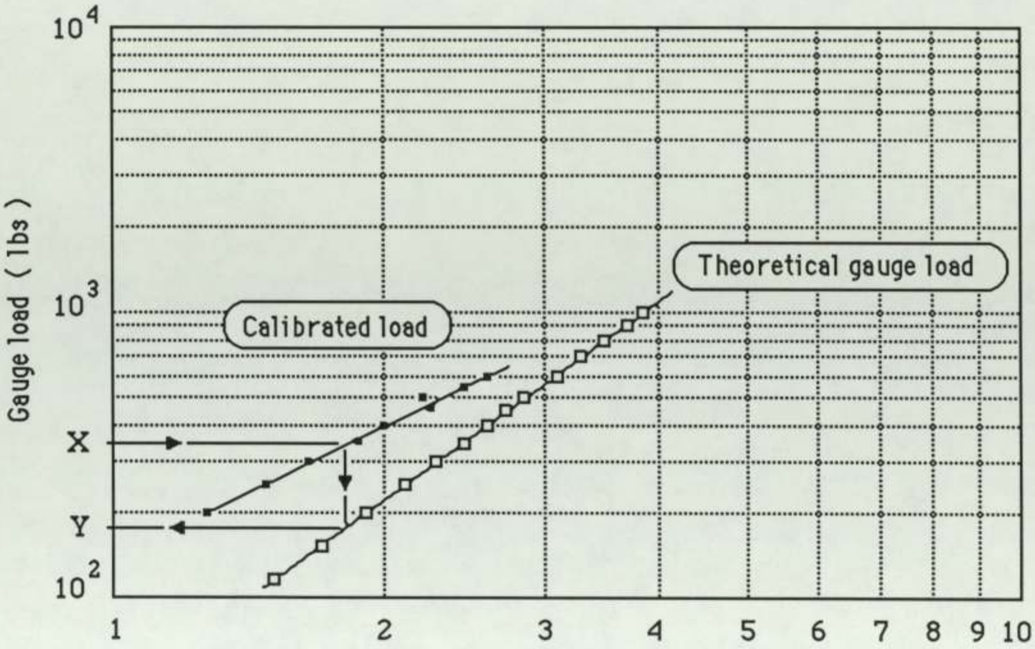

Indentation diameter (mm)

Note : Apply load X on gauge to obtain true load Y on pin

Fig.36: Calibration curve for Falex wear testing. 3000 lbs load gauge

All Falex wear testing was carried out under lubricated conditions. The lubricant used was a paraffin based oil (ISO 22) with a viscosity of 22 cSt (22 mm^2/s) at 40° C and a residual 0.7% sulphur content.

Preliminary wear tests showed that the Falex machine could overheat if long testing periods of more than 45 minutes were used, and therefore, the safety cut out device could stop the run. To avoid this undesired effect and since no standard Falex wear testing procedure for surface treated materials is available, several partial wear periods were chosen for each pin, until completion of the test, as indicated below.

The pin and two V-blocks were cleaned ultrasonically in isopropyl alcohol and weighed to an accuracy of 10^{-5} g prior to any Falex testing. The weights of the pins were determined by averaging a minimum of ten readings from the balance; the zero position was reset for each reading.

The specimens, pin and V-blocks, were placed in position ready for testing as shown schematically in Figure 35. The oil cup contained 70 ml of additive free paraffinic lubricant. The motor was activated and the load increased initially to 440 N, by means of the ratchet wheel. This load was maintained for a 1 minute run-in period, and then increased slowly to either 710 N (for coatings) or 900 N (for steels). The test was stopped after partial periods of 15 to 30 minutes so that the wear rate of the pins could be monitored by weight loss. This procedure was repeated several times, using fresh oil after each wear period, until the total wear period (up to approximately 150 minutes) had been completed. Problems of stopping and restarting tests for each pin were minimized since an intimate contact between V-blocks and test pins was generally obtained.

All testing was performed at room temperature and the oil never exceeded 50°C during any run. Table 12 shows the materials and wear couples used for the Falex wear testing; like on like material was chosen for the steels, while AISI 52100 bearing steel was used as the V-block for the coating systems. In addition to weight loss measurements, profiles of the wear tracks were obtained using a Taylor Hobson "Talylin I" apparatus, so that any change in the topography of the worn surfaces as a result of the implantation could be investigated.

4.4.2 Pin on Disc Dry Wear Testing

Conventional pin on disc wear testing was carried out in order to compare the performance of nitrogen implanted steel surfaces under dry conditions and lower loads to that of the Falex procedure as described earlier.

A schematic diagram of the wear tester, showing the main components can be seen in Figure 37. Testing was conducted generally using the same material for the pin and disc. The geometry of these test parts is illustrated in Figure 29.

Loads used throughout the experiments ranged from 9.81 to about 49 N (ie. 0.35 to 1.73 N/mm^2). Several wear tracks were performed on each disc for which the rotational speed had to be adjusted appropriately to result in the required sliding velocity of 0.5 m/s.

Table 12: Falex Wear Testing Materials

PIN			V-BLOCKS		
Material	Surface roughness (CLA)	Hardness *	Material	Hardness	Calibrated load
AISI M2	0.20 μm	62-64 HRc 850 ± 10 HV	AISI M2	62-64 HRc 850 ± 10 HV	900 N
AISI D2	0.22 μm	58-60 HRc 680 ± 10 HV	AISI D2	58-60 HRc 680 ± 10 HV	900 N
AISI 420	0.34 μm	52-54 HRc 595 ± 5 HV	AISI 420	52-54 HRc 959 ± 5 HV	900 N
Electroless Ni-P (H13 steel substrate)	0.12 μm	1100 $HV_{0.1}$	AISI 52100	62-64 HRc 850 ± 10 HV	710 N
Hard Cr coating (TypeII) (H13 steel substrate)	0.4 μm	1050 $HV_{0.1}$	AISI 52100	62-64 HRc 850 ± 10 HV	710 N
Co-W coating (H13 steel substrate)	0.4 μm	550 $HV_{0.1}$	AISI 52100	62-64 HRc 850 ± 10 HV	710 N

* Note: Hardness values are for the "unimplanted" condition - only the pins were nitrogen implanted.

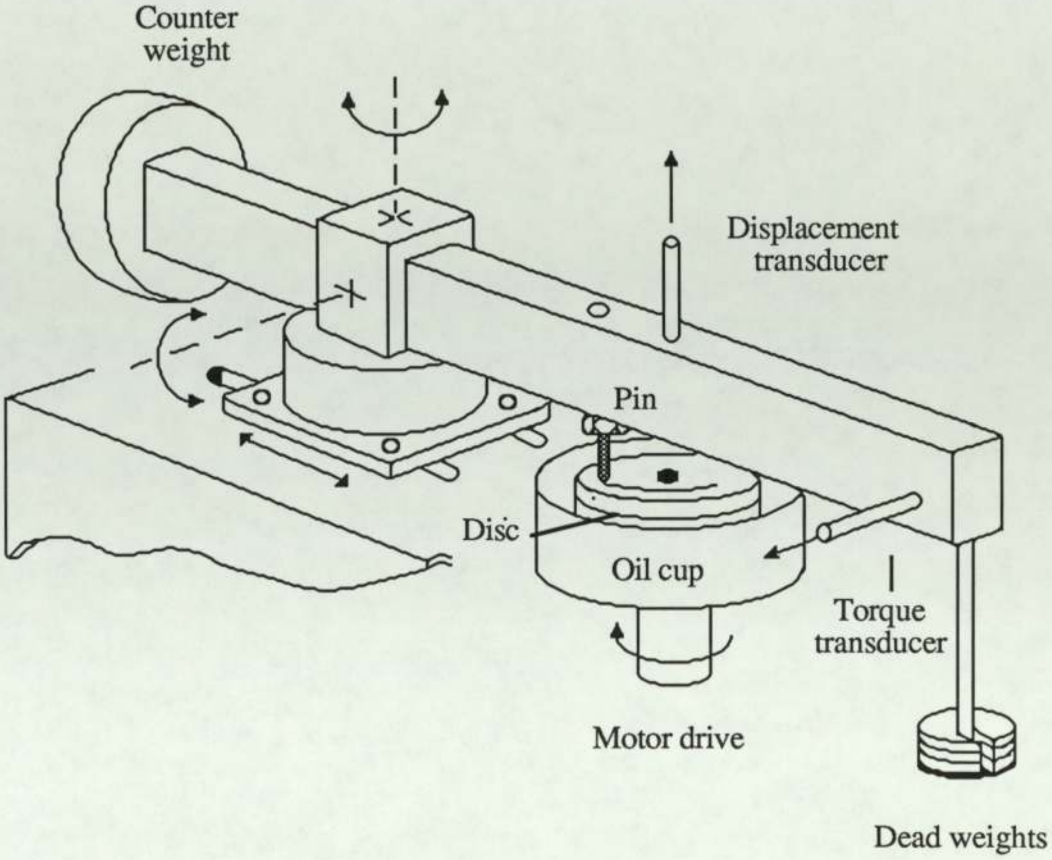

Fig.37: Schematic diagram of the pin-on-disc wear machine.

At these operating conditions the wear on the disc was very low even under prolonged testing and would not be measured accurately by surface profilometry or weight loss. Therefore, it was decided to implant with nitrogen the flat ends of the pins so that gravimetric wear rates could be more easily calculated from the pins.

Both pins and discs were degreased thoroughly prior to testing. It was very important to ensure that the contact between both parts was perfect in order to avoid a cutting effect from the edge of the pin which would increase ploughing friction and hence wear.

Once the testing materials were arranged correctly, the motor was actuated and the load applied to the arm. A chart recorder was used to display the output of the transducers. The vertical displacement transducer provides a combined measure of the wear occurring on both pin and disc, although some expansion might also be operative due to heating effects if a severe testing procedure were chosen. The torque transducer provides an indication of the frictional force, and by knowing the applied load, the dynamic coefficient of friction can be calculated.

4.5 Electron Microscopy

To investigate whether any change in wear behaviour occurred as a result of nitrogen implantation, the worn surfaces of the untreated and implanted materials were examined by scanning electron microscopy (SEM). A Cambridge Microscan Electron Microscope complemented with Energy Dispersive X-ray spectroscopy (EDS) was used in this work. X-ray analysis (EDS) is not suitable for the study of nitrogen implanted surfaces since light elements (below atomic number 11) are not detected and the depth of information, which depends on the specific density (atomic number) of the elements contained in the sample and the energy of the primary beam, ranges between 1 to 10 μm, far beyond the implantation range. However, it proved very useful for fast qualitative and semi-quantitative information on the composition of the untreated surfaces and individual features of worn areas.

To examine the microstructure of the thin implanted layer Transmission Electron Microscopy had to be conducted on special samples. These were prepared for nitrogen implantation using the same starting material as that in the tribological tests. In the case of tool steels, pins were turned down from the original annealed steel rod to 3 mm in diameter and, after suitable heat treatment (see Table 10), several discs were further reduced to a thickness of approximately 0.2 mm by grinding on silicon carbide papers using a special sample holder, prior to nitrogen implantation. The discs to be implanted were mounted on a copper block to provide a good thermal sink, which was electroless-nickel coated to avoid any possible contamination due to copper sputtering during bombardment.

The treatment was carried out with a 90 keV mixed (75% N^+, 25% N_2^+) ion beam, a dose of 4×10^{17} ions/cm^2 and a beam current density of 3.5 μA/cm^2. An infra-red temperature monitoring system indicated a bulk temperature of less than 150°C.

Hard chromium coating foils were prepared for nitrogen implantation by plating onto thin copper plates. The Cu substrate was chemically dissolved with a chromic-sulphuric acid solution following nitrogen implantation. The implanted side was protected with stopping off lacquer during the stripping of the copper substrate. Specimens of approximately 3 mm diameter were then taken from the Cr plate.

Discs for TEM examination were ion beam thinned with an argon beam, from the unimplanted side, using a low ion current (typically 80 μA, 5 kV voltage) to avoid any heating effect during thinning which might affect the structure of the implanted layer. Finally, microscopy was carried out on thinned specimens using a JEOL JEM 100B transmission electron microscope at 100 kV accelerating voltage.

4.6 Surface Analysis

4.6.1 Auger Electron Spectroscopy (AES)

To verify that nitrogen implantation had occurred as expected, chemical analyses of near surface regions of the implanted materials were determined by Auger electron spectroscopy (AES). The AES analysis was combined with sputtering of surface layers by argon ions in order to obtain a depth profile of the elements of interest.

-Physical Principles

Figure 38 illustrates the main process by which Auger electrons are generated. A bombarding electron first removes an atomic electron from a core state in a sample atom. Another electron then fills this vacated level by transitioning from a more energetic level, leaving the atom in a state with excess energy. This energy can be dissipated either by emission of a characteristic X-ray (X-ray fluorescence), which can be neglected during a typical Auger analysis(223), or by ejection of an Auger electron.

The energy of the Auger electron is a function of the energies of the electron levels involved in its production, and it is characteristic of the element giving rise to the Auger electron, allowing its identification.

In Figure 38, an initial core vacancy is shown in the K level. This is filled by an electron from the L_1 level and the excess energy is transferred to an electron in the L_2 level that is ejected as a KL_1L_2 Auger electron.

The energy of the Auger electron E_A, characteristic of the particular atom, in this case is given approximately by:

$$E_A = E_K - E_{L_1} - E_{L_2} \qquad \text{..... 4.2}$$

Only a few of the many transitions that may occur (eg. KLL, LMM, MNN, NOO...) are strong for each element and these enable the surface atoms to be clearly identified from the emitted electron energy spectrum.

Atoms from depths greater than a few monolayers (1 nm) also eject Auger electrons but these do not escape easily and so do not contribute to the emitted line spectrum. Thus AES is characteristic of the outermost atomic layers of a solid and is a very useful tool for the surface analysis of implanted materials.

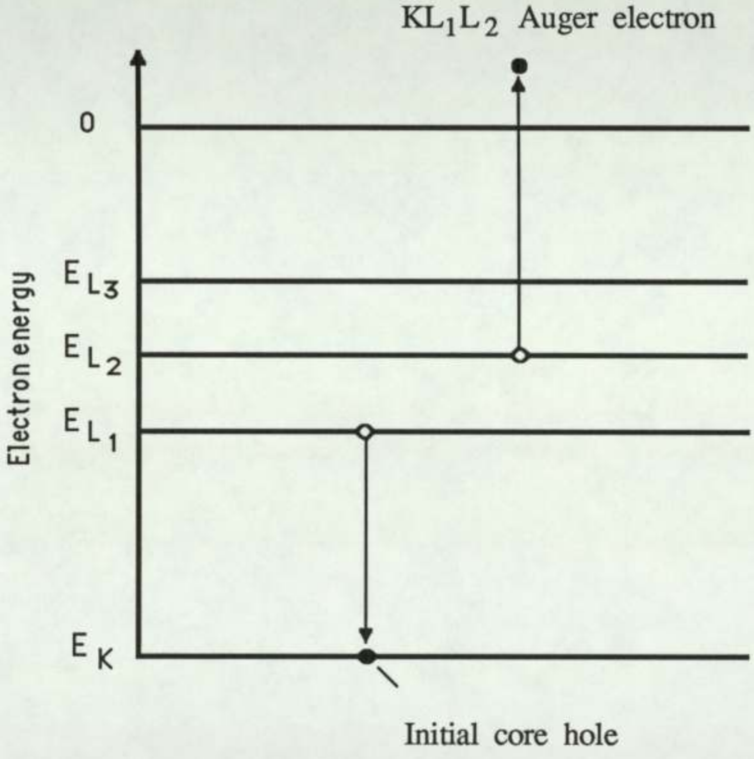

Fig.38: Schematic illustration of the generation of an Auger electron by electron bombardment.

-Experimental Details

Auger analysis was carried out using a Scanning Auger Microprobe System (X-SAM 800). The primary electron beam was operated at 5 kV and a sample current of 10 μA. Survey Auger derivative spectra were recorded for Auger electrons with energies between 100 and 1100 eV.

Depth profiling was carried out in a Ultra-High-Vacuum system (UHV), with a base pressure of 10^{-9} torr, turning into a working pressure of about 10^{-7} torr when argon was introduced. The surface was then bombarded with a beam of argon ions. The ion gun was operated at 5 kV focussing the beam over a spot size of 1000 μm, the ion beam was rastered to ensure uniformity. The normal to the analysed surface was at an angle of 60° to the ion beam direction.

Spectra were taken before ion etching and then at regular intervals after etching. The aim was to determine concentration profiles through a layer approximately 0.2 μm thick. Calibration of the sputtering rate was carried out with a standard silicon nitride specimen of known thickness. A value of 20 Å/min was obtained which corresponds to sputtering rates of 30 Å/min for iron and chromium, with an uncertainty of about 20%.

Quantitative analyses from the spectra were obtained using the normalized peak heights method and sensitivity factors as quoted in the "Handbook of Auger Electron Spectroscopy" (224).

4.6.2 X - Ray Photoelectron Spectroscopy

This technique involves the analysis of photoelectrons produced by the action of X-rays. An incident X-ray ejects a core level electron from an atom in the specimen. This electron travels to the surface of the material without losing significant energy and escapes with a kinetic energy given by:

$$KE = h\nu - BE - \text{Ø}_S \qquad ..... \; 4.3$$

where $h\nu$ is the energy of the incident X-ray photon, BE is the binding energy of the atomic orbital from which the electron originates and Ø_S is the spectrometer work function.

Figure 39 illustrates the production of a 1s photoelectron. By measuring the kinetic energies of the photoelectrons emitted, the binding energies of the levels from which they originated can be determined. This information allows identification of the element and atomic level responsible. The precise position and shape of the photoelectron line depends on the chemical state of the surface atoms, and so XPS can be used to probe the chemical state of implanted surfaces.

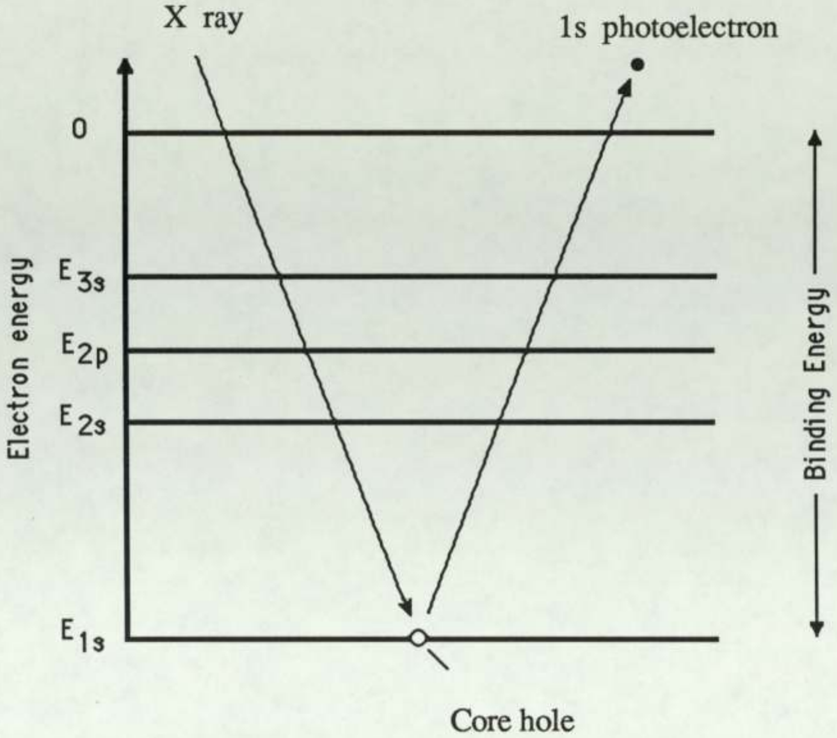

Fig.39: Schematic illustration of the production of a 1s photoelectron by X-ray bombardment.

-Experimental Details

The XPS analysis was performed on hard chromium coatings and AISI 420 martensitic stainless steel in a Kratos X SAM 800 ESCA-Auger instrument with Mg K_α - X radiation (1253.6 eV). The X-ray source was operated with a filament current of 15 mA and a voltage of 15 kV. Ion bombardment of sample surfaces, to record the spectra at various depths, was carried out with a Kratos Macrobeam I ion gun. With this gun, it is possible to raster the ion beam evenly over an area of 9 x 4 mm. Argon ions of 5 keV energy were used with a sample current of approximately 3.1 μA. The beam interacted with the surface at a glancing angle of 30°.

An ultrahigh vacuum of about 10^{-9} torr was maintained inside the sample analysis chamber while measurements were taken. Cr $2p_{3/2}$, O 1s and N 1s spectra were recorded in the case of chromium coatings. The C 1s spectra due to hydrocarbons on the specimen surfaces were also obtained as the binding energy of this line, at 284.6 eV, is often used as a reference value in XPS analysis. In order to obtain charge-corrected binding energy measurements, a thin layer of gold was evaporated onto the steel specimens to be analysed and binding energies were then calculated relative to the Au 4f $_{7/2}$ peak at 84.0 eV. In the steel material Fe $2p_{3/2}$, Cr $2p_{3/2}$, O 1s, N 1s, C 1s and Au $4f_{7/2}$ spectra were recorded after etching at different depths.

Data was collected and recorded with an Apple IIe microcomputer system linked with the spectrometer. Software was available for data analysis purposes, such as non-linear background subtraction and curve fitting. The curve-fitting procedure was based on a non-linear least squares method, as described by Sherwood(225).

4.7 Nuclear Reaction Analysis (NRA)

In this technique, charged particles in the 0.5 to 2 MeV energy range are accelerated to induce nuclear reactions on light (low Z) nuclei. The emitted charged particles are detected by means of semiconductor devices and their energy spectrum is recorded; the interpretation of these spectra allows identification of the nuclei in the target. Absolute quantities of these nuclei may be obtained by comparison to reference standards up to a depth of about 1 μm. A description of the technique and its applications to materials analysis has been presented by Amsel et al(226).

-Experimental Details

The analysis was conducted in the 3 MeV Van de Graaff accelerator at the Nuclear Physics Division (AERE, Harwell). The reaction used was ^{14}N (d,p)^{15}N, ie. Target (Projectile, Ejectile) Residual, with a 1.4 MeV incident beam energy (100 nA beam with 2 mm diameter spot size), the Q value for the nuclear reaction being 8.61 MeV.

The emitted charged particles, or backscattered protons, were detected at an angle of 160° using an Ortec surface barrier detector. Energy of the emitted particles was 8.63 MeV. A foil of 25 μm thick Al was placed in front of the detector to stop elastically scattered deuterons hitting it. The energy of the protons after transmission through this foil was 8.37 MeV.

Spectra recorded from the implanted surfaces were compared with spectra from the standard, a 991 Å thick Si_3N_4 thermally grown on Si, in order to obtain absolute nitrogen concentrations or basically the retained nitrogen dose on the implanted samples.

Additional NRA was also carried out for comparison purposes in the Dynamitron accelerator at Birmingham University's Radiation Centre . The same (d,p) reaction was used with 1.5 MeV deuterons as the incident radiation.

4.8 X - Ray Diffractometry

X-ray diffraction analysis was carried out on untreated and nitrogen implanted electroless Ni-P coatings to investigate any possible phase change which might have occurred due to bombardment effects.

The principle of the technique is as follows: a beam of X-rays of specific wavelength λ is 'reflected' at certain angles (θ) by crystal planes of appropriate spacing (d) which satisfy the Bragg equation:

$$n \lambda = 2 d \sin \theta \qquad \text{..... 4.4}$$

The angular position of diffraction peaks, their shape and intensity give information on crystal structure and physical state; the results being obtained from a thin (typically 50 μm) surface layer. Since the implanted layer is less than 1 μm and the instrument had no crystal monochromator to reduce the background of the diffracted spectrum and to facilitate the detection of weak peaks, the technique was not considered to be suitable for phase identification after nitrogen implantation. However, it would be useful to assess any possible phase change induced by bombardment heating effects occurring during implantation at high beam currents.

Testing was carried out in a Philips X-ray diffractometer, with the experimental conditions as indicated below:

Radiation	..... Cr, K_α
Filter	..... Ni
Voltage	..... 40 kV
Current	..... 20 mA
Scanning range	..... 40°-120°
Scanning speed	..... 1° min.^{-1}
Divergence slit	..... 1°
Receiving slit	..... 0.1 mm
Detector	..... Proportional counter

The diffraction patterns obtained from the Ni-P coatings were plotted on a chart recorder. Graphs being essentially a plot of intensity as a function of 2θ angles. Each line of the pattern was then numbered and tabulated together with the value of 2θ° and the intensity of the peak. Angles were converted into 'd' values by application of the Bragg law (equation 4.4) and finally the diffraction data was interpreted using the Powder Diffraction File for Inorganic Phases(227).

CHAPTER 5

RESULTS

5 RESULTS

5.1 Surface Hardness

5.1.1 Conventional (Vickers) Microhardness Testing

-Steels

Since indentation depths even at low loads are much greater than the projected range of nitrogen ions, only a percentage gain in microhardness with respect to the unimplanted material is meaningful. The relative hardness index (RHI), defined as the ratio of the nitrogen implanted hardness value to that of the untreated specimen, is a very useful parameter to assess the hardening effect brought about by the implantation.

$$\text{RHI} = \frac{\text{Hardness implanted surface}}{\text{Hardness unimplanted surface}} \qquad \text{.... 5.1}$$

Table 13 shows the RHI values for tool steels under different implantation conditions.

Table 13 - Relative hardness index for nitrogen implanted tool steels. (Vickers, 5g load)

Materials	Nitrogen dose (x 10^{17} ions/cm^2)					
(AISI code)	2	3	4	5	6	7
M2$^{(a)}$	1.02	1.12	1.15	1.15		
M2$^{(b)}$	1.26	1.33	1.38	1.37	1.39	1.38
M2$^{(b+c)}$		1.12	1.37	2		
D2$^{(a)}$	1.10	1.14	1.16	1.15		
D2$^{(b)}$	1.27	1.39	1.41	1.46	1.51	1.50
D2$^{(b+c)}$		1.30	1.87	1.97		
420$^{(a)}$	1.09	1.11	1.13	1.16		
420$^{(b)}$	1.53	1.65	1.71	1.73	1.77	1.81

Key: (a) Implantation at 6 μA/cm^2. Water cooling and rotation of samples.
(b) Implantation at 3.5 μA/cm^2. No rotation or cooling of samples.
(c) Annealed material.

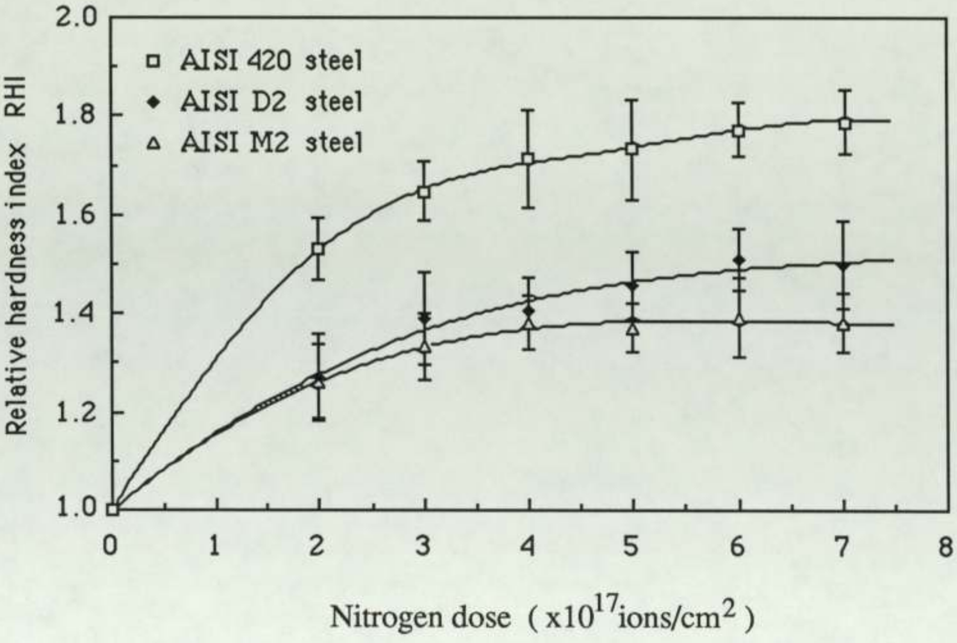

Fig.40: Variation of surface hardness of tool steels with nitrogen dose. Vickers, 5g. load.

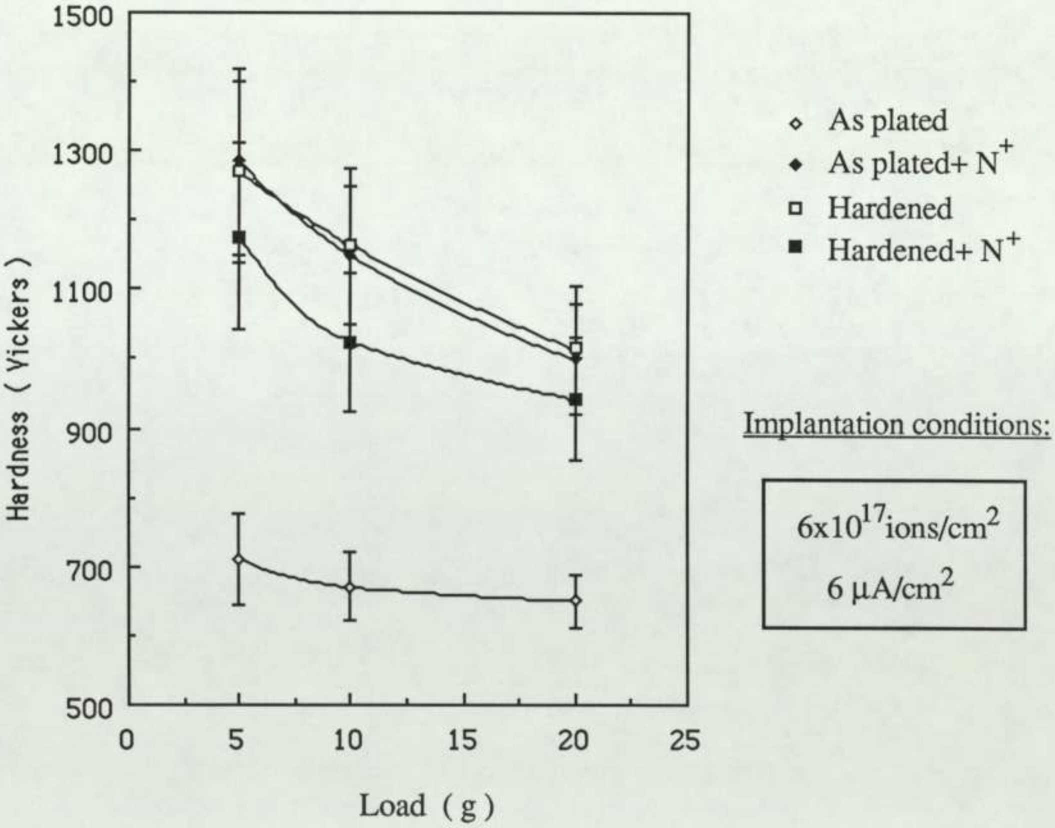

Fig.41: Effect of varying load on microhardness of electroless Ni-P coatings

It can be seen, as expected, that hardness values depend on implantation conditions and the composition of substrate material. The improvement in hardness achieved as a function of nitrogen dose for steels implanted without rotation or water cooling is indicated in Figure 40.

-Coatings

RHI values for the coating system investigated in this work are indicated in Table 14.

Table 14 - Relative hardness index for nitrogen implanted coatings

(Vickers, 5g load)

Coating	Nitrogen dose (x 10^{17} ions/cm^2) 2	3	4	5	7
Hard Cr $^{(a)}$	1.17	1.33	1.35	1.43	1.33
Ni-P $^{(a+b)}$	0.99	0.99	1		
Ni-P $^{(a+c)}$		0.98			
Co-8 % W $^{(d)}$		1.42			
Co-1.5 % W $^{(a)}$		1.07			

Key:
(a) Implantation at 3.22 μA/cm^2. Water cooling and rotation of samples.
(b) As plated coating.
(c) Hardened coating, (400°C, 1h)
(d) Implantation at 3.5 μA/cm^2. No cooling or rotation of samples.

Figure 41 illustrates the effect of varying indentation load upon hardness of as-plated and hardened electroless nickel coatings. It is shown that implantation conditions can have a significant hardening effect on coatings, especially if these are subjected to precipitation strengthening. Absolute hardness values at such low loads should be treated with caution but they provide a valid comparison between implanted and unimplanted hardness values.

Nitrogen implantation of hard chromium produces significant hardening up to a 43% increase. Figure 42 depicts the percentage hardness improvement achieved on hard chromium coatings, as a function of nitrogen dose.

5.1.2 **Ultra - Low Load Hardness Testing**

Results of ultra-shallow indentation tests on AISI 420 steel and hardened electroless Ni-P alloy before and after nitrogen implantation at 6 x 10^{17} ions/cm^2 (6 μA/cm^2), are presented in Figures 43 to 45.

An example of individual depth-load run for this technique, showing loading and unloading curves can be seen in Figure 34. Figure 43 illustrates the indentation depth (∂) against the square root of the load (P) for AISI 420 steel. Each point in the graph represents the average of typically 3 to 10 data; impressions were made at least 30 μm apart. Only loading curves are shown, with the values "off-load", ie. the elastic recovery parameter (∂'_e/∂_t) has been subtracted (see Figure 34). Figure 44 presents the same data replotted in the form of normalized hardness, relative to a standard silicon control specimen of known doping, as a function of depth. The same figure shows that even at 300 nm depth the implanted AISI 420 specimen is more than twice as hard as the untreated material.

The results for the hardened electroless Ni-P coating are illustrated in Figure 45. This graph depicts, as above, the normalized hardness as a function of depth, and a decrease in hardness value is observed after high dose nitrogen implantation.

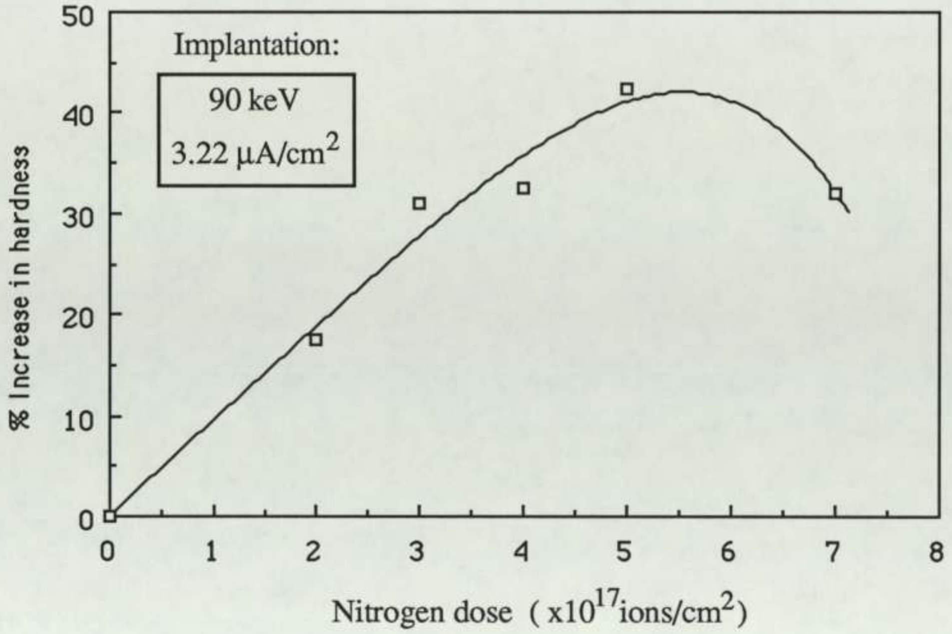

Fig.42: Effect of nitrogen implantation on hardness of hard Cr coating. Vickers, 5g load.

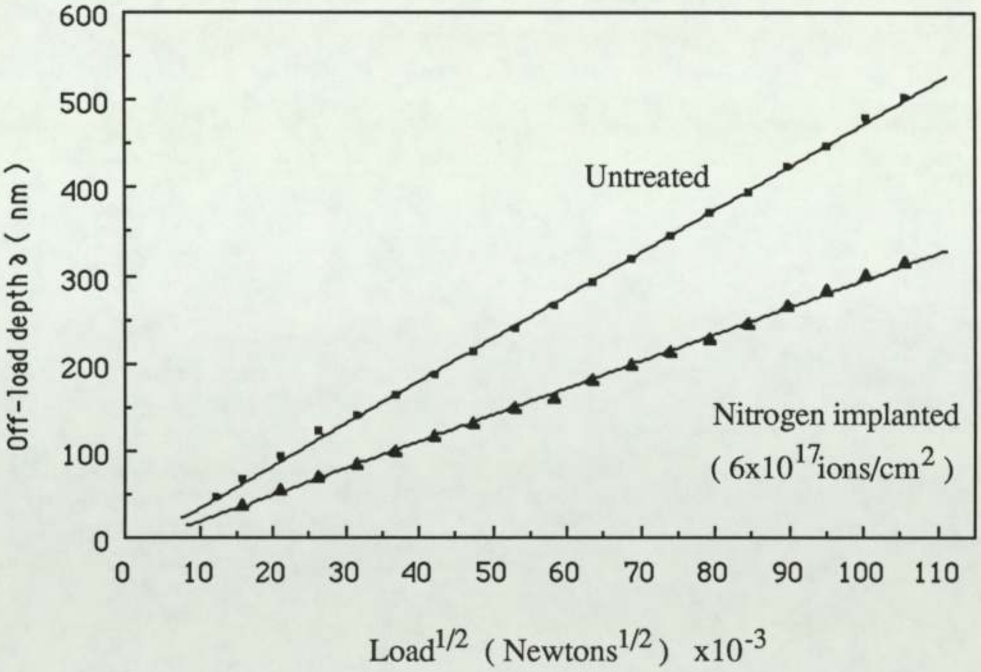

Fig.43: Indentation depth ∂ against square root of load for AISI 420 steel

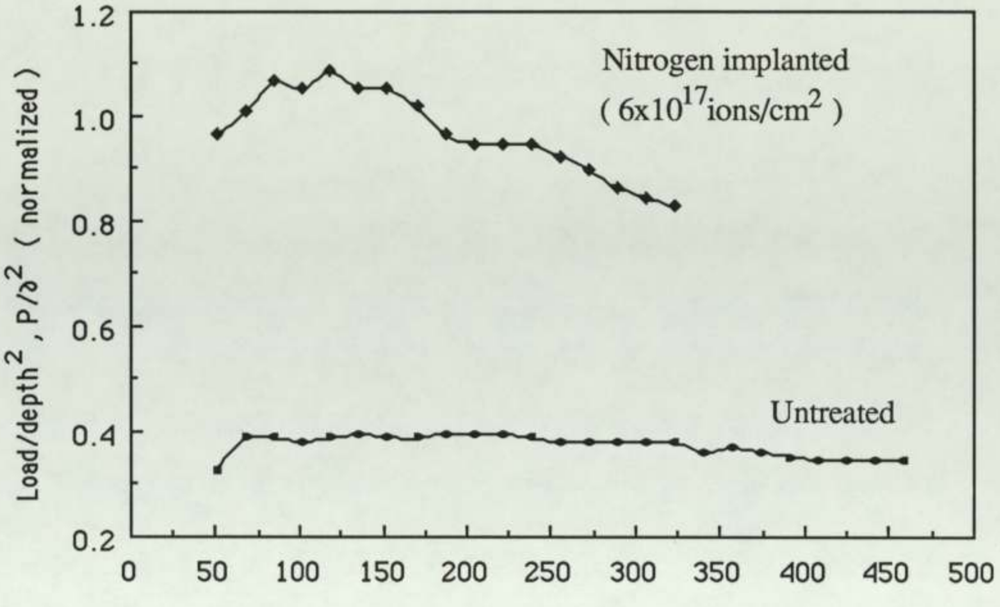

Fig.44: Normalized hardness as a function of depth for AISI 420 steel.

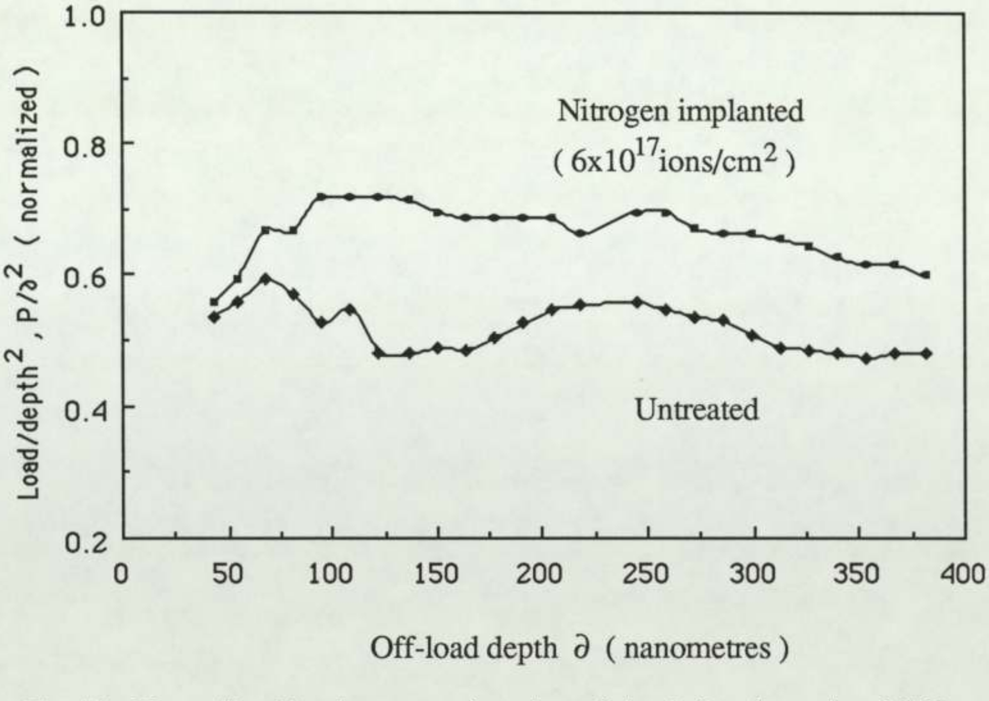

Fig.45: Normalized hardness as a function of depth for electroless Ni-P coatings.

5.2 Wear Testing

5.2.1 Lubricated "Falex" Friction and Wear

5.2.1.1 Steel Materials

The results of the Falex wear tests for tool steel materials are presented in Tables 15 to 18 and Figures 46 to 52. Tables 15 to 17 summarize the averaged results of sets of two or three pins after implantation at doses ranging from 2 to 5×10^{17} ions/cm^2. These results are also illustrated by Figures 46 to 49 for each particular steel. Based on the respective optimum nitrogen dose for every material (see Figure 49) a larger number of specimens were tested and the results are presented in Table 18 and Figure 50. This figure illustrates the variation of the pin weight loss as a function of the testing time. The set(s) of data presented in Figures 46 to 49 cannot be compared directly with that of Figure 50, since due to material restrictions, the same pair of V-blocks was used for each pin in the latter experiments. This probably accounts for any differences observed in wear rates.

Friction coefficient curves can be seen in Figures 51 and 52. The former figure illustrates the effect of nitrogen implantation dose on the friction coefficient of AISI D2 steel and Figure 52 shows the improvement in frictional properties achieved for AISI 420 as a function of wear time. A significant change in frictional behaviour was not obtained by nitrogen implantation of AISI M2 high speed steel.

Table 15 - Lubricated Falex wear testing results for AISI M2 steel.

900 N load, AISI M2 V-blocks

AISI M2 steel	Wear time (min)	Pin weight loss (mg)	Wear rate $\times 10^{-3}$ mg/min
	30	0.376 ± 0.064	12.53
Untreated	60	0.702 ± 0.044	11.70
	90	0.864 ± 0.056	9.60
	30	0.474 ± 0.039	15.80
2×10^{17} ions/cm^2	60	0.733 ± 0.022	12.22
	90	0.918 ± 0.034	10.20
	30	0.409 ± 0.054	13.63
3×10^{17} ions/cm^2	60	0.620 ± 0.046	10.33
	90	0.784 ± 0.064	8.71
	30	0.179 ± 0.012	5.97
4×10^{17} ions/cm^2	60	0.425 ± 0.030	7.08
	90	0.633 ± 0.005	7.03
	30	0.165 ± 0.016	5.50
5×10^{17} ions/cm^2	60	0.309 ± 0.032	5.15
	90	0.496 ± 0.024	5.51

Note: Final contact pressure ~ 231 MN/m^2. Each result is average of two tests.

Table 16 - Lubricated Falex wear testing results for AISI D2 tool steel. 900 N load. AISI D2 V-blocks

AISI D2 steel	Wear time (min)	Pin weight loss (mg)	Wear rate x10^{-3} mg/min
Untreated	30	0.129 ± 0.035	4.30
	60	0.291 ± 0.037	4.85
	90	0.368 ± 0.006	4.09
	150	0.604 ± 0.073	4.03
2 x 10^{17} ions/cm^2	30	0.017 ± 0.009	0.57
	60	0.170 ± 0.010	2.83
	90	0.206 ± 0.022	2.29
	150	0.362 ± 0.006	2.41
3 x 10^{17} ions/cm^2	30	0.073 ± 0.041	2.43
	60	0.123 ± 0.016	2.05
	90	0.183 ± 0.035	2.03
	150	0.356 ± 0.006	2.37
4 x 10^{17} ions/cm^2	30	0.038 ± 0.017	1.27
	60	0.231 ± 0.024	3.85
	90	0.269 ± 0.010	2.99
	150	0.462 ± 0.055	3.08
5 x 10^{17} ions/cm^2	30	0.123 ± 0.021	4.10
	60	0.212 ± 0.002	3.53
	90	0.283 ± 0.018	3.14
	150	0.478 ± 0.022	3.19

Note: Final contact pressure ~ 245 MN/m^2. Each result is average of 2 or 3 tests.

Table 17 - Lubricated Falex wear testing results for AISI 420 steel
900 N load, AISI 420 V-blocks

AISI 420 steel	Wear time (min)	Pin weight loss (mg)	Wear rate $x10^{-3}$ mg/min
Untreated	30	0.487 ± 0.087	16.23
	60	0.963 ± 0.212	16.05
	90	1.370 ± 0.108	15.22
2×10^{17} ions/cm^2	30	0.220 ± 0.016	7.33
	60	0.654 ± 0.121	10.90
	90	1.016 ± 0.205	11.29
3×10^{17} ions/cm^2	30	0.297 ± 0.051	9.90
	60	0.581 ± 0.056	9.68
	90	0.930 ± 0.163	10.33
4×10^{17} ions/cm^2	30	0.164 ± 0.034	11.27
	60	0.284 ± 0.038	4.73
	90	0.554 ± 0.175	6.16
5×10^{17} ions/cm^2	30	0.338 ± 0.005	11.27
	60	0.554 ± 0.033	9.23
	90	0.738 ± 0.062	8.20

Note: Final contact pressure ~ 252 MN/m^2 (MPa). Each result is average of 2 tests.

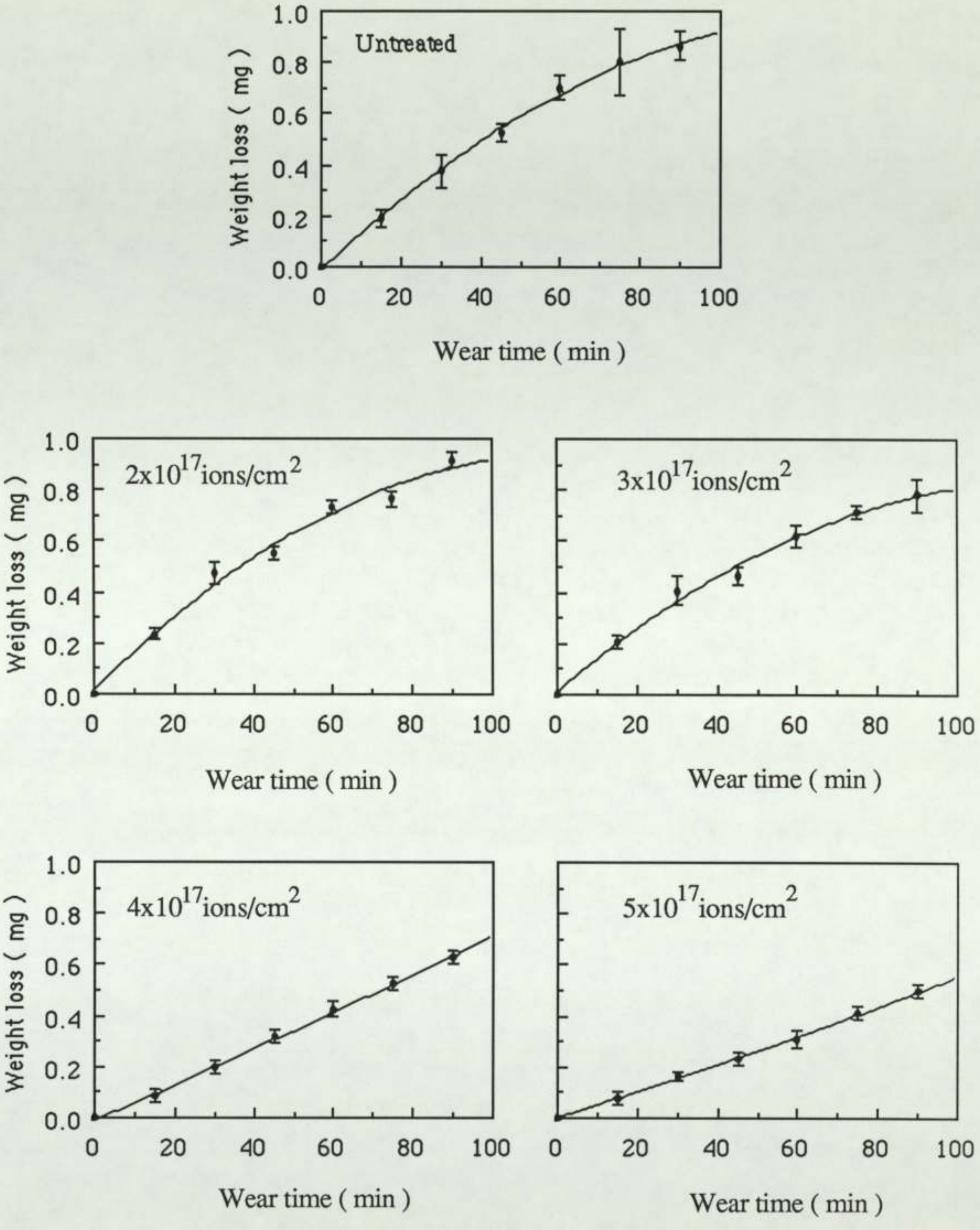

Fig.46: Falex wear results of AISI M2 high speed steel.

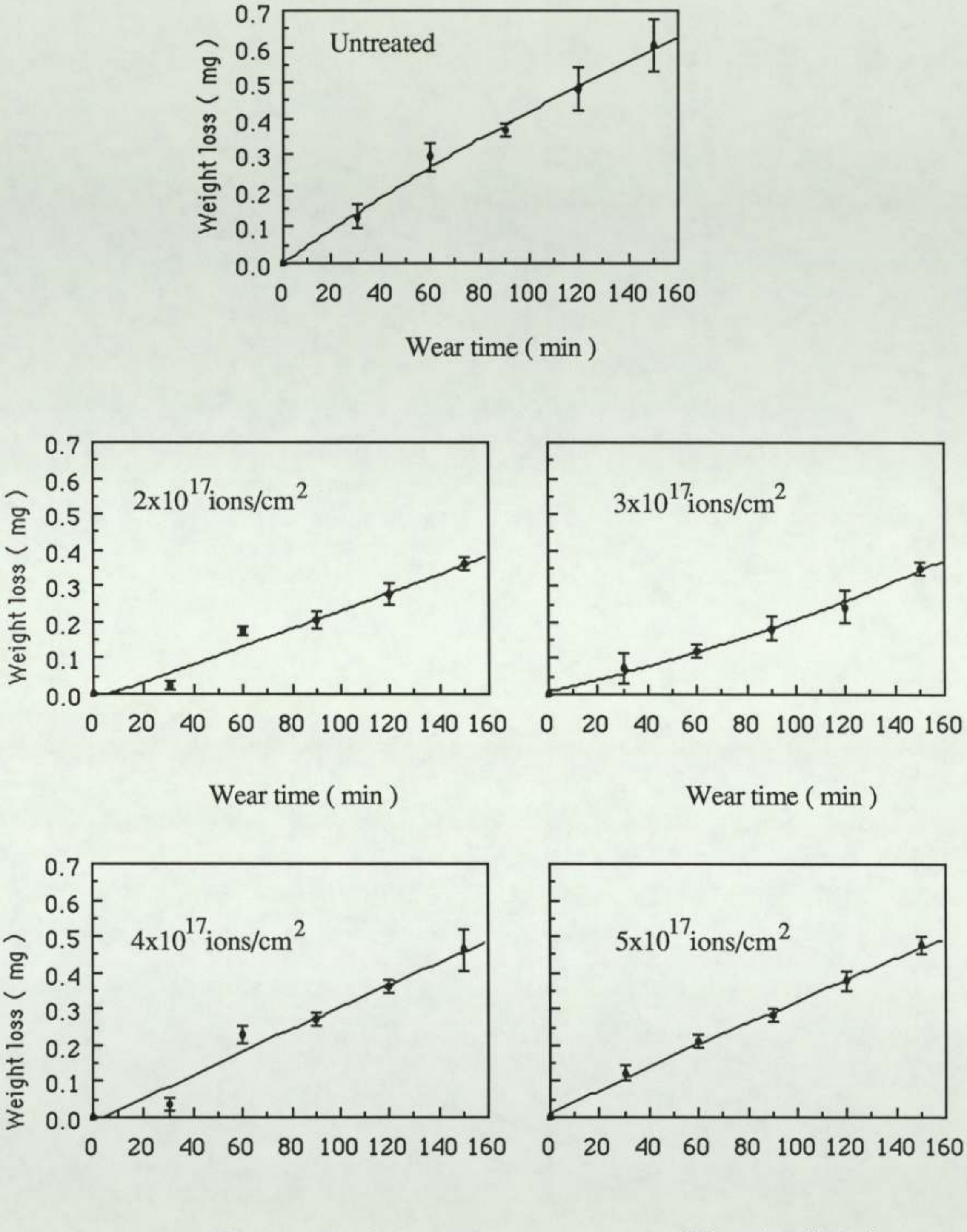

Fig.47: Falex wear results of AISI D2 cold work tool steel

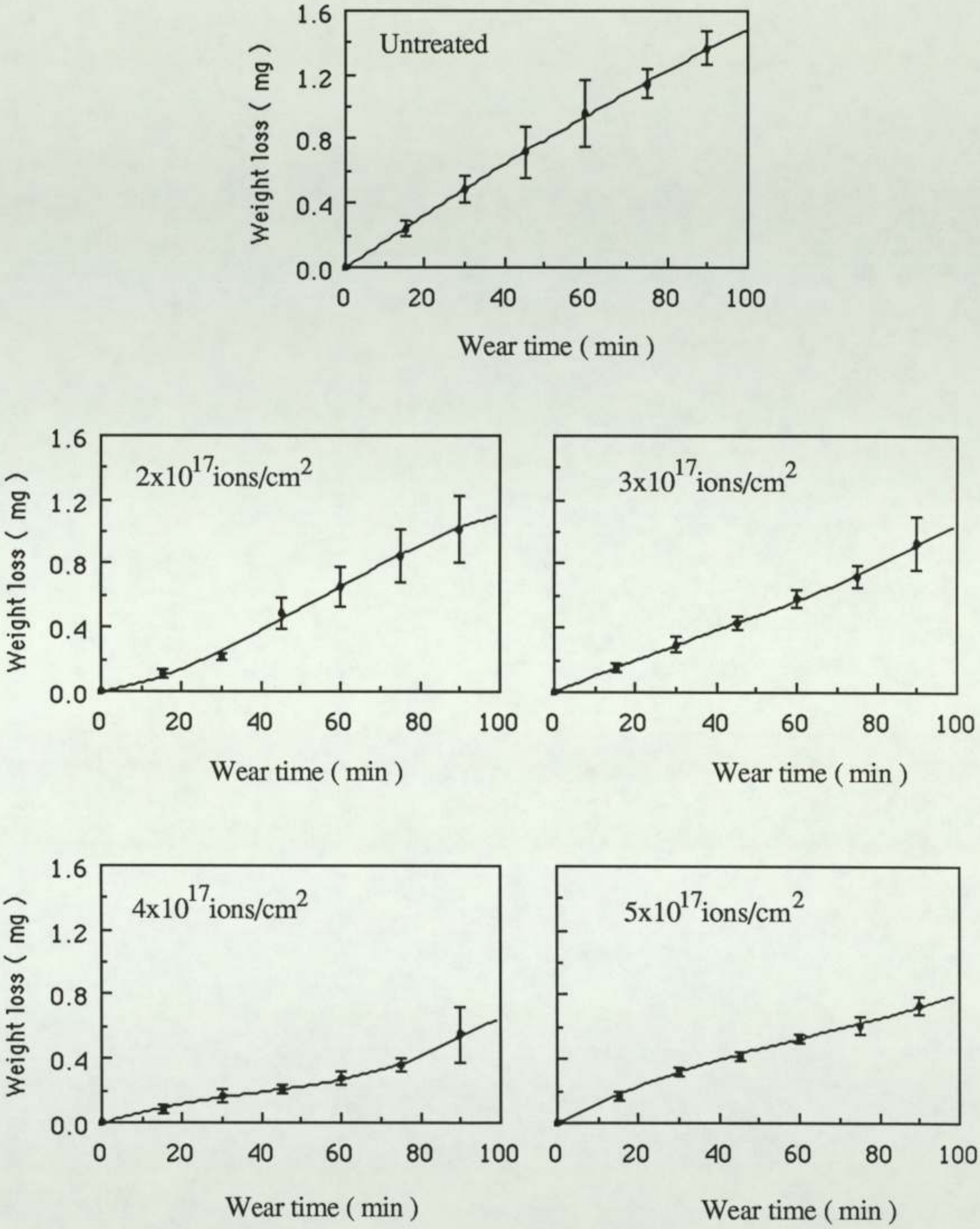

Fig.48: Falex wear results of AISI 420 martensitic stainless steel

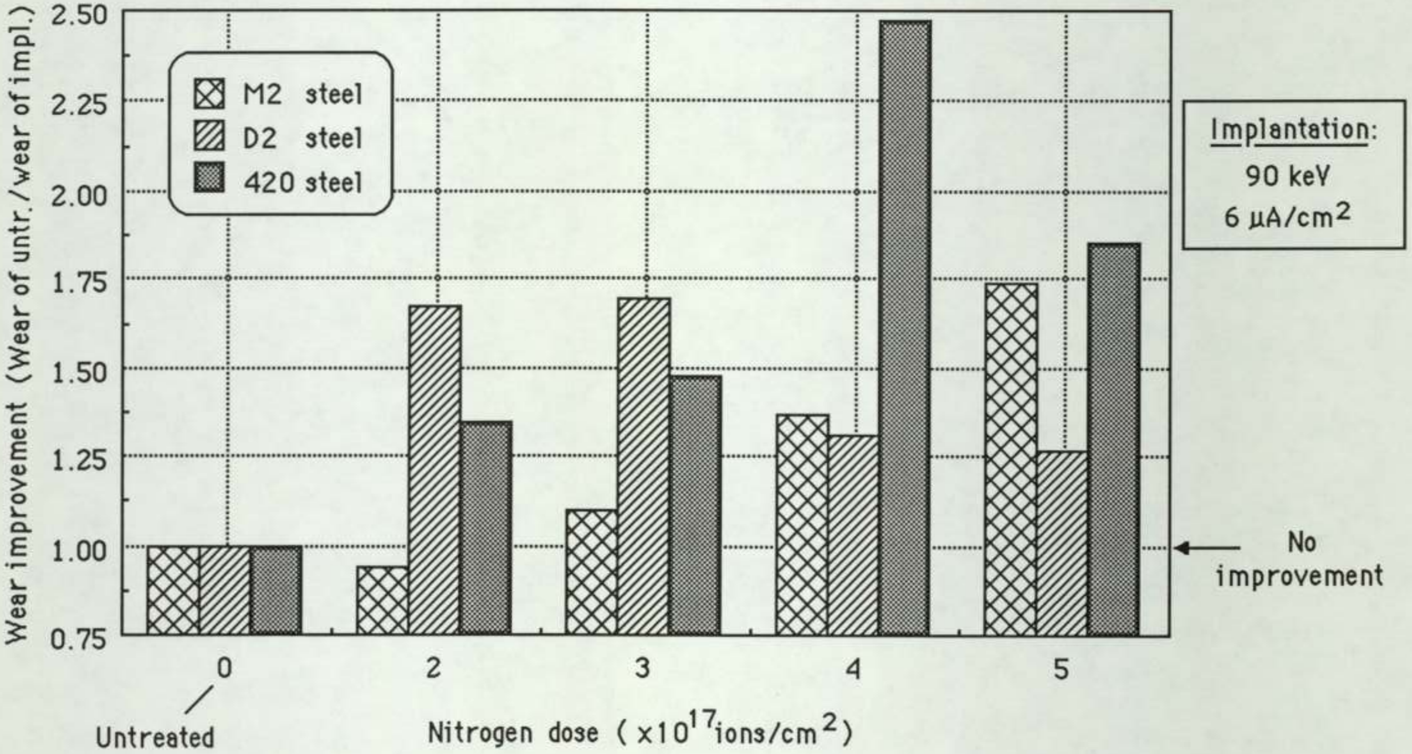

Fig.49: Wear reduction factors for AISI M2, D2 and 420 tool steels

Op. cond.: Lubricated Falex testing. 900 N load. 290 rpm

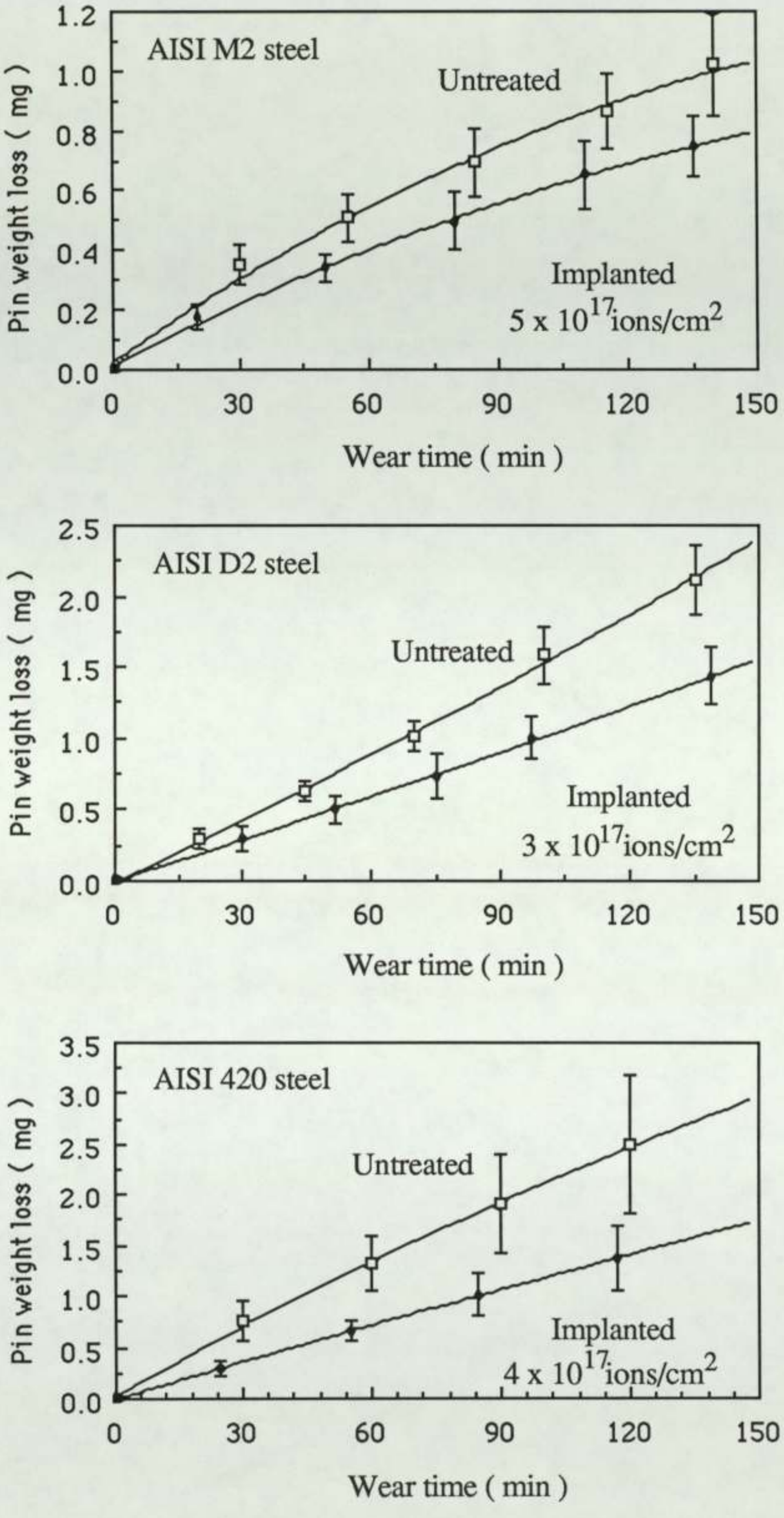

Fig.50: Falex wear results of AISI M2, D2 and 420 steels.
Like-on-like material lubricated testing. 900 N load.

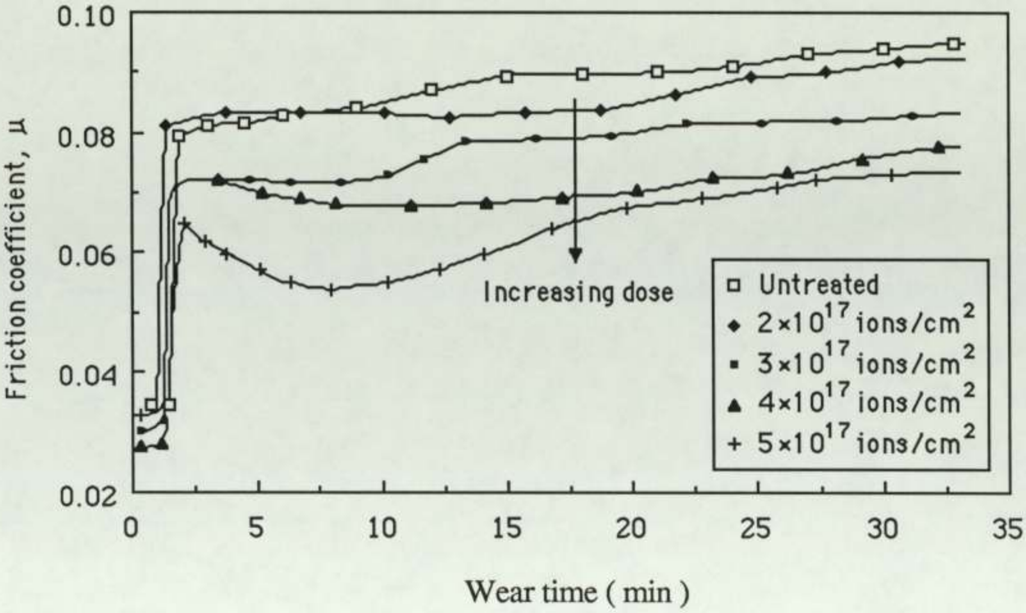

Fig.51: Variation of friction coeff. as a function of nitrogen dose for AISI D2 steel.

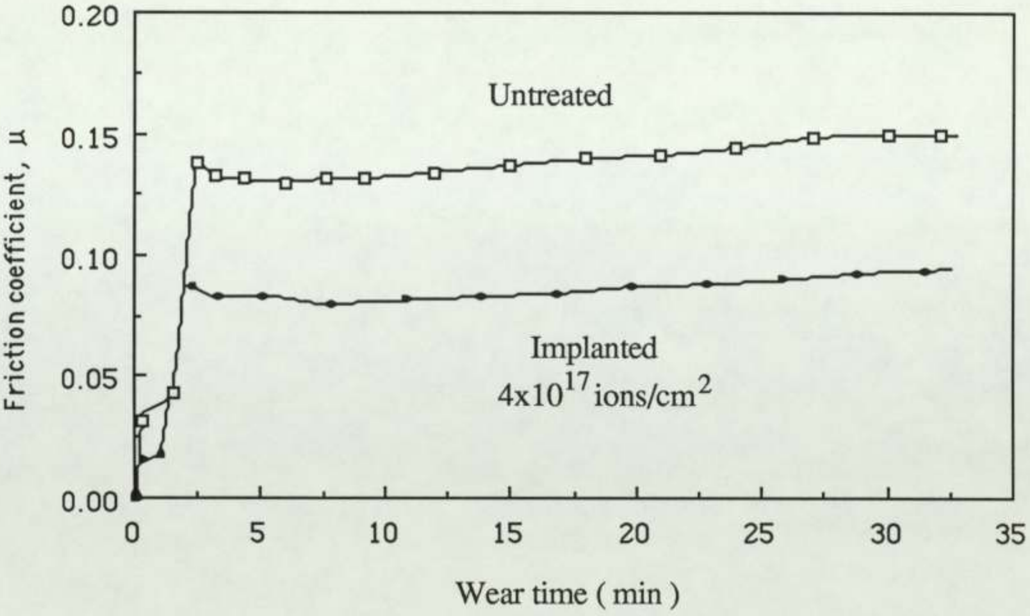

Fig.52: Friction curves for AISI 420 martensitic stainless steel.

Table 18 - Falex wear tests results for steels. Wear rate in g x 10^{-6}/min. Operating conditions: 900 N load, lubricated, 140 minutes wear time

Pin	AISI M2		AISI D2		AISI 420	
Code	Untreated	5×10^{17}	Untreated	3×10^{17}	Untreated	4×10^{17}
1	7.320	6.783	13.141	10.000	23.428*	11.070
2	6.233	5.712	18.636	8 496	25.888*	14.289
3	9.379	5.769	15.187	10.550	13.890	15.565
4	7.254	4.728	15.195	9.900	26.712*	8.850
5	6.248	4.693	16.329	12.790	15.730	9.154
Mean	7.287	5.537	15.698	10.347	20.730	11.786
St. dev.	1.282	0.867	2.005	1.562	6.431	3.025

*Test stopped due to seizure of the pin.
Note: Optimum implantation doses in ions/cm^2 for each material

5.2.1.2 Coatings

Friction and wear test results for hard chromium, electroless nickel-phosphorus and electrodeposited cobalt-tungsten coatings are presented in Tables 19 to 21 and Figures 53 to 57.

Tables 19 and 20 summarize the wear data for hard chromium and electroless Ni-P coatings after nitrogen implantation at doses from 2 to 7×10^{17} ions/cm^2. These results are also presented in Figures 53 and 55 respectively, which depict the pin weight loss as a function of wear time. Samples of chromium coatings with a "milky" appearance and softer (700 $HV_{0.1}$, Type I coating) than the conventional chromium deposits (1050 $HV_{0.1}$, Type II coating) were also nitrogen implanted and the results presented in Figure 54. It is shown that nitrogen implantation produces a significant wear improvement in chromium electrodeposits, but little or an adverse effect on already hardened electroless Ni-P coatings.

Results of hard chromium coated pins implanted at the optimum nitrogen dose (ie. 5×10^{17} ions/cm^2) are presented in Table 21 and Figure 56. Limited work was also carried out on a new high efficiency hard Cr coating (1200 $HV_{0.1}$, Type III coating) and the wear results are depicted in Figure 57. Table 22 and Figure 56 illustrate the data obtained for Co-1.5% W coatings implanted at a nitrogen dose of $3x10^{17}$ ions/cm^2. Frictional curves for both coatings, conventional hard chromium (Type II) and cobalt-tungsten, are shown in Figure 58.

Table 19 - Lubricated Falex wear testing results for hard chromium. (Type II coating) 710 N load, AISI 52100 steel V-blocks

Hard Cr coating	Wear time (min)	Pin weight loss (mg)	Wear rate $x10^{-3}$ mg/min
*Untreated	30	0.267 ± 0.110	8.90
	60	1.040 ± 0.430	17.33
	90	2.098 ± 0.697	23.31
2 x 10^{17} ions/cm^2	30	0.225 ± 0.201	7.50
	60	0.657 ± 0.550	10.95
	90	1.264 ± 1.062	14.04
3 x 10^{17} ions/cm^2	30	0.095 ± 0.080	3.17
	60	0.514 ± 0.392	8.57
	90	1.083 ± 0.752	12.03
4 x 10^{17} ions/cm^2	30	0.087 ± 0.052	2.90
	60	0.410 ± 0.246	6.83
	90	0.945 ± 0.650	10.50
*5 x 10^{17} ions/cm^2	30	0.043 ± 0.031	1.43
	60	0.248 ± 0.153	4.13
	90	0.522 ± 0.243	5.80
7 x 10^{17} ions/cm^2	30	0.054 ± 0.011	1.80
	60	0.316 ± 0.091	5.27
	90	0.679 ± 0.219	7.54

Note: Each result is the average of three tests, but (*) average of five tests.

Table 20 - Lubricated Falex wear testing results for hardened Ni-P coatings. 710 N load. AISI 52100 steel V-blocks

Electroless Ni-P	Wear time (min)	Pin weight loss (mg)	Wear rate $x10^{-3}$ mg/min
	30	0.150 ± 0.050	5.00
Untreated	60	0.348 ± 0.065	5.80
	90	0.699 ± 0.200	7.77
	30	0.269 ± 0.120	8.97
2×10^{17} ions/cm^2	60	0.821 ± 0.060	13.68
	90	1.911 ± 0.264	21.23
	30	0.284 ± 0.050	9.47
3×10^{17} ions/cm^2	60	0.699 ± 0.304	11.65
	90	0.954 ± 0.555	10.60
	30	0.186 ± 0.066	6.20
7×10^{17} ions/cm^2	60	0.408 ± 0.022	6.80
	90	0.780 ± 0.283	8.67

Note: each result is the average of 2 to 4 tests

Table 21 - Falex wear test results for hard chromium (Type II coating)

Operating conditions: 710 N, lubricated, 90 minutes wear time

	Untreated		Nitrogen implanted	
Pin code	Weight loss (mg)	Wear rate $x10^{-3}$ mg/min	Weight loss (mg)	Wear rate $x10^{-3}$ mg/min
1	3.149	34.985	0.361	4.014
2	2.052	22.801	0.779	8.655
3	2.339	25.992	0.458	5.088
4	1.451	16.111	0.771	8.564
5	1.500	16.670	0.243	2.703
Mean	2.098	23.312	0.522	5.805
St. dev.	0.697	7.741	0.243	2.696

Note: Nitrogen dose for implanted coating is 5 x 10^{17} ions/cm^2.

Table 22 - Falex wear test results for Co-1.5% W coatings

Operating conditions: 710 N, lubricated, 90 minutes wear time

	Untreated		Nitrogen implanted	
Pin code	Weight loss (mg)	Wear rate $x10^{-3}$ mg/min	Weight loss (mg)	Wear rate $x10^{-3}$ mg/min
1	3.242	36.025	0.873	9.702
2	2.217	24.639	1.183	13.145
3	2.189	24.327	0.782	8.693
4	3.102	34.465	1.245	13.836
5	2.688	29.865	1.265	14.052
Mean	2.688	29.864	1.070	11.886
St. dev.	0.487	5.410	0.225	2.502

Note: Nitrogen dose for implanted coating is 3 x 10^{17} ions/cm^2.

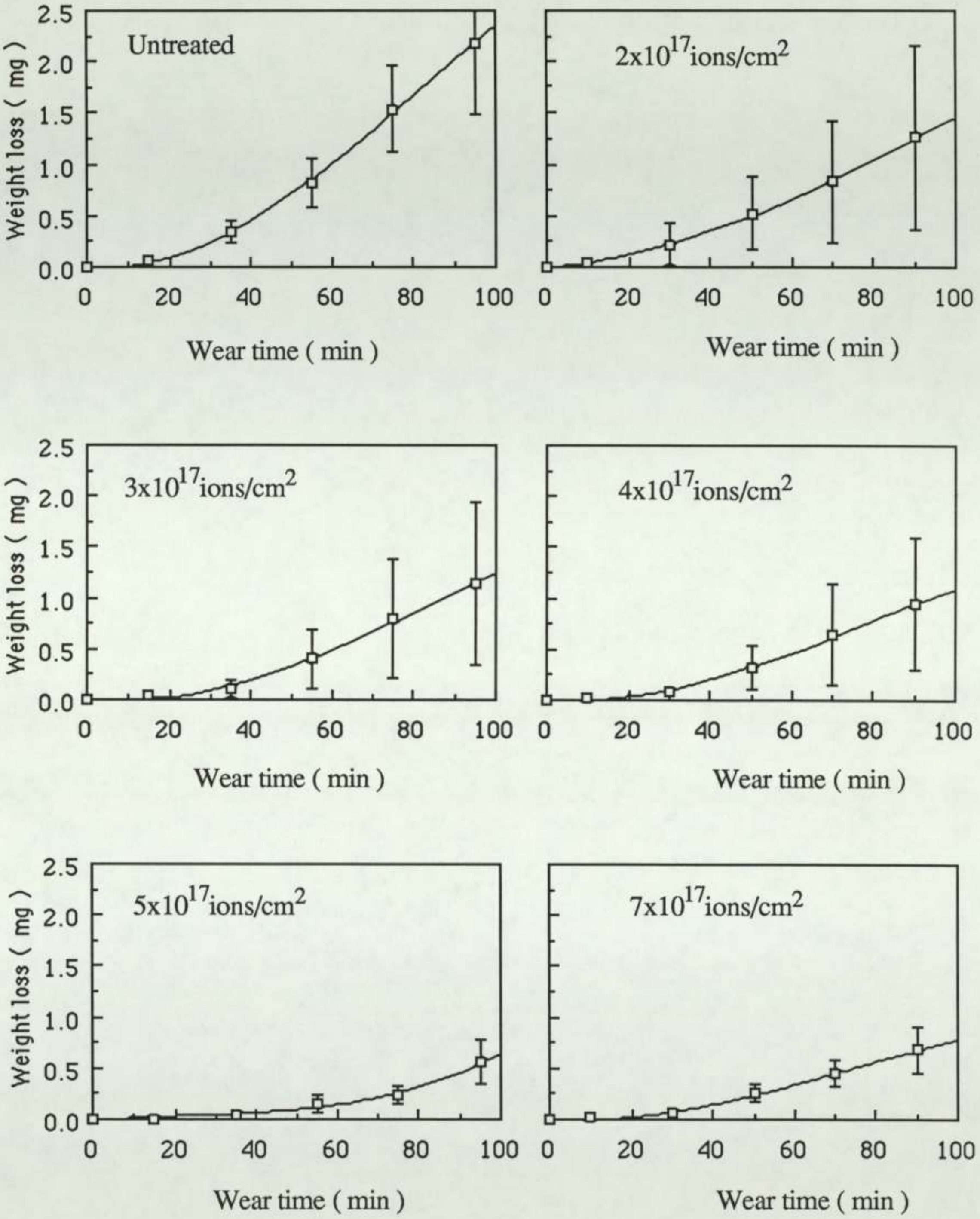

Fig.53: Lubricated Falex wear results of hard Cr coatings. (Type II, 1050 $HV_{0.1}$)

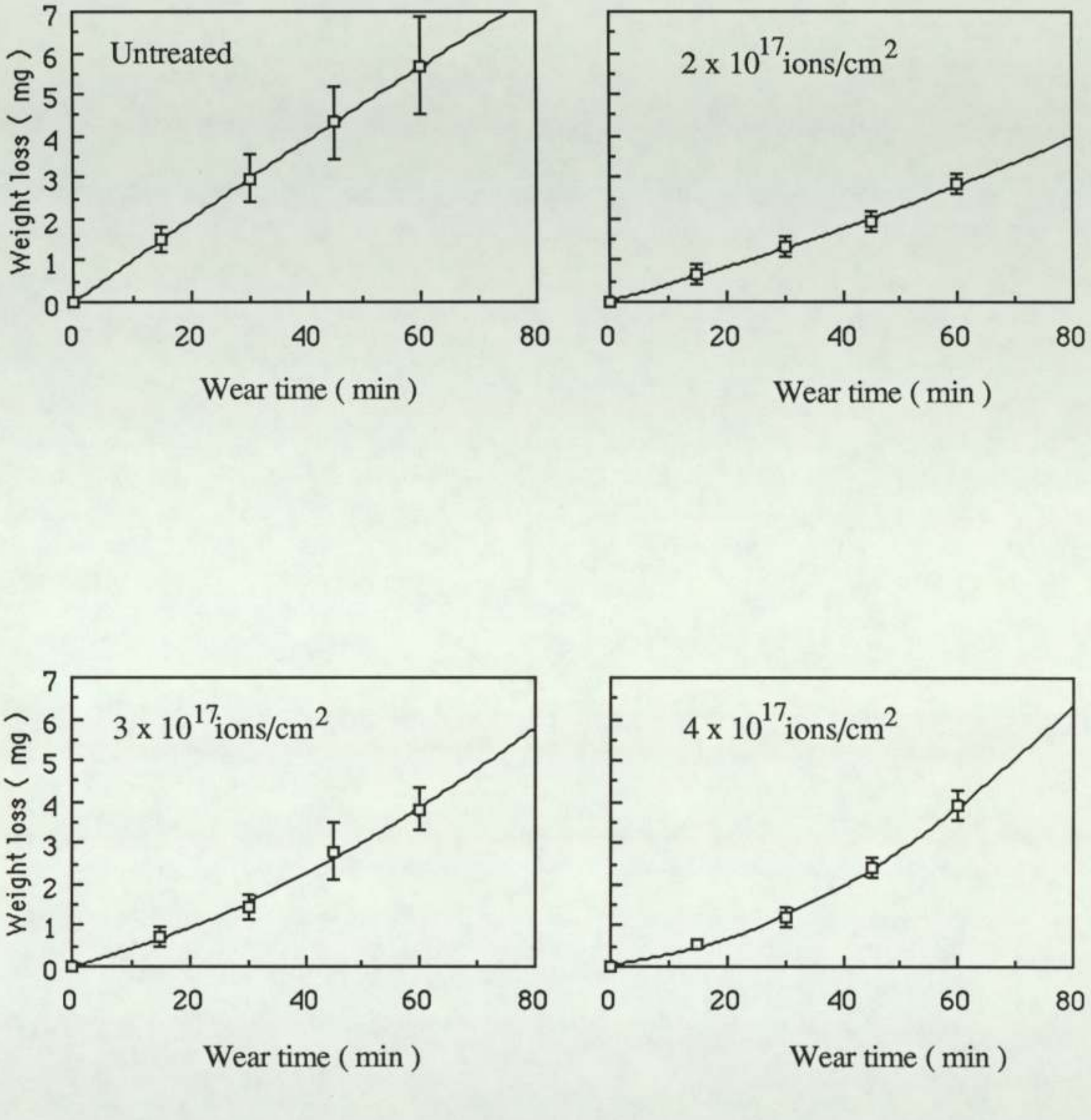

Fig.54: Lubricated Falex wear results of hard Cr coatings. (Type I, 700 $HV_{0.1}$)

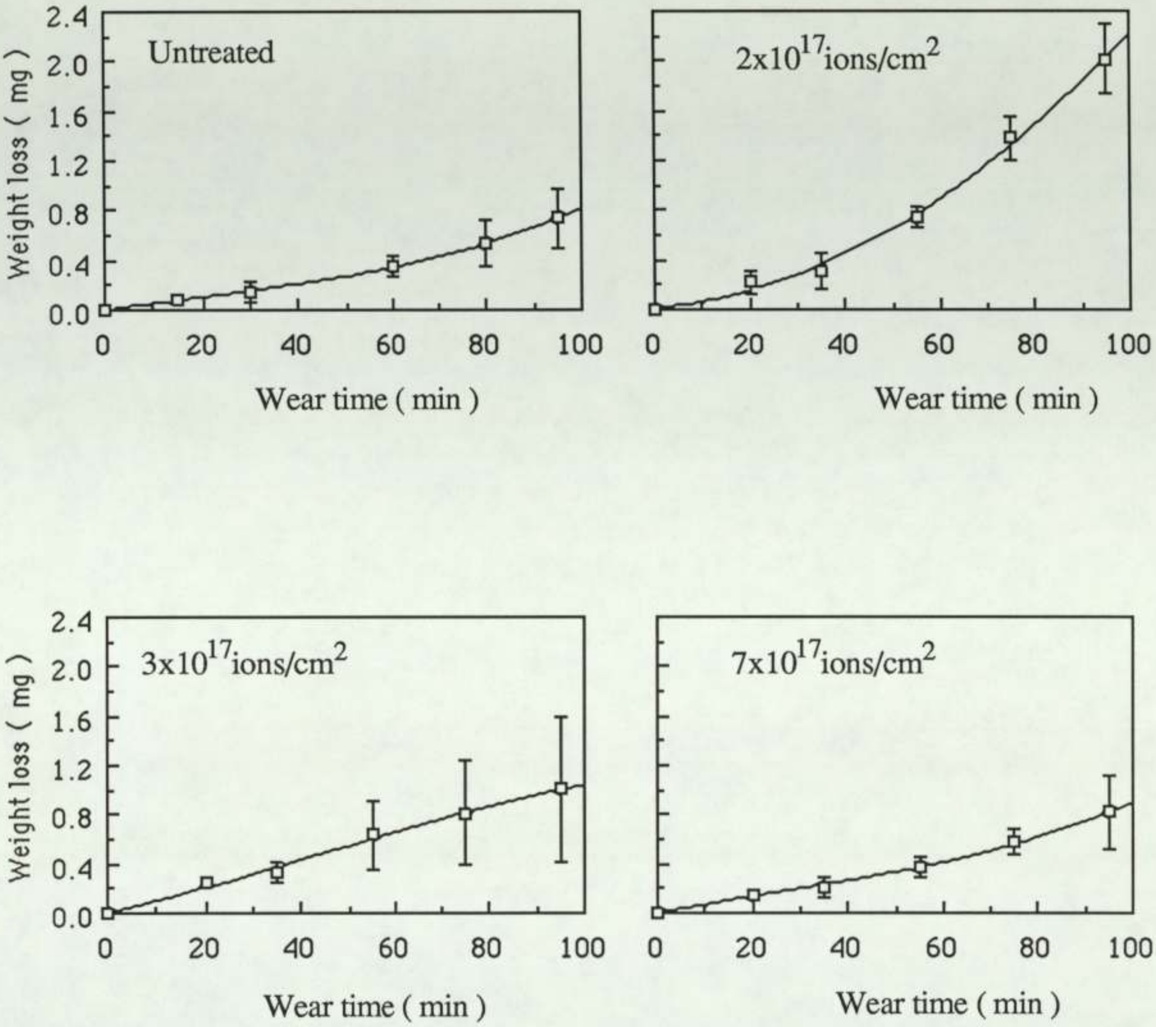

Fig.55: Lubricated Falex wear results of hardened electroless Ni-P coatings.

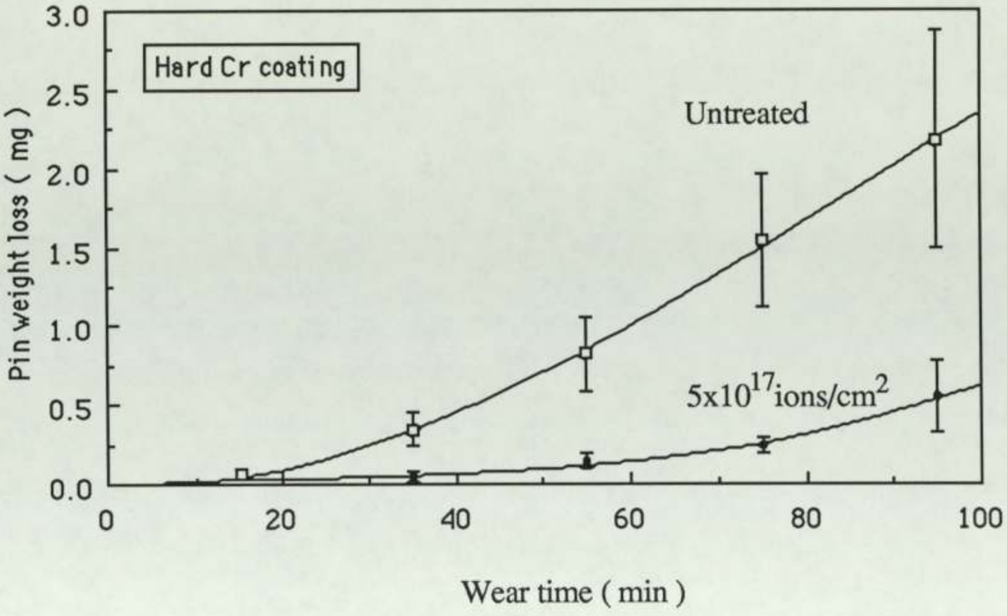

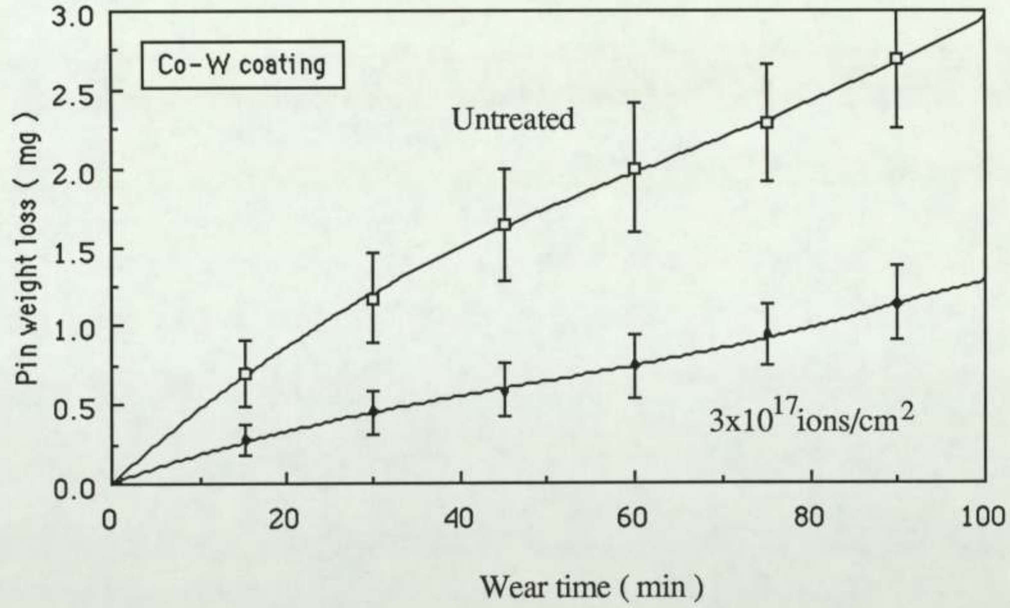

Fig.56: Lubricated Falex wear results of Hard Cr (Type II) and Co-W coatings
Oper. cond.: 710 N load. AISI 52100 steel V-blocks.

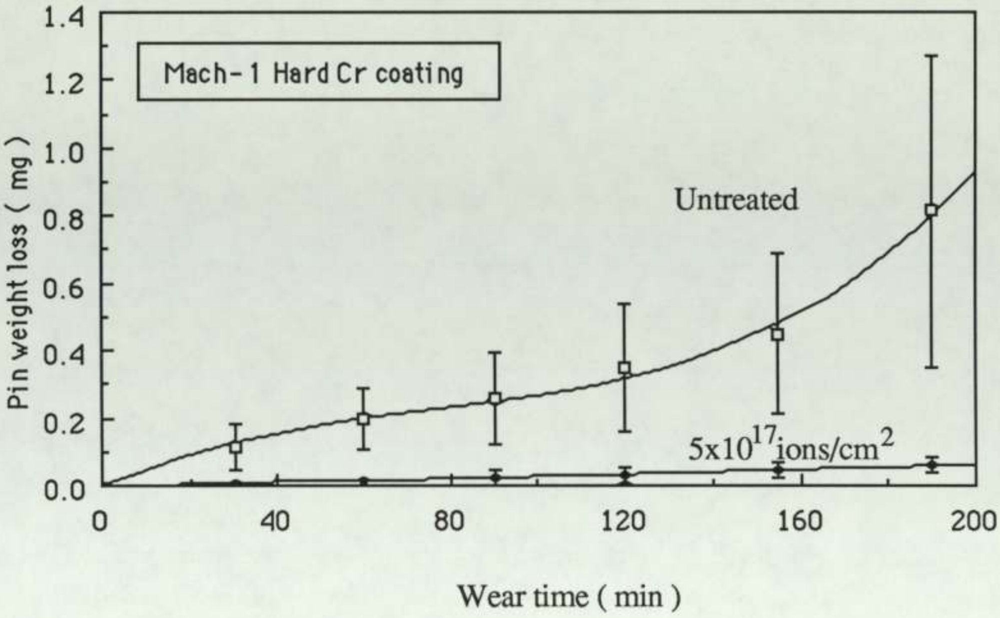

Fig.57: Lubricated Falex wear results of high efficiency hard Cr (Type III) coatings. Oper. cond.: 710 N load. AISI 52100 steel V-blocks.

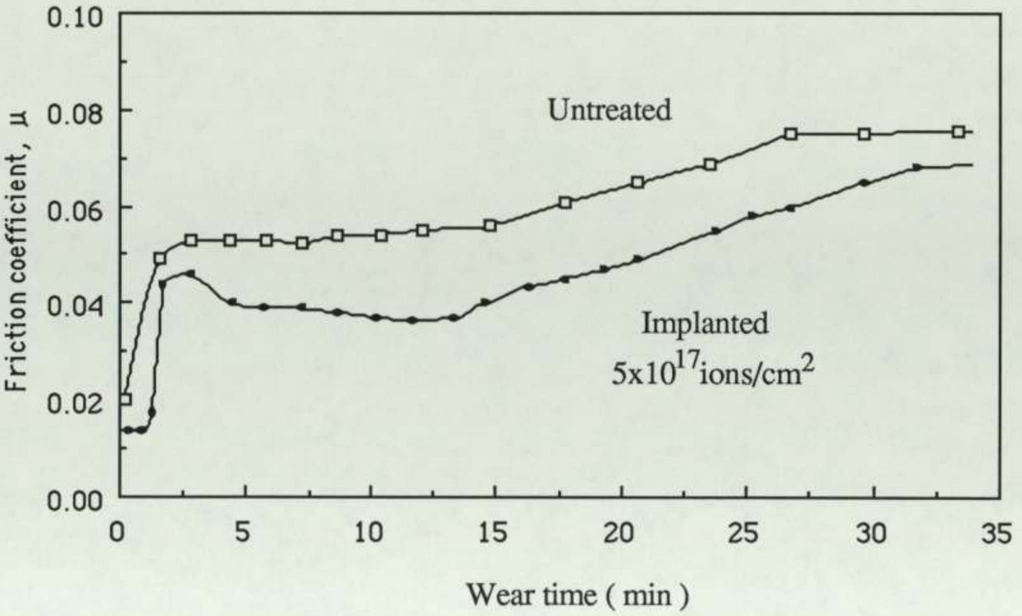

Lubricated Falex friction of hard Cr coating

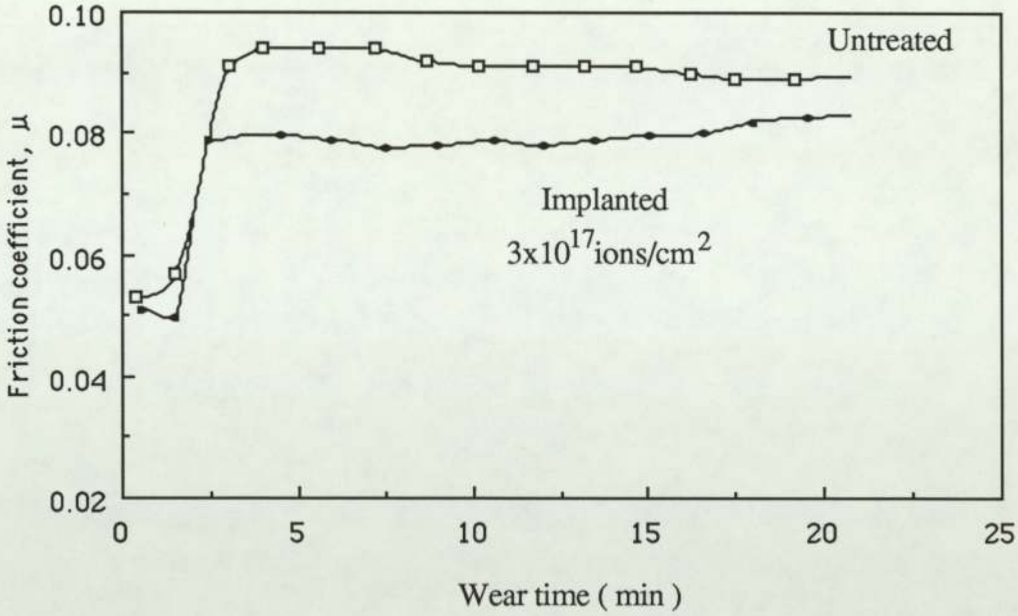

Lubricated Falex friction of Co-W coating

Fig.58: Friction curves of hard Cr (Type II) and Co-W coatings

5.2.2 Unlubricated "Pin-on-disc" Wear Testing

Pin-on-disc wear testing was conducted only on tool steel specimens and the results are summarized in Tables 23 and 24 and Figures 59 to 61.

Table 23 presents the wear results of AISI M2 high speed steel tested at loads from 9.81 to 39.23 N. In this table the gravimetric pin wear rate, K_W, is described as:

$$K_W = \frac{\text{Weight loss}}{\text{Sliding distance x Area of contact}} \qquad .... 5.2$$

and is presented as a function of the applied load. These results are also illustrated in Figure 60.

Table 24 summarizes wear data obtained with AISI D2 and 420 steels, with 9.81 N load and 0.5 m/s sliding speed operating conditions. The variation of the pin weight loss as a function of sliding distance was calculated from these experiments and illustrated in Figure 59 for untreated and nitrogen implanted steels. Tables 23 and 24 also indicate the final coefficient of friction for each particular steel and test condition. Figure 61 shows the variation in running-in friction coefficient for untreated and nitrogen implanted AISI 420 martensitic stainless steel. After running-in was completed friction values for untreated and implanted steels were approximately the same.

Table 23 - Unlubricated pin-on-disc wear results of AISI M2 high speed steel

Material	Load (N)	Slid Distance (m)	Weight loss x 10^{-3} g	K_w x10^{-3} g/m x m^2	μ_{final}
AISI M2	9.81	1772	0.280	14	0.61
	19.61	1751	0.645	26	0.62
(Untreated)	29.42	1705	1.062	37	0.72
	39.23	1243	0.236	21	0.53
AISI M2	9.81	2150	0.367	12	0.60
	19.61	2150	0.860	22	0.69
($4x10^{17}$	29.42	1556	0.768	25	0.76
ions/cm^2)	39.23	1436	0.119	7	0.52

Oper. Cond.: 0.3 to 0.5 m/s sliding speed. 57-60% relative humidity. 23° C

Table 24 - Unlubricated pin-on-disc wear results of AISI D2 and 420 steels

Material	Sliding distance (m)	Weight loss x 10^{-3} g	K_w x10^{-3}g/m x m^2	μ_{final}
AISI D2 (Untreated)	11528	2.92	9.00	0.77
	10800	1.89	6.20	0.73
	4647 *	0.86	19.64	0.91
AISI D2 (3x10^{17} ions/cm^2)	12315	2.00	5.70	0.67
	11235	11.01	3.20	0.71
AISI D2 (4x10^{17} ions/cm^2)	6600	1.47	8.00	0.75
	5161	0.38	14.60	0.77
AISI 420 (Untreated)	7207	2.43	12.00	0.65
	8355	4.73	20.00	0.71
	7215	2.88	14.10	0.74
	5832 *	3.26	19.80	0.69
AISI 420 (3x10^{17} ions/cm^2)	7808	0.21	1.20	0.77
	7785	1.25	5.70	0.62
	7218	0.33	2.10	0.71
AISI 420 (4x10^{17} ions/cm^2)	7350 *	0.82	4.00	0.77
	6204 *	0.89	5.00	0.66

Oper. cond.: 9.81N load, 0.5 m/s sliding speed, 15° C room temperature.

*Note: Tests carried out at 23° C and 57-60% R.H.

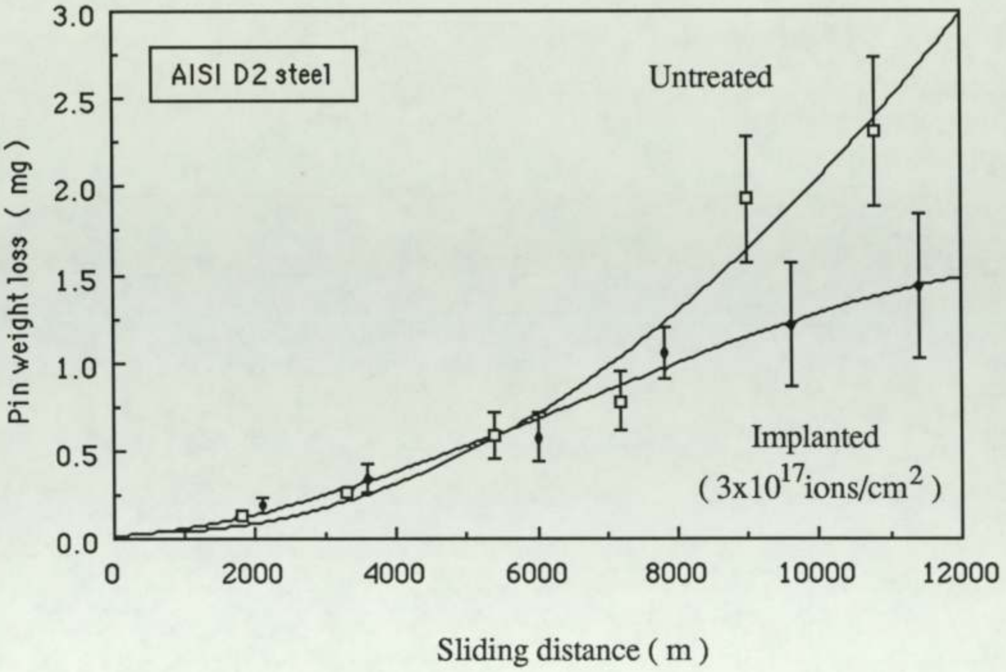

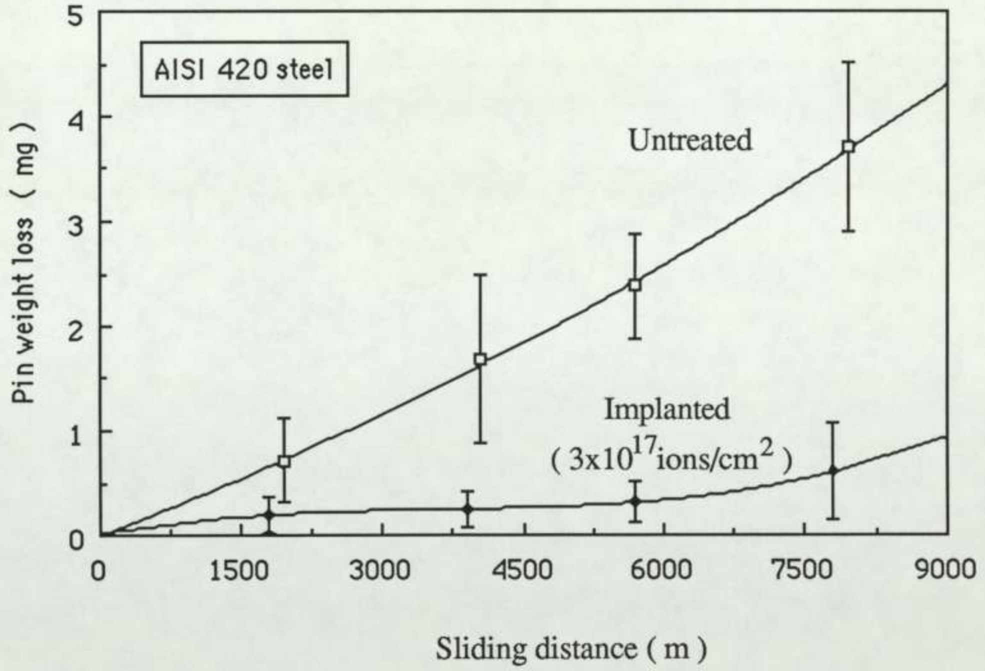

Fig.59: Unlubricated pin-on-disc wear of AISI D2 and 420 steels.
Oper. cond.: 9.81 N load. 0.5 m/s sliding speed.

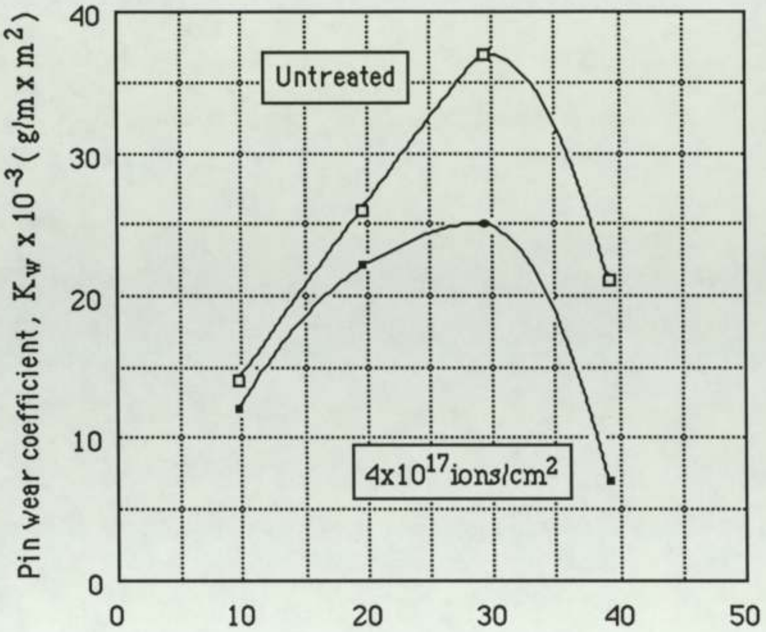

Load (Newtons)

$$K_w = \frac{\text{Weight loss}}{\text{Slid. distance x Contact area}}$$

Fig.60: The effect of load on the gravimetric wear rate of AISI M2 steel.

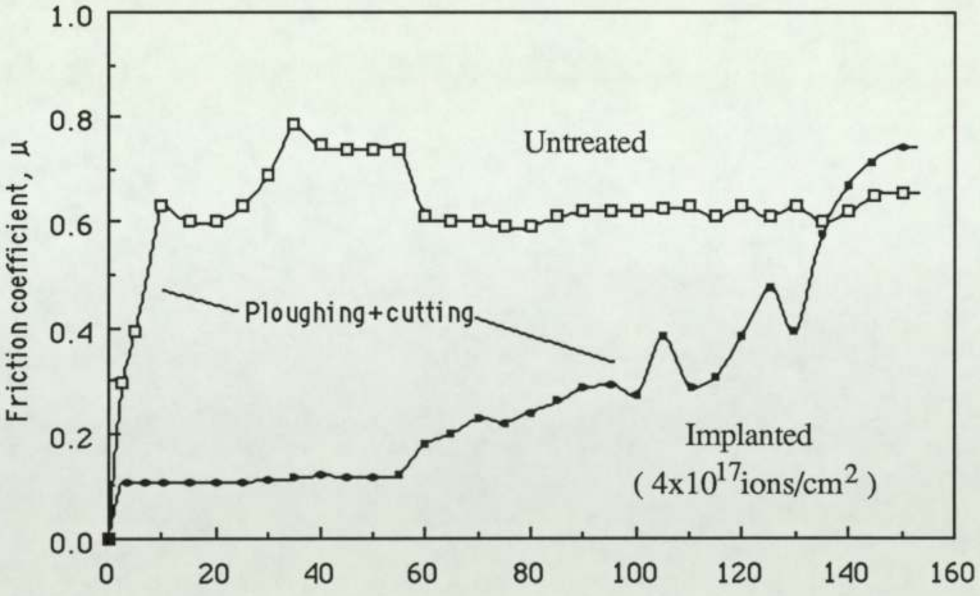

Wear time (min)

Fig.61: Unlubricated pin-on-disc running-in friction of AISI 420 steel.
Oper. cond.: 9.81 N load. 0.5 m/s sliding speed. AISI 420 steel disc.

5.3 Examination of Worn Surfaces

5.3.1 Profilometry

Some characteristic surface profiles taken from the worn areas of lubricated Falex wear testing samples are presented in Figures 62 to 64.

Figure 62 depicts profilometer traces of worn steel surfaces after approximately 140 minutes wear testing at a load of 900 N. The wear behaviour of these steels, AISI M2, D2 and 420 respectively has already been shown in Figure 50.

Figures 63 and 64 present the profiles of wear tracks on chromium and Co-W coatings. Figure 63 illustrates the traces obtained for chromium coatings (Type I - 700 $HV_{0.1}$) after 60 minutes wear at 710 N load. Similar traces after 90 minutes wear can also be seen in Figure 64 for a harder Cr coating (Type II - 1050 $HV_{0.1}$) implanted at the optimum dose of 5 x 10^{17} ions/cm^2 and a Co-1.5% W coating implanted at 3 x 10^{17} nitrogen ions/cm^2 respectively.

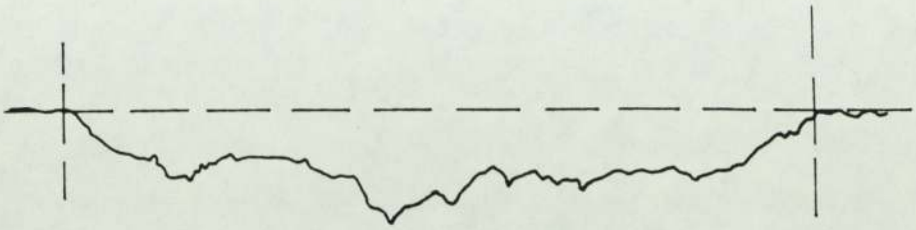

Untreated AISI M2 steel

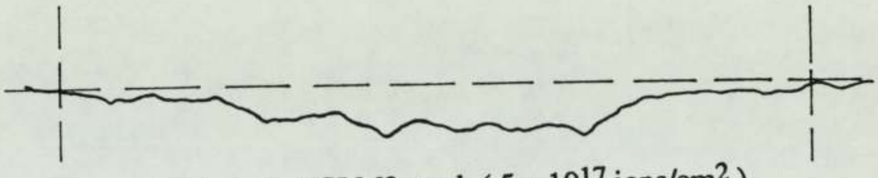

Implanted AISI M2 steel (5×10^{17} ions/cm^2)

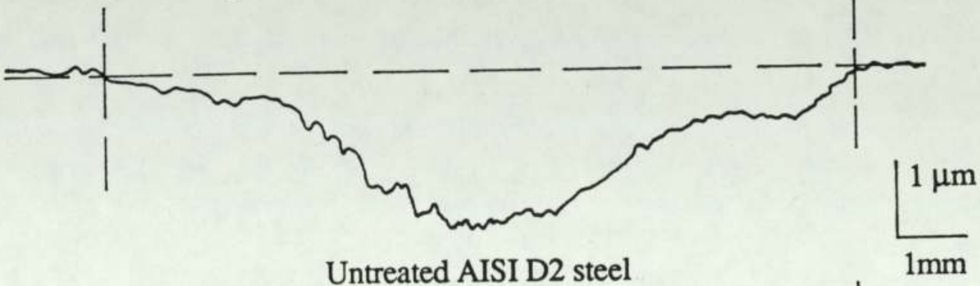

Untreated AISI D2 steel

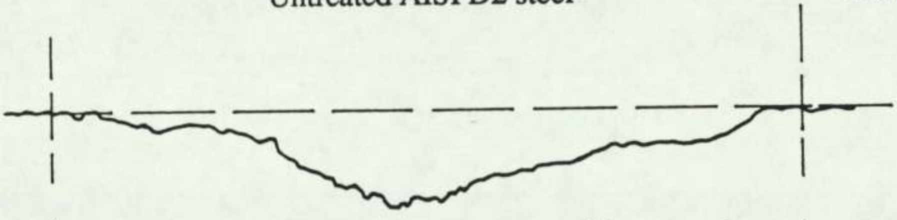

Implanted AISI D2 steel (3×10^{17} ions/cm^2)

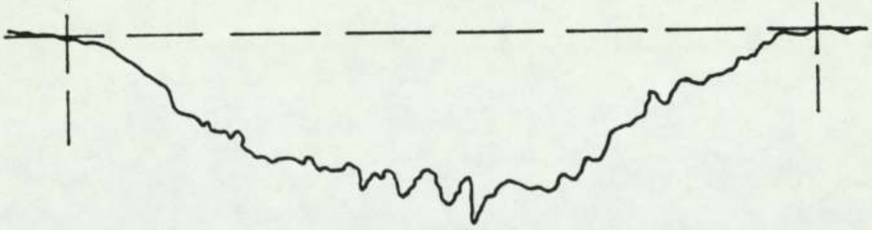

Untreated AISI 420 steel

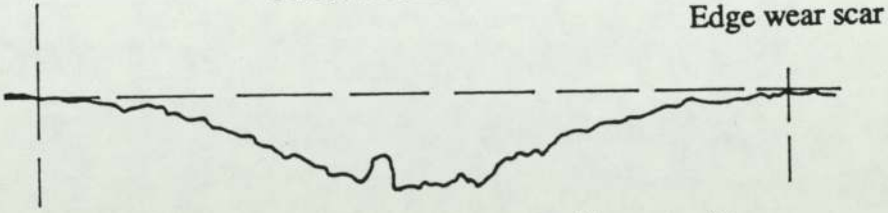

Implanted AISI 420 steel (4×10^{17} ions/cm^2)

Figure 62: Profilometer traces of worn steel surfaces after approximately 140 min. lubricated Falex wear testing at 900 N load. Implantation carried out at optimum nitrogen dose.

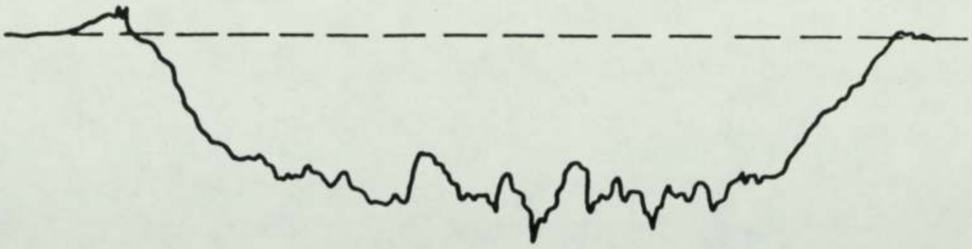

Untreated hard Cr

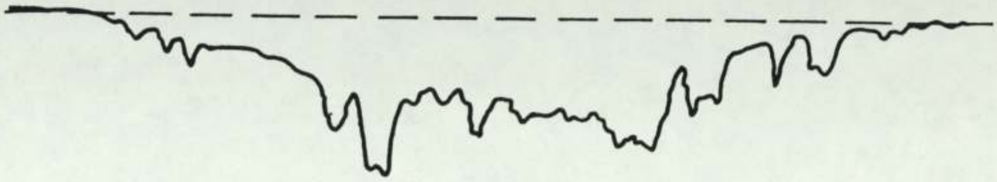

Implanted hard Cr (2 x 10^{17} ions/cm^2)

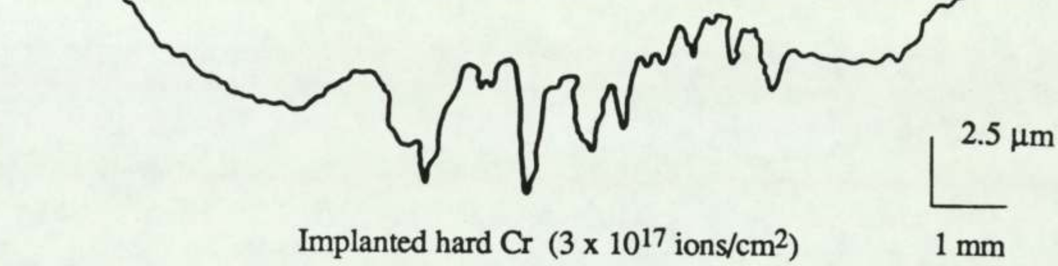

Implanted hard Cr (3 x 10^{17} ions/cm^2)

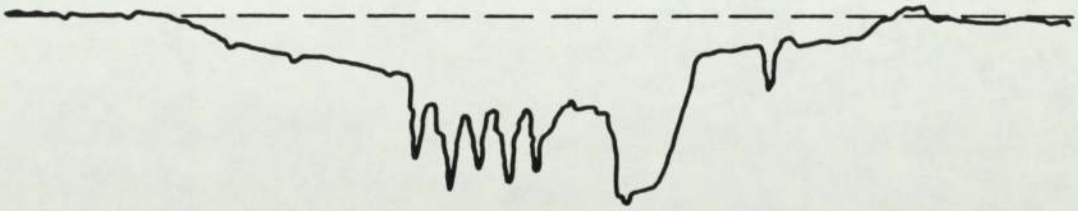

Implanted hard Cr (4 x 10^{17} ions/cm^2)

Figure 63: Profilometer traces of hard Cr coating (Type I, 700 HV$_{0.1}$) after 60 min. lubricated Falex wear testing at 710 N load.

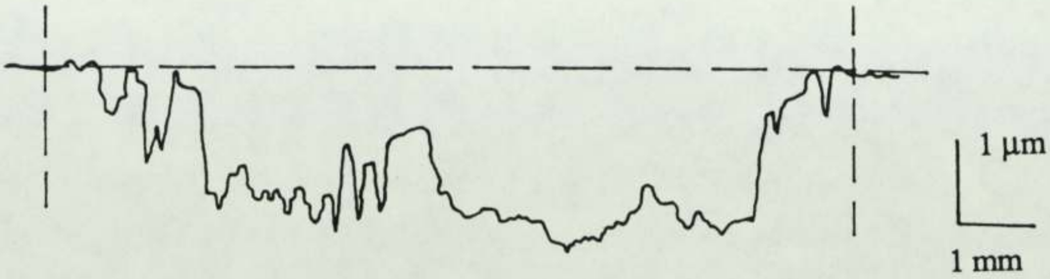

Untreated hard Cr

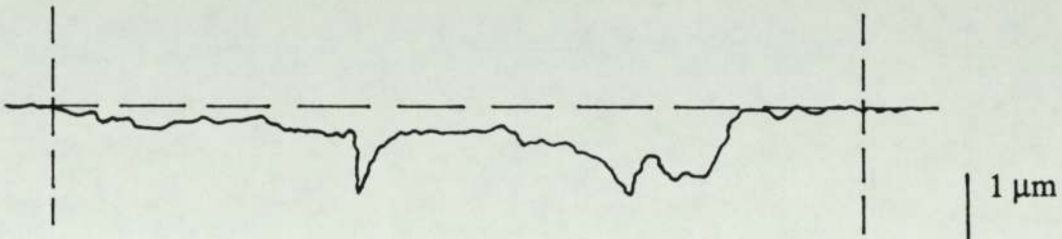

Implanted hard Cr (5 x 10^{17} ions/cm^2)

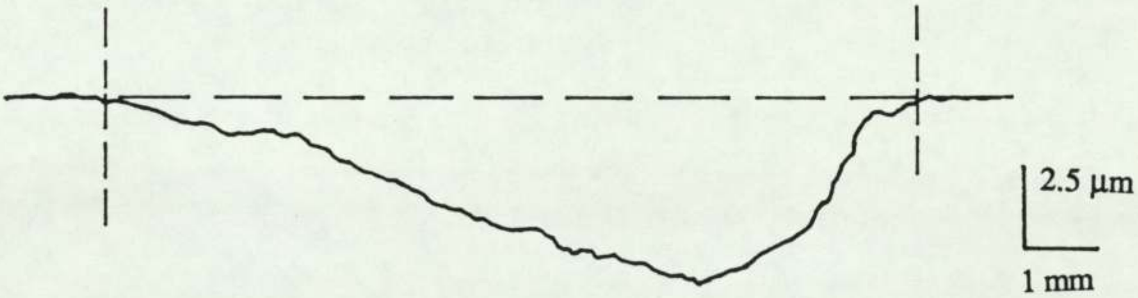

Untreated Co-1.5%W

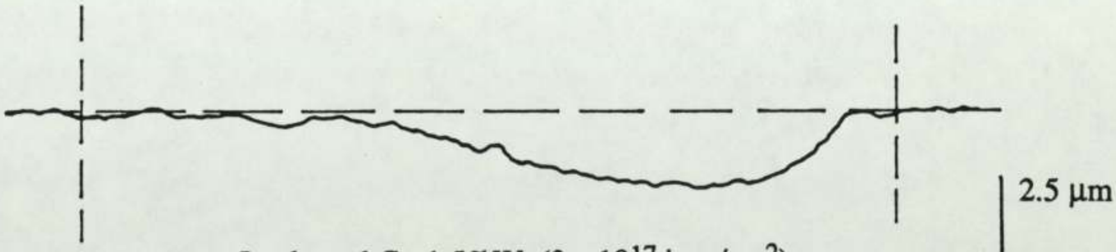

Implanted Co-1.5%W (3 x 10^{17} ions/cm^2)

Figure 64: Profilometer traces of hard Cr (Type II, 1050 $HV_{0.1}$) and Co-1.5%W coatings after 90 min. lubricated Falex wear testing at 710 N load.

5.3.2 Scanning Electron Microscopy Work

In this section the results from the SEM examination of worn surfaces are presented. In the case of nitrogen implanted materials only micrographs of those materials implanted at doses which produced the most significant tribological results are illustrated here for sake of brevity. The rest exhibited similar but less pronounced results.

5.3.2.1 Steel Materials

-Lubricated Falex Wear

Nitrogen implantation reduced wear in all three steels AISI M2, D2 and 420 and the worn surfaces from untreated and nitrogen implanted specimens showed clear differences. Figure 65 shows characteristic surfaces of AISI M2 and D2 after 90 minutes Falex lubricated wear. Ploughing is readily visible for both untreated materials (see 65A and 65C), whilst nitrogen implantation reduced considerably abrasion on the surface. As a result the amount and size of debris generated during the wear process was also reduced. Figure 66 illustrates the differences between the size of debris produced for AISI M2 when this material was untreated and nitrogen implanted. An energy dispersive X-ray analysis of one of the wear platelets generated from the untreated AISI M2 (Figure 66A) is also shown (Figure 66C).

The wear pattern from AISI 420 was similar to the above exhibited for M2 and D2 steel. However, at the high loading encountered in the Falex tests, some of the untreated samples suffered severe scuffing and adhesive wear. Figure 67A depicts the worn surface of untreated AISI 420, showing scuffing and Figure 67B illustrates a wear fragment adhered to the surface. The debris formed under these conditions had the typical shear-front lamellar structure of the chips formed in metal cutting processes (see Figure 67C). Nitrogen implantation prevented this kind of damage, reducing considerably ploughing and eliminating adhesion, as Figure 67D illustrates.

-Pin-on-Disc Dry Testing

Nitrogen implantation also changed the wear behaviour of the steels investigated under dry conditions and moderate load (9.81N) and sliding speed (0.5 m/s). Figure 68 depicts the worn surfaces of untreated (Figure 68A) and nitrogen implanted (Figure 68B) AISI D2 steel pins after a sliding distance of about 11000 m. Ploughing and some adhesive transfer of material are general features of the unimplanted surface. On the contrary the nitrogen implanted specimen showed a mild oxidative wear mechanism with elimination of the abrasion of the surface. The shape of the carbides within the martensitic matrix is clearly revealed after wear (Figure 68B).

Similarly, implanted AISI 420 steel exhibited much reduction in ploughing as Figure 69C shows. The untreated AISI 420 material also suffered heavy ploughing (see Figure 69B). The unworn surface of the pin is depicted in Figure 69(A) to illustrate the smoothing effect produced during wear by nitrogen implantation, changing the wear mechanism from adhesive or abrasive (Figure 69B) to oxidative (Figure 69C). As expected the wear debris produced from the untreated AISI 420 steel (Figure 70A) was coarser than that from the implanted material (Figure 70B).

5.3.2.2 Coating Materials

Characteristic micrographs obtained from chromium coatings (Type I, 700 $HV_{0.1}$) are presented in Figures 71A to D. Figures 71A, B illustrate worn surfaces after 30 minutes Falex wear of untreated and nitrogen implanted specimens (dose $4x10^{17}$ ions/cm^2) respectively. Ploughing was not eliminated completely by implantation but the wear volume was reduced.

Nitrogen implantation creates large stresses on the surface of the hard chromium coatings, however, evidence could not be found that this would close the inherent microcracks of the coating. Figure 71C shows an unworn area of the deposit showing a crack, similarly Figure 71D illustrates that cracks were also present in an unworn surface of a specimen implanted at 4×10^{17} ions/cm^2.

The wear behaviour of the harder chromium deposit (Type II, 1050 $HV_{0.1}$) was significantly different. Figure 72A shows the worn area of an untreated specimen after 90 minutes Falex wear testing, the track evidences ploughing and this figure also illustrates how wear debris is generated. Nitrogen implantation reduced ploughing at the optimum dose of 5 x 10^{17} ions/cm^2 and a characteristic worn area is shown in Figure 72B. The inherent microcracks of the coating did not appear to have an influence on the subsequent wear, debris was not generated preferentially at these sites, as Figure 72C indicates.

The effect of nitrogen implantation on the wear of already hardened electroless Ni-P was the opposite to that experienced with other coatings. Figure 73A shows the unworn area of an unimplanted Ni-P coating; after 95 minutes Falex wear the surface was polished and exhibited some ploughing (see Figure 73B). Nitrogen implantation did not improve the load bearing capacity of the surface, as Figure 73C indicates, and abrasion was evident.

Figure 74A shows a characteristic unworn area of a Co-1.5% W brush plated coating which illustrates the nodular structure of the deposit. Falex wear testing for 90 minutes produced a polished surface on the untreated coating (see Figure 74B) with absence of ploughing. Nitrogen implantation increased the wear resistance of the surface and produced less wearing away of the nodules, as Figure 74C illustrates.

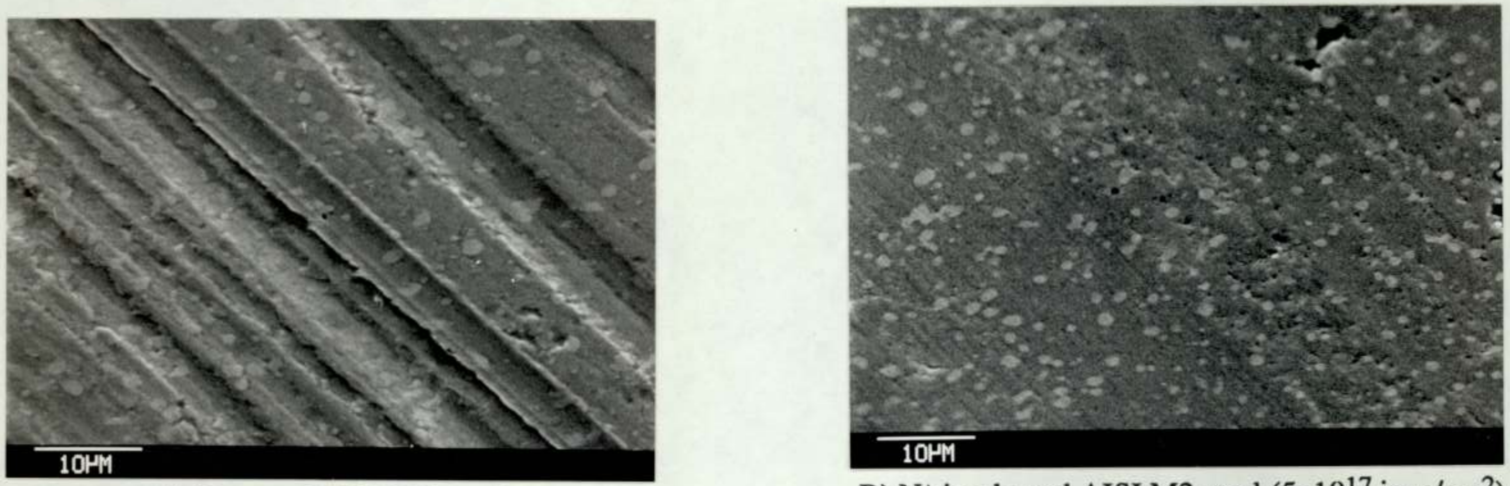

A) Untreated AISI M2 steel

B) N^+ implanted AISI M2 steel (5×10^{17} ions/cm^2)

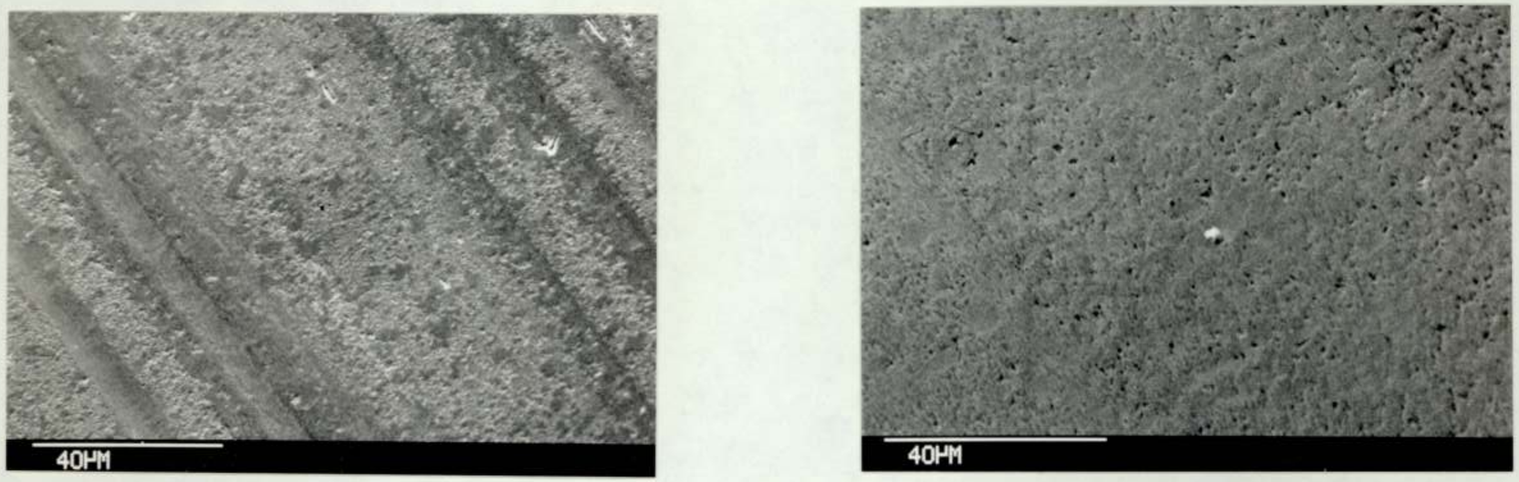

C) Untreated AISI D2 steel

D) N^+ implanted AISI D2 steel (3×10^{17} ions/cm^2)

Figure 65: Scanning micrographs of surfaces of AISI M2 and D2 steels after 90 mins. "Falex" wear testing. A) Untreated AISI M2 steel. B) N^+ implanted AISI M2 steel. C) Untreated AISI D2 steel and D) N^+ implanted AISI D2 steel.

A) Untreated AISI M2 steel

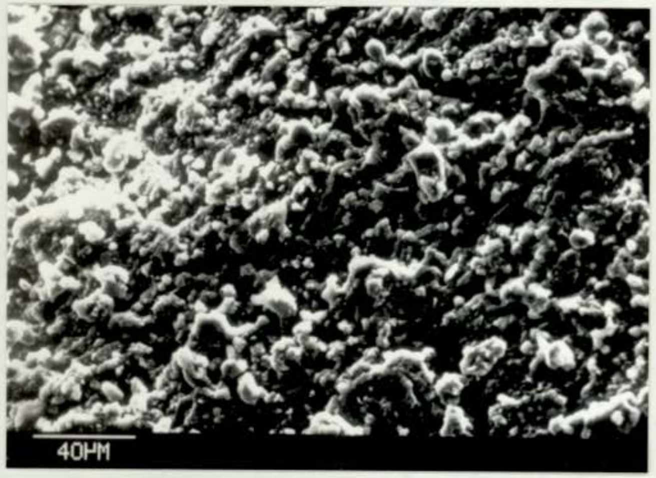

B) Nitrogen implanted AISI M2 steel

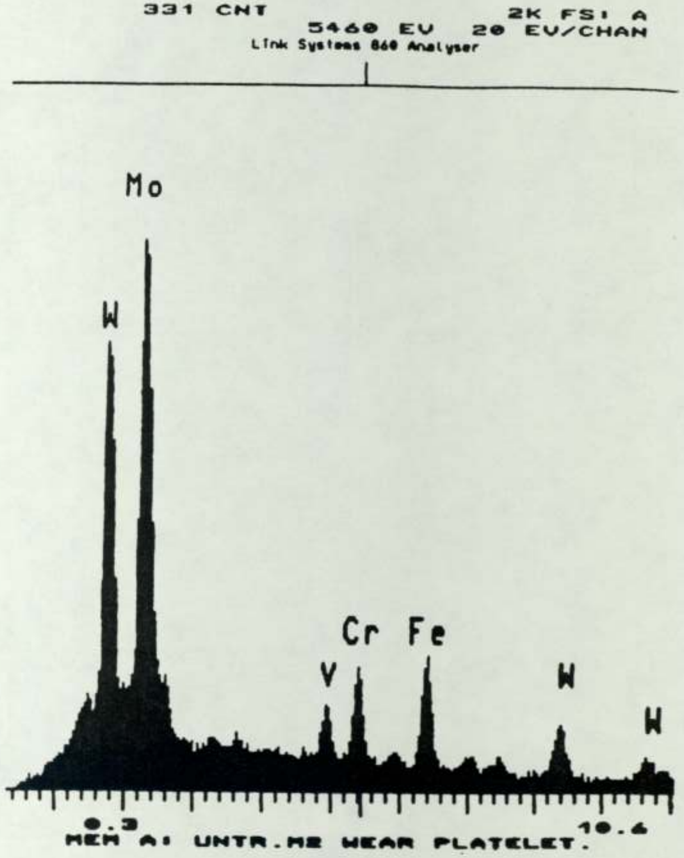

EDX analysis of particle from (A)

Figure 66: Debris generated during lubricated "Falex" wear of A) Untreated AISI M2 steel and B) N^+ implanted AISI M2 (dose: $5x10^{17}$ ions/cm^2)

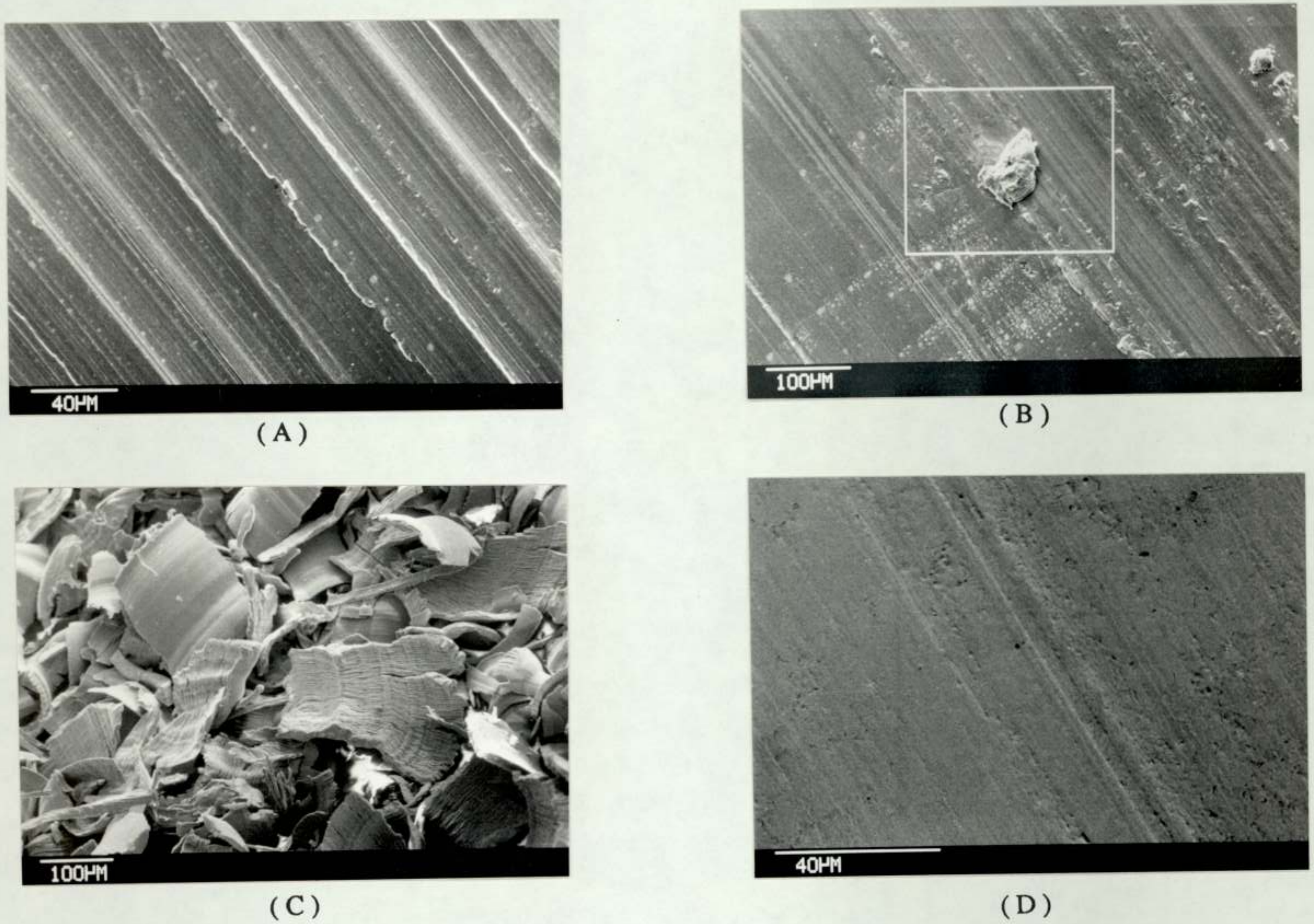

Figure 67: (A,B): Scanning micrographs of worn surfaces after Falex testing of AISI 420 steel, exhibiting (A) severe scuffing and (B) adhesive wear. Debris generated is shown in (C). (D): showing worn surface of N^+ implanted AISI 420 steel (4×10^{17} ions/cm^2).

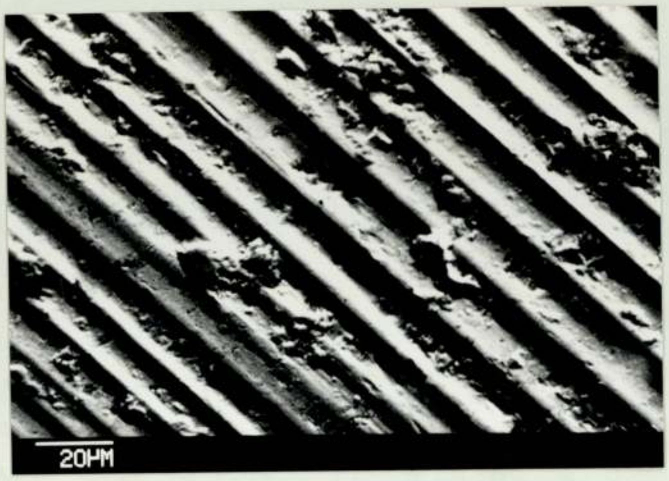

A) Untreated AISI D2 steel

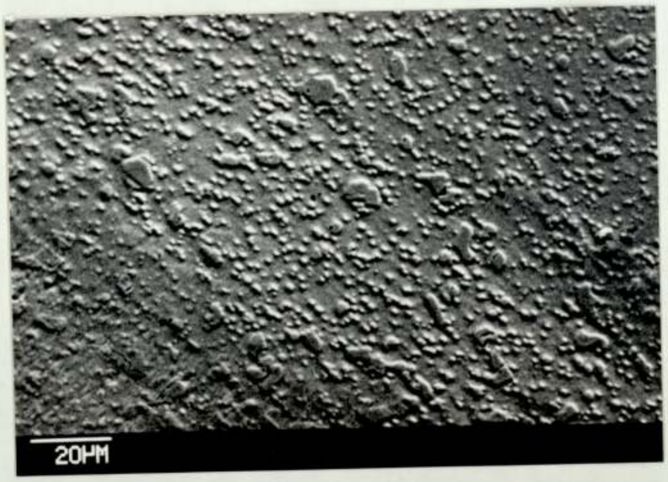

B) Nitrogen implanted AISI D2 steel

Figure 68: Scanning micrographs of worn surfaces of AISI D2 steel after pin-on-disc dry wear testing. A) Untreated AISI D2. B) N^+ implanted AISI D2 steel.

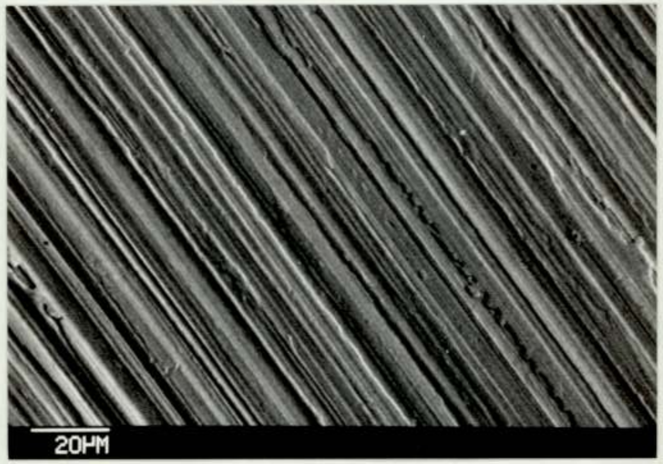

A) Unworn AISI 420 steel surface

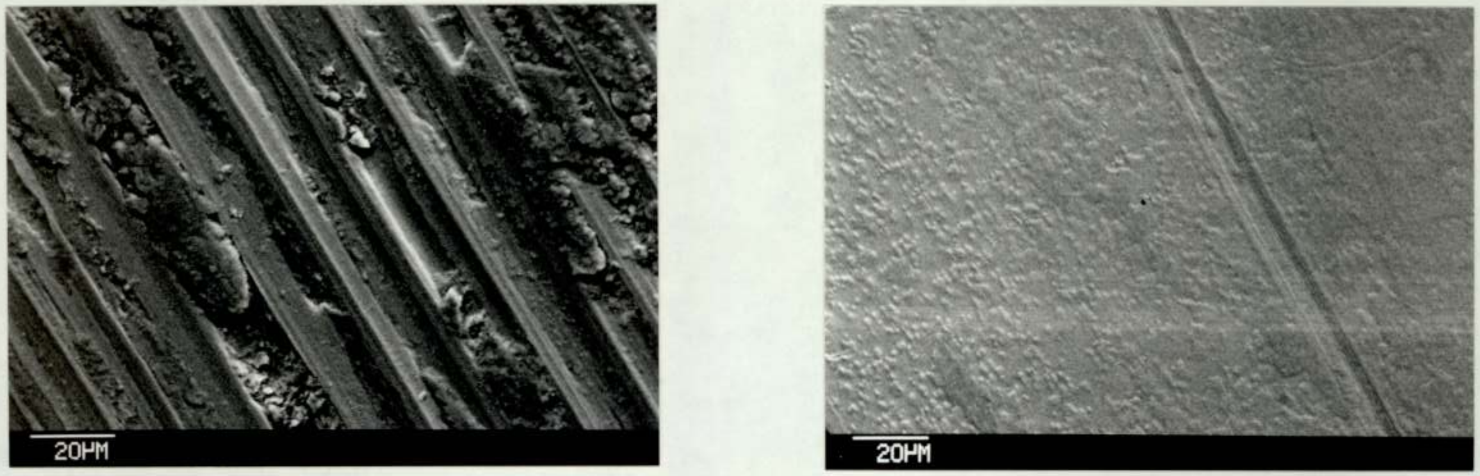

B) Worn surface of untreated AISI 420 steel

C) Worn surface of N^+ implanted AISI 420 steel

Figure 69: Scanning micrographs of surfaces of AISI 420 steel. A) Unworn surface. B) Untreated AISI 420, after about 4 hours dry pin-on-disc wear testing and C) N^+ implanted AISI 420 steel (dose: 3×10^{17} ions/cm^2) after same wear conditions.

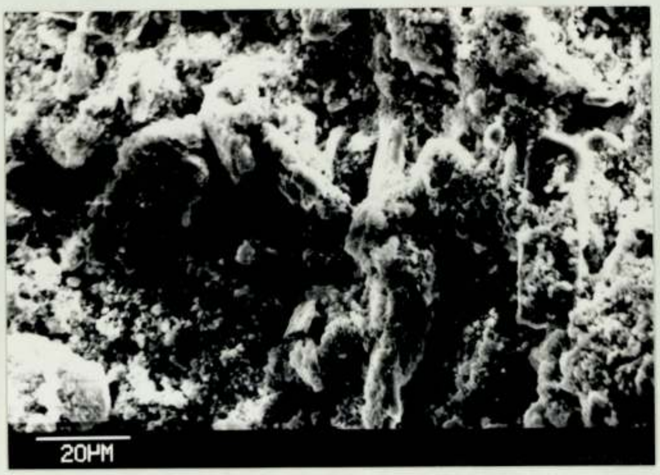

A) Untreated AISI 420 martensitic stainless steel

B) Nitrogen implanted AISI 420 martensitic stainless steel

Figure 70: Debris generated during dry pin-on-disc wear of A) untreated AISI 420 steel and B) N^+ implanted AISI 420 steel. Testing conditions: 9.81 N load, 0.5 m/s sliding speed. Like on like material testing.

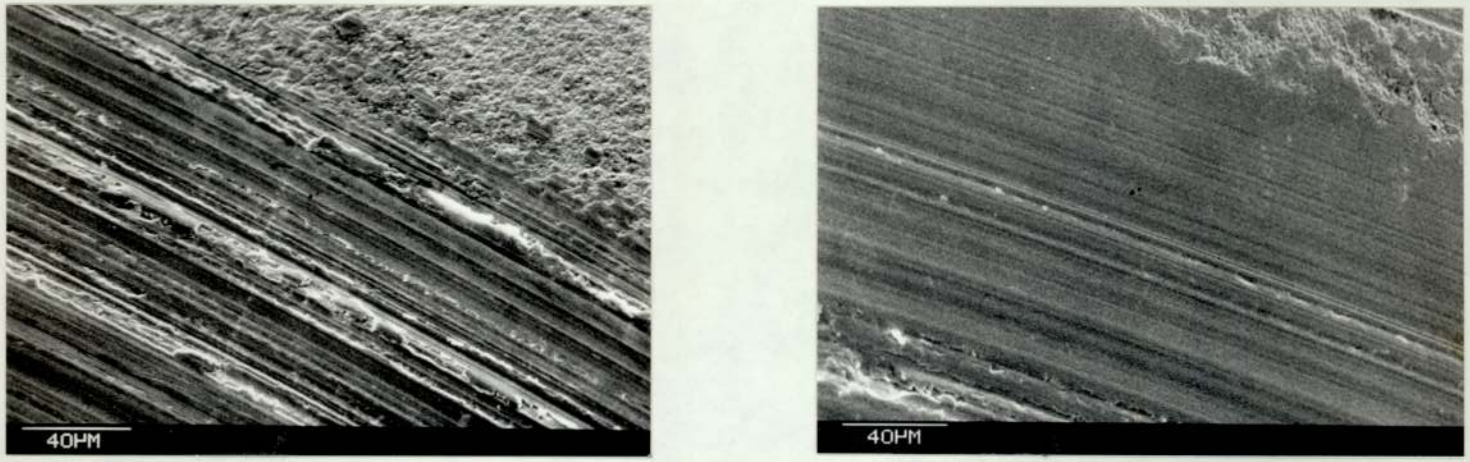

A) Untreated Cr coating after wear

B) N$^+$ implanted Cr coating after wear

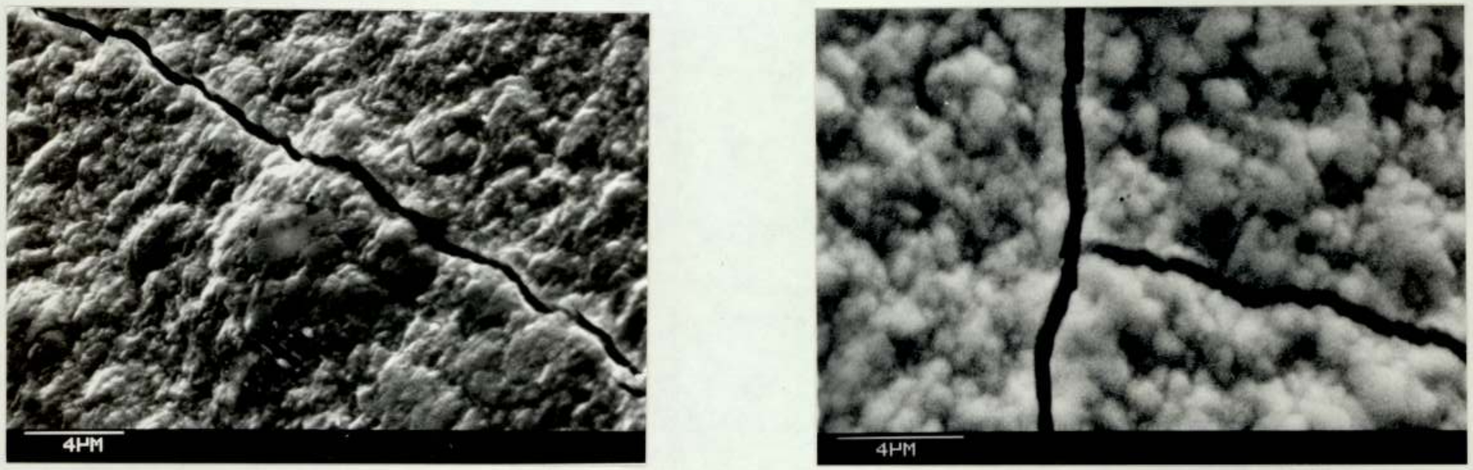

C) Unworn untreated Cr coating

D) Unworn N$^+$ implanted Cr coating

Figure 71: Scanning micrographs of Cr coatings (Type I). A) Worn area from untreated Cr after 30 min. Falex testing. B) Worn area of N$^+$ implanted Cr after similar period. C) Unworn area of untreated Cr showing cracking. D) Cracking on unworn surface of N$^+$ implanted Cr (dose: 4×10^{17} ions/cm^2).

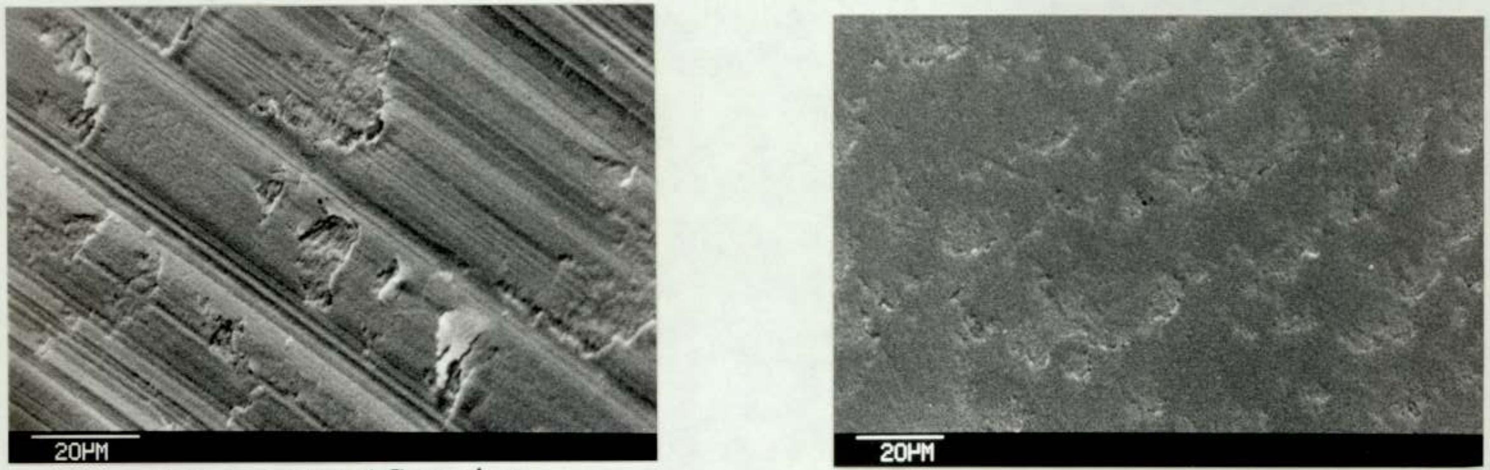

A) Untreated hard Cr coating

B) N^+ implanted hard Cr coating

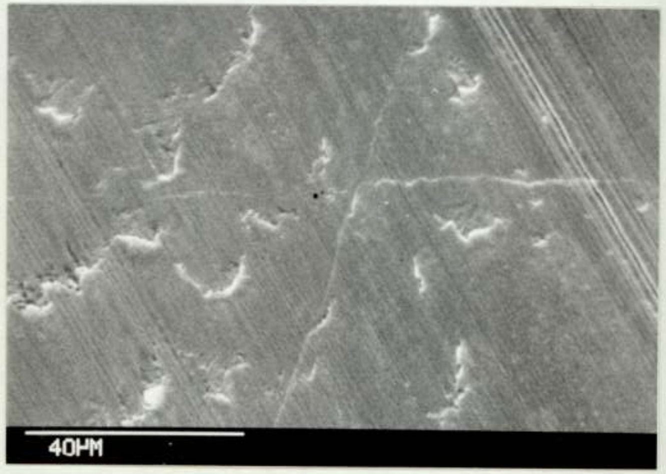

C) Microcracking in worn area of untreated Cr coating

Figure 72: Scanning micrographs showing worn areas of hard Cr coatings (Type II,1050 $HV_{0.1}$). A) Unimplanted, illustrating a particle of Cr about to be detached. B) N^+ implanted hard Cr (5×10^{17} ions/cm^2) and C) microcracking in the wear track of an untreated deposit.

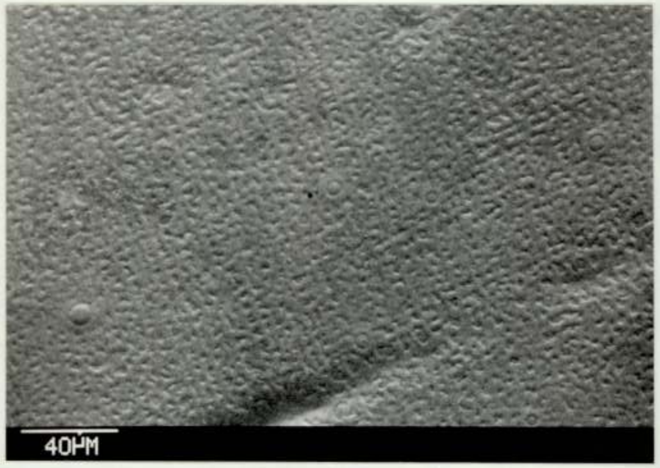

A) Unworn Ni-P coating

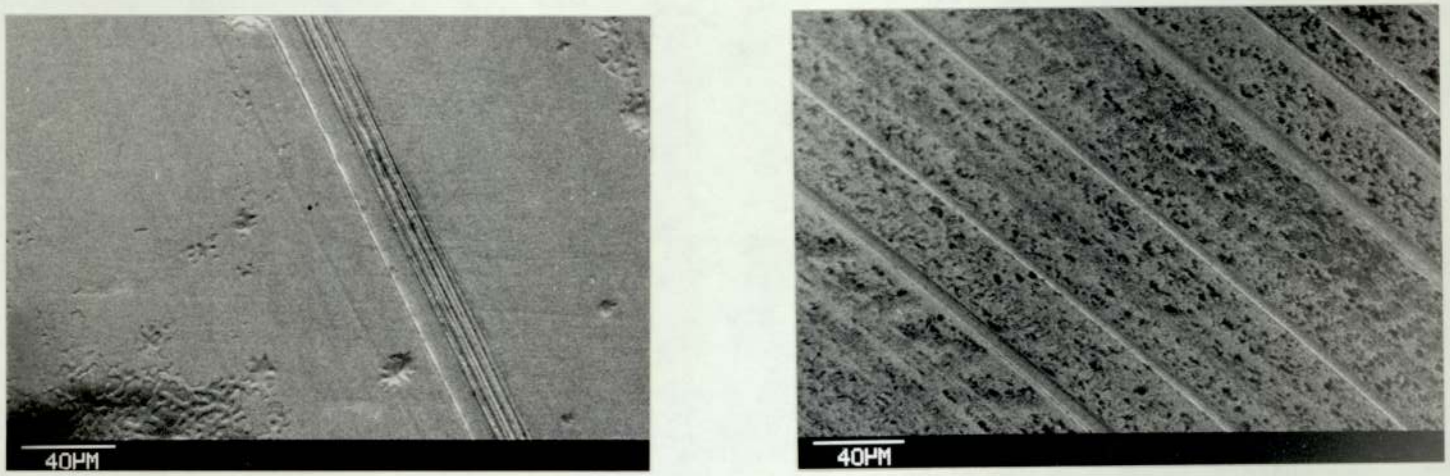

B) Unimplanted Ni-P after wear

C) N^+ implanted Ni-P coating after wear

Figure 73: Scanning micrographs of hardened electroless Ni-P coatings. A) Unworn unimplanted specimen. B) Area of unimplanted coating after 95 min. Falex wear and C) worn area of N^+ implanted Ni-P coating after a similar Falex testing period.

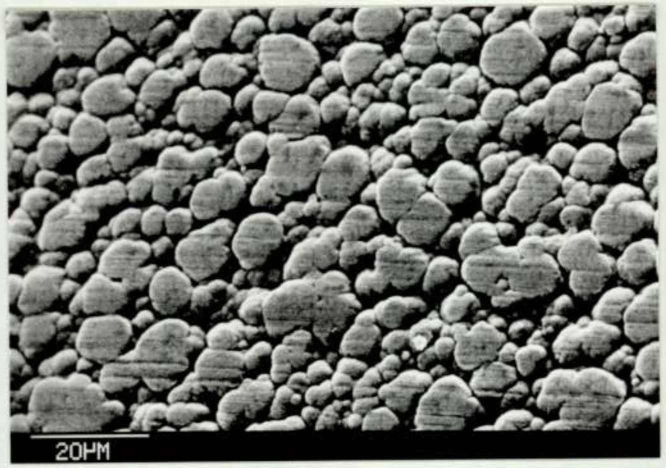

A) Unworn Co-W coating

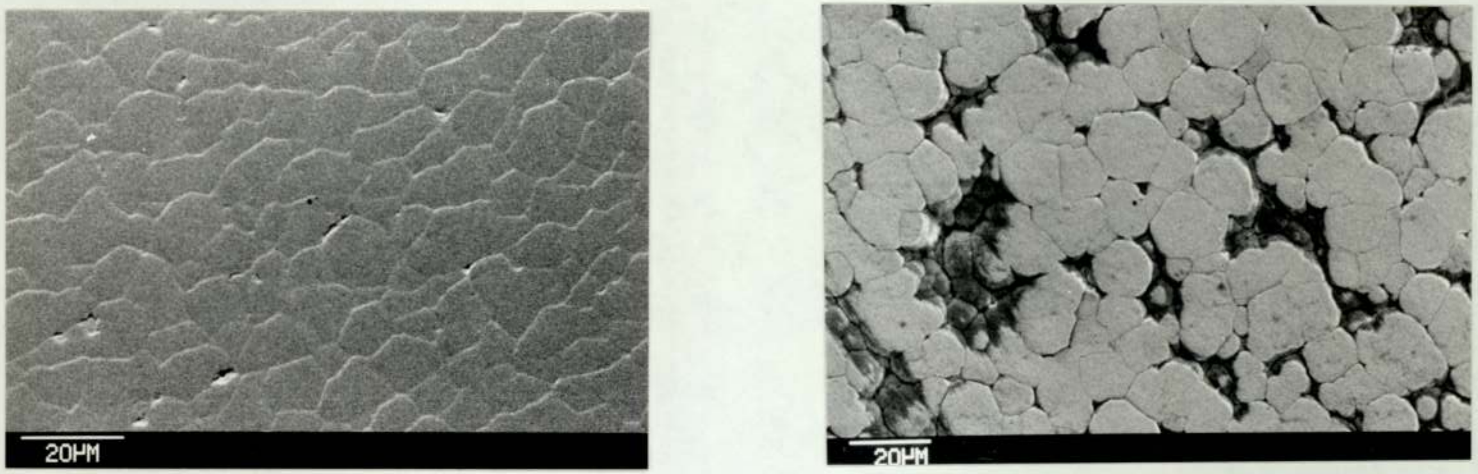

B) Untreated Co-W coating after wear

C) N^+ implanted Co-W coating after wear

Figure 74: Scanning micrographs of Co-1.5% W coatings. A) Unworn surface, to show the nodular structure of the deposit. B) Worn area of untreated coating after 90 min. Falex testing. C) Worn area of N^+ implanted coating after 90 min. Falex testing.

5.4 Surface Analysis

5.4.1 Auger Electron Spectroscopy (AES)

5.4.1.1 Steels

Results obtained from the Auger analysis of tool steels can be seen in Figures 75 to 81. Figure 75 depicts characteristic Auger spectra obtained in derivative mode for AISI 420 martensitic stainless steel after implantation at a dose of 4 x 10^{17} ions/cm^2. Depth concentration profiles for nitrogen and other elements of interest such as C, O, Fe and Cr, which were obtained from the spectra using the normalized peak heights method are presented in Figures 76 to 81. In these graphs the atomic percentage of each element is plotted against depth below the surface. The sputtering rate calibration yielded a value of 3nm/min for the argon ions.

It can be seen that nitrogen profiles have their maximum at a depth of about 90 to 120 nm normally and, as expected, the steel with the lower carbon content, ie. AISI 420 stainless steel, retained the highest nitrogen level. A maximum of approximately 29% at N was obtained for this steel implanted at 4 x 10^{17} ions/cm^2, and a higher dose only produced a flattening of the profile with deeper nitrogen penetration due to bombardment effects. Unexpectedly, the Auger profiles contained high background oxygen levels; this was thought to have been introduced during the heat treatment procedure and mechanical preparation of the samples prior to nitrogen implantation. A poor vacuum level during the Auger measurements which accounts also for the high adventitious carbon content might have also contributed to this effect.

5.4.1.2 Hard Chromium Electrodeposits

Characteristic Auger spectra obtained in derivative mode from a chromium coating implanted at 5 x 10^{17} ions/cm^2 are shown in Figure 82. Unlike those spectra obtained from the steel materials, here the nitrogen peaks identified at 379 eV electron energy are considerably larger and readily indicate higher retained nitrogen levels.

Figures 83 to 85 present the atomic concentration profiles of Cr, O, C and N elements of untreated and nitrogen implanted chromium coatings at doses of 2 x 10^{17} and 5 x 10^{17} ions/cm^2. Depth scaling was calculated as previously using a calibrated sputtering rate of about 3nm/min. These line concentration profiles exhibit a maximum nitrogen concentration of about 47 at % at a depth of approximately 60 nm (see Figure 85) for the chromium coating implanted at 5 x 10^{17} ions/cm^2. Nitrogen did not penetrate into the chromium substrate as deep as into the steel specimens, but was retained at much higher levels and this accounts for the more significant improvements in mechanical properties achieved already described in previous sections.

Auger electron analysis was also carried out on a hard chromium implanted at 5 x 10^{17} ions/cm^2 and worn, using the Falex method under lubricated conditions, to a depth exceeding the implantation range. The results are presented in Figure 86 and it can be seen that about 2.5% atomic nitrogen remains after wear. A profile of the worn area, showing schematically the area analysed by the electron beam, is also indicated in this figure.

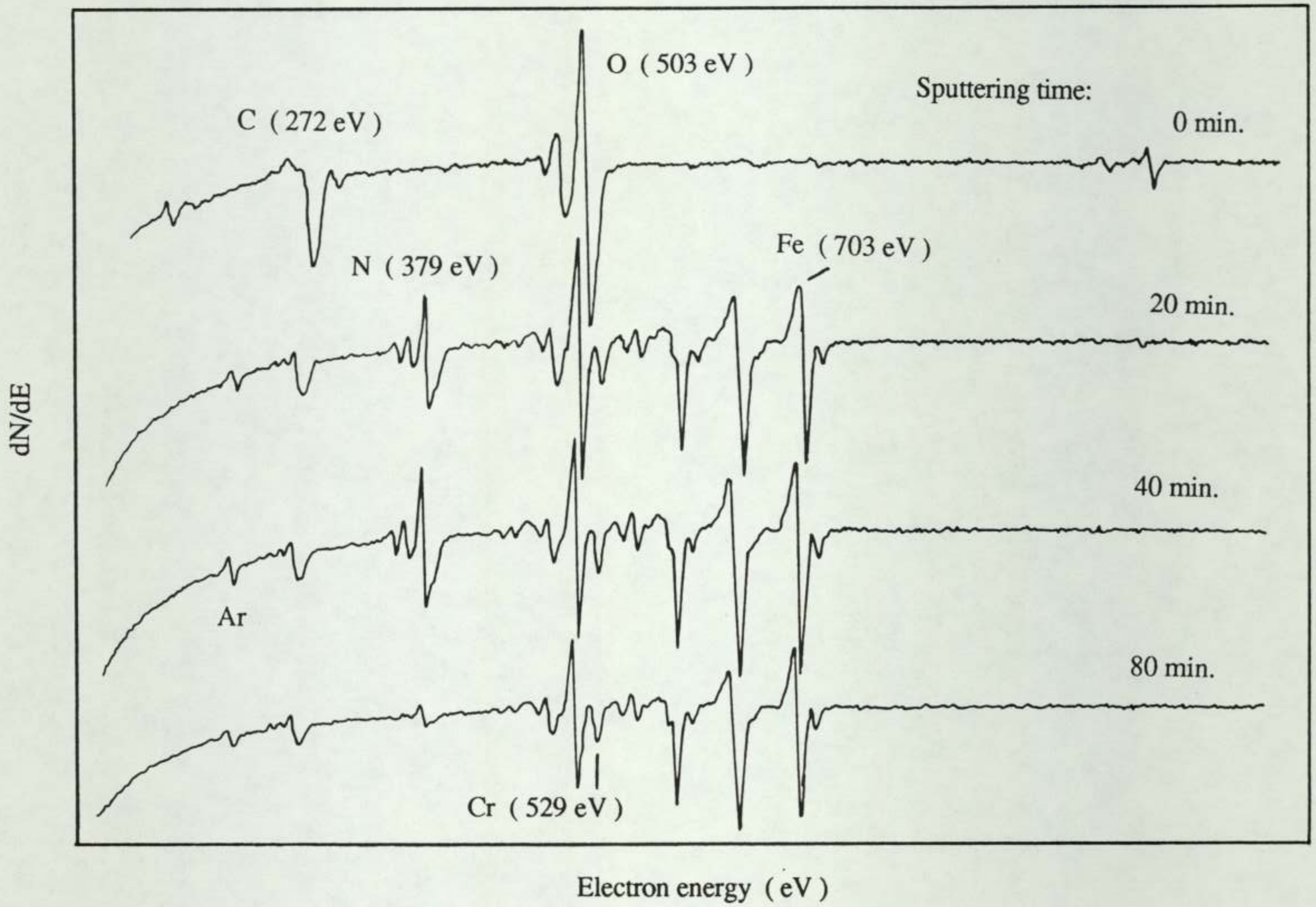

Figure 75: Typical Auger derivative spectra of AISI 420 steel implanted at 4 x 10^{17} ions/cm^2. 90 keV energy, 6 μA/cm^2 dose rate.

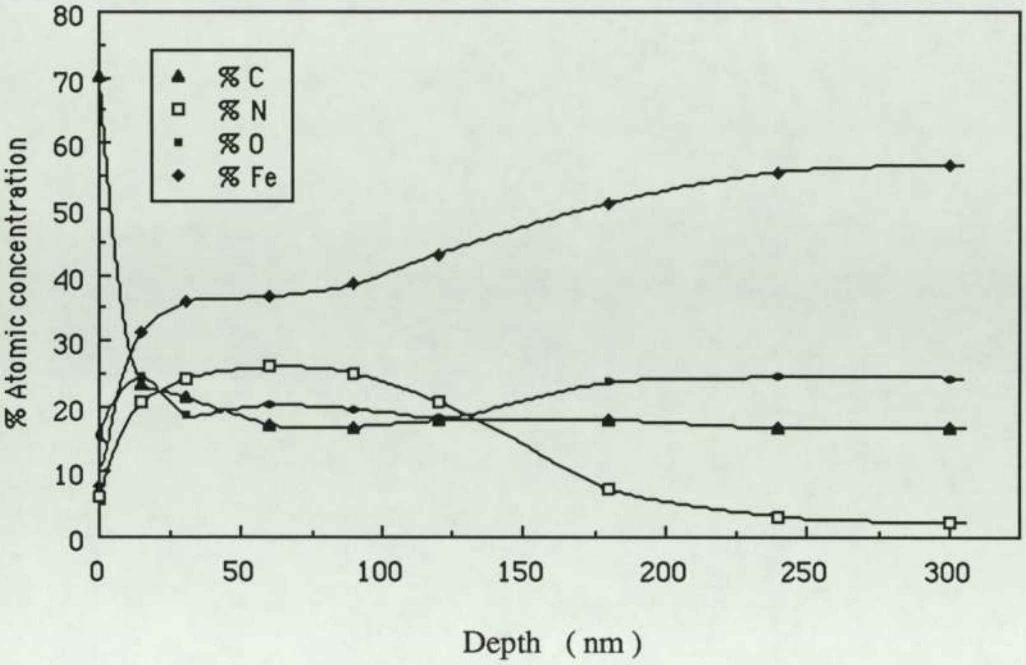

Figure 76: Depth concentration profiles of AISI M2 steel implanted at $4 \times 10^{17} N^+$ ions/cm^2
Sputtering rate: 3nm/min.

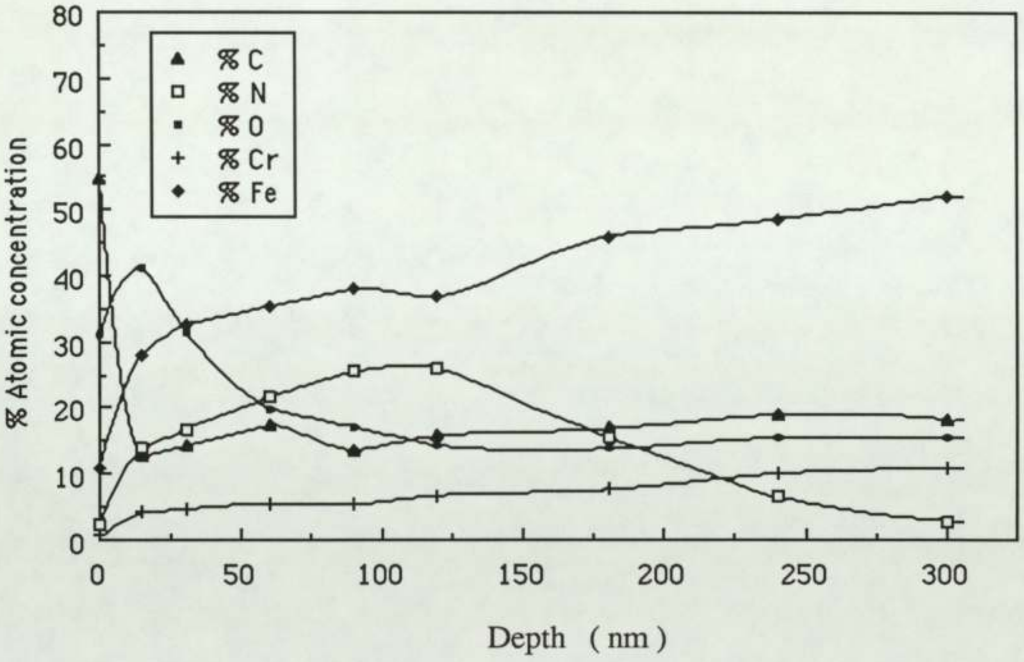

Figure 77: Depth concentration profiles of AISI D2 steel implanted at $3 \times 10^{17} N^+$ ions/cm^2
Sputtering rate: 3nm/min.

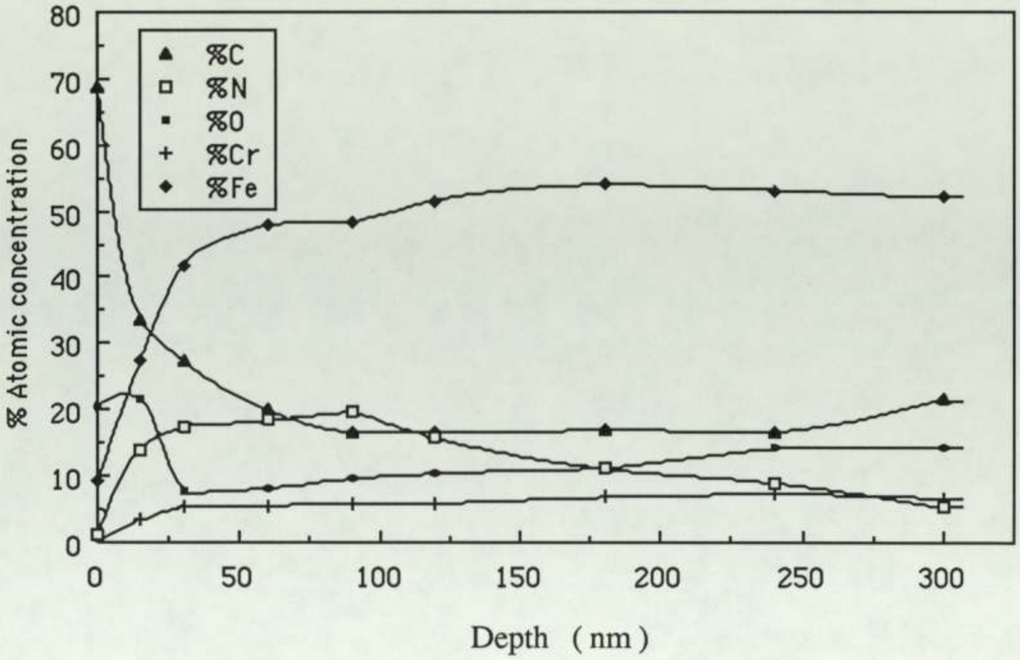

Figure 78: Depth concentration profiles of AISI D2 steel implanted at 4x10^{17}N^{+}ions/cm^{2}
Sputtering rate: 3 nm/min.

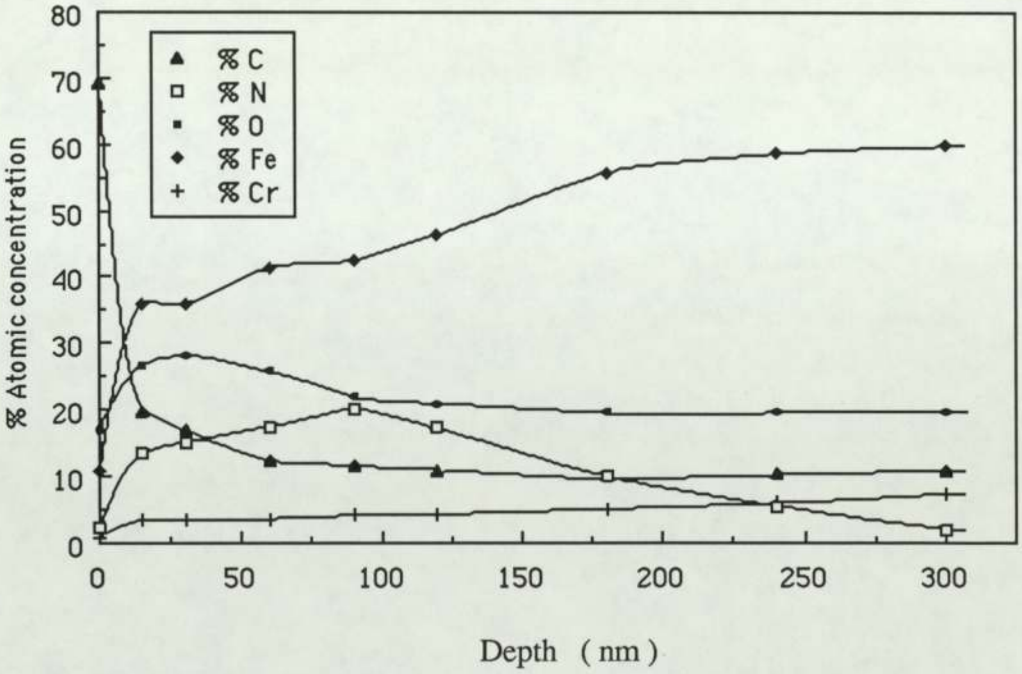

Figure 79: Depth concentration profiles of AISI 420 steel implanted at 3x10^{17}N^{+}ions/cm^{2}
Sputtering rate: 3 nm/min.

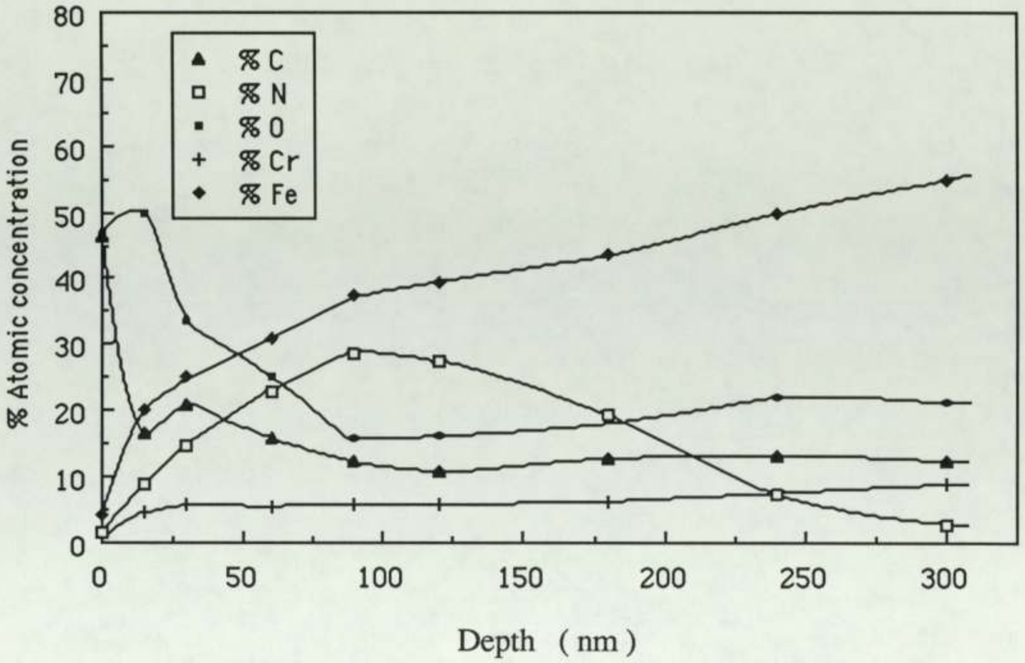

Figure 80: Depth concentration profiles of AISI 420 steel implanted at 4x$10^{17}$$N^+$ ions/cm^2
Sputtering rate: 3 nm/min.

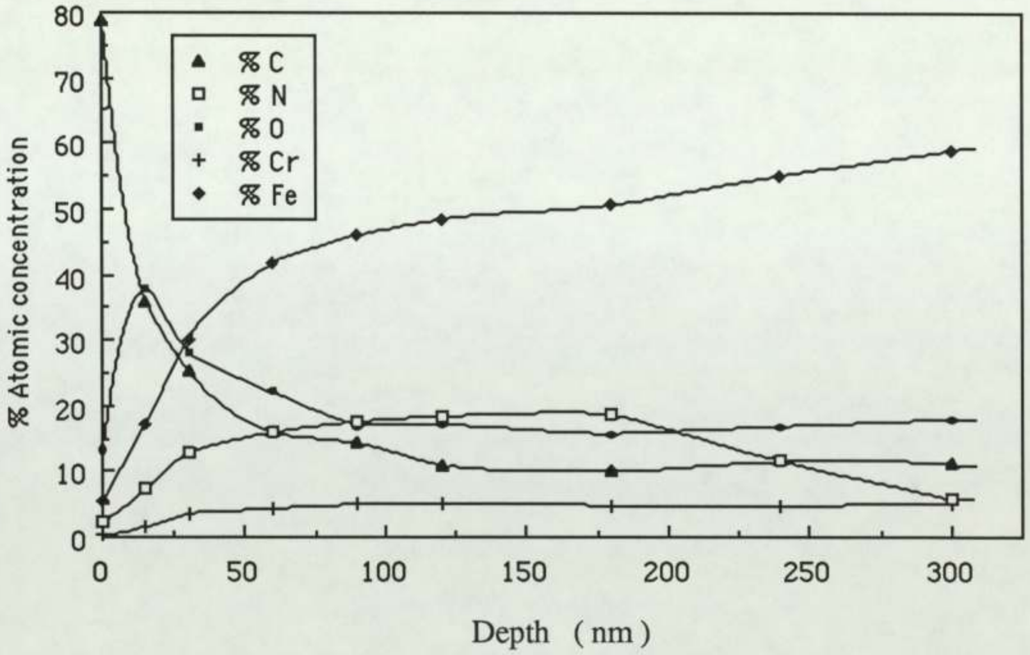

Figure 81: Depth concentration profiles of AISI 420 steel implanted at 5x$10^{17}$$N^+$ ions/cm^2
Sputtering rate: 3 nm/min.

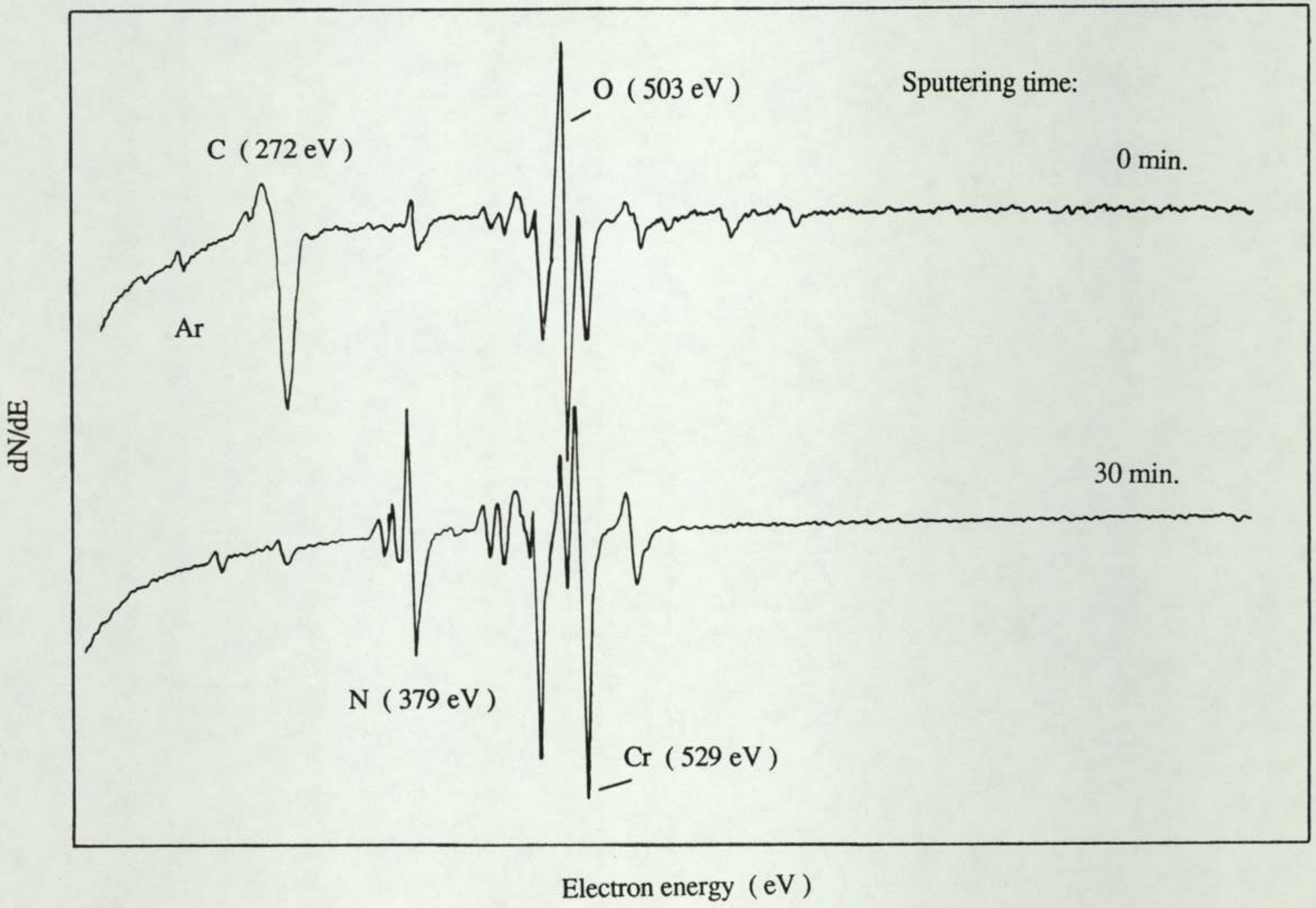

Figure 82: Characteristic Auger derivative spectra of hard chromium coating implanted at 5 x 10^{17} nitrogen ions/cm^2.

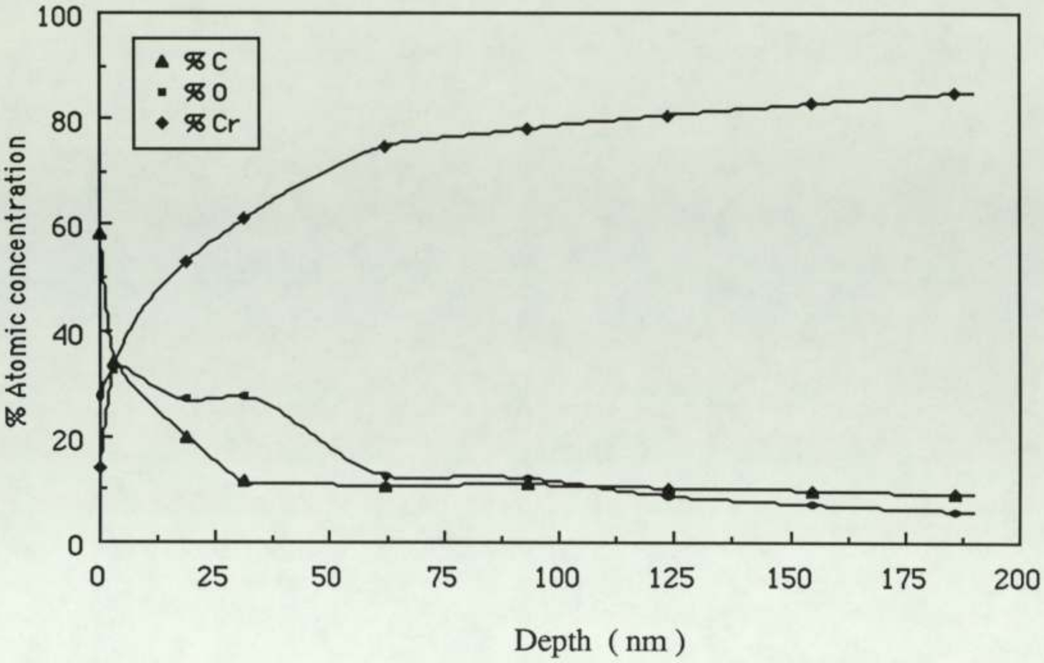

Figure 83: Depth concentration profiles of untreated hard Cr coating.
Sputtering rate: 3 nm/min.

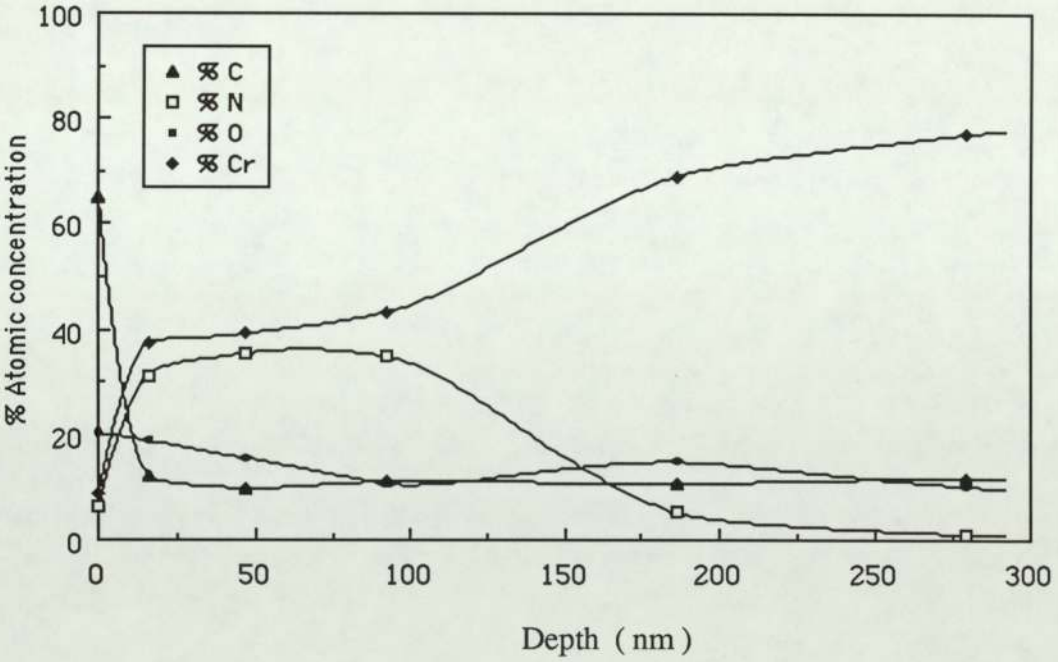

Figure 84: Depth concentration profiles of hard Cr implanted at 2x10^{17}N^{+} ions/cm^{2}
Sputtering rate: 3 nm/min.

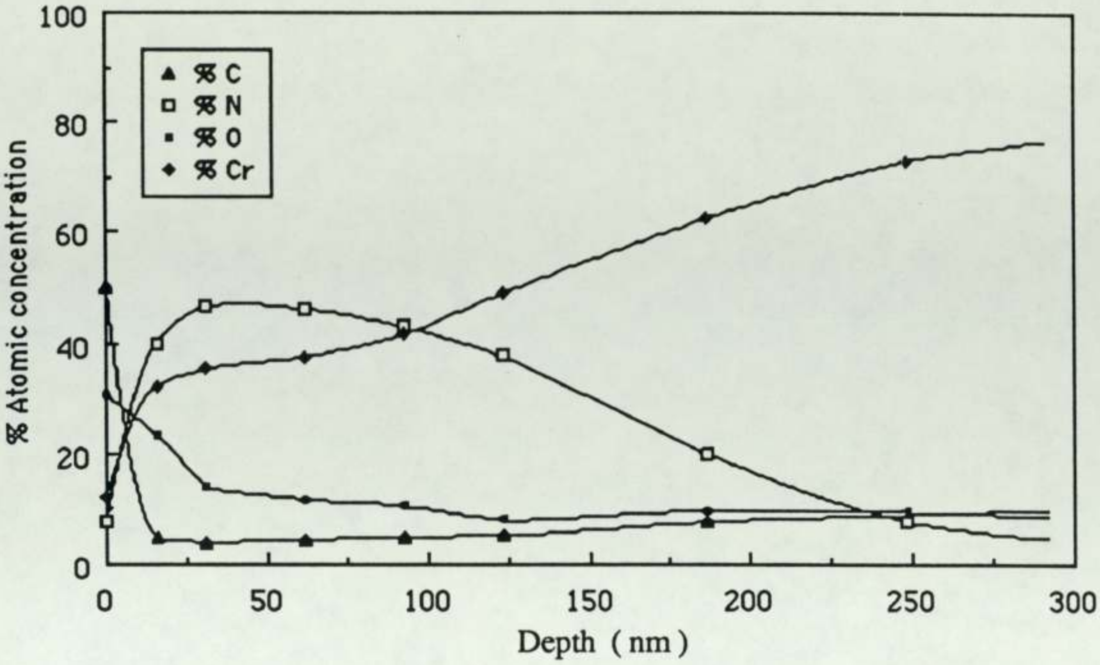

Figure 85: Depth concentration profiles of hard Cr implanted at $5x10^{17}N^{+}$ ions/cm^2
Sputtering rate: 3 nm/min.

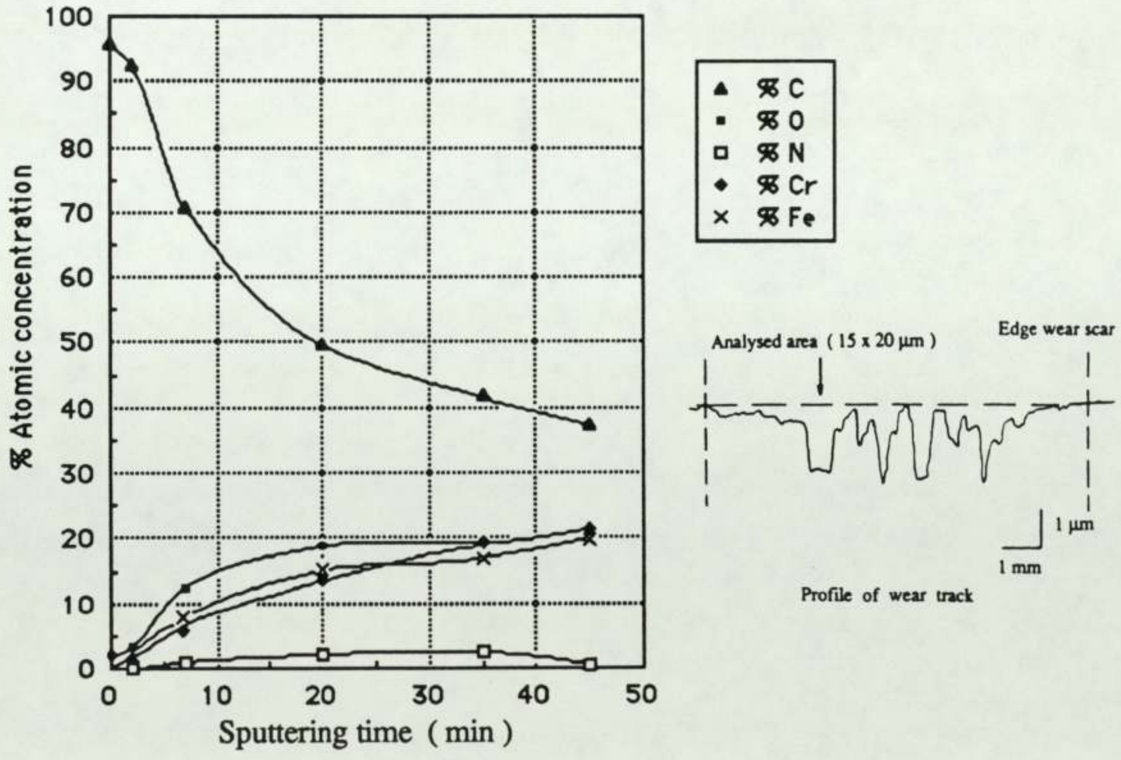

Figure 86: Auger analysis of worn hard Cr coating implanted at $5x10^{17}N^{+}$ ions/cm^2
Sputtering rate: 3nm/min

5.4.2 X-Ray Photoelectron Spectroscopy

5.4.2.1 Steels

Only the martensitic stainless steel was investigated using this technique. Fe $2p_{3/2}$ and Cr $2p_{3/2}$ peaks from the untreated AISI 420 stainless steel are presented in Figures 87 and 88 respectively. Each of these figures illustrates spectra for different etching times by Ar^+ ions (sputtering rate: 3 nm/min) reduced to 278 channels and after non-linear background subtraction. Binding energies, with an error range of ± 0.2 eV, and calculated with reference to the Au $4f_{7/2}$ line at 84.0 eV are indicated for each peak.

Figures 89 to 91 exhibit Fe $2p_{3/2}$, Cr $2p_{3/2}$ and N 1s spectra obtained from AISI 420 after implantation at a dose of $4 \times 10^{17}/cm^2$. These peaks were obtained under similar conditions and etching times as those described above.

N 1s spectra (Figure 91) show that nitrogen is retained mainly in the nitrided state. Cr $2p_{3/2}$ peaks (Figure 90) also exhibit a nitride formation, thus, chromium nitrides are preferentially produced in this steel, since significant differences cannot be observed for Fe 2p spectra from the untreated material (Figure 87) and the implanted steel (Figure 89). These spectra (see Figures 87a and 89a for example) show a three component peak corresponding to the metal and Fe_2O_3 and FeO oxides. FeO oxide can be formed at temperatures above 500°C on steel surfaces but in this case it is a product of the preferential sputtering of oxygen from the Fe_2O_3 surface layer of the steel. As expected the surface of the implanted steel (Figure 89a) contains a larger proportion of FeO than the untreated steel (Figure 87A), this is due to the bombardment effects of the implantation, sputtering the oxygen preferentially and reducing the oxide.

5.4.2.2 Coatings

Cr $2p_{3/2}$, O 1s and N 1s peaks obtained after non-linear background subtraction of spectra from hard chromium coatings are presented in Figures 92 to 98. Chemical binding information of the elements was acquired at the surface and after 30 minutes sputtering, ie. about 90 nm below the surface.

Figures 92 and 93 exhibit spectra from the untreated hard chromium coating, while Figures 94 and 95, and 96 to 98 depict the peaks obtained from nitrogen implanted chromium electrodeposits at doses of 2×10^{17} and 5×10^{17} ions/cm^2

respectively. Binding energies, calculated with reference to the C 1s line at 284.6 eV are indicated for all peaks fitted to each spectrum.

It is shown that nitrogen is almost entirely bound as nitride to chromium for both coatings implanted with nitrogen. The N 1s spectrum at the surface of the chromium coating implanted at 5 x 10^{17} ions/cm^2 is not shown due to the very low nitrogen levels obtained from the area analysed; the high adventitious carbon levels present at the surface could have masked the signals from other elements.

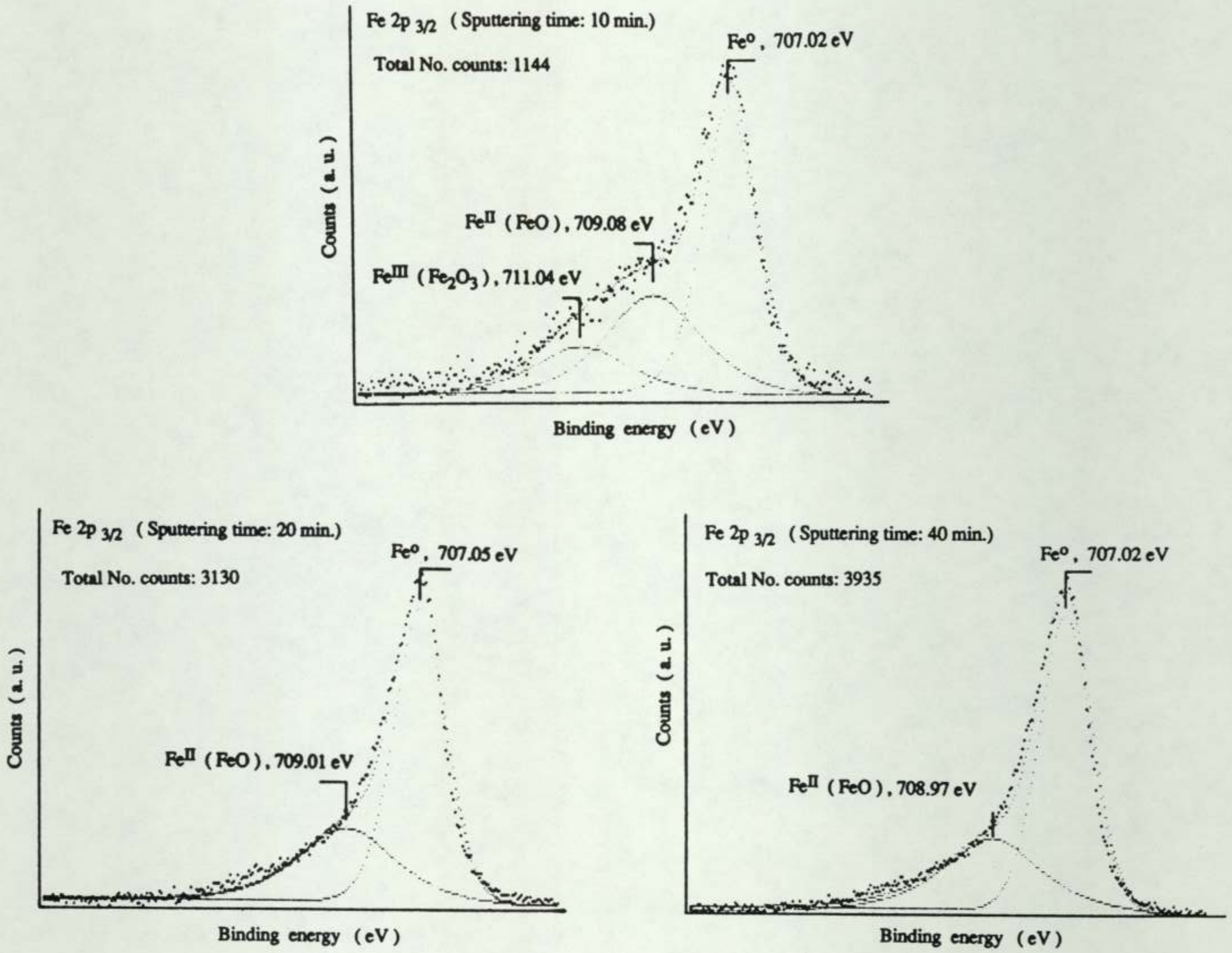

Figure 87: Fe 2p XPS spectra from untreated AISI 420 steel after A) 10 min., B) 20 min. and C) 40 min. sputtering time.

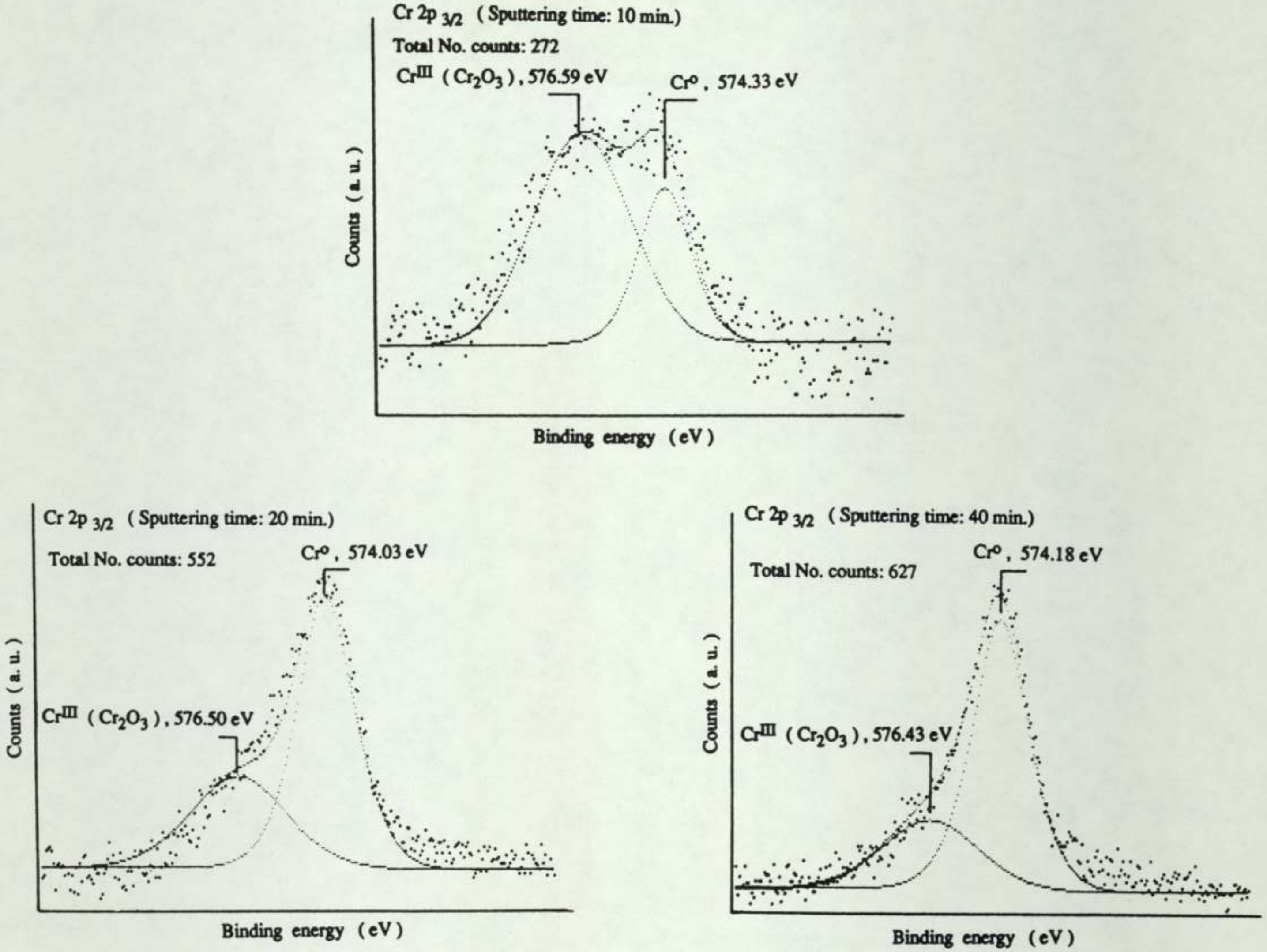

Figure 88: Cr 2p XPS spectra from untreated AISI 420 steel after A) 10 min., B) 20 min. and C) 40 min. sputtering time.

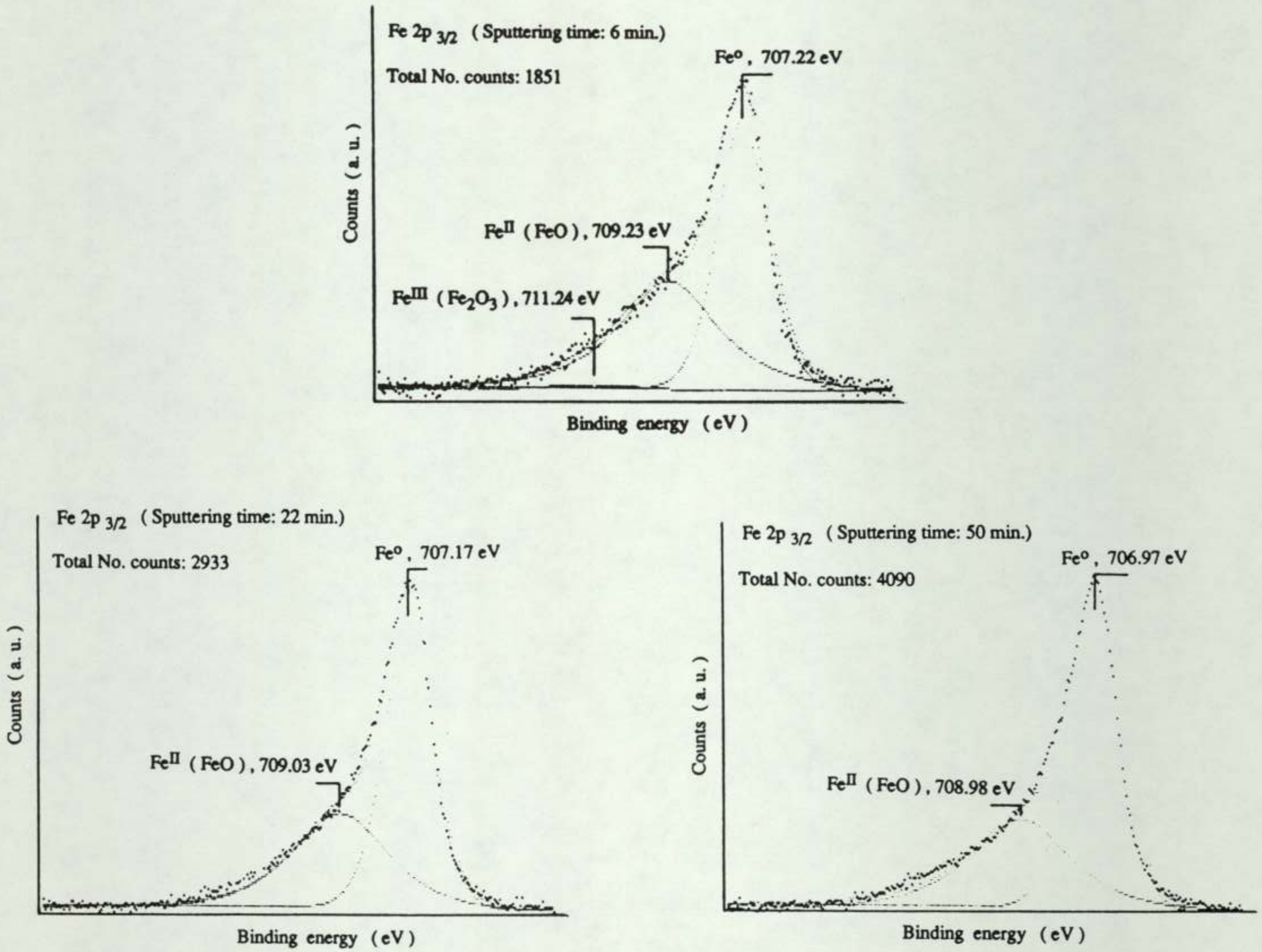

Figure 89: Fe 2p XPS spectra from implanted AISI 420 steel (4 x 10^{17} ions/cm^2) after A) 6 min., B) 22 min. and C) 50 min. sputtering time.

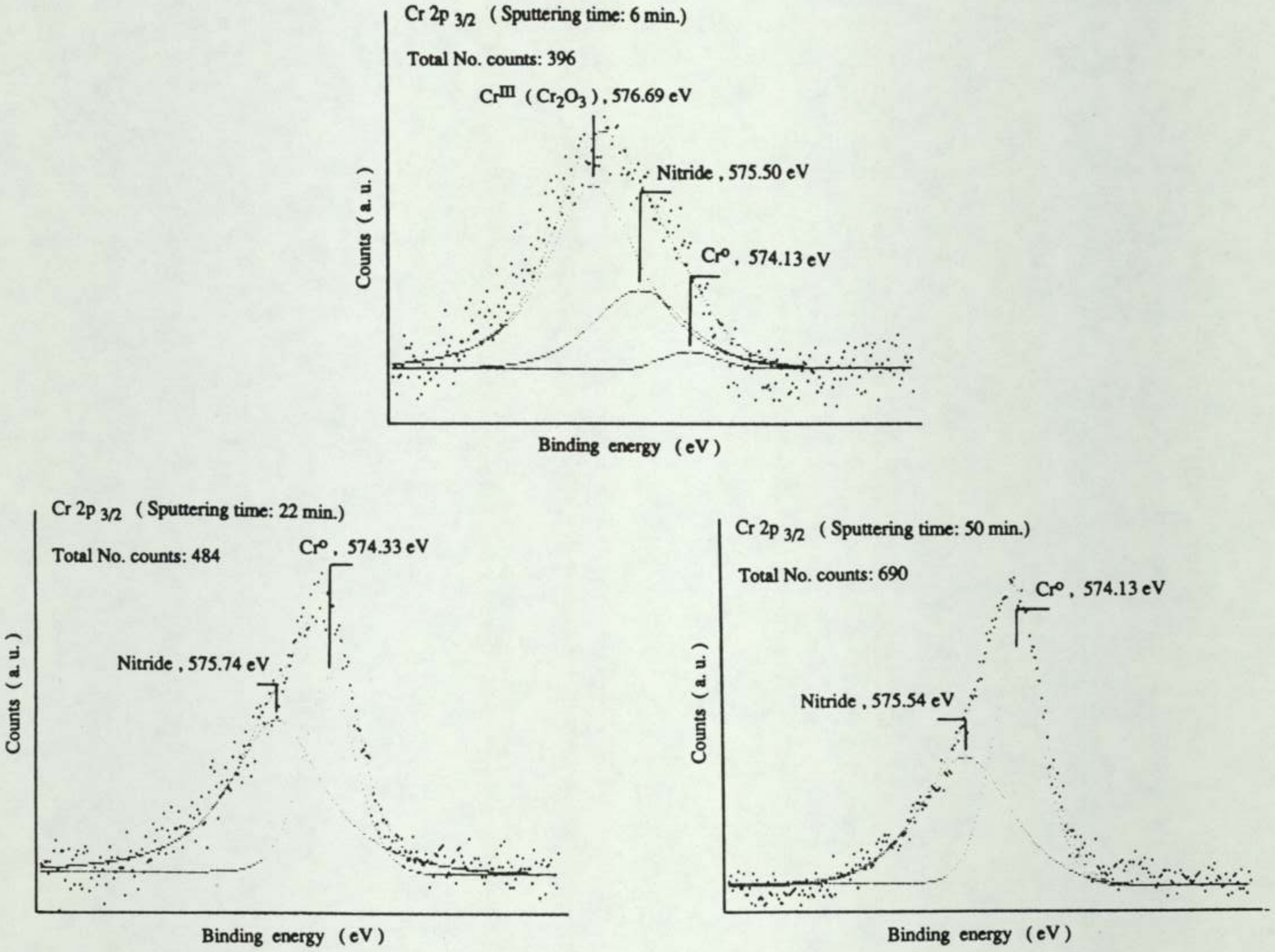

Figure 90: Cr 2p XPS spectra from implanted AISI 420 steel (4 x 10^{17} ions/cm^2) after A) 6 min., B) 22 min. and C) 50 min. sputtering time.

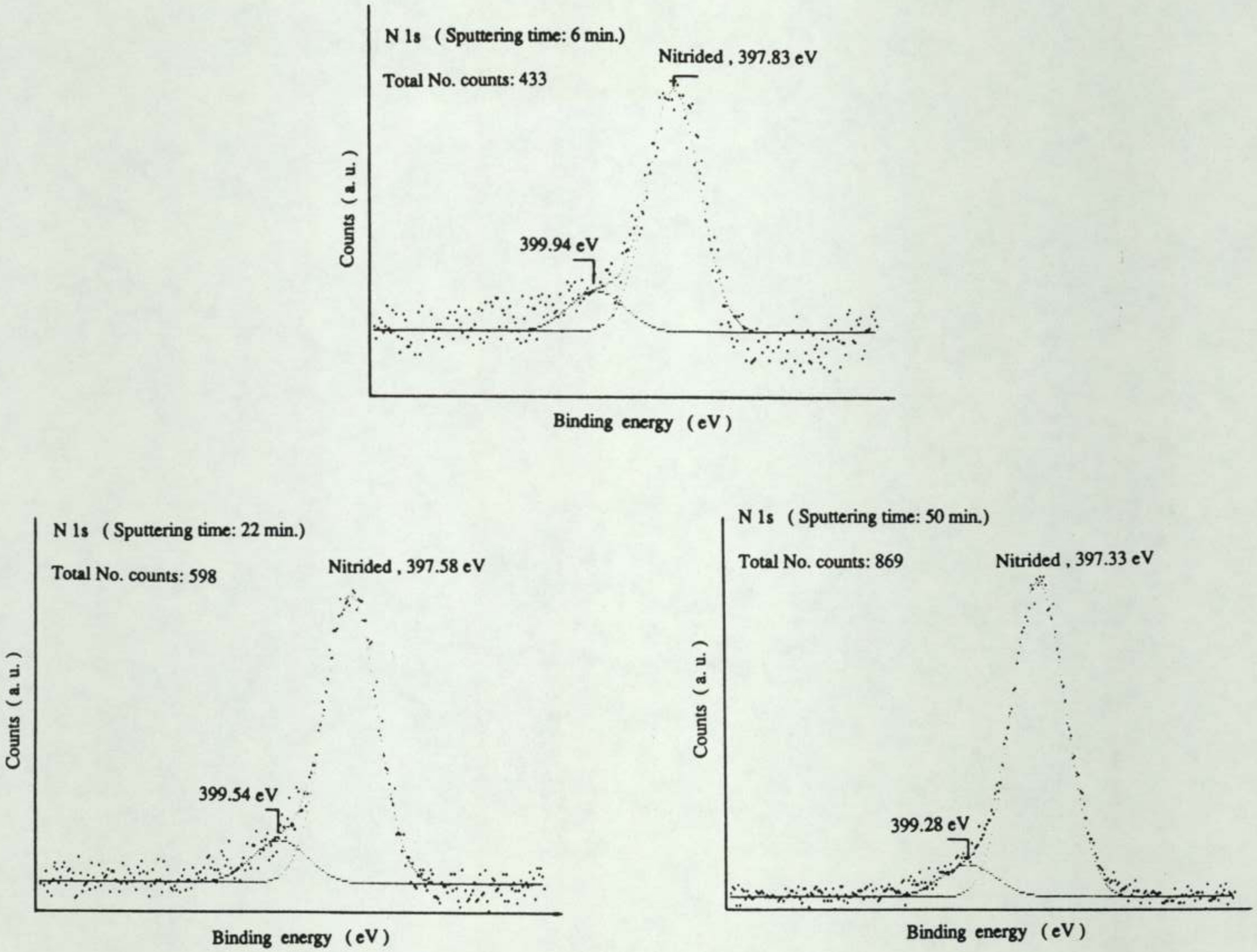

Figure 91: N 1s XPS spectra from implanted AISI 420 steel (4 x 10^{17} ions/cm^2) after A) 6 min., B) 22 min. and C) 50 min. sputtering time.

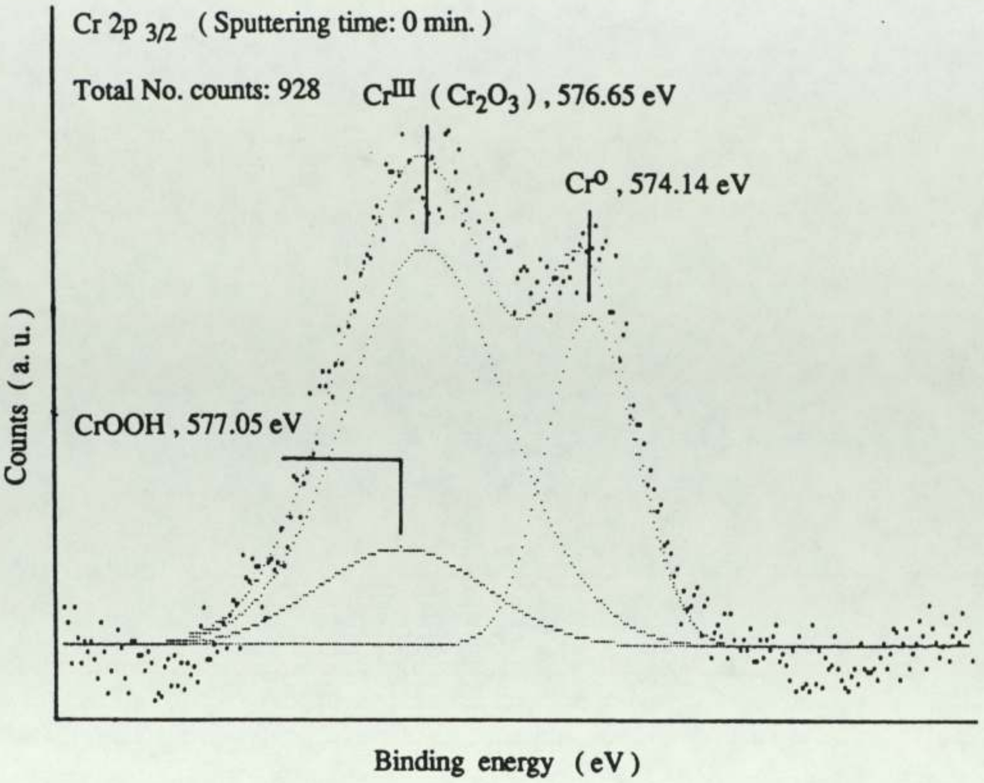

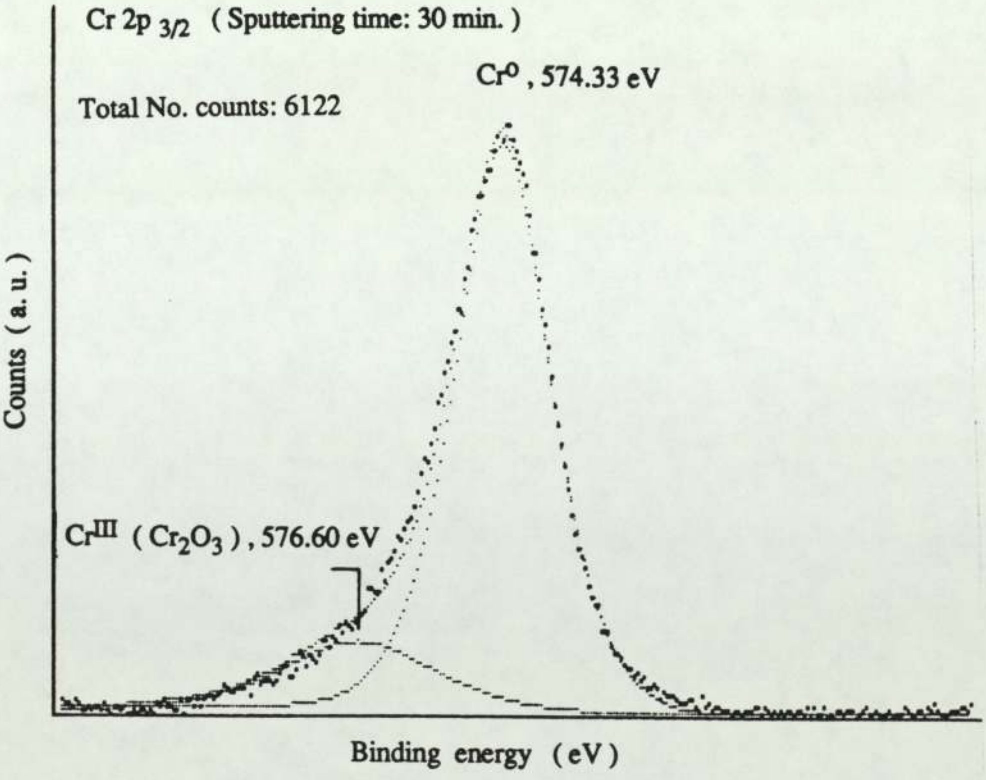

Figure 92: Cr 2p XPS spectra from untreated hard Cr coating, A) at the surface and B) after 30 min.sputtering time.

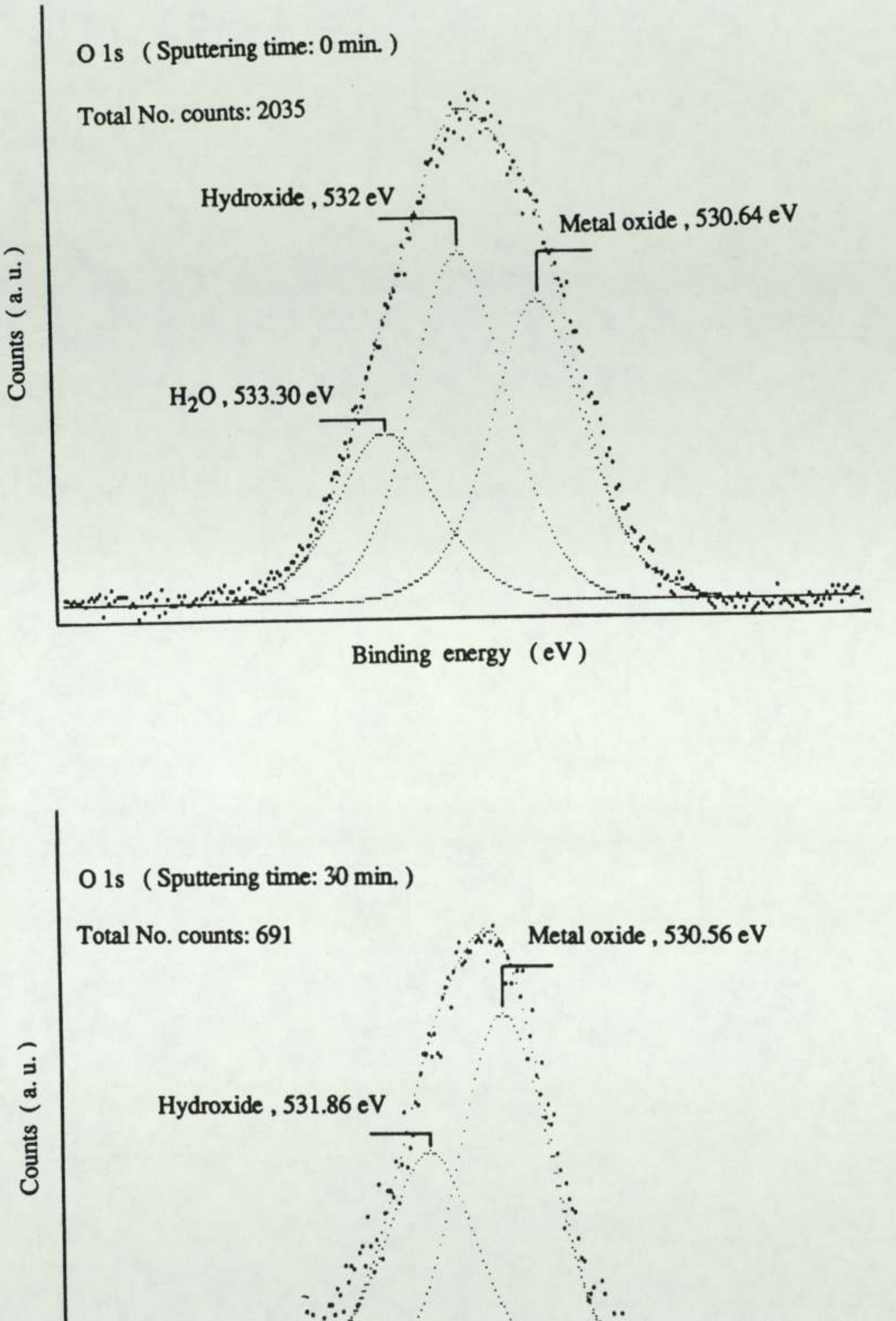

Figure 93: O 1s XPS spectra from untreated hard Cr coating, A) at the surface and B) after 30 min. sputtering time.

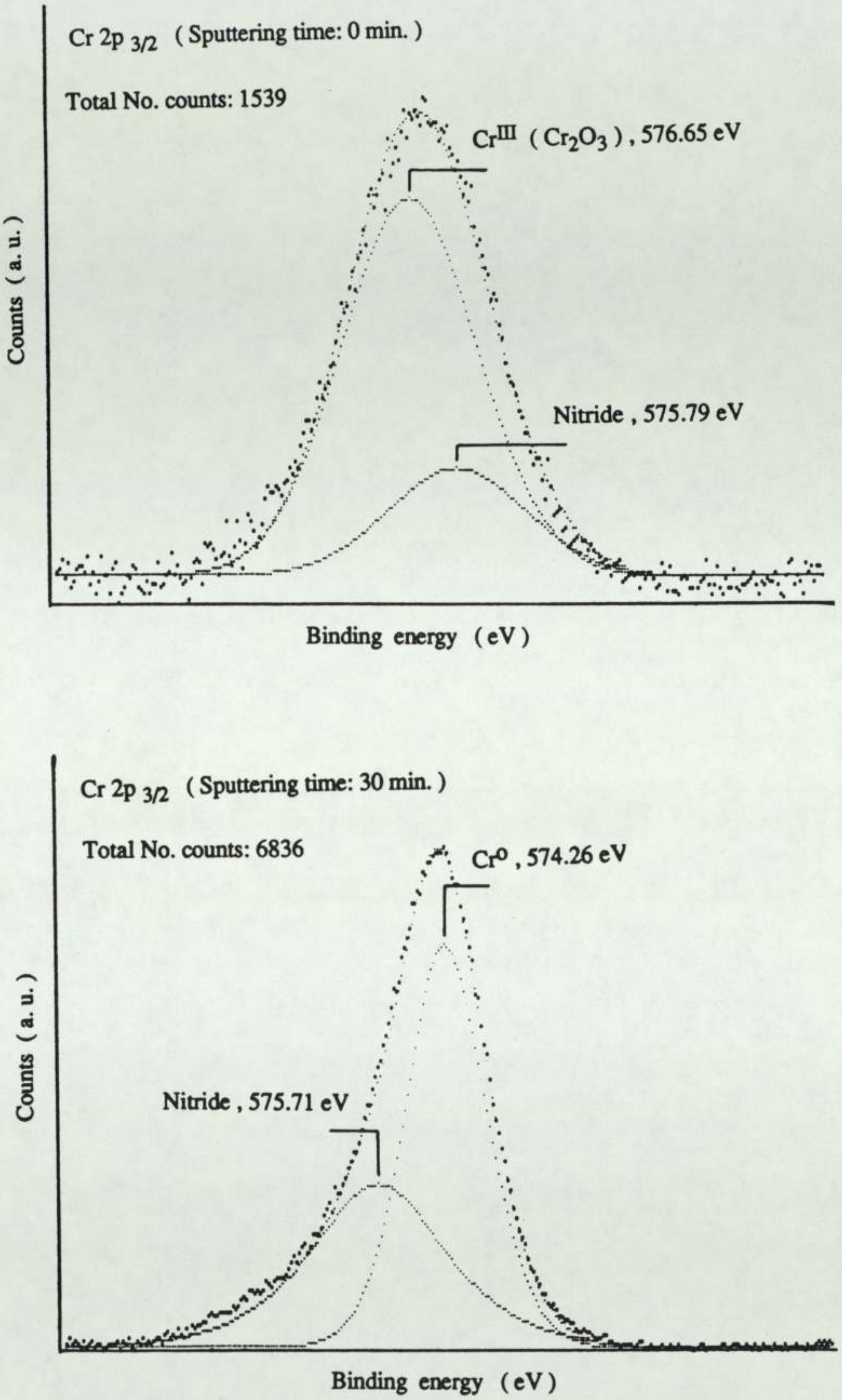

Figure 94: Cr 2p XPS spectra from implanted hard Cr coating (2 x 10^{17} N^+ ions/cm^2) A) at the surface and B) after 30 min. sputtering time.

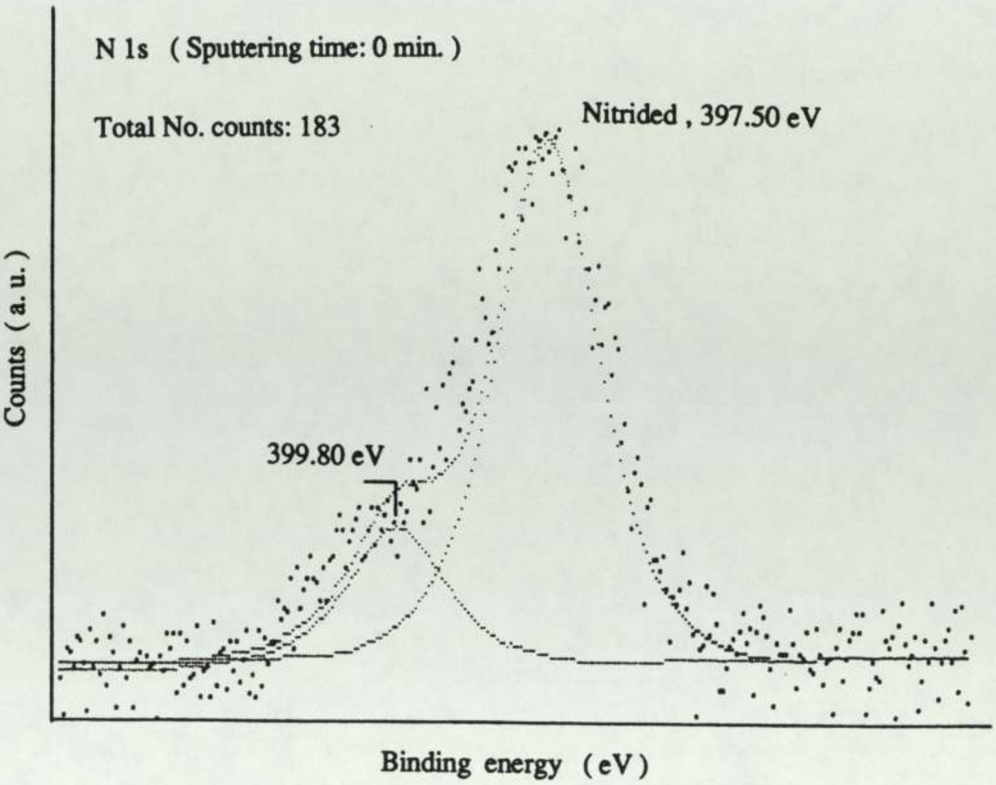

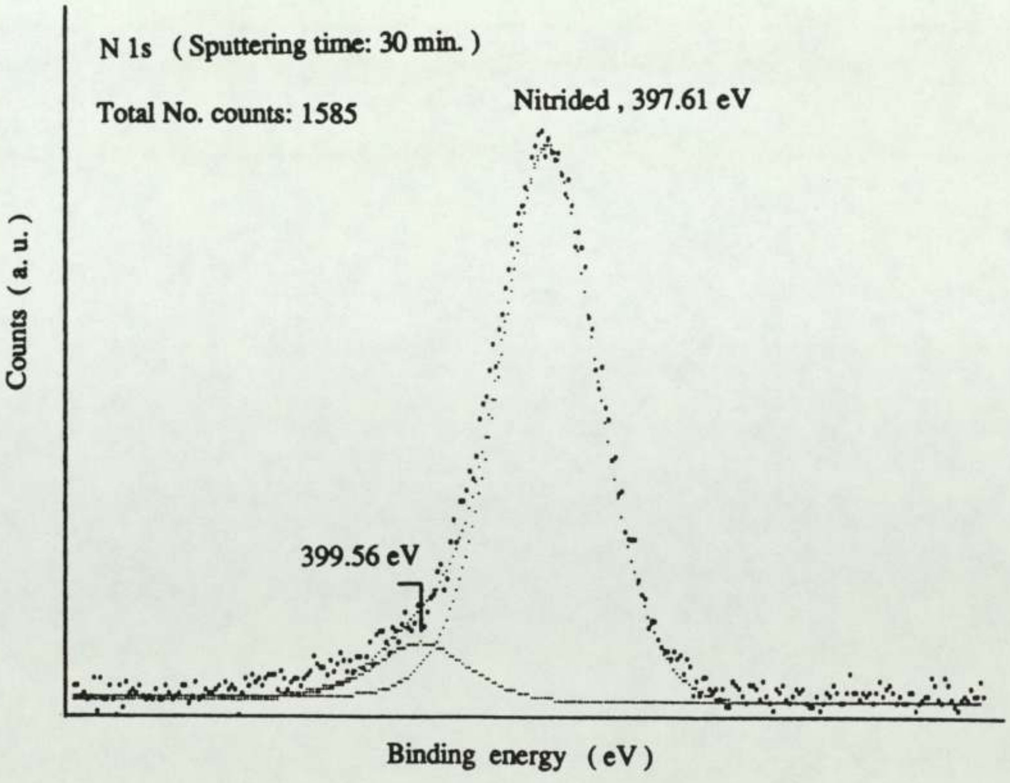

Figure 95: N 1s XPS spectra from implanted hard Cr coating (2 x 10^{17} N^+ ions/cm^2)
A) at the surface and B) after 30 min. sputtering time.

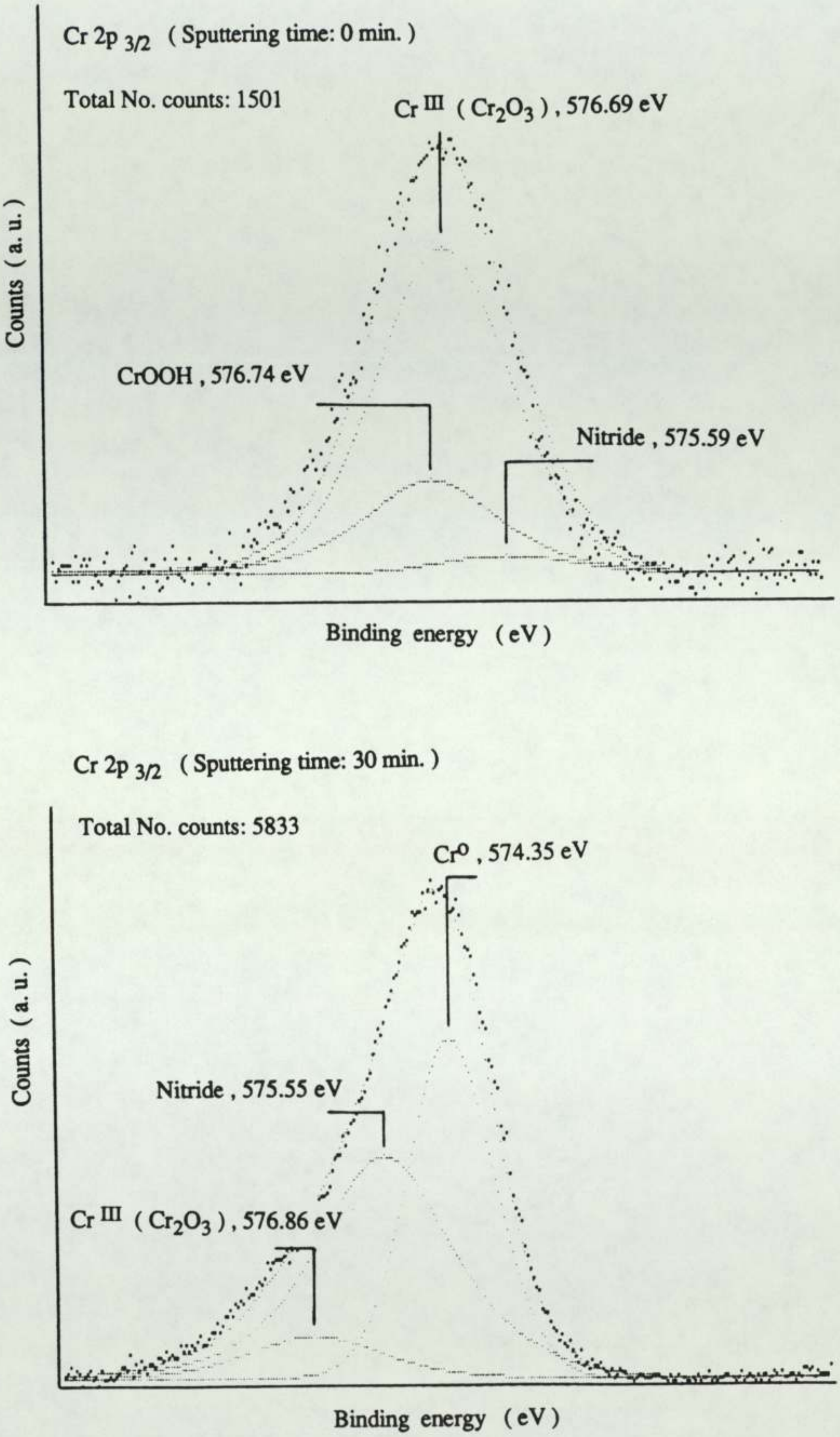

Figure 96: Cr 2p XPS spectra from implanted hard Cr coating (5 x 10^{17} N^+ ions/cm^2) A) at the surface and B) after 30 min. sputtering time.

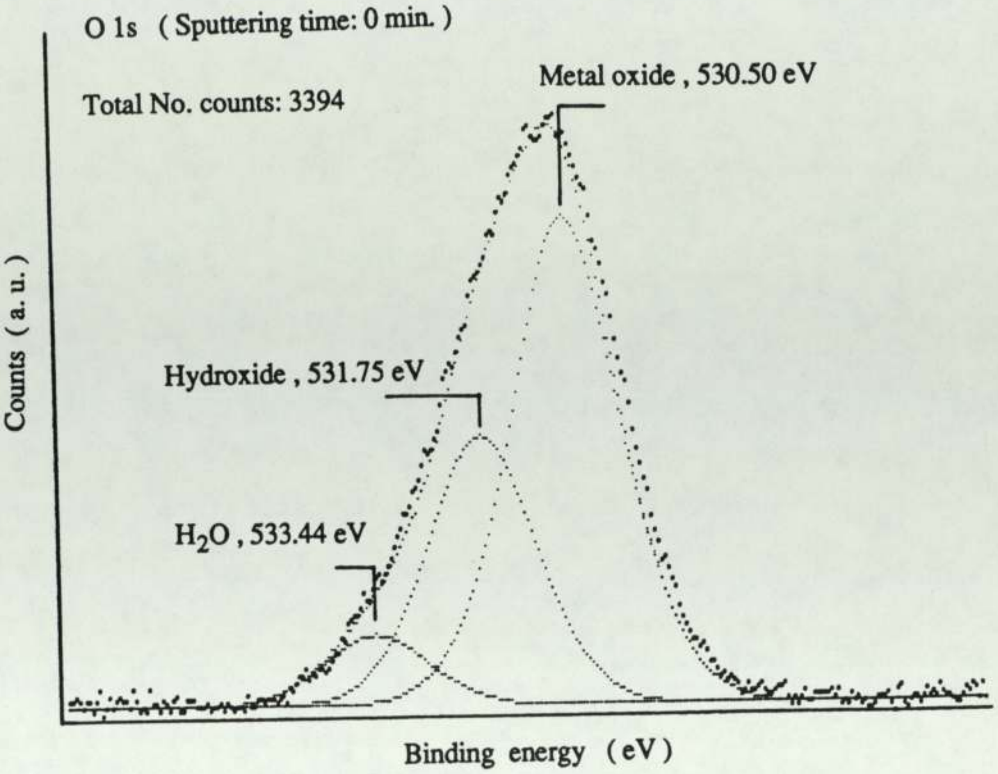

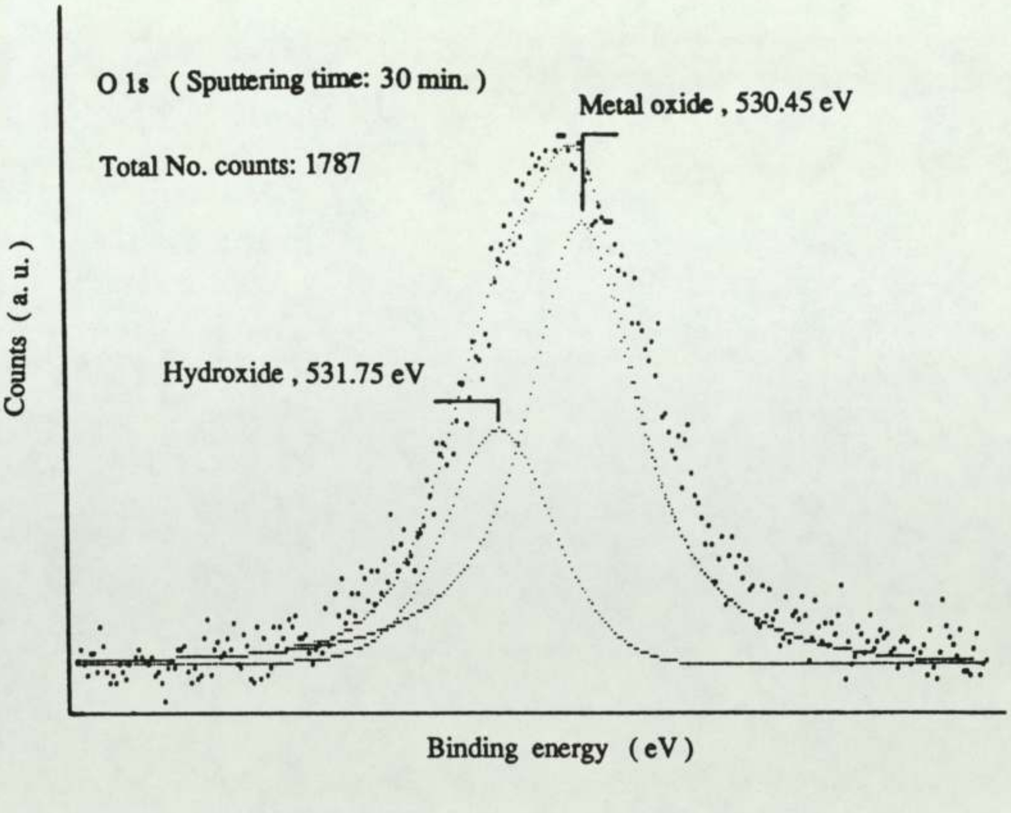

Figure 97: O 1s XPS spectra from implanted hard Cr coating (5 x 10^{17} N^+ ions/cm^2)
A) at the surface and B) after 30 min. sputtering time.

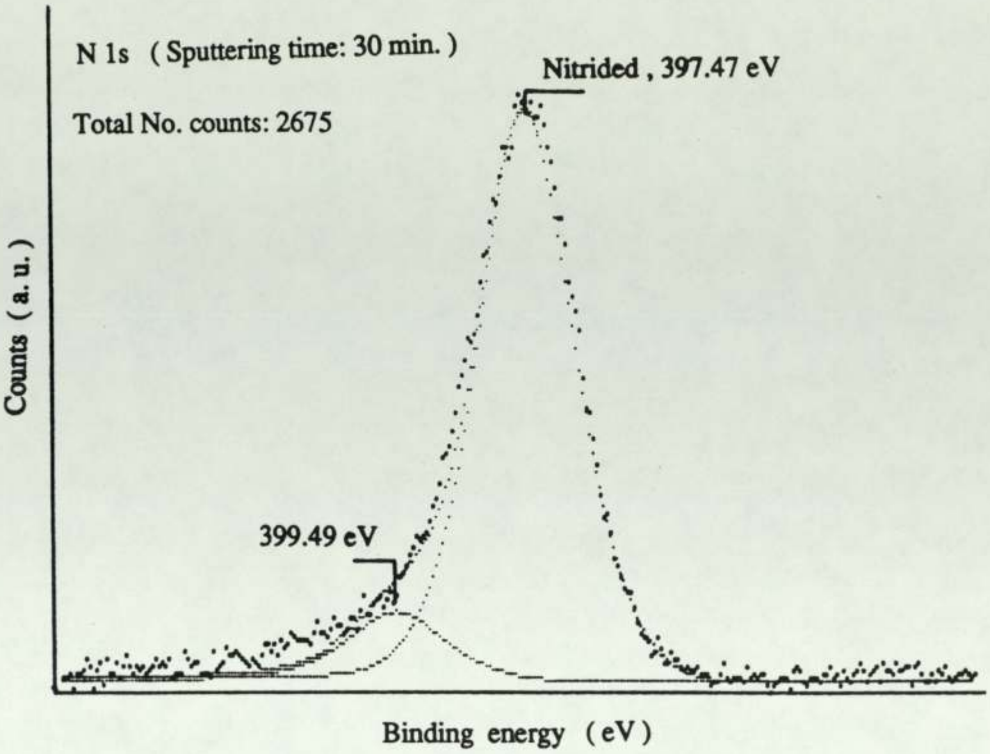

Figure 98: N 1s XPS spectrum from implanted hard Cr coating (5×10^{17} N^+ ions/cm^2) after 30 min. sputtering time.

5.5 Nuclear Reaction Analysis

$^{14}N(d,p)$ spectra obtained from AISI M2, D2 and 420 steel specimens implanted at a dose of 4 x 10^{17} ions/cm^2 are presented in Figure 99. All the peaks to the right of channel 300 are from deuteron reactions with nitrogen and below this channel the contribution is almost entirely from the bulk carbon of the steels. The small peak in the hollow at about channel 128 is from reactions with oxygen in the thin surface oxide layer. A summary of the results obtained in two different laboratories can be seen in Table 25, where the applied nitrogen dose is indicated with the retained or measured nitrogen dose calculated from the nuclear reaction analysis.

Table 25: Nuclear reaction analysis data of tool steels

Steel material	Nitrogen dose (x 10^{17} ions/cm^2)	Retained nitrogen Harwell	Retained nitrogen Birmingham Univ.
AISI M2	3		2.4
AISI D2	3		2.51
AISI 420	3	3.83	2.34
AISI M2	4	3.2	3.66
AISI D2	4	3.54	3.66
AISI 420	4	4.97	4.63

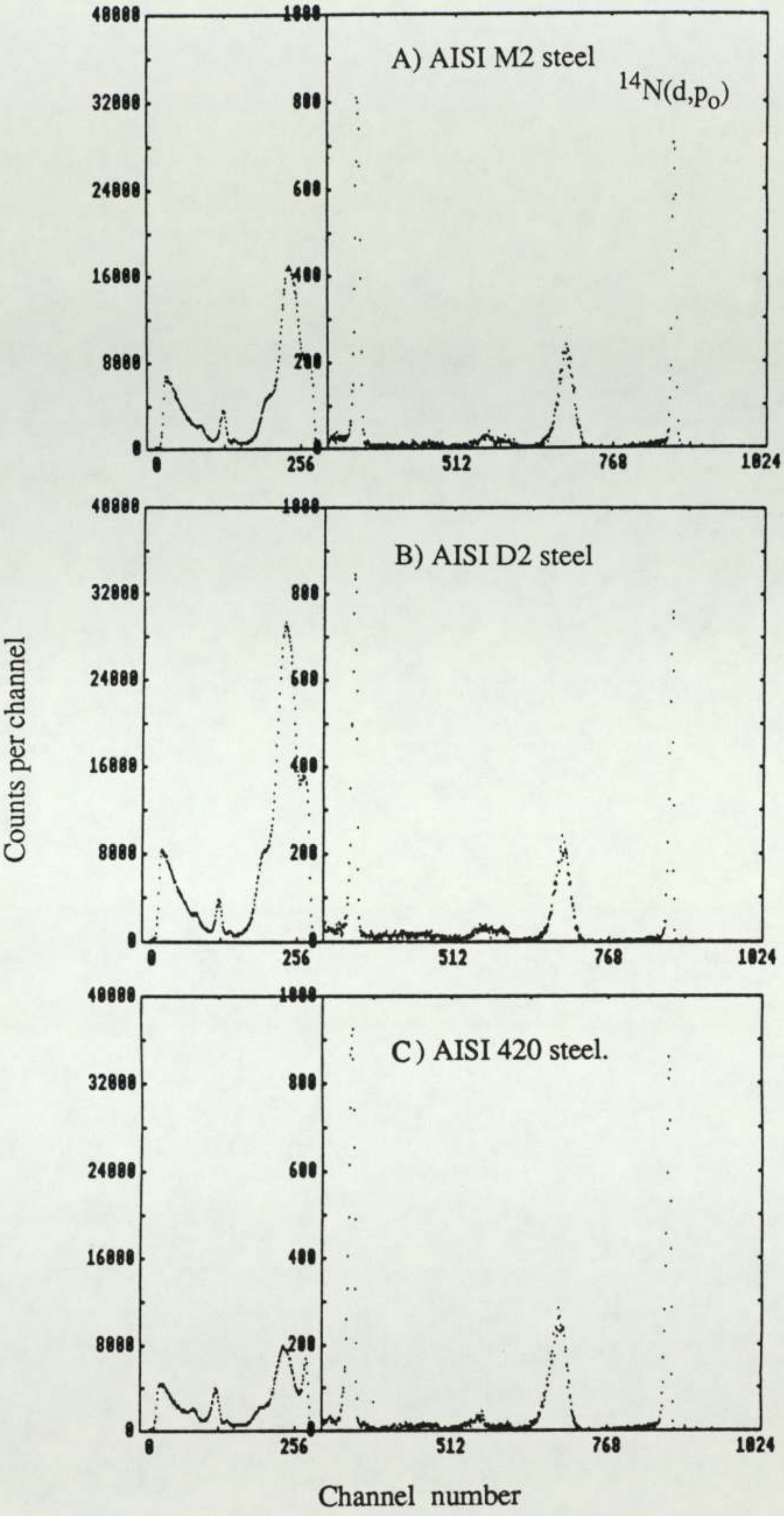

Figure 99: Nuclear reaction analysis spectra obtained from tool steels implanted at 4×10^{17} nitrogen ions/cm^2. A) AISI M2 high speed steel. B) AISI D2 cold work tool steel and C) AISI 420 martensitic stainless steel.

5.6 Transmission Electron Microscopy

TEM observation of steel specimens in the bright field mode, untreated and nitrogen implanted did not show a significant difference. The images exhibited the typical heavily dislocated structure, characteristic of martensitic steels. No attempt had been made prior to implantation to eliminate the deformed layer created by mechanical polishing of the specimens, in order to imitate common industrial practice. Implantation was carried out on this layer which might explain the difficulties experienced in observing differences in the structure.

Problems were also encountered when preparing hard chromium specimens. These were extremely brittle and implantation introduced additional stresses in the deposit. This produced curling around the electron transparent areas produced by the ion beam thinning, which in many cases made samples unsuitable for examination. The fine grained structure of the deposit is indicated in Figure 100 This shows a bright field image obtained from a chromium coating implanted at 4 x 10^{17} ions/cm^2. Owing to the limited time available for completion of this project and since chemical information had already been obtained using other techniques such as XPS, it was decided at that point not to pursue further the TEM work.

A) Untreated Cr (Type I), x150 K Magnification

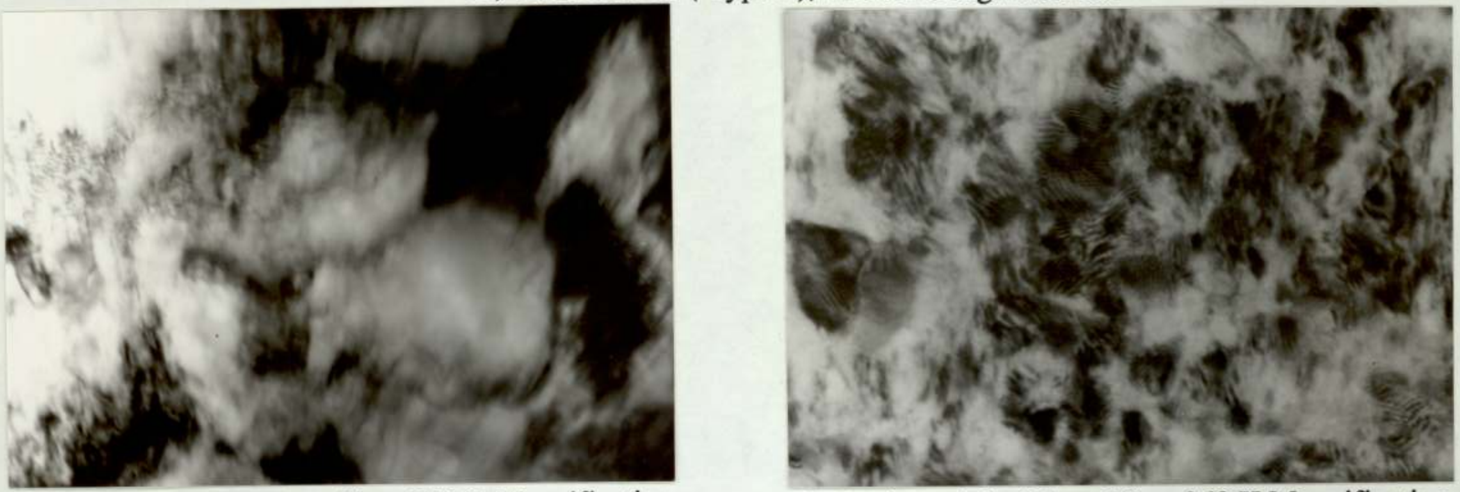

B) Implanted Cr (Type I), x250 K Magnification

C) Implanted Cr (Type II), x360 K Magnification

Figure 100: Bright field TEM images of hard Cr coatings. A) Unimplanted Cr coating (Type I, 700 $HV_{0.1}$). B) Implanted Cr coating (Type I), dose: 4 x 10^{17} ions/cm^2 and C) Implanted Cr coating (Type II, 1050 $HV_{0.1}$), dose: 4 x 10^{17} ions/cm^2.

5.7 X-Ray Diffraction Analysis

XRD was only performed on electroless Ni-P deposits. The diffraction pattern of electroless nickel-phosphorus coating in the as-plated state is indicated in Figure 101A. High dose nitrogen implantation at 6 x 10^{17} ions/cm^2 and a dose rate of 6 $\mu A/cm^2$ caused the formation of the Ni_3P phase, as the corresponding diffraction pattern shows (see Figure 101B).

Figure 102A illustrates the diffraction pattern of a hardened Ni-P coating after heat treatment at 400°C for one hour, and Figure 102B depicts similar data, but after additional high dose nitrogen implantation at the conditions described earlier. No cooling or rotation of the samples was provided during the implantation process and therefore the surface temperature of the specimens might have increased to 250°C due to the bombardment heating effect of the implantation. The nitrogen implantation treatment was carried out for about 4 hours and 30 minutes, thus effectively allowing precipitation hardening to occur in the thin electroless Ni-P coating (25 μm).

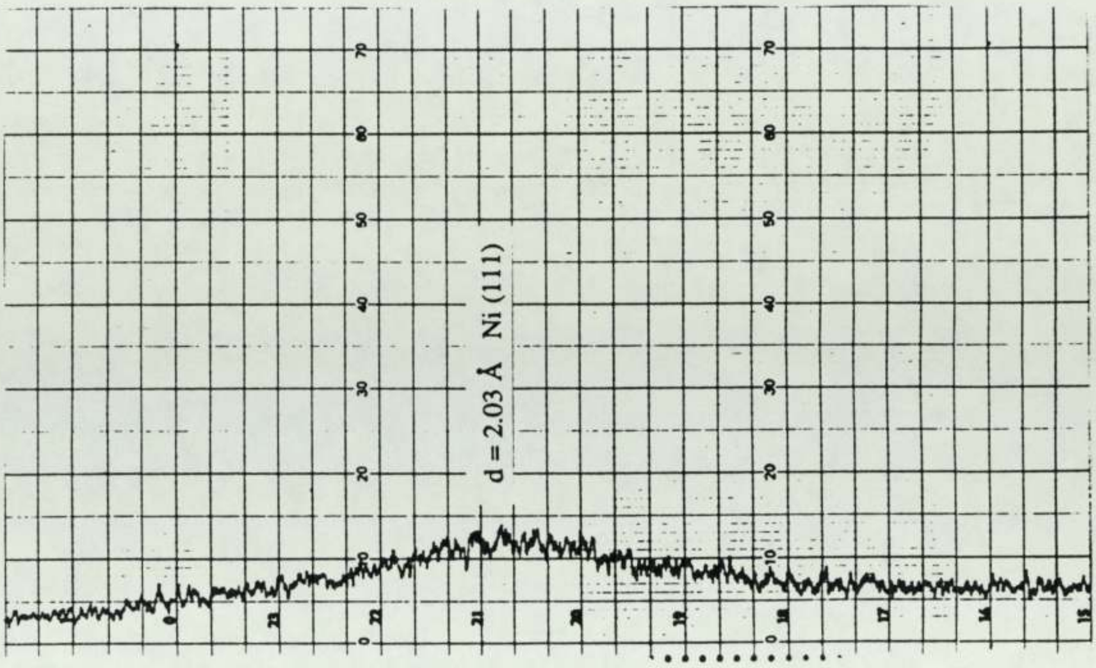

A) As plated electrolessNi-P coating

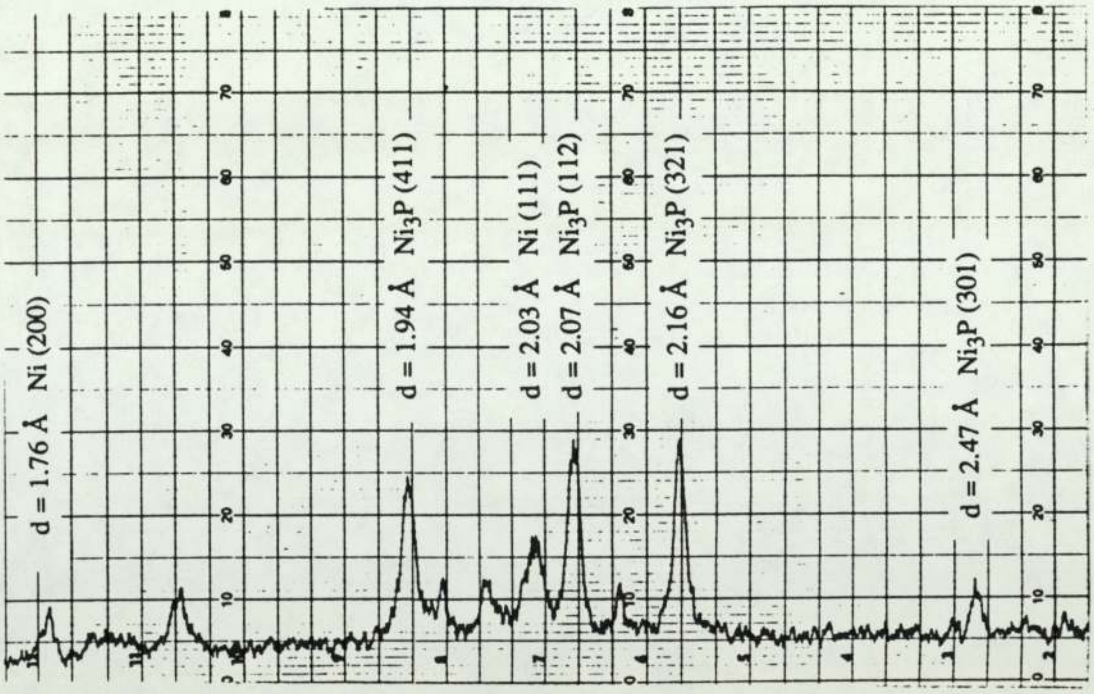

B) As plated electroless Ni-P coating, implanted at 6 x 10^{17} ions/cm^2.

Figure 101: X-ray diffraction patterns of unhardened electroless Ni-P coatings.
A) As-plated coating. B) Implanted at 6 x 10^{17} ions/cm^2.

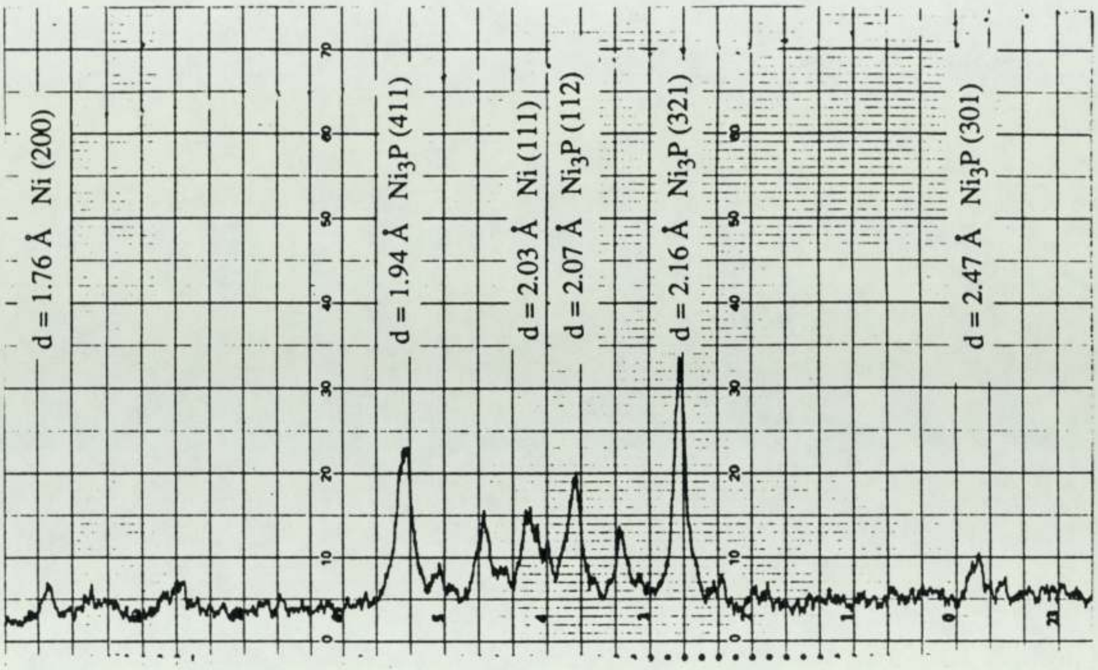

A) Hardened electroless Ni-P coating

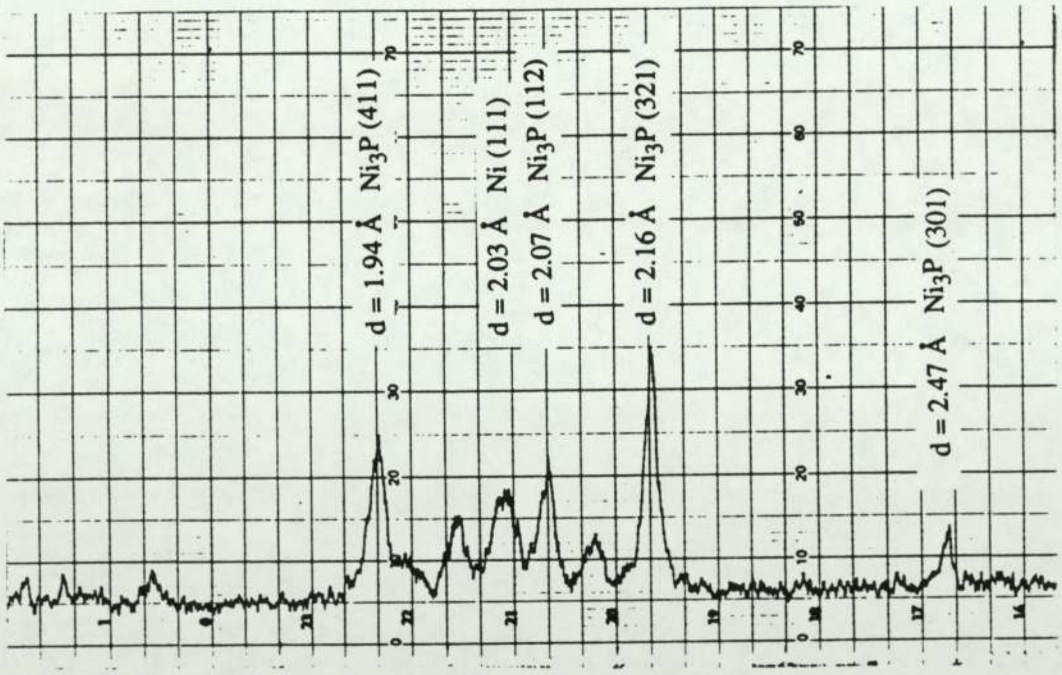

B) Hardened electroless Ni-P coating, implanted at 6 x 10^{17} ions/cm^2.

Figure 102: X-ray diffraction patterns of hardened Ni-P coatings.

A) Hardened Ni-P coating. B) Implanted at 6 x 10^{17} ions/cm^2.

CHAPTER 6

DISCUSSION OF RESULTS

6.0 DISCUSSION OF RESULTS

To obtain a better interpretation of the results described in the previous section a separate discussion will be presented below for each of the groups of materials investigated, ie. tool steels and engineering coatings, with a general description of the effect of nitrogen implantation on friction and wear of these materials.

6.1 Tool Steels

Nitrogen implantation brings about a very high improvement (up to 2 times) in the surface hardness of the steels in the annealed condition (see Table 13). This observation agrees with the results of Fui Zhai et al(98) and other workers(96, 103) for similar materials and can be explained by the fact that nitrogen implantation can strengthen the ferrite phase by interstitial or precipitation hardening. Additionally, stresses induced by implantation might contribute to the hardening. Nitrogen atoms, with a radius of 0.07 nm, prefer to reside in octahedral sites and these interstitial voids in bcc iron are 0.019 nm in radius (0.052 nm for austenite), therefore an important strain is produced. Nevertheless, this hardening effect is of limited interest since normally these steels are used hardened to optimum bulk mechanical properties for tooling applications.

Implantation of hardened and tempered steels also produced an improvement in the surface hardness as Table 13 indicates. Results seem to be rather contradictory in the extent of the hardening effect and it appears that implantation conditions can exert an important influence. In the case of efficient heat conduction during implantation, ie. water cooling and rotation of the firmly clamped specimens, hardening was limited to a maximum of 16% (RHI = 1.16) for all steels. When the specimens were positioned on a metal block which acts as a heat sink a much more significant improvement in hardness was achieved as Figure 40 illustrates. Radiation and conduction cooling during the treatment might not have been adequate, the sample size (12 mm Ø x 6 mm) was not large enough to completely store implanted energy and therefore a temperature rise could have occurred, causing some diffusion of the nitrogen.

Figure 40 shows a relative hardness index of 1.8 (ie. 80% increase) for the martensitic stainless steel AISI 420 implanted under the above described conditions. Depth of penetration of the Vickers indentor is approximately 1/7 of the diagonal length(228); using a 5g load the diagonal length for the implanted material (7 x 10^{17} ions/cm^2) was 2.8 μm (3.8 μm for the untreated AISI 420 steel), ie. a depth of penetration of 0.4 μm. Implantation at room temperature conditions produced a surface modified layer of about 0.2 μm (see as reference Figures 79 to 81); therefore if diffusion took place due to inefficient heat sink, a larger implanted area is sampled by the indentor and as a consequence more significant hardening effects can be observed. Hence, hardness of implanted layers as measured by conventional micro-indentation techniques is depth sensitive and can be subjected to considerable variations due to penetration of the nitrogen ions either by energetic or diffusional processes.

To overcome the problems encountered with conventional micro-hardness testers, special ultra-low indentation techniques are usually carried out and, as Figure 44 illustrates, a much more significant improvement in hardness exceeding 100% at depths up to about 300 nm is achieved in the implanted AISI 420. As discussed above heating effects during implantation can be considered to have caused deeper penetration of the nitrogen ions. These results are in agreement with those obtained with conventional techniques and presented in Figure 40 and the results reported by Dimigen et al(103) for a similar martensitic stainless steel.

Figure 40 shows, as expected, that the best hardening results occur for AISI 420 steel. This material contains a low carbon and a high chromium content, therefore implantation would contribute to hardening by interstitial and precipitation strengthening. X-ray photoelectron spectroscopy work (see Figures 90 and 91) indicates that most of the nitrogen in this steel is in a nitrided state and combines preferentially with Cr to form chromium nitrides. This is in close agreement with the work of Dimigen et al(103), in which XPS data of AISI 440B steel are presented.

Furthermore, nitrogen is retained in this steel at higher concentrations as indicated in Figure 103 obtained from the Auger electron spectroscopy work, and Nuclear Reaction Analysis also shows maximum retention at a dose of 4 x 10^{17} ions/cm^2 for AISI 420 steel (see Table 25). This agrees with the observations of

Principi et al(147) who reported that the threshold concentration of retained nitrogen increased with Cr content.

AISI M2 high speed steel has a microstructure consisting of a dispersion of carbides in a high carbon martensitic matrix, as shown in Figure 104. It can be considered that the available hardening mechanisms are already operative in this microstructure through its heat treatment but some slight hardening can also be expected to occur after nitrogen implantation due to nitride precipitation, since this steel contains a high alloying content in nitride forming elements.

The XPS spectra obtained from nitrogen implanted AISI 420 steel (see Figures 89 to 91) illustrate some differences when compared with those obtained from the untreated material (Figures 87 and 88). A summary of the binding energy values of peaks fitted to each spectrum can be seen in Tables 26 and 27 for untreated and implanted AISI 420 respectively. Widths at half maxima (FWHM) in eV and the area of each peak assigned are also indicated in each table, together with the chemical state.

It can be seen that nitrogen implantation produces significant changes in the surface layer and these can be observed in the chromium spectra. At the surface, most of the chromium is in the form of chromium oxide (Cr_2O_3) at a binding energy of 576.6 eV, for both untreated and implanted steel (see Table 28 for binding energies of reference compounds). However, on the implanted surface most of the metallic chromium (Cr°) has become chromium nitride (shift of ca 1.4 eV). At longer sputtering times Cr 2p spectra from the untreated material present an increasing contribution of the metallic species (Cr°) to the cost of Cr_2O_3 (see Figure 88), while in the nitrogen implanted material only metallic and the nitride contributions could be observed.

Binding energies of the chromium nitride formed, from 575.5 to 575.74 ± 0.2 eV (Table 27) agree well with those reported elsewhere(229,230) for CrN compound formation. The N 1s photoelectron peaks in the implanted steel (see Figure 91) show that nitrogen is bound almost entirely as a nitride at a binding energy of 397.3-397.8 ± 0.2 eV and a "shoulder" appears in all the peaks at higher binding energies (399.3-399.9 eV) which can be attributed to weakly adsorbed nitrogen species(141).

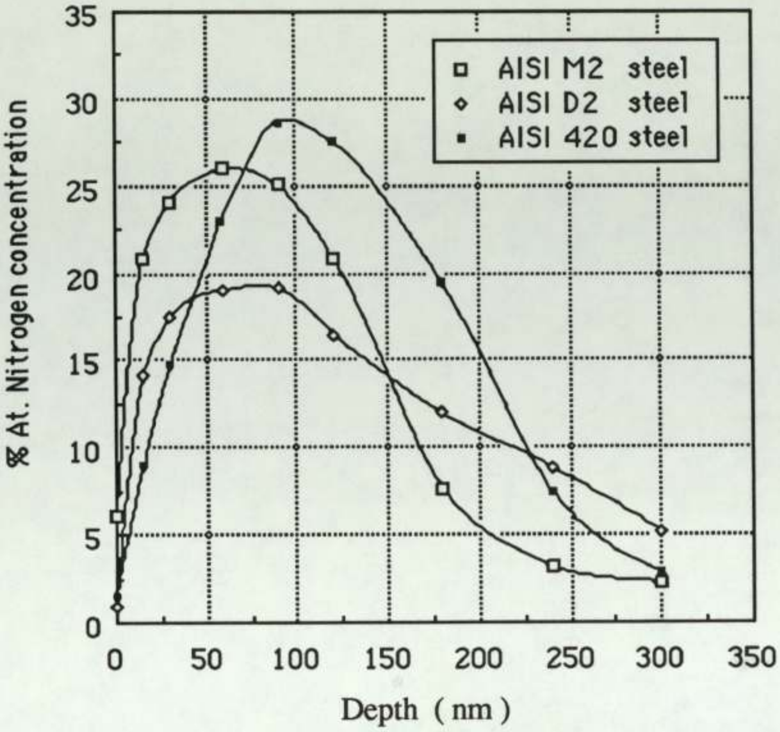

Fig.103: Nitrogen concentration profiles of AISI M2, D2 and 420 steels implanted at 4 x 10^{17} ions/cm^2.

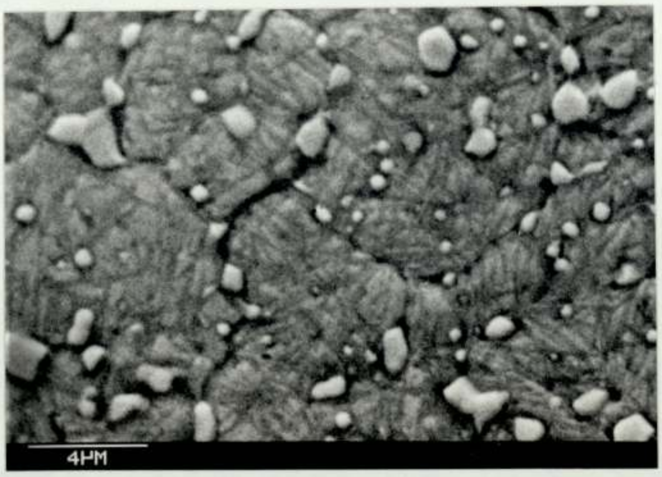

Fig.104: Scanning electron micrograph of AISI M2 high speed steel, showing a microstructure consisting of carbides in a martensitic matrix. 2% Nital etch.

Differences cannot be seen in the N 1s line to distinguish between iron and chromium nitrides. Furthermore, Fe 2p core-level binding energies for untreated and implanted steels did not show any significant differences, as Figure 87 and 89 (see also Tables 26 and 27) indicate respectively, therefore it may be concluded that at the dose investigated nitrogen bonds preferentially to chromium to form chromium nitrides. Singer and Murday(141) reported chromium nitride precipitation for an AISI 304 steel at doses above 2 x 10^{17} ions/cm^2 but when implantation was carried out at 8 x 10^{17} ions/cm^2 Cr and Fe nitrides could be identified by Auger lineshapes but not from XPS measurements. High Cr-containing steels (eg. austenitic stainless steels) have also been reported to precipitate CrN(142,144). This lends good support to the observations made in the present study and can explain the improved mechanical properties achieved in implanted steels, due to the formation of a fine dispersion of nitride particles.

Fe 2p spectra from untreated (Figure 87) and N^+ implanted steel (Figure 89) show some slight differences regarding oxide contributions. After sputtering for 6-10 minutes the spectra could be resolved into 3 peaks: metallic Fe° and the oxides Fe_2O_3 (Fe^{III}) and FeO (Fe^{II}). Longer sputtering times caused chemical reduction of the Fe_2O_3 oxide. The reduction of the initial oxide to a lower oxidation state and to metal by the Ar^+ beam is a well documented phenomenon(232), which is due to the differential sputtering effect of argon ions.

FeO is an oxide that is unstable below 570°C(233) and is not expected to be formed on unimplanted unworn steel surfaces, therefore it can be concluded that it is a product of the sputtering of Ar^+ ions during XPS analysis. FeO oxide was found to be the predominant oxide in nitrogen implanted AISI 420 steel (see Figure 89 and Table 27). During implantation nitrogen ions at much higher energy (90 keV) are bombarded towards the surface, thus, preferential sputtering mechanisms are also operative and a reduction from Fe_2O_3 to FeO takes place. The FeO outer layer formed on implanted surfaces is thermodynamically unstable in air and tends to reoxidize to Fe_2O_3, although some FeO could remain below the surface, especially in high chromium steels due to the protection given by Cr_2O_3, which is relatively impermeable to oxygen and Fe^+ cations.

Table 26: Core-level binding energies for peaks fitted to Fe and Cr $2p_{3/2}$ spectra from untreated AISI 420 steel

Fe $2p_{3/2}$

Sputter time (min.)	Binding energy BE (± 0.2 eV)	Chemical state	Peak width FWHM (eV)	Peak Area (a.u.)
10 min	707.02	Fe°	1.8	52%
	709.08	Fe^{II} (FeO)	3.2	32%
	711.04	Fe^{III} (Fe_2O_3)	3.2	16%
20 min	707.05	Fe°	1.8	67%
	709.01	Fe^{II} (FeO)	3.2	33%
40 min	707.02	Fe°	1.7	67%
	708.97	Fe^{II} (FeO)	3.2	33%

Cr $2p_{3/2}$

Sputter time (min.)	Binding energy BE (± 0.2 eV)	Chemical state	Peak width FWHM (eV)	Peak Area (a.u.)
10 min	574.33	Cr°	1.8	30%
	576.59	Cr_2O_3	3.2	70%
20 min	574.03	Cr°	1.85	65%
	576.5	Cr_2O_3	3.2	35%
40 min	574.18	Cr°	1.85	71%
	576.43	Cr_2O_3	3.2	29%

Table 27: Core-level binding energies for peaks fitted to spectra from N^+ implanted AISI 420 steel (4 x 10^{17} ions/cm^2)

Fe $2p_{3/2}$

Sputter time (min.)	Binding energy BE (± 0.2 eV)	Chemical state	Peak width FWHM (eV)	Peak Area (a.u.)
6 min	707.22	Fe°	1.7	53%
	709.23	Fe^{II} (FeO)	3.2	45%
	711.24	Fe^{III} (Fe_2O_3)	3.2	2%
22 min	707.17	Fe°	1.7	60%
	709.03	Fe^{II} (FeO)	3.2	40%
50 min	706.97	Fe°	1.7	61%
	708.98	Fe^{II} (FeO)	3.2	39%

Cr $2p_{3/2}$

Sputter time (min.)	Binding energy BE (± 0.2 eV)	Chemical state	Peak width FWHM (eV)	Peak Area (a.u.)
6 min	574.13	Cr°	1.7	3%
	575.5	Nitrided	3.0	28%
	576.69	Cr_2O_3	3.0	69%
22 min	574.33	Cr°	1.7	38%
	575.74	Nitrided	3.0	62%
50 min	574.13	Cr°	1.7	50.5%
	575.54	Nitrided	3.0	49.5%

N 1s

Sputter time (min.)	Binding energy BE (± 0.2 eV)	Chemical state	Peak width FWHM (eV)	Peak Area (a.u.)
6 min	397.83	Nitrided	1.7	85.4%
	399.94	Adsorbed	1.8	14.6%
22 min	397.58	Nitrided	1.7	87%
	399.54	Adsorbed	1.8	13%
50 min	397.33	Nitrided	1.7	90.6%
	399.28	Adsorbed	1.8	9.4%

Table 28: Reported binding energies of Cr $2p_{3/2}$, Fe $2p_{3/2}$ and N 1s electron levels in stainless steel substrates and reference compounds.

	Binding energy (± 0.2 eV)			
	Cr 2p	Fe 2p	N 1s	O 1s
*N^+-AISI 304 (141)	574.8	707.1	397.7	
*Nitrided AISI 304(141)	574.8	707.1	397.2	
*AISI 304 (unimpl.)(141)	574.6	706.8	-	
*AISI 304 (unimpl.)(111)	574.3	706.8		531.7
*N^+-AISI 304 (111)	574.0	706.9	399.9,397.2	531.6
Fe metal(231)		707.3		
Wustite FeO(231)		710.3		530.1
α-Fe_2O_3(231)		711.4		530.2
Fe metal(230)		706.8		
FeO(230)		709.2		530.1
Fe_2O_3(230)		711.0		530.1
Cr metal(229)	574.2			
Cr metal(230,141)	574.1			
*CrN(229)	575.7		396.8	
CrN(230)	575.5			
*Cr_2N(229)	576.1		397.4	
CrO_2(230)	576.1			
Cr_2O_3(230)	576.6			530.2

* No curve-fitting provided

Wear resistance

The wear resistance of all three steels investigated was improved by nitrogen implantation, as Tables 15 to 17 and Figures 46 to 48 show for the lubricated wear at 900 N load. The best wear improvement factor (of 2.47) was obtained for AISI 420 stainless steel at a dose of 4 x 10^{17} ions/cm^2. This agrees with the observation that also the best hardening effects were obtained in this steel, but according to Figure 40 higher nitrogen doses should also produce better wear behaviour. It can be concluded that although surface hardness is a good measure of the influence of nitrogen implantation, there is no simple relationship between hardness and wear behaviour and microstructural factors, such as volume and composition of precipitates, plasticity, fracture toughness and residual stress states can exert an influence.

Figure 49 summarizes the wear reduction factors for these steels at the doses investigated and, as it is shown, the most significant improvements do not occur at the same dose for all the materials. A dose of 3 x 10^{17} ions/cm^2 produces the best wear improvements in AISI D2 but a higher dose of 5 x 10^{17} ions/cm^2 is required to bring about a more significant wear reduction in AISI M2 steel.

It is reasonable to think that since alloying elements and composition of the steels, as indicated in Table 9, are different, the effect of nitrogen implantation will not be the same for a given dose in these materials. Figure 105 depicts nitrogen concentration profiles of AISI D2 and 420 steels implanted under the same conditions as the wear experiments. It is shown that higher nitrogen levels were obtained for AISI D2 at a dose of 3x10^{17} ions/cm^2 and for AISI 420 when implantation was carried out at 4 x 10^{17} ions/cm^2. These doses correspond to those which produced the best wear improvement (see Figure 49). Therefore, it can be concluded that the best wear behaviour occurred at the saturation dose and additional nitrogen bombardment would lead to a microstructure having inferior mechanical properties.

However, caution should be exercised, since two problems can arise experimentally. First, it is normal to have a relatively large scatter in the results of accelerated wear tests and secondly, the results of Auger spectroscopy are very sensitive to carbonaceous and oxide contamination layers, which might provide unexpected results.

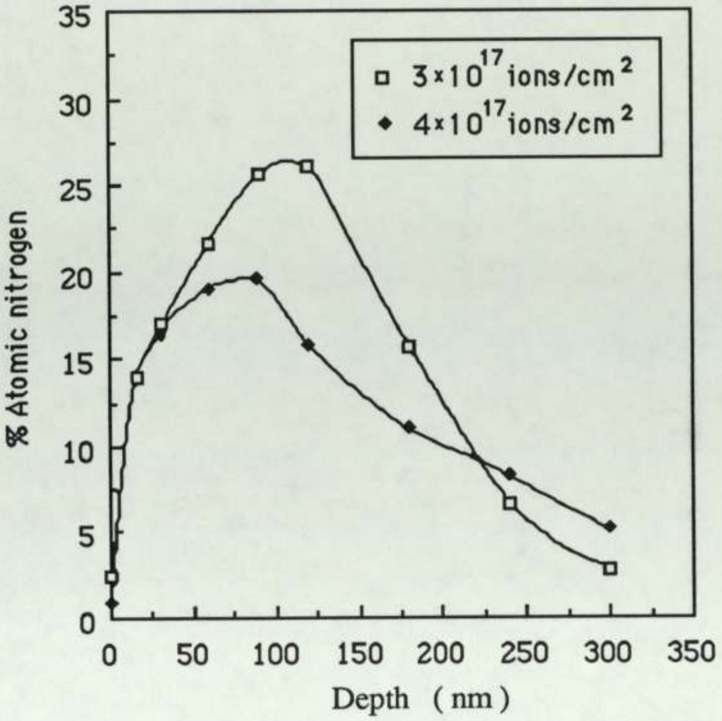

A) AISI D2 cold work tool steel.

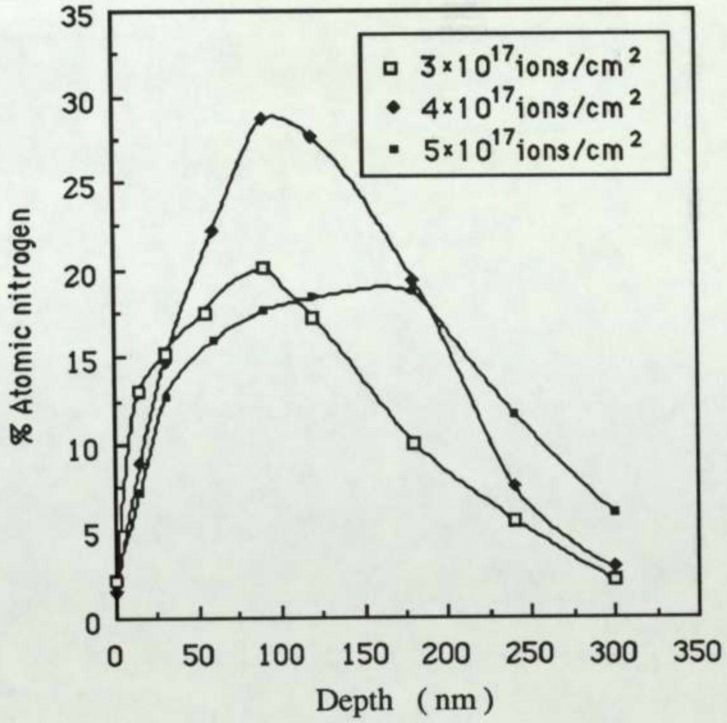

B) AISI 420 martensitic stainless steel

Fig.105: Nitrogen concentration profiles of implanted AISI D2 and 420 steels.

Figure 50 and Table 18 show the results obtained from AISI M2, D2 and 420 steels implanted at the optimum doses respectively, when a larger number of samples were tested. Results differ from those already discussed (see Figures 46 to 48) because of a different testing procedure imposed by material restrictions.

Figure 50 shows that both higher wear rates and the best wear resistance improvement after N^+ implantation are achieved for the softer AISI 420 stainless steel and, as expected, the harder AISI M2 steel exhibits the least improvement.

The wear results described above were also accompanied by a decrease in the friction coefficient, at least during the running-in period. Increasing nitrogen dose caused a marked improvement in the frictional characteristics of AISI D2 steel (see Figure 51) and a similar behaviour was exhibited by the AISI 420 steel (see Figure 52). Friction curves had an upward trend, as opposed to the general trend in dry friction to attain a steady-state value as the test proceeds. At the start of the Falex test a lubricant film is created on the rubbing surfaces preventing them from coming into full contact. Friction coefficient values for D2 under these conditions suggest a mixed lubricant regime (see Figure 11 as reference for lubricant regimes). This lubricant film is thin enough to permit contact between surface asperities and friction arises from adhesion between asperities, shearing of the lubricant film and ploughing of hard asperities into the softer counterface. As wear takes place under the high load, frictional heating causes the oil temperature to rise and viscosity to diminish thus affecting the lubricious film which causes a shift to a boundary regime. In this regime more metal to metal contacts occur between surfaces, ploughing and adhesion become more important and friction values rise.

A thin adventitious carbon layer from the diffusion pump oil in the implanter vacuum system is normally deposited on the implanted surfaces, additionally the bombardment process can affect the stoichiometry and adhesion of the oxide surface films to the base metal, causing a reduction in friction. Moreover, if nitrogen implantation improves the load bearing capacity of the surface the ploughing component of friction will also be reduced.

The wide range of implantation conditions and testing procedures used in the literature makes difficult the study and comparison of results. Nevertheless, the results reported here agree with those published elsewhere for similar steels. As a general rule, nitrogen implantation does not seem to improve frictional behaviour in low alloyed and high carbon steels(165,159,157), however significant reductions in friction have been found for stainless steels both in lubricated(98,112,162) and dry wear conditions(150,160). Nitrogen implantation reduces the galling tendency of these steels, probably by stabilizing the lubricious oxide film on the surface. This effect will be discussed below in light of the dry wear test results.

Wear behaviour under dry wear conditions and lower loads was also improved by nitrogen implantation. Table 23 and Figure 60 illustrate the gravimetric pin wear rate, K_w, of AISI M2 steel and it can be seen that the most significant effects occur at 30 to 40 N load. The reduction in K_w values for both untreated and N^+ implanted materials at 40 N load seems to indicate that a change in wear regime takes place; at this load frictional heating could have promoted a mild oxidative wear improving performance.

The wear resistance of AISI D2 and 420 steels also benefitted significantly after nitrogen implantation as Figure 59 depicts. The best wear improvement (a factor of 5.5) was obtained for the martensitic stainless steel. Table 24 summarizes the wear data and it is shown that room temperature and humidity can affect the wear results. Running-in friction was generally reduced by nitrogen implantation and this is supported by the observations of Feller et al(150) who tested similar materials also under dry conditions. However, no general trend was observed for final friction values for D2 and 420 steels. As mentioned above differences in the environment can explain the discrepancies observed for wear rates shown in Table 24 for identical materials and treatments. Humidity in the environment is known to have a marked effect on the wear of materials, but there is little agreement as to the direction or severity of this effect(234).

Figure 61 presents the running-in friction curves obtained from AISI 420 tested at 23°C and 57-60% RH (see Table 24). In this like on like material set of tests, severe wear by a combined ploughing and cutting mechanism was evident in the untreated material after few minutes, causing a sharp rise in the friction coefficient to a steady state value. Nitrogen implantation (see Figure 61) under the same testing and environmental conditions did not eliminate, but delayed this form of wear. Once the implanted layer was worn away the friction coefficient increased to similar values to those obtained for the untreated material. This severe wear mechanism was not always experienced, room temperature and humidity seemed to have a role to play, but friction values showed the same tendency.

As discussed earlier, the wide spectrum of wear testing procedures and implantation parameters used by different researchers hamper the possibility of a meaningful comparison between results. Few attempts have been made to determine the optimum nitrogen implantation parameters for a particular material and testing procedure. Probably, the most systematic study was by Iwaki et al(110), in which a range of tool steels including AISI D2, 420 and H13 were investigated by means of a pin-on-disc apparatus and implantation of 150 keV N_2^+ ions at doses from 10^{17} to 10^{18} ions/cm^2. No agreement was reached as to the optimum dose, different values were obtained for each material corroborating the idea that implantation is sensitive to alloying content. AISI D2 presented a saturation effect above 5 x 10^{17} ions/cm^2, while AISI 420 showed the best wear improvement between 2 to 5 x 10^{17} ions/cm^2 and above these doses wear behaviour deteriorated. Testing in Iwaki's work was limited to very short distances and light loads, conditions very different from those used in the present work.

Fayeulle and Treheux(164) reached the conclusion that the optimum implantation dose for AISI 304 austenitic stainless steel was of 2 x 10^{17} ions/cm^2 when the treatment was carried out at 40 keV energy. At lower energies higher concentrations can be obtained for a given dose closer to the surface, therefore saturation can take place at lower doses; additional implantation does not introduce more nitrogen due to sputtering processes and no further benefits in tribological performance are achieved. In the present work a higher energy 90 keV mixed ion beam (N^+ and N_2^+ species) was used, therefore optimum doses should be expected to lie in the range 3 to 5 x 10^{17} ions/cm^2, as reported, depending on base material.

Wear results described in this work show a much lower improvement than those reported in the literature, especially in the case of lubricated testing and this is due to the severity of this test. Nevertheless, it has been shown that under these conditions nitrogen implantation can also provide a significant influence. Daniels and Wilbur(185) also used very high loads (up to 2670 N) with a ring-on-block configuration lubricated test, and a 25% reduction in wear volume was reported for AISI M2 high speed steel, which is in agreement with the present findings. Hence, contrary to the suggestions(157,192) that nitrogen implantation does not produce additional improvement in martensitic structures, evidence proves that this process can improve hardness, friction and wear characteristics significantly providing that the treatment is carried out at optimum parameters to achieve its full potential. The choice of inadequate implantation treatment and inappropiate test procedures can lead to misleading conclusions.

Tribological tests are of limited significance if no attempt is made to understand the degradation mechanisms operating at surfaces and to investigate the influence that the implantation can exert on them. Characteristic profilometer traces from worn steel surfaces after lubricated Falex testing (see Figure 62) show that the wear volume is reduced by the implantation treatment. Under this sort of testing nitrogen implantation improved the load bearing capacity of the surfaces, as shown in Figures 65 and 67, reducing the grooving or cutting effect of hard asperities or work hardened wear particles that can become entrapped between contacting surfaces, thus, decreasing the amount of material removed. There was some evidence (see Figure 66) that the wear debris resulting from implanted surfaces was finer than that from untreated material, the latter containing a number of larger wear platelets with carbide particles as identified in the EDX analysis. This suggests that the implanted martensitic matrix is worn away, primarily by abrasion and plastic deformation, so that carbide particles can be more easily plucked out. Ion implantation strengthens the martensitic phase and can also induce extremely high surface compressive stresses(123) due to a large concentration of interstitials and the formation of precipitates which attempt to expand the lattice. These compressive stresses can close partially existing microcracks or influence the crack nucleation stage during wear, therefore delaying or preventing the detachment of plate-like particles by the tensile stresses introduced during sliding. In addition residual compressive stresses would reduce the cyclic fatigue damage caused during sliding wear by decreasing the total tensile stress operating at the surface.

It was observed that some of the untreated AISI 420 steel specimens when tested under high loads in the Falex apparatus suffered a high torque and severe adhesive-abrasive wear (see Figures 67A and 67B). Like on like material testing of this steel at high loads can produce galling especially if metal to metal contact occurs. The adhered particles or work-hardened debris originated by this wear mechanism can become entrapped and accelerate degradation of surfaces by a cutting process, producing metallic debris (see Figure 67C) which exhibits the typical lamellar structure of chips formed in metal cutting processes. This phenomenon was not observed in the implanted surfaces, as shown in Figure 67D; nitrogen implantation improved abrasion resistance and reduced the adhesion tendency between surfaces.

Observation of surfaces of steel pins worn under dry conditions and lower loads (pin-on-disc procedure) revealed some interesting features. Figure 68A illustrates how the surface of an untreated AISI D2 steel pin is severely worn, showing that abrasion or ploughing is the dominant degradation process. Nitrogen implantation eliminated abrasion as indicated in Figure 68B, producing to the eye a smooth tarnished surface, a characteristic which indicates that oxidative wear was the preferential mechanism. The martensitic matrix was strengthened by the implantation and exhibited lower wear rate. The worn surface revealed the shape of the harder carbide particles, mainly of $(Cr,Fe)_7C_3$ composition, in this high carbon high chromium cold work tool steel. Nitrogen implantation might also have affected the mechanical properties of the carbide phase, a consideration that is often neglected, probably due to the difficulties experienced in measuring the effects of the process on different phases of a same material. Implantation into carbides may also result in a radiation/solid-solution hardened surface or an apparently tougher surface with increased resistance to crack propagation(235).

Similar features were observed for the martensitic stainless steel (see Figure 69). In this figure the unworn as ground surface prior to implantation and testing is shown to assist in understanding the topographical evolution of the surface during mechanical degradation (see Figure 69A). The untreated material (Figure 69B) exhibited severe wear, damage occurring mainly by abrasion with the production of metallic laminar particles and oxidized debris (Figure 70A). Some evidence for adhesive wear was also observed as illustrated by Figure 106. Under repeated rubbing the metallic particles remaining in the wear track can be fractured due to the loading forces, becoming smaller and oxidized. The oxide particles can then agglomerate in the wear scars, as shown in Figure 69B, thereby reducing metal to metal contact and causing a steady-state friction.

On the contrary, the effect of wear on the implanted surface was to produce a flattening of asperities (see Figure 69C), a smooth oxidized surface and induce a rapid transition to mild wear. The more adherent oxide film formed on the implanted surface acted as a lubricant layer, reducing friction and the stresses transmitted to the substrate material, therefore, reducing the extent of wear. The wear debris generated from the implanted surface was characterized as fine oxidized debris (see Figure 70B). Asperity tops being "worn off" to provide flat contact regions have also been observed by Sreenath and Raman(236) during running-in of a different tribosystem. However, from their results it is not clear whether the action of the wear process was to develop flat asperities or to polish the original ones(233), since the depth of material removed before flattening was apparently exceeded by 4 times the average roughness of the surface.

In the present work the approximate depth of material removed during wear can be calculated easily from weight loss measurements knowing the density of the material investigated. In the case of AISI 420 steel pins from 1 to 6 μm of material were removed, larger than the initial range of the implantation treatment and yet the beneficial wear mechanism persisted, therefore, suggesting that nitrogen implantation initiates good wear conditions. Unfortunately, no Auger spectroscopy work could be carried out on the worn surfaces to investigate whether any nitrogen had diffused to such depth to explain the sustained wear conditions by interstitial or precipitation strengthening. Hale et al(178, 179) also reported a sustained beneficial wear mechanism for implanted SAE 3135 steel under a lubricated Falex wear test at depths beyond the implanted range, although no nitrogen could be detected. In addition, they tentatively explained this effect as being due to the oxide formed on the surface during wear, but

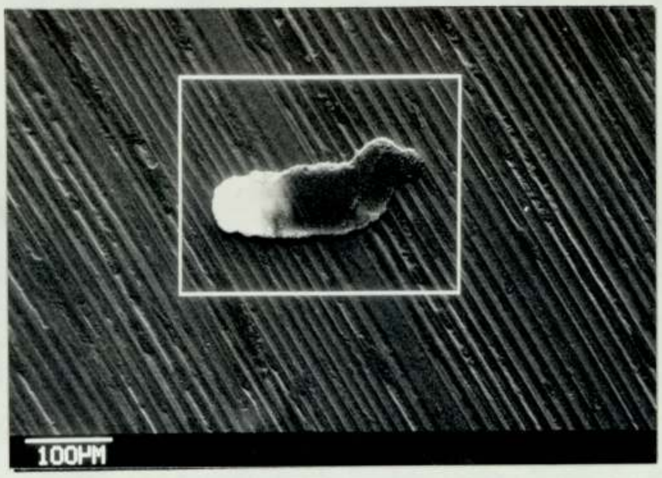

A) Worn area of untreated AISI 420 steel.

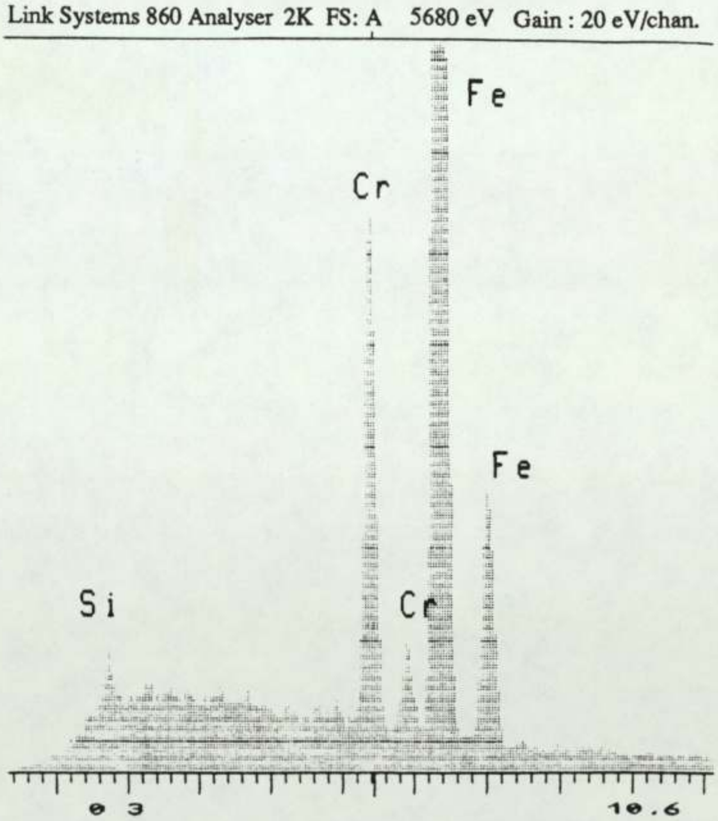

B) EDX analysis of adhered debris.

Figure 106: A) Worn surface of untreated AISI 420 steel, after pin-on-disc testing, showing adhesive wear.
B) EDX analysis of adhered debris.

the precise role and characteristics of the oxide layer in this mechanism were not clearly investigated. Similarly, Goode et al(182) discussed their results of nitrogen implanted iron specimens under lubricated pin-on-disc testing in terms of a mild abrasive or oxidative wear situation, but they failed to provide enough experimental evidence to support fully this model.

Oxides will inevitably form on lubricated or dry ferrous surfaces operated in air(237); therefore, oxidation of both unimplanted or N^+ implanted surfaces is expected to occur during wear. Hence, it is important to understand the changes that nitrogen implantation induces on surface mechanical properties, but also to investigate the bombardment effects on oxide layers and the oxides formed on implanted surfaces during sliding and their relevance to wear properties.

Little attention has been dedicated to the effect of nitrogen implantation on the oxidation of surfaces during wear. Dearnaley(91) suggested that implantation might reduce oxidative wear rates by surface alloying, increasing the critical oxide thickness to spalling by reducing oxide growth stresses, raising the fracture toughness of the oxide or matching the hardness of oxide layer and substrate.

As already discussed, nitrogen implantation increased the hardness of all the steels, therefore it will raise the load-carrying capacity of the oxide and reduce the oxidative wear. Oxidative wear is also controlled by the oxidation rate and mechanical properties of the oxide. The influence of nitrogen implantation on oxide film growth is not clear as yet and only tentative explanations can be provided. The principal ways in which implantation could affect the oxidation rate are(157):

(i) the formation of a coherent protective barrier layer
(ii) the blocking of short-circuit diffusion paths such as grain boundaries and dislocations
(iii) modification of the plasticity of the oxide layer and
(iv) modification of the oxide defect population and thus the bulk diffusion rates.

Nitrogen implantation produces second-phase particles (nitrides) and their main effect in growing oxide films is to block diffusion through the oxide, therefore leading to a slow growth by inward oxygen transport. Evidence of lower oxidation rates has been provided by Doyle et al(207) and other workers(208), who found reduced oxide levels on wear tracks of N^+ implanted AISI 304 and mild steel specimens respectively. In addition, Pollock and co-workers(208) have suggested that the formation of iron or other transition metal nitrides as a result of the implantation reduces the availability of oxide-forming elements, but this reduction is not below the level needed to form a lubricating layer.

The blocking of lattice point defect diffusion would also suppress scale decohesion and would provide good keying as a result of the metal-oxygen reaction that occurs at the internal interface(238). In addition the precipitates formed by nitrogen implantation could influence the oxide plasticity, improving the resistance against cracking and spallation during wear(238). The time required for rupture of an oxide film depends on its level of adhesion to the substrate and the acting stresses. Preferential sputtering during implantation leads to the formation of FeO oxide as discussed above (Figure 89). According to the Pilling-Bedworths rule adhesion between oxide and substrate will be better the smaller the ratio of the individual volumes of oxide and base metal, for FeO it is 1.72, while for Fe_2O_3 and Fe_3O_4 are 2.15 and 2.10 respectively(67).

To conclude, evidence has been presented in this work that nitrogen implantation reduces abrasion of the surface (Figures 68 and 69 for AISI D2 and 420 respectively) and the adhesive wear in materials with a tendency to scuffing (Figure 106A). Nitrogen implantation improves the hardness and load bearing capacity of the surface; initial running-in wear results in a flattening of the asperities, producing a "burnished" wear track (see Figure 69C). This results in a thin more adherent lubricant oxide layer on the surface, therefore initiating a mild oxidative wear mechanism. Nitrogen implantation might alter oxide composition and reduce the growth rate of this oxide layer by blocking the diffusion paths through the oxide, thus delaying the onset of wear.

Figure 107A shows the surface of a N^+ implanted AISI 420 steel pin after prolonged wear under dry conditions. This surface is almost covered by an oxide film (darker areas) giving protection to the underlying material and having a marked influence on friction and wear behaviour. This oxide layer reduces adhesion between contacting surfaces, hence reducing the friction coefficient, and transfers less shear stress to the underlying substrate, therefore reducing deformation and the amount of debris generated, which is characterized by fine oxidized debris. When the oxide film attains a critical thickness, typically about 3 μm(90), plastic deformation occurs but is not sufficient to relieve the stresses and the oxide spalls off, as indicated in Figure 107B.

A schematic diagram of the possible wear evolution of N^+ implanted and unimplanted steel surfaces is presented in Figure 108. During running-in nitrogen implantation reduces abrasion or adhesion tendency of asperities due to precipitation strengthening mechanisms operative and the existence of an oxide film better supported by the underlying substrate. At this stage wear could also be reduced by the well known mechanism of locking of dislocations by interstitial solutes, proposed by Dearnaley and co-workers(8,35). These conditions favour the formation of a lubricant oxide layer on the surface due to frictional heating and a shift to a mild oxidative wear mechanism. This wear mode is able to propagate itself with low surface degradation, providing external factors such as load, temperature or environment do not change, since these could affect the oxidation kinetics at the surface and hence the oxide growth and the onset of wear.

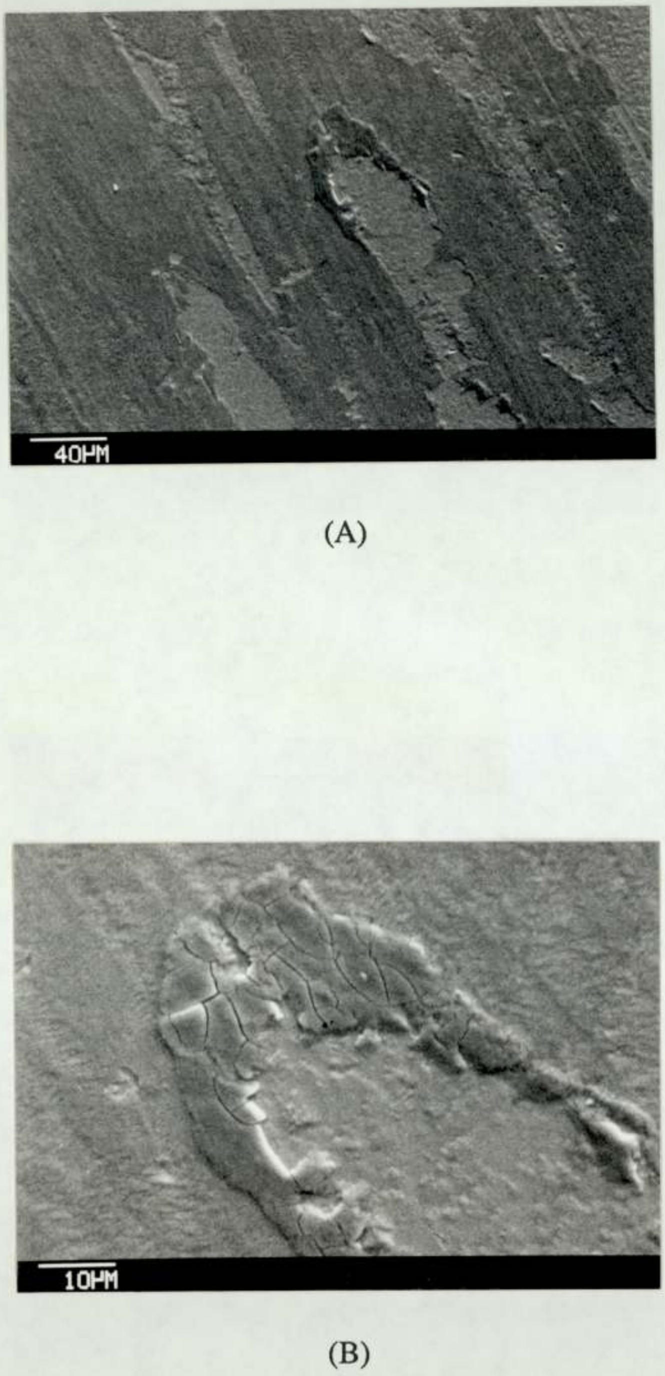

Fig.107: A) Characteristic worn oxidized surface of implanted AISI 420 steel
(3×10^{17} ions/cm^2) after pin-on-disc testing.
B) Spalling-off of a thicker oxide film.

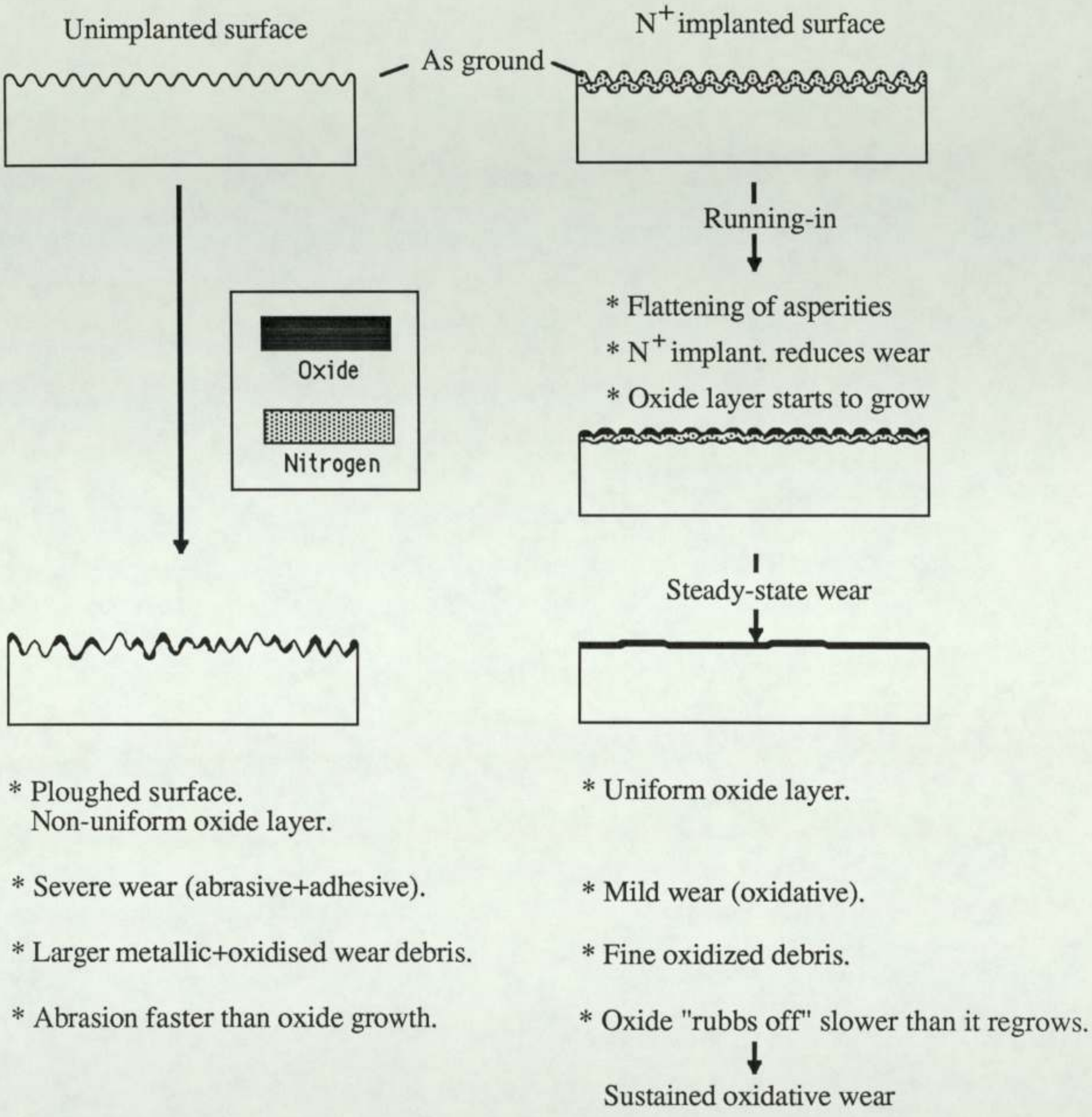

Fig.108: Schematic diagram of wear evolution of unimpl.and N^+implanted steel surfaces.

6.2 Coatings

Nitrogen implantation produced differing results in the three coatings investigated in this work: hard chromium, Co-W and electroless Ni-P. Significant improvements were obtained for hard Cr and Co-W coatings, which will be explained in terms of a precipitation strengthening mechanism that changes the wear behaviour, but an adverse effect was observed in already hardened Ni-P coatings. In order to obtain a better appreciation of the results obtained in the present work, these will be discussed separately.

6.2.1 Electroless Ni-P Coatings

Initial hardening results for Ni-P coatings were very promising. Figure 41 shows that a significant increase in hardness was produced when as-plated Ni-P was nitrogen implanted at a high dose (6 x 10^{17} ions/cm^2), and the hardness levels attained approached those of a precipitation hardened Ni-P coating. This hardening effect could be due mainly to one of two mechanisms, a result of bombardment-induced heating effects during the implantation or nitride precipitation as a result of the implantation. Analysis of the X-ray diffraction patterns (see Figure 101) conclusively showed that the hardening was related to the formation of the nickel phosphide phase (Ni_3P), extending beyond the depth of the implantation (X-rays penetrate deeper than the implantation range), corroborating the idea of the induced target heating.

Nitrogen implantation was carried out at 6 μA/cm^2 on small testing coupons (~25 x 25 x 2 mm), with no provision for cooling of the samples, therefore target heating in excess of 250°C could have occurred in the samples during implantation providing the deceptive hardening results. The work of Sadeghi et al(239) indicates that heat treatment of a Ni-8%P coating at that temperature for several hours brings about structural transformation and hence the hardening effect. Additional hardening in the electroless nickel coating as a direct result of implantation can be considered unlikely to occur, since the precipitation hardening mechanism is already effective in this coating when fully hardened.

Nitrogen implantation on an already hardened deposit produced a "softening" effect (see Figure 41) and this observation was also supported by the ultramicrohardness testing, sampling hardness at depths within the implanted layer (see Figure 45). This suggests that some coarsening of the Ni_3P precipitates could have taken place due to the above mentioned bombardment-induced heating effect. When nitrogen implantation was carried out at a sufficiently low temperature with a good thermal sink for the workpieces, surface hardness was not significantly changed, only a slight decrease in the relative hardness index was experienced (see Table 14).

As expected, in view of the hardness results, the wear and friction behaviour of hardened electroless Ni-P coatings was not improved by nitrogen implantation (see Figure 55 and Table 20). Observation by scanning electron microscopy revealed that nitrogen implantation decreased the abrasive resistance of the coating, ploughing becoming apparent, as Figure 73 illustrates. Implantation degraded the surface of the coating, making it less abrasion resistant and this is thought to be due to a coarsening of the precipitates during the treatment causing an overageing effect, detrimental in wear situations.

6.2.2 Brush plated Co-W coatings

Limited work was carried out with this coating due to time restrictions within the research programme, but nitrogen implantation produced significant effects at the only dose investigated (3×10^{17} ions/cm^2). Table 14 shows that a significant hardening effect can be produced by nitrogen implantation and this depends on the tungsten content in the deposit. A hardness increase of 42% (RHI = 1.42) was achieved for the Co-8%W while a less pronounced effect was observed for the Co-1.5%W (7% increase). It is only meaningful to consider the relative hardness index or percentage gain in hardness with respect to the unimplanted coatings, since indentation depths are greater than the thickness of the implanted layers. More accurate hardening effects could be attained by using an ultra-microhardness technique, limiting penetration of the indentor to depths within the treatment range.

The hardening effect produced by the implantation can be explained in terms of residual stresses, solid solution and precipitation strengthening; the latter thought to provide the major contribution. No published information is available to date on the effects of the implantation on Co-W electrodeposited coatings. A review by Kelly(240) on the phases that can be formed on metals implanted with nitrogen suggests that Co_4N nitride can be formed. The results obtained in the present work (Table 14) appear to indicate that implantation of a coating with higher tungsten content results in a considerable hardening effect, probably by the formation of tungsten nitrides; although some unusual penetration of the ions due to heating effects might have also operated yielding a higher hardness value. More recent work by En Ma et al(241) on Co and W thin films provides evidence for Co_3N and W_2N and WN respectively after implantation in the dose range 10^{16} to 8 x 10^{17} ions/cm^2. The molar volume expansion ratio for these nitrides ranges from 1.10 to 1.29, therefore, nitrogen implantation would be expected to induce surface compressive stresses and precipitation hardening also in the Co-W deposit. There is prior knowledge that this type of alloy can be hardened by an age hardening mechanism(242).

The microstructure of electrodeposited Co-W films depends on the plating conditions and can be either amorphous or crystalline with a hcp, fcc or mixed lattice(243). The structure and alloy content of the deposit will influence the properties achieved by nitrogen implantation; hence, a further detailed study is still needed to take full advantage of the process.

Nitrogen implantation reduced the wear volume (or weight loss) of the Co-W coatings after Falex testing, as the profilometer traces (see Figure 64) and Table 22 and Figure 56 indicate. This significant (x 2.5 times) reduction in wear was accompanied by a slight reduction in the running in friction as Figure 58 shows. Despite such an improvement in wear and friction behaviour, the wear mechanism did not seem to change in the implanted surfaces (see Figure 74). Nitrogen implantation increased the load-bearing capacity of the Co-W coating, by raising the hardness and abrasion resistance, and the surfaces showed partially worn nodules (Figure 74C). In the unimplanted coating (Figure 74B) the absence of any ploughing is evident, but the characteristic nodules of the as-plated coating have disappeared giving rise to a very smooth surface. After prolonged wear testing, the pin weight loss vs wear time curves of untreated and nitrogen implanted Co-W coatings approached to similar values (see Figure 56). This appears to indicate that once the implanted layer is worn away the benefits of nitrogen implantation do not persist.

6.2.3 Hard Chromium Coatings

The results obtained in the present work for hard chromium coatings show that hardness and wear resistance are significantly improved by nitrogen implantation. Hardness, as measured by a 5g load Vickers indentor, was improved by a maximum of 43% at a dose of 5 x 10^{17} ions/cm^2 (see Figure 42), although higher doses produced a lower value probably due to a saturation of nitrogen and an annealing effect produced by the prolonged bombardment. These results agree with those obtained by Oliver et al(101), who reported a 30% improvement in hardness when an electrodeposited Cr coating was implanted at 3.5 x 10^{17} ions/cm^2 (90 keV). Terashima and co-workers(168) also found a reduction in the indentor penetration from 0.3 to 0.1 μm as a result of nitrogen implantation when an ultramicrohardness test was conducted.

This hardening effect can be explained by the known processes of residual stress, solid solution and precipitation strengthening. The role of residual stresses in hardening for a number of ions and thin metallic films was studied by Robic et al(121), who concluded that no correlation existed between hardness and induced stress. However, a more specialized ultramicrohardness test(101,104) is required to sample hardness at depths in which the stress profile is expected to be at a maximum.

As-deposited hard chromium coatings have very small grain size (see Figure 100) and high internal tensile stresses which result in bulk hardness of about 1000 HV. Thus, little interstitial or solid solution hardening is likely to occur by implantation. Chromium nitrides have a hardness of about 1500 HV, thereby the increase in hardness obtained in the present work seems realistic if the formation of precipitates is the major strengthening mechanism. Nitrogen concentration profiles derived from Auger spectroscopy revealed a very high nitrogen content, with a maximum of approximately 47% at. nitrogen concentration at the optimum dose of 5 x 10^{17} ions/cm^2, as Figure 109 indicates. Hardening is directly related to the nitrogen concentration retained after implantation, as inferred from these results.

The XPS results presented in Figures 94 to 98 show conclusively that nitrogen implantation produces chromium nitrides, which account for the hardening

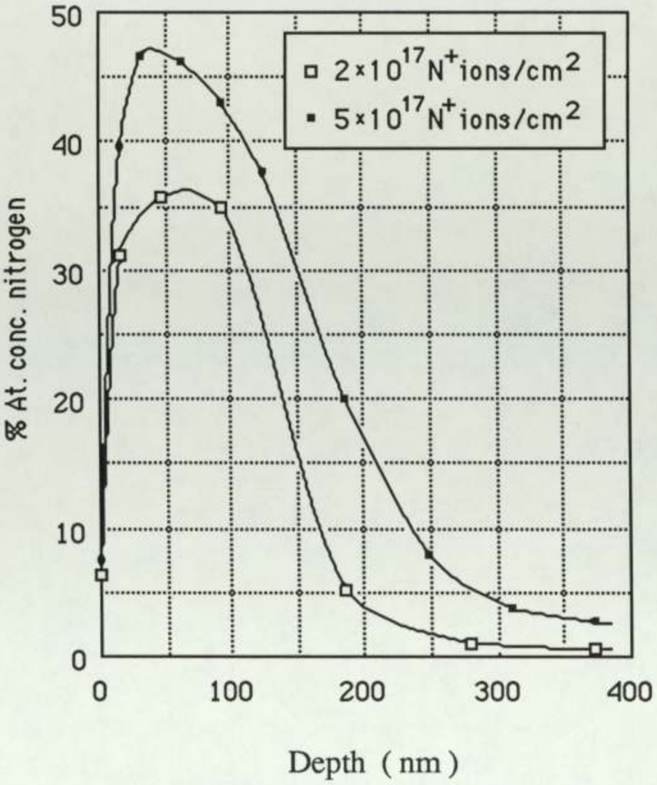

Fig.109: Nitrogen concentration profiles from Auger analysis of implanted hard chromium coatings.

effects. Data from the XPS work are summarized in Tables 29 and 30 for untreated and implanted hard chromium coatings respectively. In these tables binding energies with an accuracy of ± 0.2 eV and chemical states for all peaks fitted to each spectrum are indicated.

The untreated Cr coating is covered by an oxide layer of Cr_2O_3 at the surface (see Figures 92 and 93). Nitrogen implantation probably reduces the oxide by preferential sputtering but it reoxidizes again readily in contact with air as shown in Table 30. Some chromium nitride contribution at the surface is also evident, but after 30 minutes sputtering by Ar^+ ions this becomes more important as shown in the Cr 2p spectra (Figures 94 and 96) or N 1s spectra (Figures 95, 98). In the latter N 1s spectra a small shoulder at higher binding energies of 399.5 to 399.8 eV can be seen, which is attributed to weakly adsorbed nitrogen species. The binding energy obtained for the N 1s peaks of 397.5 ± 0.2 eV is characteristic of a nitrided state (Table 30) and this is further corroborated by the Cr 2p spectra which show peaks for the implanted specimens at a binding energy of 575.5 ± 0.2 eV, corresponding to chromium nitride formation.

Some confusion arises as to which of the nitrides are formed by nitrogen implantation either the cubic CrN or hcp Cr_2N or both. Terashima et al(168) also carried out XPS work on hard chromium coatings and concluded that Cr_2N was formed as a result of N^+ implantation. However, Pethica et al(100) in similar experiments reported CrN precipitation. These workers did not mention the procedure followed for energy referencing and did not carry out curve fitting in their spectra to prove conclusively the formation of Cr_2N or CrN, although the presence of nitrides was evident. Romand and Roubin(229) reported binding energies (BE) for both nitrides, (see Table 28), which were prepared by nitriding Cr substrates with a NH_3-H_2 mixture. The reported value of 575.5 eV (Cr $2p_{3/2}$) for CrN formation lends good support to the results obtained in this work, although some discrepancies are found for the binding energy values obtained from the corresponding N 1s peak. Romand and Roubin(229) found a value of 396.8 eV and 397.4 eV in the N 1s spectra for CrN and Cr_2N respectively. In the present study a value of 397.5 ± 0.2 eV was obtained for N 1s electron levels in the implanted hard chromium coatings (Table 30) and similar values were obtained for the martensitic stainless steel implanted with nitrogen (Table 27), with reference to the Au $4f_{7/2}$ line at 84.0 eV.

Singer and Murday(141) found in their work that binding energies for chromium nitride powder samples could not be reproduced accurately because of charging or binding energy shifts due to excessive oxygen contamination. Discrepancies in binding energies for these compounds could also be due to differences in calibration procedures and sensitivity of the instruments used. Additional XPS studies of reference compounds with curve fitting procedures should be carried out to determine more precise energy values of nitrides.

Hutchings(122) reported the formation of a continuous layer of fine grained Cr_2N by electron diffraction work on a hard Cr coating implanted at a dose of 3.5×10^{17} ions/cm^2. The work of Belii et al(46) on Cr films revealed the formation of not only the hcp Cr_2N phase, but also the cubic CrN, the latter increasing in importance with nitrogen dose, and at 4×10^{17} ions/cm^2 (60 keV N_2^+) only CrN could be detected. From these and the present work it can be concluded that both nitrides can be formed by nitrogen implantation, their precipitation seems to depend on the particular nitrogen dose employed and/or nitrogen concentration profile achieved which can affect their stoichiometry.

Table 29: Core-level binding energies for untreated hard Cr coating

Cr $2p_{3/2}$

Sputter time (min)	Binding energy (± 0.2 eV)	Chemical state	Peak width FWHM (eV)	Area (a.u.)
0 min	574.14	Cr°	1.75	27%
	576.65	$Cr_2O_3(Cr^{III})$	3.0	59%
	577.05	CrOOH	3.0	14%
30 min	574.33	Cr°	1.8	84%
	576.6	Cr_2O_3	3.0	16%

O 1s

Sputter time (min)	Binding energy (± 0.2 eV)	Chemical state	Peak width FWHM (eV)	Area (a.u.)
0 min	530.64	Metal oxide	2.0	37%
	532	Hydroxide	2.0	42%
	533.3	H_2O	2.1	21%
30 min	530.56	Metal oxide	2.0	59%
	531.86	Hydroxide	2.0	41%

Table 30: Core-level binding energies for N^+ implanted hard Cr coatings

A) Dose: 2×10^{17} ions/cm^2

Cr $2p_{3/2}$

Sputter time (min)	Binding energy (± 0.2 eV)	Chemical state	Peak width FWHM (eV)	Area (a.u.)
	575.79	Nitride	3.0	22%
0 min	576.65	Cr_2O_3	3.0	78%
	574.26	Cr°	1.8	58.6%
30 min	575.71	Nitride	3.0	41.4%

N 1s

Sputter time (min)	Binding energy (± 0.2 eV)	Chemical state	Peak width FWHM (eV)	Area (a.u.)
	397.5	Nitrided	1.8	80%
0 min	399.8	Adsorbed	1.8	20%
	397.61	Nitrided	1.8	91%
30 min	399.56	Adsorbed	1.8	9%

Table 30: (continued)

B) Dose: 5 x 10^{17} ions/cm^2

Cr $2p_{3/2}$

Sputter time (min)	Binding energy (± 0.2 eV)	Chemical state	Peak width FWHM (eV)	Area (a.u.)
	575.59	Nitride	3.0	3.6%
0 min	576.69	Cr_2O_3	3.0	74.4%
	576.74	CrOOH	3.0	22%
	574.35	Cr°	1.85	43.2%
30 min	575.55	Nitride	3.0	48.2%
	574.86	Cr_2O_3	3.0	8.6%

O 1s

Sputter time (min)	Binding energy (± 0.2 eV)	Chemical state	Peak width FWHM (eV)	Area (a.u.)
	530.5	Metal oxide	2.0	59.6%
0 min	531.75	Hydroxide	2.0	32.3%
	533.44	H_2O	2.0	8.1%
	530.45	Metal oxide	2.0	70%
30 min	531.75	Hydroxide	2.0	30%

N 1s

Sputter time (min)	Binding energy (± 0.2 eV)	Chemical state	Peak width FWHM (eV)	Area (a.u.)
	397.47	Nitrided	1.8	90%
30 min	399.49	Adsorbed	1.8	10%

The wear resistance of hard Cr coatings was also improved significantly and can be explained in view of the precipitation strengthening produced by chromium nitrides. The extent of the wear reduction achieved depended upon the type of Cr coating, the softer coating (Type I) exhibited higher wear rates and a more moderate improvement by nitrogen implantation (Figure 54). Nitrogen implantation reduced the wear volume but did not change the wear mechanism as Figures 63 and 71 indicate. The softer Cr substrate did not support fully the nitrogen implanted layer during the high load Falex test and ploughing was evident in both untreated and implanted surfaces.

When implantation was carried out on conventional hard chromium coatings (Type II) with a bulk hardness of 1050 $HV_{0.1}$ a more significant improvement of about 4 times reduction in wear was obtained at the optimum dose of 5 x 10^{17} ions/cm^2 as Table 21 and Figure 53 indicate. Wear reduction for this type of coating followed a similar trend to that of the improvement in hardness, as Figure 110 illustrates. The best dose for improvement of these mechanical properties was 5 x 10^{17} ions/cm^2 at 90 keV nitrogen; higher doses produced a softening effect in both hardness and wear resistance. Saturation of the nitrogen content could have occurred and prolonged ion bombardment induced softening due to an in-situ annealing effect during implantation, similar to that produced when hard chromium coatings are heat treated to avoid hydrogen embrittlement or to improve fatigue characteristics. The chromium coatings were not baked prior to implantation, since for wear applications as in the case of plastics processing, in which nitrogen implantation has shown its benefits(200), fatigue is not generally a problem. During implantation two competing processes can occur simultaneously: hardening mainly by precipitation strengthening and softening due to target heating by the high energy beam. It is therefore of practical interest to carry out implantation at room temperature to avoid deleterious effects which could limit the benefits imparted by the treatment.

Friction behaviour was also improved on nitrogen implanted surfaces during the early stages of wear, as Figure 58 illustrates, due to less penetration of surface asperities of the counterface material into the surface of the coating. After longer periods, friction coefficients for both untreated and implanted surfaces approached the same values, as a result of increased ploughing. Nitrogen implantation produced a light tan colour on the surface of the coating, this was initially thought to result from a slight low temperature oxidation induced by the nitrogen beam(199), but it is probably due to carbon contamination from the vacuum system, since O 1s spectra for both untreated (Figure 93) and implanted (Figure 97) Cr coatings revealed the presence of Cr_2O_3 oxide and Auger concentration profiles did not show a significant difference in oxygen content (Figures 83 and 85).

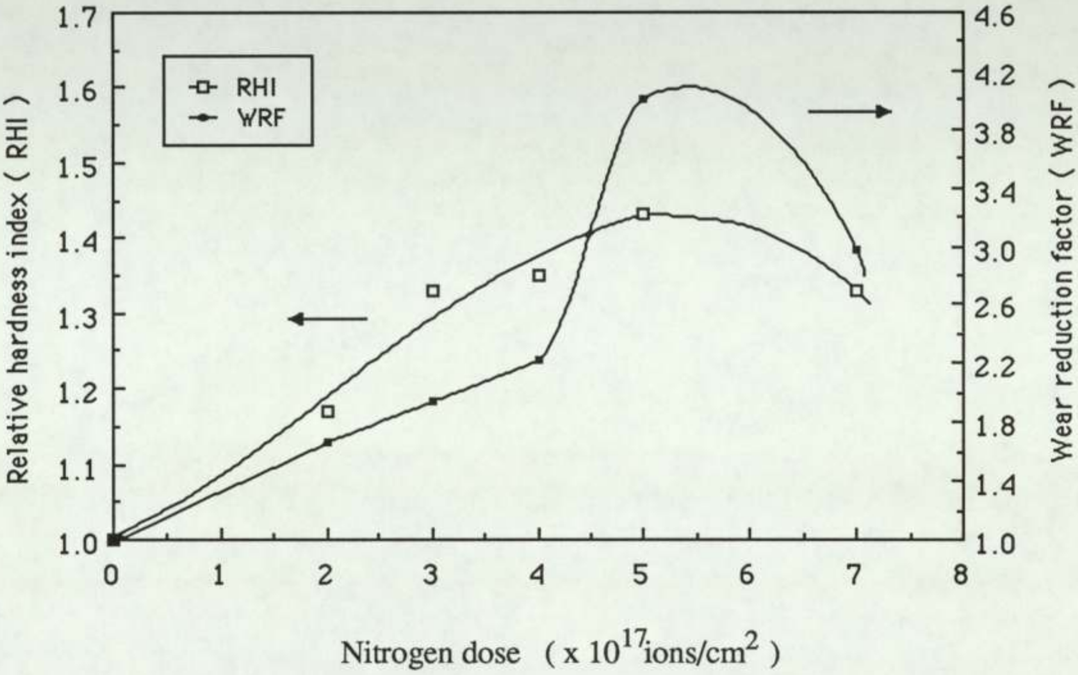

$$RHI = \frac{\text{Hardness implanted}}{\text{Hardness unimplanted}} \qquad WRF = \frac{\text{Wear unimplanted}}{\text{Wear implanted}}$$

Fig.110: Relative hardness index and wear reduction factors of implanted hard chromium coatings as a function of nitrogen dose.

As mentioned earlier, during implantation absorption of carbon from residual gas molecules from the diffusion pump takes place and some degree of "atomic mixing" due to the ion beam occurs leading to a slight "carburization" process, as revealed by the C 1s spectra (see Figure 111) obtained from implanted surfaces. A similar effect has been reported elsewhere(244) for Ti^+ implantation, due to the high affinity of this element for carbon. Chromium is also a strong carbide former and

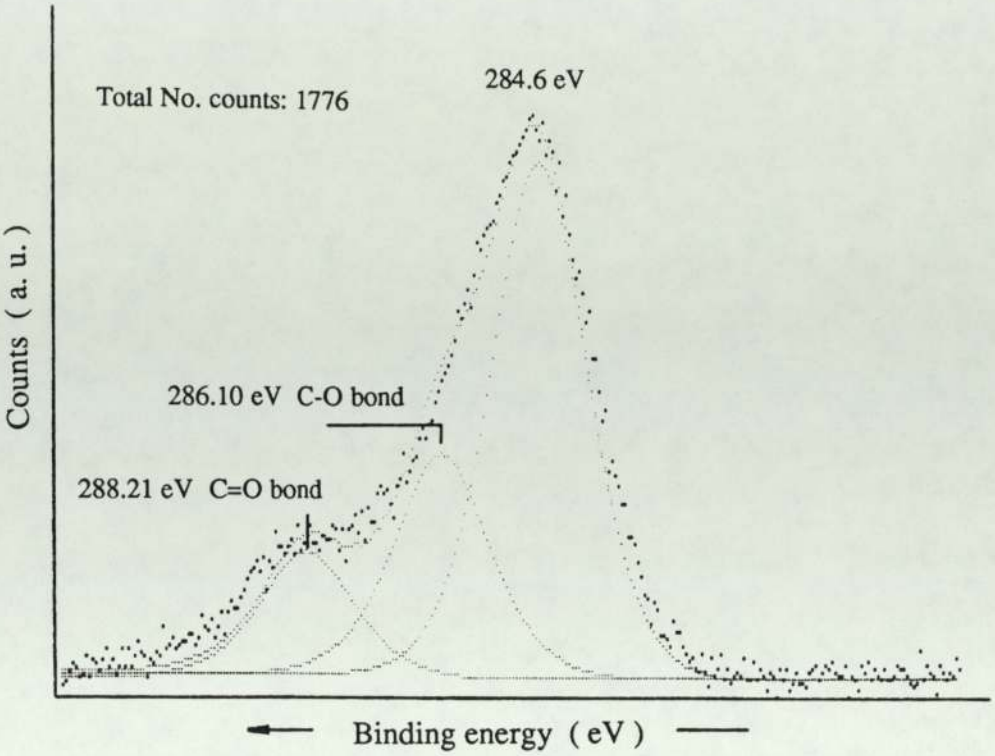

C 1s spectrum from untreated hard chromium coating. 0 min. sputtering

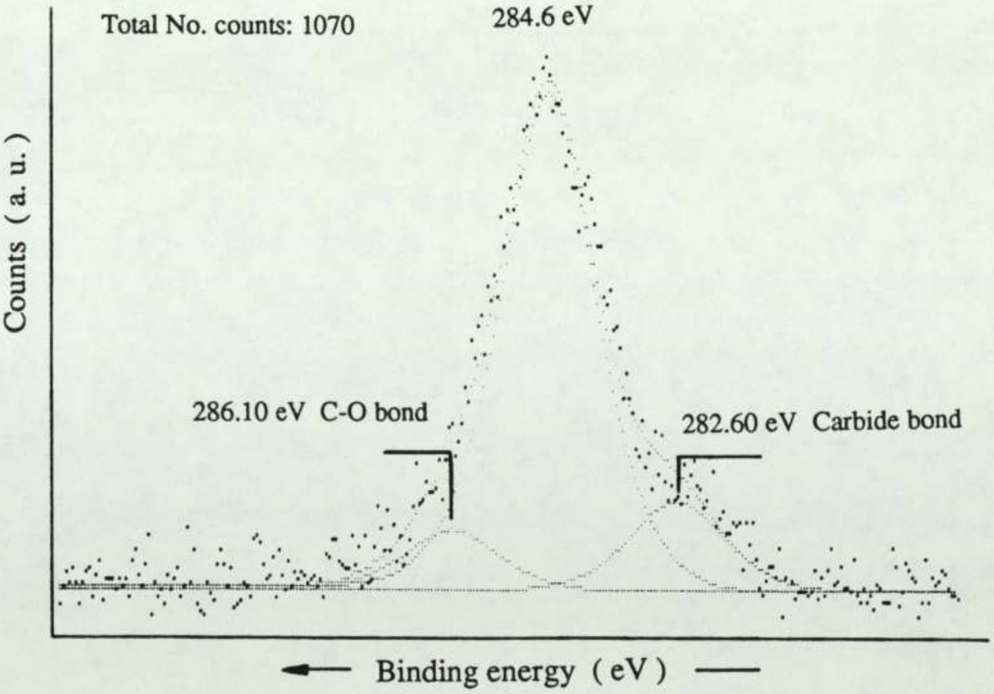

C 1s spectrum from implanted hard Cr coating (5 x 10^{17} ions/cm^2).30 min. sputtering

Figure 111: C 1s spectra from untreated and nitrogen implanted hard Cr coatings.

therefore implant-assisted carburized layers can also be formed. This carburization may also assist in the reduction in the friction coefficient by decreasing the adhesive tendency of counteracting surfaces under load.

Limited work was conducted on a new hard Cr coating (Mach-1, Type III) and the results are presented in Figure 57. Untreated surfaces exhibited little wear as compared to the other types of Cr coatings tested, and degradation of the implanted surface was negligible (Figure 57). Wear behaviour of Types II and III Cr coatings is summarized in Figure 112 and as shown the new Cr deposit (Type III) provided very good results. However, it had a better surface finish in the as-plated condition (0.2 µm CLA) which could have influenced the lubricated regime during wear testing thus reducing friction and wear. The conventional hard Cr (Type II) coating was centreless ground and polished to 0.4 µm CLA and this has been reported(245) to produce a coating with decreased abrasion resistance. A more detailed study is, thus needed to compare directly the performance of both Cr coatings. Plating under the same conditions, ie. current density and plating temperature and surface grinding to similar finishes should provide a firm basis for comparison. Nevertheless, these results show that regardless of the metal coating condition, nitrogen implantation does improve considerably its wear resistance.

The wear results obtained in the present work are in agreement with those reported by Oliver and co-workers(101,102) who found a 23 times wear reduction factor for hard Cr coatings using a low load ball-on-disc test. Watkins and Dearnaley(199) and other researchers(168) have also found an improved wear behaviour under induced abrasive wear conditions.

Nitrogen implantation changed the wear mechanism of hard Cr (Type II) coatings, as Figure 72 indicates. Wear of the untreated coating showed significant grooving (Figure 72a) with some ductile tearing perpendicular to the sliding direction and transverse shear cracks which led to the formation of metallic debris. These wear particles if entrapped at the interface can cause progressive damage to the surface by ploughing, which accelerates degradation of the coating and explains the higher wear rates obtained after prolonged wear (see Figure 112). A hard layer of chromium nitrides in the implanted coating would increase the load bearing capacity of the surface and reduce ploughing by hard particles (Figure 72b). The surface is more vulnerable to penetration when this layer is worn away. Auger analysis of a deeply worn hard Cr coating (Figure 86) revealed a marginal nitrogen contribution; however, presence of Fe was also evident. One explanation for this Fe "contamination" is that of wear debris embedded on the surface, therefore, it could also be argued that the nitrogen comes from remnant debris at the root of the grooved area, and not from diffusion to such depths. After implantation most of the nitrogen was found to be in a nitrided state by XPS analysis (Table 30) and chromium nitrides are known to be stable up to temperatures well in excess of those expected to occur at asperity contacts(46). Therefore, an enhancement of wear properties at greater depths than the implanted layer by decomposition of nitrides through frictional heating seems unlikely to occur. This observation does not lend good support to the mobile interstitial model initially suggested by the Harwell group(35, 170). Nitrogen ions are tightly bound to Cr and it is unlikely that free nitrogen would be readily available to diffuse during wear and so block dislocations according to the well reported "Cottrell" model(204). Furthermore, this mechanism might not be fully effective in a high dislocation and fine grained structure as that of electrodeposited chromium.

The formation of chromium nitrides leads to a volume expansion in the lattice ranging from 22 to 50% (Cr_2N=22%, CrN=50%)(103), which creates a large compressive stress in the implanted layer, due to constraint of the underlying material. Hutchings(122) has suggested that the inherent microcracks in as-plated chromium coatings are preferential sites for the nucleation of wear debris and their closure as a result of the large stresses created by implantation would produce an improvement in wear resistance. In the present work evidence could not be found for this phenomenon. Figures 71C and D show that nitrogen implantation does not lead to closure of the microcracks. Moreover, microcracks would extend beyond the implanted depth (0.1-0.2 μm) and their closure would be marginal. The recent work of Terashima et al(168) which also showed conclusively that microcracks are not closed by high dose nitrogen implantation supports the present findings.

During electroplating of chromium, metal can be deposited as an unstable fcc or hcp chromium hydride which decomposes to bcc chromium. The stress produced in the chromium coating by decomposition of the hydride is relieved in part by cracking(246). When nitrogen implantation is carried out on as-plated chromium deposits, further decomposition of the remaining hydride and release of occluded hydrogen occurs due to bombardment target heating and additional cracking can be observed, as illustrated by the work of Terashima and co-authors(168). The compressive stresses induced by the nitride formation on Cr coating counteract this effect but not sufficiently to close microcracks. Moreover, surface grinding and polishing of chromium plated components prior to nitrogen implantation would mask the microcracks and their possible influence during wear would be diminished for both treated or untreated coatings, as Figure 72C illustrates. In conclusion, the closure effect on wear resistance reported by Hutchings(122) can be considered to be negligible, the major role in the improvement of wear behaviour being played by nitride precipitation.

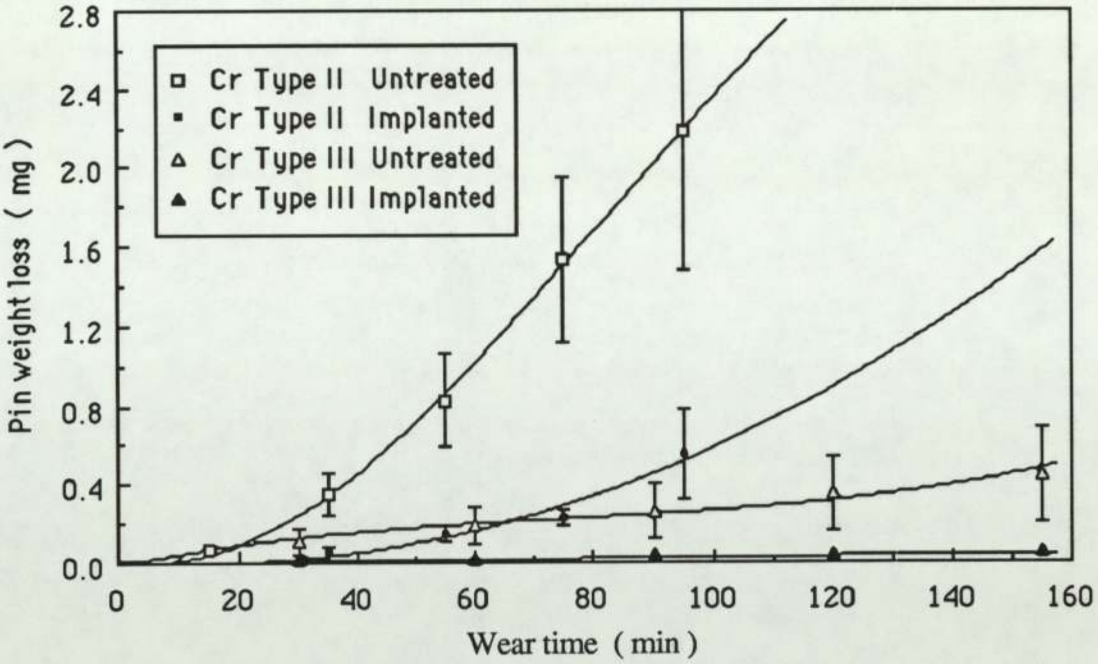

Fig. 112: Lubricated Falex wear results of hard Cr coatings (Types II and III).
Implantation dose: 5×10^{17} nitrogen ions/cm^2.
Oper. cond.: 710 N load. AISI 52100 steel V-blocks.

CHAPTER 7

CONCLUSIONS AND RECOMMENDATIONS FOR FURTHER WORK

7 CONCLUSIONS AND RECOMMENDATIONS FOR FURTHER WORK

7.1 Conclusions

Nitrogen implantation improved considerably the running-in wear and friction behaviour of most of the materials investigated in the present work. This enhancement in mechanical properties is due mainly to a precipitation strengthening mechanism acting within the implanted surface layer, although some slight contribution from a solid solution hardening has also to be considered. Implantation did not improve the mechanical properties of hardened electroless nickel coatings since precipitation strengthening mechanisms are already fully operative in this alloy system, and implantation improved more moderately the tribological performance of AISI M2 high speed steel because little room for additional strengthening by nitrogen is available in this high carbon martensitic alloy steel.

Nitrogen implantation was found to provide a long lasting improvement in the wear life of the steels investigated and this effect has been associated with a clear change in wear mechanism from abrasive + adhesive to a mild oxidative wear mode which , providing the environment does not change (eg. no changes in temperature, load or contact pressures acting on the surfaces), can sustain itself regardless of any remaining nitrogen at the interacting surfaces. However, this prolonged wear behaviour seemed to be a characteristic of the tribological system rather that of a particular implanted metal, since for example a sustained mild oxidative wear behaviour was not found by other workers on implanted surfaces that were operated under dry conditions at very high loading. The oxide film initiated on the surface due to frictional heating was easily worn off under such conditions providing no benefit after running-in had been completed and this can explain the large scatter of results obtained by different researchers when severe loading conditions are employed.

The major conclusions drawn from the present work can be summarized as follows:

1 Nitrogen implantation improved the wear resistance of all steels investigated in this work. The best results were obtained for AISI 420 martensitic stainless steel with a factor of 5.5 wear resistance improvement under low load dry testing and 2.5 improvement under high load lubricated wear testing.

2 The wear resistance of hard chromium coatings was enhanced by 4 times and a lower wear improvement factor of 2.5 was achieved for Co-W alloy electrodeposits. However, no enhancement of wear properties was experienced for electroless Ni-P coatings after nitrogen implantation.

3 Nitrogen implantation reduced the running-in friction of AISI D2 and 420 steels and hard Cr and Co-W coatings.

4 The optimum doses for wear resistance were material dependent and lie within a range of 3 to 5 x 10^{17} ions/cm^2 for the conditions studied in this work. These doses were associated with a maximum nitrogen retention, additionally the materials that showed higher nitrogen levels, ie. hard chromium coating and AISI 420 steel, provided the best results.

5 Nitrogen implantation did harden martensitic structures and coatings, providing the substrate material was highly alloyed with elements that form nitrides readily.

6 A hardness improvement of 2 times was achieved for AISI 420 steel after nitrogen implantation when an ultra-microhardness technique was used to sample the hardening effect within the implanted layer. Conventional Vickers (5 g load) microhardness revealed also a hardening but less significantly. Ultra-microhardness techniques are therefore necessary to reveal the true hardness of implanted layers, although conventional hardness methods, which are influenced by the underlying substrate can provide a useful indication of the hardening effect by ion implantation.

7 Nitrogen implantation improved by a 40% the hardness of hard chromium at the optimum dose, higher doses resulted in a less significant improvement due to softening of the coating by bombardment heating induced during implantation.

8 The extent of the hardening in steels and coatings depended on the strengthening mechanisms already operative in the materials prior to nitrogen implantation. For example, no benefits were obtained for hardened electroless nickel coatings because precipitation strengthening by Ni_3P particles was already fully operative.

9 After implantation XPS analysis of hard chromium coatings and AISI 420 steel revealed that nitrogen was almost entirely bound to chromium, forming chromium nitrides. Nitride formation explains the hardening and wear resistance improvements achieved by implantation.

10 By creating a hard nitride layer, nitrogen implantation increased the load bearing capacity of the surface of coatings (Cr and Co-W) and steels improving their resistance to abrasion by wear particles or hard asperities.

11 Nitrogen implantation favoured the formation of an adherent oxide layer on the surfaces of steels during wear. This was often associated with a change in wear mechanism from abrasive or adhesive to mild oxidative, depending on the tribological system. This improvement in wear behaviour could persist after running-in had been completed and did not seem to depend on any nitrogen remaining on the surface.

12 Implantation is therefore an effective method of treating components or tools made from the steels investigated or coated with Cr or coatings that contain nitride forming elements, providing conditions of operation are not so severe that the implanted layer is eliminated in short times.

7.2 **Recommendations for further work**

Auger and X-ray photoelectron spectroscopy work should also be conducted on Co-W alloy coatings of varying W content, implanted at different doses in order to obtain the nitrogen concentration and to seek any binding effect between nitrogen and cobalt and/or tungsten. Wear tests would provide information of the best combination of nitrogen dose and alloying content.

Further X-ray photoelectron spectroscopy should be carried out after wear of implanted steels to investigate the nature of the oxides formed and their relevance in tribological performance. It is also of interest to investigate under which conditions sustained oxidative wear is operative, eg. load, sliding speed, lubrication etc.. This would have important commercial implications.

"Welsh" curves for a given steel material, ie. wear rate vs loads for different sliding speeds, would provide information on the influence of nitrogen implantation on the transition loads from mild to severe wear.

Glancing X-ray diffraction work is of great interest to investigate phase changes after implantation either in worn or unworn surfaces. This would provide a standard basis of comparison for XPS work and would help to clarify the formation of both types of chromium nitrides.

Multiple energy implants to provide a more uniform nitrogen profile should also be considered. Ultra-microhardness and wear tests would provide relevant information of the benefits of the process.

The influence of other interstitial elements already present in the substrate material, eg. carbon in steel, on the mechanical properties of implanted surfaces should be investigated. This work has relevance to optimize the commercial application of this process to ferrous materials.

Further work should be carried out on the new high efficiency hard chromium deposits in view of the promising results obtained. The effect on as plated and ground surface finishes (different surface roughness) should be studied.

The influence of nitrogen implantation on corrosion resistance has not been considered in this work but often wear resistance in a corrosive environment is important. Consequently this needs to be investigated.

Finally, ion beam mixing of elements that readily form hard nitrides should also be considered, especially for those materials in which strengthening by nitrogen implantation is less significant, eg. AISI M2. This would broaden the scope of ion beam modification of surfaces for metal cutting and forming operations.

LIST OF REFERENCES

8. LIST OF REFERENCES

1 Hartley NEW, Swindlehurst WE, Dearnaley G and Turner JF. "Friction changes in ion implanted steel". J. of Materials Science, 1973, **8**, 900-904.

2 Hartley NEW. "The tribology of ion implanted metal surfaces". Tribology International, 1975, **8**, 65-72.

3 Hartley NEW. "Tribological effects in ion implanted metals". Applications of Ion Beams to Materials. Inst. Phys. Conf. Series, No 28. Eds.: Carter G, Colligon JS and Grant WA. Inst. of Physics (Bristol), 1976, 210-223.

4 Williams JS. "Materials modification with ion beams". Reports on Progress in Physics, 1986, **49** (5), 491-587.

5 Vardiman RG. "The modification of fatigue properties by ion implantation". Ion Plating and Implantation. Applications to Materials. Ed.: Hochman RF. American Society for Metals, 1986, 107-113.

6 Hubler GK. "DoD applications of implantation-modified materials". Metastable Materials Formation by Ion Implantation. Eds.: Picraux ST and Choyke WJ. North-Holland (New York), 1982, 341-354.

7 Hirvoven JK, Carosella CA, Kant RA, Singer I, Vardiman R and Rath BB. "Improvements of metal properties by ion implantation". Thin Solid Films, 1979, **63**, 5-10.

8 Hartley NEW. "Friction and wear of ion implanted metals. A review". Thin Solid Films, 1979, **64**, 177-190.

9 Herman H. "Surface mechanical properties-effects of ion implantation". Nuclear Instruments and Methods, 1981, **182/183**, 887-898.

10 Ingram DC and Bhattacharya RS. "MeV ion beam modification of metals and special metal coatings". Ion Plating and Implantation. Applications to Materials. Ed.: Hochman RF. American Soc. for Metals, 1986, 55-62.

11 Dearnaley G. "Thermal oxidation". Ion Implantation. Treatise on Materials Science and Technology, Vol 18. Ed.: Hirvonen JK. Academic Press (New York), 1980.

12 Ashworth V, Procter RPM and Grant WA. "The applications of ion implantation to aqueous corrosion". Ibid., 176-256.

13 Wolf GK. "Chemical properties of ion implanted materials". Ibid., 373-414.

14 Meyer O. "Superconductivity". Ibid., 415-445.

15 North JC, Wolfe R and Nelson TJ. "Applications of ion implantation to magnetic bubble devices". J. Vac.Sci. and Tech. 1978, **15** (5), 1675-1684.

16 Lindhard J and Scharff M. "Energy dissipation by ions in the keV region". Physical Review, 1961, **124** (1), 128-130.

17 Townsend PD, Kelly JC and Hartley NEW. Ion implantation, sputtering and their applications. Academic Press. 1976.

18 Lindhard J, Sharff M and Schiott HE. "Range concepts and heavy ion ranges". Mat. Fys. Medd. Dan Vid. Selsk., 1963, **33** (14).

19 Ryssel H and Ruge I. Ion implantation. John Wiley & Sons (Chichester), 1986, 8-12.

20 Winterbon KB. Ion implantation range and energy deposition distributions. Vol 2. Low incident ion energies. Plenum Press (NewYork), 1975.

21 Hirvonen JK. Ion implantation: Vol 18. Treatise of Materials Science and Technology. Academic Press (New York), 1980, 2.

22 Davis JA and Howe LM. "Basic implantation processes". Site Characterization and Aggregation of Implanted Atoms in Materials. Eds.: Perez A and Coussement R. Plenum Press, 1980, 7-32

23 Brandt W. "Channelling in crystals".Scientific Amer.,1968,**218**(3),90-102.

24 Pathak AP. "The effect of defects on charged particle propagation in crystalline solids". Radiation Effects, 1982, **61**, 1-46.

25 Carter G, Katardjiev IV, Nobes MJ and Whitton JL. "Sputtering-induced surface topography on FCC metals". Materials Science and Engineering, 1987, **90**, 21-32.

26 Liu BX, Johnson WL, Nicolet MA and Lau SS. "Amorphous film formation by ion mixing in binary metal systems". Nuclear Instruments and Methods, 1983, **209/210**, 229-234.

27 Winterbon KB, Sigmund P and Sanders JB. "Spatial resolution of energy deposited by atomic particles in elastic collisions". Kong. Danske Vidensk. Selsk. Mat. - Fys. Medd. 1970, **37** (14), 5-61.

28 Lanore JM. "Simulation of the evolution of defects in a lattice by the Monte Carlo method". Radiation Effects, 1974, **22** (3), 153-162.

29 Biersack JP and Haggmark LG. "A Monte Carlo computer program for the transport of energetic ions in amorphous targets". Nuclear Instruments and Methods, 1980, **174**, 257-269.

30 Kinchin GH and Pease RS. "The displacement of atoms in solids by radiation". Reports on Progress in Physics, 1955, **18**, 1-51.

31 Sigmund P. "On the number of atoms displaced by implanted ions or energetic recoil atoms". Applied Physics Letters, 1969, **14** (3), 114-117.

32 Dearnaley G. "Ion implantation for improved resistance to wear and corrosion". Materials in Engineering Applications, 1978, **1**, 28-41.

33 Nowich AS and Berry BS. "Unelastic relaxation in crystalline solids". Academic Press (New York), 1972.

34 Cottrell AH. Dislocations and plastic flow in crystals. Clarendon Press (Oxford), 1953.

35 Dearnaley G. "The effects of ion implantation upon the mechanical properties of metals and cemented carbides". Radiation Effects, 1982, **63**, 1-15.

36 Herman H. "Modification of the surface mechanical properties of ferrous alloys by nitrogen ion implantation". Ion Implantation into Metals. Eds.: Ashworth V, Grant WA and Procter RPM. Pergamon Press, 1982, 103-110.

37 Hartley NEW. "Ion implantation case studies". Surface treatments for protection. Papers presented at the Spring Review Course, Cardiff, 7-10 April 1978. Ed.: Evans HW. Institution of Metallurgists, 1978, 197-209.

38 Carter G and Colligon JS. Ion Bombardment of Solids. Elsevier (New York), 1968.

39 Sigmund P. "Theory of sputtering. I. Sputtering yield of amorphous and polycrystalline targets". Physical Review, 1969, **184** (2), 383-416.

40 Liau ZL and Mayer JW. "Limits of composition achievable by ion implantation". Journal of Vac. Science and Tech. 1978, **15** (5), 1629-1635.

41 Andersen HH. "Ion-bombardment-induced composition changes in alloys and compounds". Ion implantation and Ion Beam Processing. Eds: Williams JS and Poate JM. Academic Press (New York), 1984, 127-187.

42 Poate JM and Cullis AG. "Ion implantation metallurgy - metastable alloy formation". Ion Implantation. Treatise on Materials Science and Engineering. Vol 18. Ed.: Hirvonen JK. Academic Press (New York), 1980, 85-134.

43 Sood DK and Dearnaley G. "Ion-implanted surface alloys in copper and aluminium". Applications of Ion Beams to Materials. Inst. Physics Conf. Series. No 28. Eds.: Carter G, Colligon JS and Grant WA. Inst. of Physics (Bristol), 1976, 196-203.

44 Martin G and Barbu A. "Implantation, ion beam mixing and solid state solubility". Nuclear Instruments and Methods, 1983, **209/210**, 203-201.

45 Pavlov PV. "Implantation phases in solids". Nuclear Instruments and Methods, 1983, **209-210**, 791-798.

46 Belii IM, Komarov FF, Tishkov VS and Yankovskii VM. "Formation of chemical compounds by ion bombardment of thin transition metal films". Phys. Status Solidi (A), 1978, **45**, 343-352.

47 Picraux ST. "Equilibrium phase formation by ion implantation". Site Characterization and Aggregation of Implanted Atoms in Materials. Eds.: Perez A and Coussement R. Plenum, 1980, 307-323.

48 Herman H, Hu WW, Clayton CR, Hirvonen JK, Kant R and MacCrone RK. "Modification of mechanical properties through ion implantation" IPAT '79. Ion Plating and Allied Techniques (Proc Conf) London, 1979, CEP Consultants Ltd, 255-264.

49 Kant RA, Myers SM and Picraux ST. "Experimental study of precipitation in an ion-implanted metal: Sb in Al" Journal Applied Physics, 1979, **50** (1), 214-222.

50 Hirvonen JK. "Industrial applications of ion implantation". Technology Vectors (Proc. Conf.) 29th National SAMPE Symposium. Reno, Nevada, April, 1984, 813-827.

51 Pope LE, Yost FG, Follstaedt DM, Knapp JA and Picraux ST. "Effects of ion implantation on friction and wear of stainless steels". Wear of Materials (Int. Conf.) Virginia, April 1983. ASME (New York), 1983, 280-287.

52 Sioshansi P. "Tailoring surface properties by ion implantation". Materials Engineering, 1987, **104** (2), 19-23.

53 Amontons M. "De résistance caus ee dans les machines" Mémories de l'Academie Royale, 1699, 203-222.

54 Bowden FP and Tabor D. The friction and lubrication of solids. Part I. Clarendon Press (Oxford), 1954.

55 Bowden FP and Tabor D. "Friction, lubrication and wear: a survey of work during the last decade". British J. of Appl. Physics, 1966, **17**, 1521-1544.

56 Bowden FP and Tabor D. The friction and lubrication of solids. Part II. Oxford University Press, 1964.

57 Archard JF. "Contact and rubbing of flat surfaces". Journal of Applied Physics, 1953, **24**, 981.

58 Archard JF. "Elastic deformation and the laws of friction". Proc .Royal Society, 1957, **A243**, 190.

59 Quinn TFJ. The application of modern physical techniques to tribology. Newnes-Butterworths, 1971, 14.

60 Kragelsky IV. "Molecular-mechanical theory of friction". In: Friction and wear of machines. Vol. 3, Acad. Sci. USSR, Moscow, 1949, 179-183.

61 Hersey MD. Theory and research in lubrication. Willey (New York), 1966.

62 Kapsa Ph and Martin JM. "Boundary lubricant films: a review". Tribology International, 1982, **15** (1), 37-42.

63 Dowson D and Higginson GR. Elastohydrodynamic lubrication. Pergamon Press (New York), 1977.

64 Cann P, Spikes HA and Cameron A. "Thick film formation by zinc dialkyldithiophosphates". ASLE Transactions. 1983, **26** (1), 48-52.

65 Komvopoulos K, Saka N and Suh NP. "Ploughing friction in dry and lubricated metal sliding". Journal of Tribology, 1986, **108**, 301-313

66 Sliney HE. "Solid lubricant materials for high temperatures - a review". Tribology International, 1982, **15** (5), 303-315.

67 Kragelsky IV, Dobychin MN and Kombalov VS. Friction and wear, calculation methods. Pergamon Press, 1982.

68 Eyre TS."The mechanisms of wear". Tribology Int.,1978, **11** (2), 91-96.

69 Moore MA. "Abrasive wear". Fundamentals of friction and wear of materials. Ed.: Rigney DA. American Soc. for Metals, 1981, 73-118.

70 Kruschov MM. "Principles of Abrasive Wear". Wear, 1974, **28**, 69-88.

71 Mulhearn TO and Samuels LE. "The abrasion of metals: a model of the process". Wear, 1962, **5**, 478-498.

72 Mutton PJ and Watson JP. "Some effects of microstructure on the abrasion resistance of metals". Wear, 1979, **48**, 385-398.

73 Popov VS and Nagornyi PL. "Influence of carbides on the abrasive wear resistance of alloys". Russian Casting Prod. 1969, **8**, 337.

74 Miller AE. "Wear in steels". Journal of Metals. 1983, **35** (1), 56-62.

75 Richardson RC. "Wear of metals by relatively soft abrasives". Wear, 1968, **11**, 245.

76 Misra A and Finnie I. "On the size effect in abrasive and erosive wear". Wear, 1981, **65**, 359-373.

77 Misra A and Finnie I. "Some observations on two-body abrasive wear". Wear. 1981, **68**, 41-56.

78 Rabinowicz E. Friction and wear of materials. Wiley (New York), 1965.

79 Rabinowicz E. "The physics and chemistry of surfaces". ASTM Standardization News, Sept. 1974, 18-21.

80 Archard JF. "Contact and rubbing of flat surfaces". J. Applied Physics, 1953, **24**, 981.

81 Verbeek HJ. "Tribological systems and wear factors". Wear, 1979, **56**, 81.

82 Welsh NC. "The dry wear of steels". Phil. Trans. Royal Soc. Series A, 1965, **257**, 31-70.

83 Cohen M. "The strengthening of steel". Transactions of the Metallurgical Society of AIME, 1962, **224**, 638-656.

84 Eyre TS and Baxter A. "The formation of white layers at rubbing surfaces". Metals and Materials, 1972, **6**, 435-439.

85 Kimura Y. "The role of fatigue in sliding wear". Fundamentals of friction and wear of materials. Ed.: Rigney DA. American Society for Metals, 1981, 187-220.

86 Suh NP. "The delamination theory of wear". Wear, 1973, **25**, 111-124.

87 Suh NP. "An overview of the delamination theory of wear". Wear, 1977, **44**, 1-16.

88 Marcinkowski MJ. "A surface dislocation model of wear". Journal of Materials Science, 1984, **19**, 1296-1306.

89 Tao FF. "A study of oxidation phenomena in corrosive wear". ASLE Transactions, 1969, **12** (2), 97-105.

90 Quinn TFJ. "Review of oxidational wear. Parts I and II". Tribology International, 1983, **16**, (5), 257-271 and (6), 305-315.

91 Dearnaley G. "Adhesive, abrasive and oxidative wear in ion implanted metals". Materials Science and Engineering 1985, **69**, 139-147.

92 Gabovich MD, Budernaya LD, Poritskii VY and Protensko IM. All Soviet Meeting on Ion Beam Physics, Proc. Conf., Kiev, (USSR).1974. (As quoted in Ref. 3).

93 Kanaya K, Koga K and Toki K. "Extraction of high current ion beams with laminated flow". Journal of Physics E: Sci. Instr., 1972, **5**, 641-648.

94 Li HT, Liu PS, Chang SC, Lu HC, Wang HH and Tao K. "Some experimental studies on metal implantation". Nuclear Instruments and Methods, 1981, **182/183**, 915-917.

95 Bolster RN and Singer IL. "Surface hardness and abrasive wear resistance of ion implanted steels". ASLE Transactions, 1981, **24** (4), 526-532.

96 Ramous E, Principi G, Giordano L, Lo Russo S and Tosello C. "Thermal effect of nitrogen implantation on high carbon steels: influence of current density". Ion Assisted Surface Treatments, Techniques and Processes. (Proc. Conf.), University of Warwick, 1982. Metals Society, 1982, 11.1-11.6.

97 Iwaki M, Okabe Y, Hayashi H, Kohno A, Takahashi K and Yoshida K. "Surface characteristics of ion implanted steels". Ibid 10.1-10.6.

98 Fu-Zhai C, Heng-De L and Xiao-Zhong Z. "Modification of tribological characteristics of metals after nitrogen implantation". Nuclear Instruments and Methods, 1983, **209/210**, 881-887.

99 Pethica JB. "Microhardness tests with penetration depths less than ion implanted layer thickness". Ion Implantation into Metals. Eds.: Ashworth V, Grant WA and Procter RPM, Pergamon, 1982, 147-156.

100 Pethica JB, Hutchings R and Oliver WC. "Composition and hardness profiles in ion implanted metals". Nuclear Instruments and Methods, 1983, **209/210**, 995-1000

101 Oliver WC, Hastings R and Pethica JB. "The wear behaviour of nitrogen implanted metals". Metallurgical Transactions A, 1984, **15A**, 2221-2229.

102 Hutchings R, Oliver WC and Pethica JB. "Hardness and wear correlations in nitrogen implanted metals". Surface Engineering. Surface Modification of Materials. Eds: Kossowsky R and Singhal SC. Martinus Nijhoff Publ. (The Netherlands), 1984, 170-184.

103 Dimigen H, Kobs K, Leutenecker R, Rysell H and Eichinger P. "Wear resistance of nitrogen implanted steels". Materials Science and Engineering, 1985, **69**, 181-190.

104 Newey D, Pollock HM and Wilkins MA. "The ultramicrohardness of ion implanted iron and steel at sub-micron depths and its correlation with wear resistance". Ion Implantation into Metals. Eds: Ashworth V,Grant WA and Procter RPM. Pergamon, 1982, 157-166.

105 Pollock HM, Maugis D and Barquins M. "Characterization of submicrometre surface layers by indentation". Microindentation Techniques in Materials Science and Engineering. ASTM STP 889. Eds.: Blau PJ and Lawn BR.Amer. Soc. for Testing and Mater. (Philadelphia), 1986, 47-71.

106 Jones WR and Ferrante J. "Tribological characteristics of N^+ implanted Fe". ASME/ASLE Lubrication Conference. Washington, 1982. ASLE Preprint No 82-LC-3D-2.

107 Tosto S. "Wear behaviour of 38NCD4 N-ion implanted steel". Journal of Materials Science. 1983, **18**, 899-902.

108 Hohmuth K, Kolitsch A and Rauschenbach B. "Beeinflussung mechanischer Eigenschaften durch Ionenimplantation". Neue Hütte,1984, **29** (5),174-178.

109 Oliver WC, Hutchings R, Pethica JB, Singer IL and Hubler GK. "Hardness as a measure of wear resistance". Ion Implantation and IonBeam Processing of Materials. North Holland. Elsevier Science Publ. Inc. (New York), 1984, 603-608.

110 Iwaki M, Fujihana T and Okitaka. "Mechanical and electrochemical properties of various tool steels implanted with nitrogen or NO ions". Materials Science and Engineering. 1985, **69**, 211-217.

111 Kothari DC, Nair MR, Rangwala AA, Lal KB, Prabhawalkar PD and Raole PM. "XPS studies at various temperatures of nitrogen implanted 304 stainless steel". Nuclear Instruments and Methods in Physics Research, 1985, **B7/8**, 235-241.

112 Bunshah RF and Suri AK. "Friction and wear of stainless steels, titanium and aluminium with various surface treatments, ion implantation and overlay hard coatings". IPAT '79. Ion Plating and Allied Techniques (Proc. Conf., London, 1979), CEP Consultants, 1979, 230-241.

113 Singh A, Fiset M and Knystautas EJ. "Effect of nitrogen implantation with overlay coatings on microhardness in 4145 steel". Solid State Communications, 1985, 54 (7), 607-610.

114 Dearnaley G, Minter FJ, Rol PK, Saint A and Thompson V. "Microhardness and nitrogen profiles in ion implanted tungsten carbide and steels". Nucl. Instrum. and Methods in Phys. Res., 1985, **B7/8**, 188-194.

115 Dienel G, Kreissig U and Richter E. "Wear behaviour of ion implanted steel surfaces". Vacuum, 1986, **36** (11-12), 813-815.

116 Prabhawalkar PD, Raole PM, Kothari DC and Nair MR. "XPS studies at various depths of low energy N_2^+ ions implanted on 304 stainless steel". Vacuum, 1986, **36** (11-12), 817-820.

117 Eyre BL. "Small clusters and their influence on mechanical properties in irradiated metals". International Metallurgical Reviews, 1974, **19**, 240-246.

118 Pavlov AV, Pavlov PV, Zoria EI and Tetelbaum DI. Proc. All Soviet Meeting on Ion Beam Physics, Kiev, 1974. (As quoted in Ref. 3).

119 Oppel GW. "Biaxial Elasto-plastic analysis of load and residual stresses". Experimental Mechanics, 1964, **4** (5), 135-140.

120 Eernisse EP. "Sensitive technique for studying ion implanted damage". Applied Physics Letters, 1971, **18** (12), 581-583.

121 Robic JY, Piaguet J and Gailliard JP. "Some measurements of hardness, wear and stresses in ion implanted thin metallic films". Nuclear Instruments and Methods, 1981, **182/183**. 919-922.

122 Hutchings R. "The subsurface microstructure of nitrogen implanted metals". Materials Science and Engineering, 1985, **69**, 129-138.

123 Hartley NEW. "Surface stresses in ion implanted steel". Journal of Vacuum Science and Technology, 1975, **12** (1), 485-489.

124 Swanson ML, Howe LM, Jackman JA, Jackman TE, Griffiths K and Quenneville AF. "Lattice location of ^{15}N in Fe". Nuclear Instruments and Methods in Physics Research, 1985, **B7/8**, 85-90.

125 Gleiter H. "Fundamentals of strengthening mechanisms". Strength of metals and alloys. (ICSMA 6), Vol 3, Ed.: Gifkins RC. Pergamon Press (Oxford), 1983, 1009-1024.

126 Bykov VN, Zdorovtseva GG, Troyan VA and Ivanyushkin EM. "Mössbauer spectra and structure of iron films irradiated with helium and nitrogen ions". Sov. Phys. Solid State, 1976, **18** (1), 118-121.

127 Longworth G and Hartley NEW. "Mössbauer effect study of nitrogen implanted iron foils". Thin Solid Films, 1977, **48**, 95-104.

128 Drako JM and Gumanskij GA. "Structural changes on iron after nitrogen and carbon ion implantation". Radiation Effects, 1982, **66**, 101-108.

129 Rauschenbach B and Kolitsch A. "Formation of compounds by nitrogen ion implantation in iron". Physics Status Solidi (A), 1983, **80**, 211-222.

130 Rauschenbach B, Hohmuth K and Kastner G. "Microstructural investigations of iron implanted with nitrogen ions at the temperature of liquid nitrogen. Part I: Implantation in the dose range $1x10^{16}$ to $1x10^{17}$ N^+ ions/cm^2". Nuclear Instrum. and Methods in Phys. Res. (to be published).

131 Rauschenbach B. "Microstructural investigations of iron implanted with nitrogen ions at the temperature of liquid nitrogen. Part II: Implantation in the dose range $1x10^{17}$ to $1x10^{18}$ N^+ ions/cm^2". Nuclear Instruments and Methods in Physics Research. 1986, **B18**, 34-46.

132 Hohmuth K, Rauschenbach B, Kolitsch A and Richter E. "Formation of compounds by metalloid ion implantation in iron". Nuclear Instruments and Methods. 1983, **209/210**, 249-257.

133 Kolitsch A, Rauschenbach B and Richter E. "Formation of compositions by implantation in Fe". Radiation Effects Letters, 1983, **76** (6), 193-202.

134 Principi G, Matteazzi P, Ramous E and Longworth G. "Mössbauer surface study of nitrogen implanted high carbon martensite". Journal of Materials Science, 1980, **15**, 2665-2668.

135 Jata KV and Starke EA. "Surface modification by ion implantation. Effects on fatigue". Journal of Metals, Aug. 1983, 23-27.

136 Marest G, Skoutarides C, Barnavon T, Tousset J, Fayeulle S and Robelet M "Conversion electron Mössbauer spectroscopy and (p,$\alpha\gamma$) nuclear reaction studies of ^{15}N implanted steels". Nuclear Instruments and Methods, 1983, **209/210**, 259-265.

137 Marest G, Moncoffre N and Fayeulle S. "Nitrogen evolution study after wear in an implanted 42CD4 steel". Applications of Surface Science, 1985, **20**, 205-214.

138 Barnavon T, Jaffrezic H, Marest G, Moncoffre N,Tousset J and Fayeulle S. "Influence of temperature on nitrogen implanted steels and iron". Materials Science and Engineering, 1985, **69**, 531-537.

139 Carbucicchio M, Bardani L and Tosto S. "Surface Mössbauer analysis of 38NCD4 steel ion implanted with nitrogen". Journal of Applied Physics, 1981, **52** (7), 4589-4592.

140 Carbucicchio M and Tosto S. "Microstructure of nitrogen implantation-induced phases on 38NCD4". Metallography, 1983, **16**, 161-170.

141 Singer IL and Murday JS. "Chemical state of ion implanted nitrogen in Fe18Cr8Ni steel". Journal of Vac. Sci. and Tech., 1980, **17** (1), 327-329

142 Baron M, Chang Al, Schreurs J and Kossowsky R. "Nitrogen distribution and nitride precipitation in $^{14}N^+$ ion implanted 304 and 316 steels". Nuclear Instruments and Methods, 1981, **182/183**, 531-538.

143 Dos Santos CA, Behar M, de Souza JP and Baumvol IJR. "Composition and thermal evolution of nitrogen implanted steels: a systematic study". Nucl. Instrum. and Methods, 1983, **209/210**, 907-912.

144 Yost FG, Picraux ST, Follstaedt DM, Pope LE and Knapp JA. "The effects of N^+ implantation on the wear and friction of type 304 and 15-5PH stainless steels". Thin Solid Films, 1983, **107**, 287-295.

145 Bone WM, Colton RJ, Singer IL and Gossett CR. "Summary abstract: SIMS, Auger and Nuclear Reaction Analysis of nitrogen implanted iron alloys". Journal of Vacuum Science and Technology A, 1984, **2**, 788-789.

146 Whitton JL, Ewan GT, Ferguson MM, Laursen T, Mitchell IV, Plattner HH Swanson ML, Drigo AV, Celotti G and Grant WA. "Chromium nitride and martensite formation in nitrogen implanted single crystal stainless steel". Materials Science and Engineering, 1985, **69**, 111-116.

147 Principi G,Lo Russo S and Tosello C. "Surface nitride formation in nitrogen implanted Cr steels".Journal of Physics F: Met. Phys.,1985,**15**,L207-L211.

148 Fayeulle S, Treheux D and Esnouf C. "TEM study of the structural changes of nitrogen implanted iron alloys". Nuclear Instruments and Methods in Physics Research. 1985, **B7/8**, 171-176.

149 Fayeulle S, Treheux D and Esnouf C. "TEM characterization of a nitrogen implanted austenitic stainless steel".Appl. Surf. Science,1986, **25**, 288-304.

150 Feller HG, Klinger R and Benecke W. "Tribo-enhanced diffusion of nitrogen implanted into steel". Materials Science and Engineering, 1985, **69**, 173-180.

151 Arnaud Y, Brunel M, de Becdelievre AM, Romand M, Thevenard P and Robert M. "Use of grazing incidence X-ray diffraction for the study of nitrogen implanted stainless steels". Appl. Surf. Science. 1986, **26**,16-26.

152 Cavalleri A, Guzman L, Ossi PM and Rossi I. "On the wear behaviour of nitrogen implanted 304 stainless steel". Scripta Metallurgica, 1986,**20**,37-42

153 Fayeulle S, Treheux D, Esnouf C and Moncoffre N. "Microstructural study of a nitrogen implanted iron-chromium alloy". Radiation Effects, 1984, **83**, 279-289.

154 Hartley NEW. "Tribological and Mechanical Properties". Ion implantation. Vol 18. Treatise on Materials Science and Technology. Ed.: JK Hirvonen. Academic Press (New York), 1980, 321-371.

155 Shepard SR and Suh NP. "The effects of ion implantation on friction and wear of materials". Journal of Lubrication Technology. 1982, **104**, 29-38.

156 Dearnaley G. "Improvement of wear resistance in cemented tungsten carbide by ion implantation". Science of hard materials. Eds: Viswanadham RK, Rowcliffe DJ and Gurland J., Plenum, 1983, 467-483.

157 Carosella CA, Singer IL, Bowers RC and Gossett CR. "Friction and wear reduction of bearing steel via ion implantation". Ion Implantation Metallurgy. Eds.: Preece CM and Hirvonen JK. TMS/AIME, 1980, 103-115

158 Iwaki M, Okabe Y, Namba S and Yoshida K. "Comparison between properties of steels implanted with unseparated ions and a selected ion". Nuclear Instruments and Methods, 1981, **189**, 155-159.

159 Hartley NEW and Hirvonen JK. "Wear testing under high load conditions. The effect of "anti-scuff" additions to AISI 3135, 52100 and 9310 steels introduced by ion implantation and ion beam mixing". Nuclear Instruments and Methods. 1983, **209/210**, 933-940.

160 Pope LE, Yost FG, Follstaedt DM, Picraux ST and Knapp JA. "Friction and wear reduction of 440 C stainless steel by ion implantation". Ion Implantation and Ion Beam Processing of Materials. North Holland. Elsevier Science Publ. Inc. (New York), 1984, 661-666.

161 Hirano M and Miyake S. "Extension of bearing endurance life by ion implantation". Applied Physics Letters, 1986, **49** (13), 779-781.

162 Kirk JA, Egerton GW and Sartwell BD. "Wear and friction of nitrogen ion implanted steel". Journal of Lubrication Technology, 1983, **105**, 239-244.

163 Ecer GM, Wood S, Boes D and Schreurs J. "Friction and wear properties of nitrided and nitrogen implanted 17-4 PH stainless steel". Wear, 1983, **89**, 201-214.

164 Fayeulle S and Treheux D. "Friction and wear of a nitrogen implanted austenitic stainless steel". Nuclear Instruments and Methods in Physics Research, 1987, **B19/20**, 216-220.

165 Singer IL and Jeffries RA. "Friction, wear and deformation of soft steels implanted with titanium and nitrogen". Ion Implantation and Ion Beam Processing of Materials. North Holland. Elsevier Science Publ. Inc. (New York), 1984, 667-672.

166 Danroc J, Aubert A and Gillet R. "Hard chrome and molybdenum coatings prepared by magnetron sputtering". 2nd Int. Conf. Surface Eng. Stratford-upon-Avon, U.K., June 1987. The Welding Institute, 1987, 26/1-26/7.

167 Madakson P. "Mechanical properties of nitrogen-implanted 18W-4Cr-1V bearing steel". Materials Science and Engineering, 1987, **90**, 287-290.

168 Terashima K. Minegishi T, Iwaki M and Kawashima K. "Surface modification of electrodeposited chromium films by ion implantation". Materials Science and Engineering, 1987, **90**, 229-236.

169 Hartley NEW. "Ion implantation and surface modification in tribology". Wear, 1975, **34**, 427-438.

170 Dearnaley G and Hartley NEW. "Ion implantation into metals and carbides". Thin Solid Films, 1978, **54**, 215-232.

171 Yu Kun, Li Hen-De, Zhang Xiao-Zhong and Tian Jia-He. "Some practical aspects of nitrogen implantation in various steels related to wearing". Nuclear Instruments and Methods, 1983, **209/210**, 1063-1070.

172 Singer IL, Bolster RN and Carosella CA. "Abrasive wear resistance of titanium and nitrogen implanted 52100 steel surfaces". Thin Solid Films, 1980, **73**, 283-289.

173 Fayeulle S. "Tribological behaviour of nitrogen implanted material". Wear, 1986, **107**, 61-70.

174 Fayeulle S,Treheux D,Guiraldenq P, Barnavon T, Tousset J and Robelet M. "Nitrogen migration during wear in an implanted steel".Scripta Metallurgica, 1983, **17**, 459-462.

175 Hale EB, Meng CP and Kohser RA. "Measurement of the wear properties of metallic solids with a Falex lubricant testing machine". Review Scientific Instruments, 1982, **53** (8), 1255-1260.

176 Hale EB, Kaiser TH, Meng CP and Kohser RA. "Effects of nitrogen ion implantation on the wear properties of steel". Ion Implantation into Metals. Eds.: Ashworth V, Grant WA and Procter RPM. Pergamon, 1982, 111-116.

177 Hale EB, Muehlemann MM, Baker W and Kohser RA. "Parameter induced changes in the wear behaviour of ion implanted steel under heavy loading". Surface Engineering. Surface Modification of Materials (Proc. of NATO Advanced Study Inst. on Surf Eng. Les Arcs. France, July 1983) Eds.: Kossowsky R and Singhal SC. Martinus Nijhoff Publ. (The Netherlands), 1984, 158-169.

178 Hale EB, Kohser RA and Reinbold R. "Ion implantation and thermal oxidation as treatments to initiate sustained oxide wear in steels". Applied Physics Letters, 1986, **49** (8), 447-449.

179 Hale EB, Reinbold R and Kohser RA. "Nitrogen implantation of steels: a treatment which can initiate sustained oxidative wear". Materials Science and Engineering, 1987, **10**, 273-280.

180 Harding SE. "The improvement in wear resistance of ion implanted materials".MSc Thesis. Dep. of Appl. Physics. Brighton Polytechnic. 1977.

181 Varjoranta T, Hirvonen J and Anttila A. "Measuring the wear of nitrogen implanted steel". Thin Solid Films, 1981, **75**, 241-245.

182 Goode PD, Peacock AT and Asher J. "A study of the wear behaviour of ion implanted pure iron". Nucl. Instrum. and Methods,1983,**209/210**, 925-931

183 Deutchman AH and Partyka RJ. "Wear resistant performance of ion implanted alloy steels". Surface Engineering. Surface Modification of Materials. Eds.: Kossowsky R and Singhal SC. Martinus Nijhoff Publ. (The Netherlands), 1984, 185-196.

184 Pollock JTA, Kenny MJ and Paterson PJK. "Enhancement of ferrous alloy surface mechanical properties by nitrogen implantation". Ion Implantation and Ion Beam Processing of Materials. (Proc .Conf. Boston. Mass. - USA- Nov 1983). North Holland. Elsevier Science Publ. Inc. (New York). 1984, 691-697.

185 Daniels LO and Wilbur PJ. "Effects of nitrogen ion implantation on load-bearing capacity and adhesive wear behaviour in steels". Nuclear Instruments and Methods in Physics Research 1987, **B19/20**, 221-226.

186 Kustas FM, Misra MS and Tack WR. "Nitrogen implantation of type 303 stainless steel gears for improved wear and fatigue resistance". Materials Science and Engineering, 1987, **90**, 407-416.

187 Goode PD and Baumvol IJR. "The influence of ion implantation parameters on the surface modification of steels". Nuclear Instruments and Methods, 1981, **189**, 161-168.

188 Hirvonen JP and Mayer JW. "Fretting wear of nitrogen implanted AISI 304 stainless steel". Materials Letters, 1986, **4** (1), 404-408.

189 Vardiman RG, Bolster RN and Singer IL. "The effect of nitrogen implantation on martensite in 304 stainless steel". Metastable Materials Formation by Ion Implantation. Materials Research Society Symp. Proc. Vol 17, Eds.: Picraux ST and Choyke WJ. North Holland. Elsevier Science Publ. 1982, 269-274.

190 Lo Russo S, Mazzoldi P, Scotoni I, Tosello C and Tosto S. "Effect of nitrogen ion implantation on the unlubricated sliding wear of steel". Applied Physics Letters, 1979, **34** (10), 627-629.

191 Hohmuth K, Richter E, Rauschenbach B and Blochwitz C. "Fatigue and wear of metalloid ion implanted steels". Materials Science and Engineering, 1985, **69**, 191-201.

192 Singer IL. "Tribomechanical properties of ion implanted metals". Ion Implantation and Ion Beam Processing of Materials. (Proc .Conf. Boston, Mass., USA, Nov. 1983). North Holland. Elsevier Science Publ. Inc. (New York), 1984, 585-595

193 Wolf GK and Westheide H. "The effect of nitrogen implantation on the wear of tools during backward extrusion of cans". Materials Science and Engineering, 1985, **69**, 219-220.

194 Weist C, Wolf GK and Ballhause P. "Improving the wear resistance of metal forming tools by ion implantation". Materials Science and Engineering, 1987, **90**, 399-405.

195 Xie Zhong-Yin, Tu You-Mo, Qiao-Yong and Lin Cheng-Ru. "Ion implantation for improving wear resistance of metals". Ion Implantation into Metals. Eds: Ashworth V, Grant WA and Procter RPM. Pergamon (Oxford), 1982, 117-125.

196 Zhao Jie, Su Yawen, Lu Guangyuan, Liu Fu Run, Ye Weiyi and Li Wang. "The improvement in the wear properties of GCr15-QBe2 wear pairs by ion implantation". Materials Science and Engineering, 1987, **90**, 291-295.

197 Hamilton S. Tech-Ni-Plant Ltd. Aston Science Park, Love Lane, Birmingham B7 4BJ. Private communication.

198 Delves BG. "The use of ion implantation for improved abrasive wear resistance". Ion Implantation into Metals. Eds: Ashworth V, Grant WA and Procter RPM. Pergamon (Oxford), 1982, 126-134.

199 Watkins REJ and Dearnaley G. "Engraved Printing Cylinders. The effects of ion implantation on the durability of hard chromium plating". AERE Harwell. Private communication.

200 Oñate JI, Dennis JK and Hamilton S. "The effect of nitrogen implantation on the properties of coatings". Transactions of the Institute of Metal Finishing, 1987, **65**, 99-104.

201 Delves BG and Dearnaley G. "The use of ion implantation for the improvement of abrasive wear resistance". IPAT '79. Ion Plating and Allied Techniques (Proc. Conf., London) CEP Consultants Ltd.,1979,264-271.

202 Dearnaley G, Goode PD, Minter FJ, Peacock AT, Hughes W and Proctor GW. "Ion implantation and ion assisted coating of metals". Vacuum, 1986, **36** (11-12), 807-811.

203 Dearnaley G and Goode PD. "Techniques and equipment for non-semiconductor applications of ion implantation". Nuclear Instruments and Methods, 1981, **189**, 117-132.

204 Cottrell AH, Hunter SC and Nabarro FRN. "Electrical interaction of a dislocation and a solute atom". The Philosophical Magazine 1953, **44** (357), 1064-1067.

205 Moncoffre N. "Nitrogen implantation into steels". Materials Science and Engineering. 1987, **90**, 99-109.

206 Dos Santos CA and Baumvol IJR. "Nitriding of steels: conventional processes and ion implantation". Ion Implantation Equipment and Techniques. Springer Series in Electrophysics. Vol 11. Eds.: Ryssel H and Glawischnig H. Springer-Verlag (Berlin), 1983, 347-356.

207 Doyle BL, Follstaedt DM, Picraux ST, Yost FG, Pope LE and Knapp JA. "Nuclear microprobe analysis of wear tracks on ^{14}N implanted steels". Nuclear Instrum. and Methods in Physics Research, 1985, **B7/8**, 166-170.

208 Pollock JTA, Clissold RA, Paterson PJ and Veitch CJ. "Nitrogen implanted steels - aspects of oxidation and diffusion during wear". Nuclear Instruments and Methods in Physics Research, 1987, **B19/20**, 263-267.

209 Sommerer TJ, Hale EB, Burris KW and Kohser RA. "Characterization of wear modes in ion-implanted steel from Auger measurements". Materials Science and Engineering, 1985, **69**, 149-154.

210 Wang JJ, Welsch G, Bakhru H, Mashayekhi A and Gibson W. "TEM evaluation of ion-implanted and fatigued metal surface layers". Nucl. Instruments and Methods in Physics Research, 1985, **B7/8**, 228-234.

211 Goldenstein AW, Rostoker W, Schossberger F and Gutzeit G. "Structure of chemically deposited nickel". Journal of the Electrochemical Society, 1957, **104** (2), 104-110.

212 Ziehlke KT, Dritt WS and Mahoney CH. "Heat treating electroless nickel coatings". Metal Progress, 1960, **77** (2), 84-87.

213 W Canning Materials Ltd., Great Hampton Street, Birmingham B18 6AS

214 Dennis JK and Jones D. "Brush plating". Surface Technol., 1981,12,57-73

215 Lodge KJ, Still FA, Dennis JK and Jones D. "The application of brush-plated cobalt alloy coatings to hot and cold-work dies". Journal of Mechanical Working Technology, 1979, **3**, 63-75.

216 Lodge KJ, Dennis JK and Jones D. "Brush plating for wear resistant applications". Trans. of the Inst. of Metal Finishing, 1979, **57**, 164-168.

217 Zymet Inc. (Eaton Corp.). 33 Cherry Hill Drive. Danvers, Massachussets 01923 (USA).

218 Drozda TJ. "Ion implantation. Manufact. Engineering,1985,**94**(1),51-56

219 Faville-Le Vally Corporation,2055 Comprehensive Dr,Aurora,Illinois 60505

220 ASTM Designations: D-2625-69, D-2670-67, D-3233-73.

221 Parker K. "Hardness and wear resistance tests of electroless nickel deposits" Plating, 1974, **61**, 834-841.

222 Ma U and Gawne DT. "Wear of electroless nickel-phosphorus coatings". Transactions of the Institute of Metal Finishing, 1985, **63**, 64-69.

223 Joshi A, Davis LE and Palmberg PW, in: "Methods of Surface Analysis" Chapter 5. Ed.: Czanderna AW. Elsevier (New York), 1975.

224 Davis IE (Ed.). Handbook of Auger Electron Spectroscopy. Physical Electronics Industries, Eden Prairie, MN, 1976.

225 Sherwood PMA. "Data analysis in X-ray photoelectron spectroscopy". Practical Surface Analysis by Auger and X-ray Photoelectron Spectroscopy. Eds.: Briggs D and Seah MP. John Wiley and Sons Ltd. (Chichester, 1983), 445-475.

226 Amsel G, Nadai JP, D'Artemare E, David D, Girard E and Moulin J. "Microanalysis by the direct observation of nuclear reactions using a 2 MeV Van de Graaff. Part II: Applications to materials analysis". Nuclear Instruments and Methods, 1971, **92**, 481-498.

227 Powder Diffraction File for Inorganic Phases. The Joint Committee for Powder Diffraction Standards. Swarthmore, Pennsylvania, 1981.

228 Dengel D and Rossow. "Comparison between the Vickers and Knoop hardness values". Härterei-Techn. Mitt., 1971, **26** (1),21-27.

229 Romand M and Roubin M. "ESCA studies of chromium and vanadium nitrides". Analusis, 1976, **4** (7), 308-312.

230 Wagner CD, Riggs WM, Davis LE and Moulder JF. Handbook of X-ray photoelectron spectroscopy. Ed. Muilenberg GE. Perkin Elmer Corporation Physical Electronics Division. Eden Prairie, Minnesota, 1979.

231 Allen GC, Curtis MT, Hooper AJ and Tucker PM. "X-ray photoelectron spectroscopy of iron-oxygen systems". J. Chem.Soc.Dalton, 1974, 1525-30

232 Brundle CR, Chuang TJ and Wandelt K. "Core and valence level photoemission studies of iron oxide surfaces and the oxidation of iron". Surface Science, 1977, **68**, 459-468.

233 Ludema KC. "A review of scuffing and running-in of lubricated surfaces, with asperities and oxides in perspective". Wear, 1984, **100**, 315-331.

234 Bentley RM and Duquette DJ. "Environmental considerations in wear processes". Fundamentals of friction and wear of materials. Ed.:Rigney DA American Society for Metals, 1981, 291-329.

235 Burnett PJ and Page TF. "Criteria for mechanical property modifications of ceramic surfaces by ion implantation". Radiation Effects, 1986, **97**,283-296

236 Sreenath AV and Raman N. "Mechanism of smoothing of cylinder liner surface during running-in". Tribology International, 1976, **9**, 55.

237 Kubaszewski O and Hopkins BE. Oxidation of metals and alloys. Butterworths (London), 1962.

238 Galerie A, Caillet M and Pons M. "Oxidation of ion implanted metals". Materials Science and Engineering, 1985, **69**, 329-340.

239 Sadeghi M, Longfield PD and Beer CF. "Effects of heat treatment on the structure, corrosion resistance and stripping of electroless nickel coatings". Transactions of the Institute of Metal Finishing, 1983, **61**, 141-146.

240 Kelly R. "On the nature of phases formed when metals are implanted with oxygen or nitrogen". Radiation Effects, 1982, **64**, 205-220.

241 En Ma, Bai-Xin Liu, Xin Chen and Heng-de Li. "Formation of metal nitrides by nitrogen implantation". Thin Films-Interfaces and Phenomena (Part of Fall'85 Meeting of Mat. Res. Soc., Boston, Dec. 1985). Materials Research Society, 1986, 617-622.

242 Still FA. "Electrodeposited cobalt alloy coatings and their use on hot forging dies". PhD thesis. The University of Aston in Birmingham. Sept. 1974.

243 Admon U, Dariel MP and Grünbaum E. "Microstructure of electrodeposited Co-W thin films". Journal of Applied Physics, 1986, **59** (6),2002-2009.

244 Singer IL. "Compositions of metals implanted to very high fluences". Vacuum, 1984, **34** (10/11), 853-859.

245 Saltzman GA. "Wet-sand rubber wheel abrasion test for thin coatings". Selection and use of wear tests for coatings. Ed.: Bayer RG. ASTM STP 769, 1982, 71.

246 Snavely CA. "A theory for the mechanism of chromium plating; a theory for the physical characteristics of chromium plate". Transactions of the Electrochemical Society, 1947, **92**, 532-577.

HEAT TREATMENT
OF METALS
1987.3 p.77–82

Nitrogen Implantation of Tool Steels

J. I. OÑATE and J. K. DENNIS (Aston University)
and
S. HAMILTON (Tech-Ni-Plant Ltd.)

In certain circumstances, ion implantation offers an alternative or an addition to traditional surface heat treatments and other processes aimed at improving properties such as resistance to wear, fatigue and corrosion, and surface hardness. In this article, the authors review the principle of the process, its advantages and limitations, some of the properties conferred, and the applications. The emphasis is on implantation with nitrogen, the element most commonly used in the treatment of plastic-moulding dies, cold-work tools and engineering components. The process is also applicable to plated coatings.

INTRODUCTION

Ion implantation is a relatively new low-temperature technique which enhances the surface characteristics of materials whilst avoiding dimensional changes or surface degradation. As such it offers an effective treatment for tools or components finished to a high precision.

The process had its origin in the electronics industry in the 1960's, having been used extensively since then for the doping of silicon and other semiconducting materials with impurity elements such as boron, phosphorus or arsenic. Research on the effects of implantation on the mechanical properties of metals started approximately a decade ago in Great Britain at AERE, Harwell[1,2]. Results of this preliminary work were so encouraging, in terms of wear and frictional properties imparted, that they inspired all the subsequent research in this area in several centres around the world. These projects have demonstrated[3,4] that ion implantation can modify the surface of metals, improving properties such as resistance to fatigue, corrosion, wear, oxidation, friction and surface hardness, without the adhesion problems associated with coating processes such as PVD and electroplating.

In particular, the many results accumulated have demonstrated the improvements in wear resistance obtained by the implantation of nitrogen in ferrous-based materials, tungsten carbides, titanium and several coatings. However, the physico-chemical changes produced and their influence on tribological behaviour are not understood completely. The effects of nitrogen implantation are related to a material's composition, and the wide spectrum of materials and implantation parameters used make it difficult to compare results obtained by different researchers.

Other than a systematic study by Iwaki et al[5], using moderate loading in wear tests, there has been only limited work published[6] on the effect of nitrogen implantation of tool steels, despite the considerable commercial success of the treatment on a wide range of tooling, as illustrated by the examples in *Table 1* drawn from the production experience of customers of Tech-Ni-Plant. This review incorporates results of investigations, conducted in conjunction with that company, into the effect of nitrogen implantation of AISI M2, D2, and 420 tool steels on their wear behaviour at high loading, a condition more commonly encountered in industrial situations. The improvement that can be achieved on plated tool steels is also considered.

Table 1. Some production applications of nitrogen implantation to tooling

Application	Material	Result
Paper slitters	1.6% Cr/1%C steel	Cutting life × 2
Punches for acetate sheet	Cr-plated steel	Improved product
Taps for phenolic resin	M2 high-speed steel	Life increase up to × 12
Thread-cutting dies	M2 high-speed steel	Life increase × 5
Slitters for synthetic rubber	Co-cemented WC	Life increase × 12
Progression tools	High-speed steel & ASP23	Life increase × 6
Plastics extrusion tooling	Cr-plated brass	Life increase × 3
Drills	High-speed steel	Life increase × 4
Spark-eroded tool finishes	Various	Maintained surface × 4
Injection-moulding tool	Aluminium	Life increase × 3
Injection-moulding nozzle	Tool steel	Life increase × 5
Swaging dies for steel	Co-cemented WC	Life increase × 2

THE PROCESS

Ion implantation is a process in which atoms of the desired element are ionised and accelerated in an electric field at energies usually in the range 50 to 200 KeV, under a vacuum of about 10^{-6} torr. The ions, in a focussed beam, reach the surface of the parts and penetrate it, coming to rest at a controlled depth, once they have lost their energy mainly by nuclear collisions with the host atoms.

The system is shown in *Fig. 1*. The process is controlled by varying the implantation time, which is dependent not only

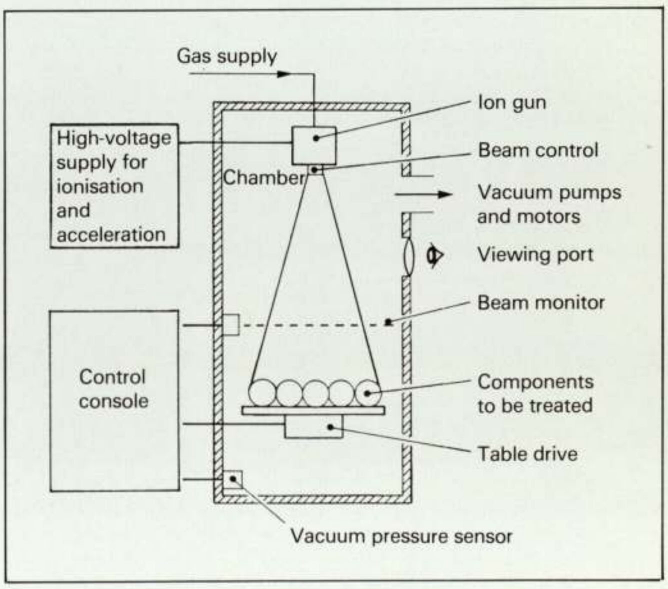

Fig. 1. Schematic diagram of the ion implantation system.

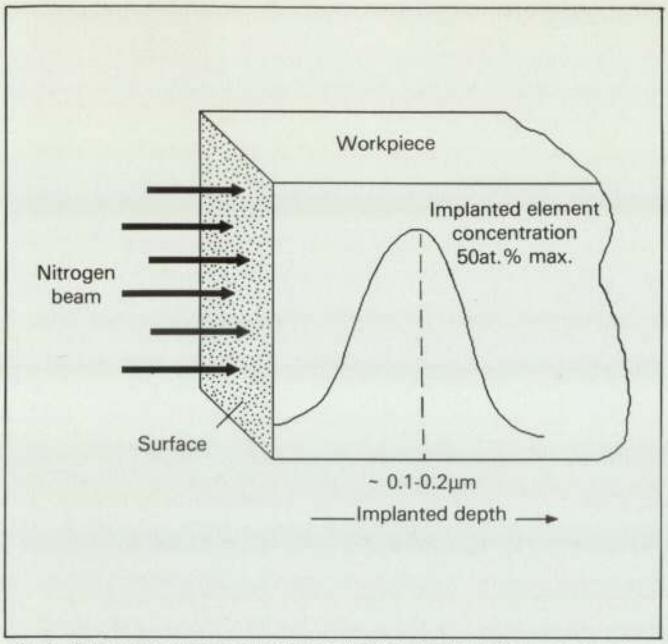

Fig. 2. Schematic representation of the ion implantation process. Ions penetrate the surface, forming an approximate Gaussian depth profile.

Table 2. Advantages and limitations of nitrogen implantation as a surface treatment

Advantages

1. Low-temperature process.
2. Negligible dimensional changes.
3. No degradation of surface finish.
4. No sacrifice of bulk properties.
5. No adhesion problems since there is no sharp interface.
6. Solid solubility limit of implanted species can be exceeded.
7. A fine dispersion of precipitates is created. Optimum wear behaviour.
8. Clean vacuum process.
9. Minimum masking costs. Ability to treat selective areas.
10. Highly reproducible and controllable process.

Limitations

1. Line-of-sight process. Manipulation under vacuum necessary.
2. Shallow penetration.
3. Relatively expensive equipment.

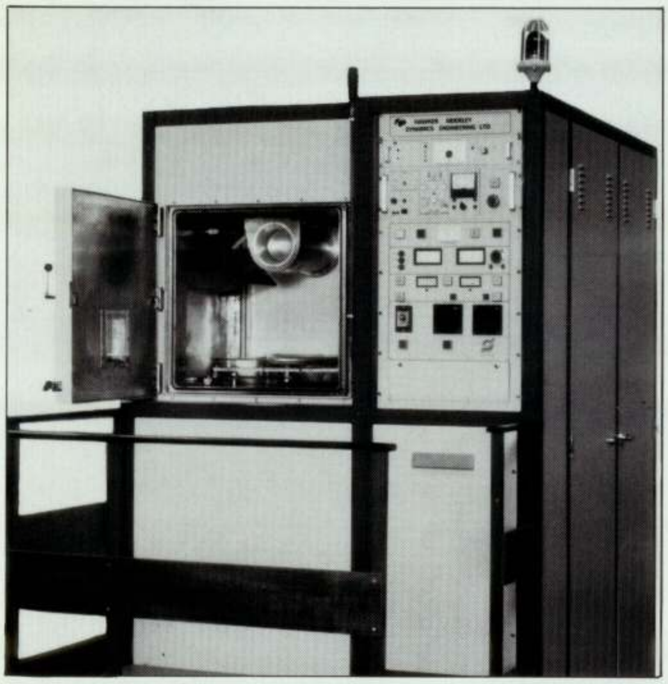

Fig. 3. The Type 222 ion implantation machine at Tech-Ni-Plant Ltd. used in the research programme. Incorporating a 610mm-cube vacuum chamber, it is capable of implanting gaseous ions with a maximum energy of 100KeV.

on the ion dose required, but also on the surface area to be treated by the beam. The beam is scanned on a pre-planned programme and the workpiece rotated and tilted as necessary to ensure exposure of all the surfaces requiring treatment. Total times of 2-10 hours are typical, depending on the component size and geometry. The beam itself is monitored to ensure the correct dose is imparted. This form of process control ensures the reproducibility of the operation.

The implanted ions follow an approximate Gaussian distribution with its peak at a depth of 0.1 to 0.2μm below the surface for the energies used commercially (see *Fig. 2*). This gradual change in concentration of the implanted element avoids problems of poor adhesion, which are possible with coating systems.

A characteristic effect of ionic bombardment is the production of a great number of point defects. The occurrence of these zones with a high concentration of vacancies and interstitial elements can create large compressive stresses at the surface. These stresses occur because the implanted surface layer is prevented from expanding by the underlying steel, and have a beneficial effect on wear resistance, fatigue behaviour and hardness. Improvements are pronounced at high doses such as those used in nitrogen implantation (i.e. $>10^{17}$ ions/cm^2). At these doses, the implanted element is at a concentration well above equilibrium and can produce unusual metallurgical phases with different properties to those produced by diffusional surface treatments, such as gas nitriding.

This process does not require high temperatures; penetration of the ions is not achieved, in general, by diffusion but is due to their high kinetic energy. Nitrogen implantation is normally carried out below 150°C and problems of distortion, softening or degradation of the surface finish of the tooling are therefore avoided or negligible. Consequently, implantation can be carried out as the final step in the surface preparation of the tooling.

Advantages and limitations

Nitrogen implantation provides a number of advantages over coatings or thermochemical surface treatments (see *Table 2*). One of the attractions is, undoubtedly, its low

Table 3. The tool steels studied

AISI designation	Analysis, %wt							Hardness HRC
	C	Si	Mn	Cr	Mo	V	W	
M2	0.87	—	—	4.2	5	1.9	6.4	62 – 64
D2	1.55	0.3	0.3	12	0.8	0.8	—	58 – 60
420	0.38	0.8	0.5	13.6	—	0.3	—	52 – 54

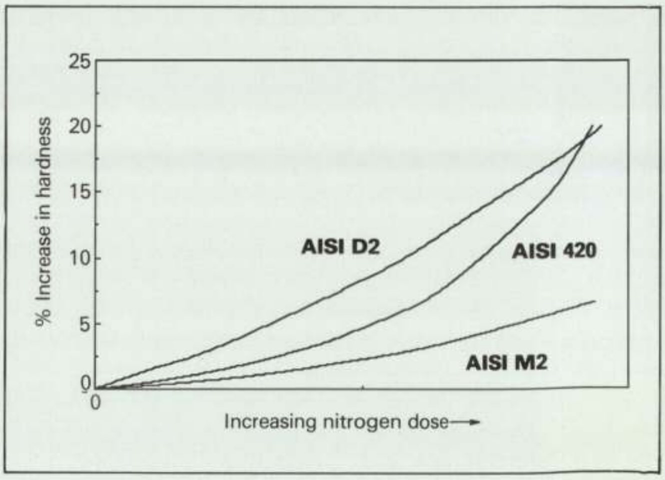

Fig. 4. The effect of nitrogen implantation on the surface hardness (Vickers, 5g load) of the tool steels.

temperature and therefore the absence of distortion or surface degradation of the parts. This makes it an ideal process for treating relatively expensive tools or components, especially if finished with a high precision. Nevertheless, the treatment has some disadvantages, as *Table 2* also indicates. A basic limitation of implantation is that of being a "line-of-sight" process, only those surfaces that receive the ion beam being treated. In order to provide uniform treatment on tools of complicated shape, special jigging systems can be designed or supplied.

The limited penetration of the ions in the range of commercially-used machines (~100 KeV) might suggest that the implantation has a limited value for engineering applications. However, there are many situations in which the effects of the implanted nitrogen persist to a greater depth (e.g. 5μm) than the initial depth of implantation (~0.2μm), providing an effective protection against wear. Additionally, nitrogen implantation can promote a beneficial oxidative wear mechanism that persists even after the nitrogen has been depleted.

PROPERTY ASSESSMENT

In a programme of research at Aston University, the effects of nitrogen implantation on hardened and tempered AISI M2, D2 and 420 tool steels *(Table 3)* have been studied. These steels are widely used in cutting, forming and plastic moulding operations respectively, areas in which nitrogen implantation is being used commercially. 25μm-thick coatings of hard chromium and cobalt-tungsten alloys have also been evaluated after implantation; in both cases, the substrate was H13 steel.

The treatment was carried out in an implantation machine consisting of a high-vacuum system and a high-voltage unit with a maximum output of 100 KeV *(Fig. 3)*. All implantations were conducted at energies in the region of 90 KeV and doses above 10^{17} ions/cm^2. The beam current density was chosen so that the temperature of the test samples did not exceed 100°C.

Surface Hardness

In order to measure the surface hardness of implanted layers, it is essential to use a low load (e.g. 5g Vickers) which limits the penetration of the indentor, minimising the influence of the substrate and, therefore, producing a more representative microhardness value for the implanted surface. At this low load, the hardness results cannot be considered as absolute values but they provide a useful comparison between implanted and untreated surfaces. The percentage increase in surface hardness of the tool steels, as a function of nitrogen dose, is illustrated in *Fig. 4*. Doses above 10^{17} ions/cm^2 are necessary to provide a hardening effect in the steels. Similar results, with hardness increases of up to 40%, were observed with the implanted coated samples.

Nitrogen implantation increased the surface hardness of D2 and 420 steels by at least 20%. Similar or better results have been obtained by Iwaki et al[5] and other workers[6], using conventional microhardness techniques. With these techniques (Vickers or Knoop) the indentor penetrates deeper than the implanted layer, and so the true surface hardness, which would be greater, is not evaluated. The use of ultra-microhardness equipment, such as that described by Newey and co-workers[7] provides more precise information on the effect of implantation on hardness. With this technique, and using loads below 1g, an increase of about 200% in surface hardness has been obtained[8] for nitrogen implanted AISI 420 steel.

The surface hardness of M2 high-speed steel was not modified significantly by implantation at the dose investigated in this work. This steel, with a bulk hardness of

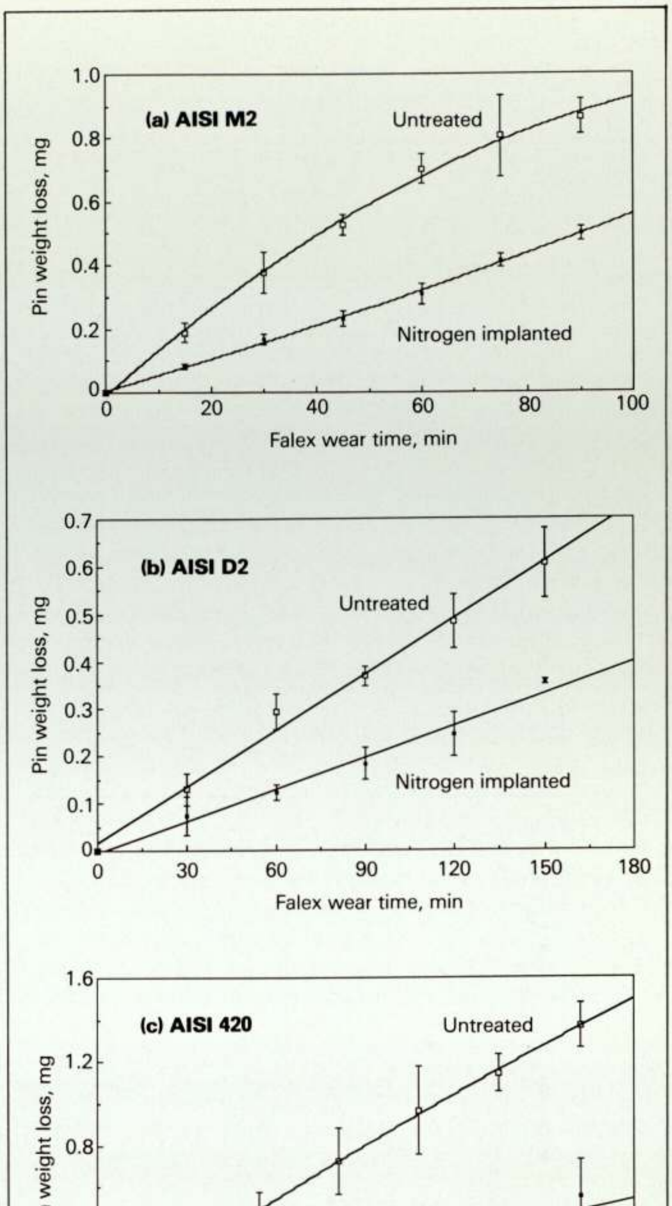

Fig. 5. The results of Falex wear testing under lubricated conditions: (a) AISI M2 steel, 890N load; (b) AISI D2 steel, 890N load; (c) AISI 420 steel, 890N load; (d) 25μm hard chromium coating on BH13 tool steel hardened and tempered to 52HRC, 710N load. In cases (a)-(c), the V-blocks were of the same material as the pin, but not implanted. In (d) the V-blocks were AISI 52100, heat treated to 64-65HRC.

Table 4. Relative wear coefficients after 90 minute Falex test at 890N load

AISI designation	Relative wear coefficient	
	Without implantation	Implanted
M2	1	0.35 (× 2.9 improvement)
D2	1	0.53 (× 1.9 improvement)
420	1	0.40 (× 2.5 improvement)

62-64 HRC, has a mainly martensitic structure with a dispersion of carbides and, therefore, additional hardening would be limited. Similar effects have been found in AISI 52100 bearing steel[6,9]. Research is in progress, however, to study the hardening effect at higher doses.

The increase in hardness is attributable to ion bombardment effects, compressive stresses, formation of a solid solution of interstitial elements (e.g. N or C) and the creation of a dispersion of hard precipitates. AISI D2 and 420 steels have a high Cr content. This element has a great affinity for nitrogen and therefore, at high doses, chromium nitrides are expected to occur. Preliminary studies by the present authors, conducted using a transmission electron microscope, appear to demonstrate the formation of the cubic CrN in the implanted AISI 420 steel. The work of Dimigen et al[6] also indicates a combination of Cr and N for a similar steel. Information about the effect of nitrogen on this type of martensitic stainless steel suggests the formation of CrN[10-12] and the hexagonal phase Cr_2N[13]. The precipitation of these nitrides seems to depend on the nitrogen dose[11]. Furthermore, the implantation of nitrogen in ferrous materials produces iron nitrides[14-16], bringing an additional hardening effect.

Wear and friction

Wear tests were performed with a Falex machine[17], the use of which, with implanted materials, has been described by several workers[18,19]. All testing was conducted using test pieces and V-blocks made of the same material, but only the test pieces were nitrogen implanted. Tests were carried out under lubricated conditions (paraffinic mineral oil — ISO 22), with a constant load of 890 N along the transverse direction, for several periods, each of about 30 minutes.

The results, shown in *Figs. 5a-c*, illustrate that nitrogen implantation clearly improves the wear resistance of the tool steels by up to three times under high loading conditions. Implanted coatings behave similarly, as indicated by way of example for hard chromium in *Fig. 5d* where the load employed was 710 N. The relative wear coefficient, or ratio of the wear of implanted parts to that of the untreated ones, is a useful parameter to illustrate the improvements produced by implantation. This value is indicated in *Table 4* after 90 minutes wear testing.

It is generally agreed that resistance to deformation of a material is related to its hardness and the presence of nitrides improves the wear behaviour of surfaces. Nitrogen implantation at low temperatures produces a higher density of micro-precipitates than that produced by diffusion-type surface treatments[20]. This effect has been stressed by Madakson[21] and it produces optimum results for the pinning of dislocations during wear and friction processes. *Figs. 6a and b* show the difference in wear behaviour during Falex testing for unimplanted and implanted M2 test pieces. Implantation increases the load-bearing capacity of the surface, reducing or eliminating the ploughing of hard asperities into the surface. Moreover, it appears to cause a change in the wear mechanism. In the untreated steel, there is plastic deformation of the surface and an abrasive type of wear. However, a mild oxidative mechanism seems to be predominant on the implanted surface, an effect that has also been observed elsewhere[5]. A fine oxide layer can reduce adhesion between contacting surfaces and deformation of the substrate which can also lower the friction coefficient. *Fig. 7* shows the beneficial effect of nitrogen implantation on the frictional behaviour of AISI D2.

Adhesion between surfaces and friction characteristics are properties sensitive to the composition of contacting surfaces. Implantation modifies the chemical affinity of the surfaces, changes the growth of oxides and, therefore, improves the tribological behaviour of surfaces.

Nitrogen penetration

In order to obtain chemical information about the surfaces after implantation, Auger electron spectroscopy has been carried out, with sputtering of atoms from the surface with argon ions to reveal the composition at various depths below the surface. *Fig. 8* shows the Auger emission spectra for AISI 420 steel, implanted at a dose above 10^{17} ions/cm^2, in which a maximum concentration of 20 at.% was attained. One of the most interesting aspects of nitrogen implantation on steel substrates is the persistence of its effects at depths 10 times greater than the original implanted depth[22,23]. Hartley[24] relates this to the formation of nitrides during implantation and their decomposition during wear, due to the frictional temperature rise in the contacting areas. The liberated nitrogen is able to move and block the movement of dislocations, hardening the surface by means of the Cottrell effect[25].

Fig. 8 also shows the Auger spectrum after 90 minute's wear. If it is assumed that uniform wear of the contacting surfaces takes place, a layer 0.57μm thick would have been removed; this is approximately three times the initial

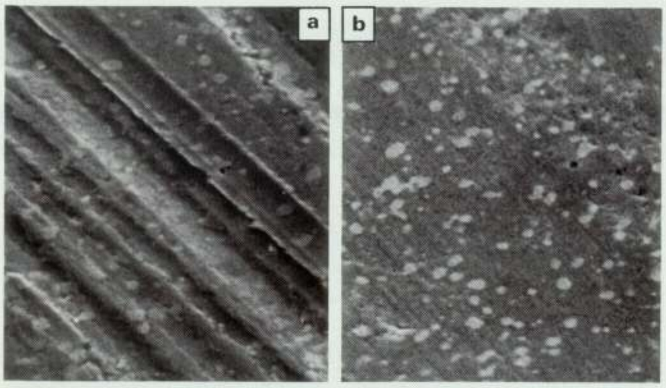

Fig. 6. Scanning electronmicrographs showing worn surfaces of (a) untreated AISI M2 steel, with ploughing readily visible, and (b) nitrogen-implanted AISI M2 steel, with ploughing virtually eliminated. Magnification: x1300.

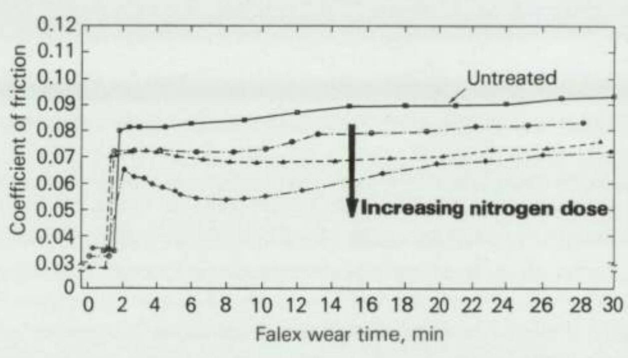

Fig. 7. The variation of the friction coefficient of implanted AISI D2 steel as a function of nitrogen dose and wear time. Lubricated wear test, 890N load.

implanted depth, and yet 40% of the implanted nitrogen was retained. This indicates the diffusion capability of the nitrogen towards the interior of the substrate. Further tests are to be carried out to confirm the model described by Hartley.

In addition to this much-discussed model, there is experimental evidence indicating that nitrogen implantation creates a thin adherent oxide film during wear. This can also contribute to the enhanced wear resistance beyond the implanted layer by promoting a beneficial mild oxidative wear mechanism[26].

APPLICATIONS

It should be pointed out that the benefits of nitrogen implantation depend on the base material and application. They are unlikely to persist at tool operating temperatures above 500°C where the implanted nitrogen diffuses readily inwards or, alternatively, is consumed by severe oxidation. The process is ideal for applications where mild abrasive erosive wear is encountered, but is not effective in severe metal-to-metal adhesive wear systems.

As indicated previously in *Table 1*, nitrogen implantation has proved to be a very successful treatment for overcoming abrasive wear problems suffered in production situations. The process has been available commercially for over three years, and has demonstrated its capability of prolonging the life of both plastic-processing moulds and machine parts *(Figs. 9 and 10)*, punches, progression and press tools, dies and forms, and slitting knives.

The performance of all ferrous-base materials can be improved by implantation but, in general, extensions in tool life are greater when higher-quality steels are used. In tooling applications where even higher performance standards are essential to provide extended continuous production, coatings such as hard chromium have been used. These provide improved wear performance, better friction characteristics, higher surface hardness and an easier release of product in plastics processing. Nitrogen implantation following plating serves to further enhance the improvements offered by chromium. The abrasion resistance of the surface is increased by the formation of chromium nitrides, to a point that is greater than the material being processed or the work-hardened debris, and hence wear is reduced substantially.

Metal-working tools that are often chromium-plated include piercing punches, forming dies, special taps and certain drawing tools. In the plastics processing industry, chromium is far more commonly used and is applied to all tooling areas which will suffer high material feed resulting in considerable wear. The major wear points in injection moulding include sprue bushes, runner blocks and gate areas, all of which show marked improvements following both chromium deposition and nitrogen implantation. The moulding cavities of impression blocks suffer wear after a period of time, but when spark-machined or chemically-etched to produce a product with a textured finish, deterioration of the surface can be almost immediate. The peaks and troughs of the texture are soon polished by the abrasive polymer and smooth areas result on the product. This is unacceptable and refurbishment is required which is both costly and time consuming.

Implantation of chromium-plated cavities significantly improves their life expectancy, generally by a factor of three or four times. *Fig. 10* shows a mould cavity which produces a jug kettle handle from abrasive phenolic material. The chromium-plated tool produced approximately 25,000 items prior to unacceptable wear. Following refurbishment, the chromium plate was nitrogen implanted and in excess of 100,000 items were moulded.

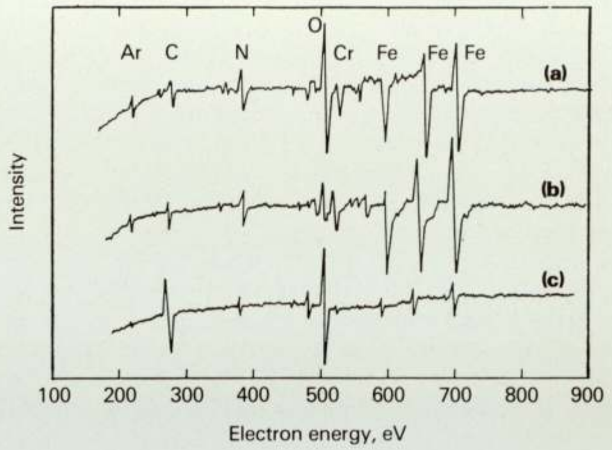

Fig. 8. Auger spectra for AISI 420 nitrogen-implanted steel. (a) and (b) relate to sputter etch times of 10 and 120 minutes. (c) relates to the situation after 90 minutes' wear in a Falex test.

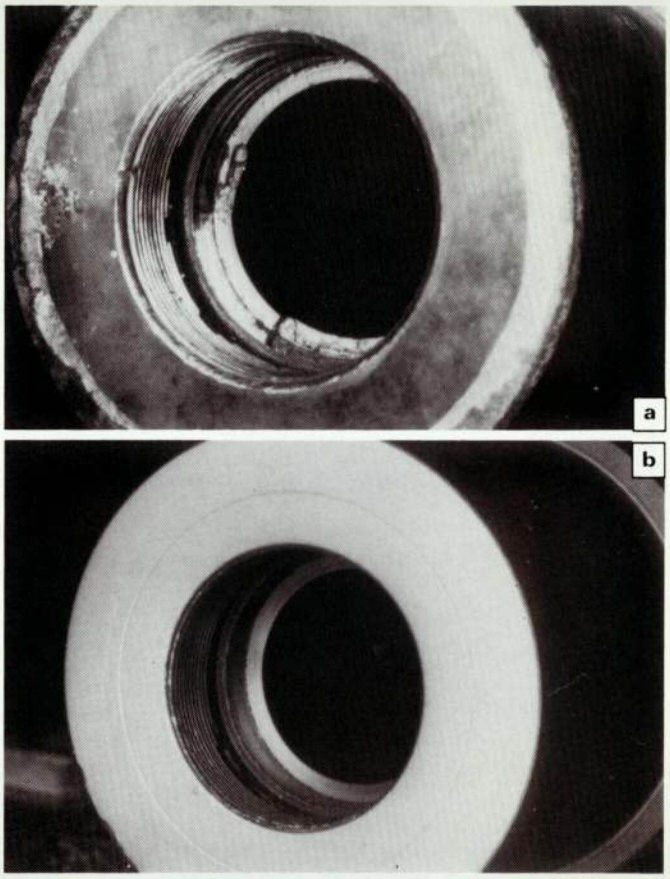

Fig. 9. Injection moulding barrels after 5½ month's use: (a) untreated heavily-worn barrel removed for refurbishment; (b) nitrogen-implanted barrel, relatively unscathed.

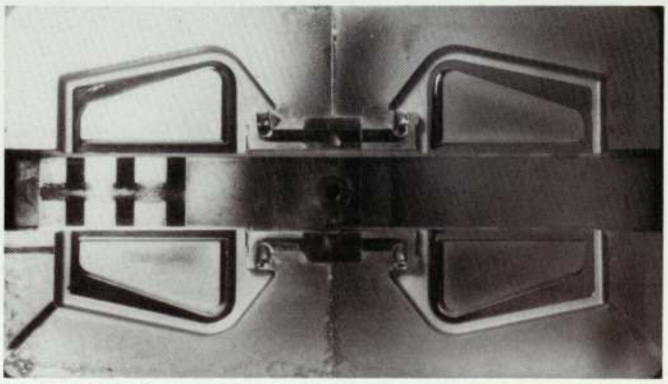

Fig. 10. The life of this hard chromium plated mould for jug kettle handles, in highly-abrasive thermoset plastic, was increased by 400% by nitrogen implantation.

CONCLUSIONS

Nitrogen implantation at high doses increases significantly the hardness of martensitic steels and coatings such as hard chromium; ultra-microhardness techniques are necessary to reveal the true hardness of thin implanted layers.

Implantation, by creating a hard nitride layer, increases the load-bearing capacity of the surface, reducing ploughing and deformation, and therefore improving the abrasive wear resistance of steels and coatings.

The treatment favours the formation of an oxy-nitride lubricant layer on the surface and can change the wear mechanism from adhesive or abrasive to a mild oxidative wear. This lubricant layer lowers the friction coefficient between contacting surfaces during the first stages of wear.

Nitrogen implantation produces striking improvements in wear resistance of both metal-processing and plastic-moulding tools.

ACKNOWLEDGEMENTS

One of the authors, J.I. Oñate, would like to thank the Basque Government's Department of Education for its financial support throughout this work. The authors are also indebted to G. Cooper (Tech-Ni-Plant Ltd.) for carrying out the implantation treatments and for valuable discussions during the present work.

REFERENCES

1. **Hartley N.E.W., Swindlehurst W.E., Dearnaley G. and Turner J.F.** Friction changes in ion-implanted steel. *Journal of Materials Science. 1973, Vol. 8, 900*
2. **Hartley N.E.W.** The tribology of ion-implanted metal surfaces. *Tribology International. 1975, Vol. 8, 65-72.*
3. **Dearnaley G.** Ion implantation for improved resistance to wear and corrosion. *Materials in Engineering Applications. Sept. 1978, Vol. 1, 28-41.*
4. **Hirvonen J.K.** Ion implantation in tribology and corrosion science. *Journal of Vacuum Science and Technology. 1978, Vol. 15, No. 5, 1662-1668.*
5. **Iwaki M., Fujihana T. and Okitaka K.** Mechanical and electrochemical properties of various tool steels implanted with nitrogen or NO ions. *Materials Science and Engineering. 1985, Vol. 69, 211-217.*
6. **Dimigen H., Kobs K., Leutenecker R., Ryssel H. and Eichinger P.** *Ibid., 181-190.*
7. **Newey D., Pollock H.M. and Wilkins H.A.** The ultramicrohardness of ion implanted iron and steel at sub-micron depths and its correlation with wear resistance. *Ion Implantation into Metals. Pergamon, 1982, 157-166.*
8. **Oñate J.I., Dennis J.K. and Hamilton S.A.** The effect of ion (nitrogen) implantation on the properties of martensitic steels. *Paper presented at the 2nd International Conference on Surface Engineering, Stratford-upon-Avon, 16-18 June 1987. The Welding Institute, Cambridge, Proceedings P18/1-18/18.*
9. **Oliver W.C., Hutchings R. and Pethica J.B.** The wear behaviour of N-implanted metals. *Metallurgical Transactions A. 1984, Vol. 15A, 2221-2229.*
10. **Baron M., Chang A.L., Schreuss J. and Kossowsky R.** Nitrogen distribution and nitride precipitation in $^{14}N^+$ ion implanted 304 and 316 steels. *Nuclear Instruments and Methods. 1981, Vol. 182/183, 531-538.*
11. **Bone W.M., Colton R.J., Singer I.L. and Gosset C.R.** Summary abstract: SIMS, Auger and nuclear reaction analysis of N-implanted Fe alloys. *Journal of Vacuum Science and Technology A. 1984, Vol. 2, 788-789.*
12. **Singer I.L. and Murday J.S.** Chemical state of ion implanted nitrogen in Fe18Cr8Ni steel. *Journal of Vacuum Science and Technology. 1980, Vol. 17, No. 1, 327-329.*
13. **Whitton J.L., Ewan G.T., Ferguson M.M., Laursen T., Mitchell I.V., Plattner H.H., Swanson M.L., Drigo A.V., Celotti G. and Grant W.A.** Chromium nitride and martensite formation in nitrogen implanted single crystal stainless steel. *Materials Science and Engineering. 1985, Vol. 69, 111-116.*
14. **Hohmuth K., Rauschenbach B., Kolitsch A. and Richter E.** Formation of compounds by metalloid ion implantation in iron. *Nuclear Instruments and Methods. 1983, Vol. 209/210, 249-257.*
15. **Dos Santos C.A., Behar M., de Souza J.P. and Baumvol I.S.R.** *Ibid., 907-912.*
16. **Barnavon Th, Jaffrezic H., Marest G., Moncoffre N., Tousset J. and Fayeulle S.** Influence of temperature on nitrogen implanted steels and iron. *Materials Science and Engineering. 1985, Vol. 69, 531-537.*
17. Falex Lubricant Testing Machine. Faville-Levally Corporation, 2055 Comprehensive Dr., Aurora, Illinois 60505, USA. *ASTM designations: D-2625-69, D-2670-67, D-3233-73.*
18. **Hale E.B., Meng C.P. and Kohser A.** Measurement of the wear properties of metallic solids with a Falex lubricant testing machine. *Review Scientific Instruments. 1982, Vol. 53, No. 8, 1255-1260.*
19. **Hartley N.E.W. and Hirvonen J.K.** Wear testing under high loading conditions. The effect of anti-scuffing additions to AISI 3135, 52100 and 9310 steels introduced by ion implantation and ion beam mixing. *Nuclear Instruments and Methods. 1983, Vol.209/210, 933.*
20. **Herman H., Hu W.W., Clayton C.R., Hirvonen J.K., Kant R. and MacCrone R.K.** Modification of mechanical properties through ion implantation. *IPAT'79, Ion Plating and Allied Techniques (Proc. Conf., London). CEP Consultants Ltd., 1979, 255-264.*
21. **Madakson P.B.** Effect of the implantation dose on the hardness, friction and wear of Sb-implanted Al. *Journal Applied Physics. 1984, Vol. 55, No. 9, 3308-3314.*
22. **Feller H.G., Klinger R. and Benecke W.** Tribo-enhanced diffusion of nitrogen implanted into steel. *Materials Science and Engineering. 1985, Vol. 69, 173-180.*
23. **Lo Russo S., Mazzoldi P., Scotoni I., Tosello C. and Tosto S.** Effect of nitrogen-ion implantation on the unlubricated sliding wear of steel. *Applied Physics Letters. 1979, Vol. 34, No. 10, 627-629.*
24. **Hartley N.E.W.** Friction and wear of ion-implanted metals. A review. *Thin Solid Films. 1979, Vol. 67, 177-190.*
25. **Cottrell A.H.** Dislocations and Plastic Flow in Crystals. *Clarendon Press, Oxford, 1953.*
26. **Pollock J.T.A., Clissold R.A., Paterson P.J. and Veitch C.J.** Nitrogen implanted steels — aspects of oxidation and diffusion during wear. *Nuclear Instruments and Methods in Physics Research. 1987, Vol. B19/20, 263-267.*

AUTHORS' ADDRESSES

Mr Oñate and Dr. Dennis are respectively postgraduate research student and Senior Lecturer in the Department of Mechanical and Production Engineering, Aston University, Aston Triangle, Birmingham B4 7ET. Miss Hamilton is Managing Director, Tech-Ni-Plant Ltd., Aston Science Park, Love Lane, Birmingham B7 4BJ.

Estimation of electroless metal deposition rate from measured bath potential

A. Oni
Department of Metallurgical Engineering, Federal University of Technology, Akure, Nigeria.

R. Cottis and G. E. Thompson
Corrosion Centre, University of Manchester, Institute of Science and Technology, Manchester.

SUMMARY – Studies have indicated that the potential changes in an electroless metal plating system is affected by chemical constituents of the baths. A hypothesis is tested to estimate metal deposition rates from the potential changes. A comparison has been made between the theoretical and experimental estimates.

INTRODUCTION

Electroless deposition of a metal consists of two electrochemical reactions; the reduction of metal ions and the oxidation of a reducing agent. Simultaneously, the potential of metal plating bath changes. The extent of potential change depends on the change in the chemical composition of the bath. The purpose of this paper is to compare the experimentally determined metal deposition rates with the theoretical rates estimated from a hypothesis based on mixed potential theory and the potential/current curves of the electrochemical reactions.

Various electroless nickel and cobalt bath formulations with hypophosphite or hydrazine as the reducing agent have been described in the literature,[1] but hypophosphite has found much more extensive technical application probably due to its high reducing power. However, a high hypophosphite concentration is not desirable because it results in bulk reduction of metal ions as opposed to selective catalytic deposition on the metal surface to be coated. In other words, bath stability decrease is a direct function of hypophosphite concentration.[1] In this work, sodium hypophosphite was used as the reducing agent for nickel and cobalt ions in electroless systems and the influence of increasing metal ion concentration was studied.

EXPERIMENTAL PROCEDURES

Mild steel specimens were pretreated by being dipped in 30% HCl for 60 seconds, rinsed in deionized water, dried, weighed and stored in a desiccator. All chemicals used in preparing plating solutions were of analytical grade. The water used was deionized. Bath pH was adjusted with concentrated ammonia solution or concentrated H_2SO_4. The following electroless plating formulations were used:

$NiSO_4$	Variable*
Sodium hypophosphite	10g/l
Glycine	40g/l
Acetic acid	10g/l
pH	5
Temp.	90°C

*50, 100 and 150g/l Ni ion

Cobalt Chloride	Variable†
Sodium hypophosphite	20g/l
NH_4Cl	50g/l
Thiourea	17g/l
pH	9.5
Temp.	85°C

†25, 50 and 75g/l Co ion

Potentials were measured using freshly deposited nickel or cobalt using the equipment shown in Fig 1. The auxiliary electrode (1cm^2 platinum sheet), the working electrode and the reference electrode already immersed in the plating solution were connected to the appropriate terminals of the potentiostat. The reference electrode (SCE) was used in combination with a Luggin capillary whose tip was placed 0.5mm from the 1cm^2 working electrode. Plating kinetics were obtained from the cathodic polarization data with the sweep-generating unit set at 50mVmin^{-1} for a sweep time of 30 minutes. The current was monitored on the chart recorder.

RESULTS AND DISCUSSION

The Wagner and Traud[2] theory of mixed potential postulates that the rate of a Faradaic process is independent of other Faradaic processes occurring simultaneously at the electrode and thus depends only on the electrode potential. Plating of metals involves a reaction proceeding at a rate controlled by activation and diffusion. In the case of Ni and Co plating, the polarization curves (Figs 2 and 3) show that diffusion is insignificant. The cathodic reactions are predominantly activation controlled.

Theoretical plating rate estimation

It is assumed that electroless plating electrochemical reactions is composed of the following reactions:

$R = R^x + xe^-$ $(H_2PO_2)^-$ oxidation

$M^x + xe = M$ Metal deposition

When these two reactions are at steady state, the plating rate, i_p is given by $i_p = i_m = i_R$, where i_m and i_R are respectively the cathodic and anodic reaction rates.

A. Oni, R. Cottis and G. E. Thompson
Trans IMF 1987, **65,** 105

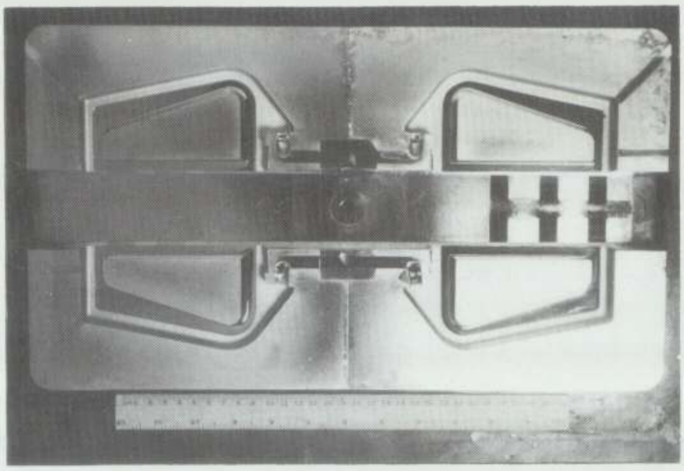

Fig 13a. Hard chromium plated mould cavities.

Fig 13b. Textured domestic items produced from nitrogen implanted chromium plated moulds.

mium plated include, piercing punches, forming dies, special taps and certain drawing tools. In the plastics processing industry chromium is far more commonly used and is applied to all tooling areas which will suffer high material feed and result in high wear. The major wear points in injection moulding include sprue bushes, runner blocks and gate areas, all of which show marked improvements following both chromium deposition and nitrogen implantation. The moulding cavities of impression blocks suffer wear after a period of time, but when spark machined or chemically etched to produce a product with a textured finish, deterioration of the surface can be almost immediate. The peaks and troughs of the texture are soon polished by the abrasive polymer and smoother areas result on the product. This is unacceptable and refurbishment is required which is both costly and time consuming.

Implantation of chromium plated mould cavities, significantly improves their life expectancy, generally by a factor or three or four times. Figure 13a shows a mould cavity which produces a jug kettle handle from abrasive phenolic material. The tool with chromium plate produced approximately 25,000 items prior to unacceptable wear. Following refurbishment the chromium plate was nitrogen implanted and 100,000 items plus were moulded. Figure 13b details a number of these textured domestic items.

CONCLUSIONS

1. Nitrogen implantation at high doses increases the hardness of hard chromium and Co/8%W by about 40%. This is due to the presence of a very thin surface layer that has a true hardness which is even greater and results from the formation of nitrides.
2. Implantation favours the formation of an oxy/nitride lubricant layer on the surface of hard chromium coatings. This layer lowers the friction coefficient between contacting surfaces during the first stages of wear.
3. Nitrogen implantation, by creating a hard nitride layer, increases the load bearing capacity of the surface, reducing ploughing by wear particles or hard asperities and therefore improves the abrasive wear resistance of the coatings.
4. Nitrogen implantation is an effective method of treating components or tools coated with deposits that contain elements which readily form hard nitrides.

ACKNOWLEDGEMENTS

One of the authors, J. I. Oñate, thanks the Basque Government for financial support throughout this work.

Gratitude is also expressed to Mr. G. Cooper (Tech-Ni-Plant Ltd) for carrying out the implantation treatments and for useful discussions about the research.

REFERENCES

1 Guides to Practice in Corrosion Control, No. 16, Engineering Coatings – Their Applications and Properties. HMSO, Dd 8825944.

2 "Wear resistant surfaces in engineering – a guide to their production, properties and selection", HMSO, 1986.

3 G. Dearnaley, "Applications of ion implantation in metals", *Thin Solid Films*, 1983, **107,** 315.

4 J. K. Hirvonen, "Industrial applications of ion implantation" Technology Vectors (Proc Conf) 29th National SAMPE Symposium, Nevada, April 1984, 813.

5 C. J. McHargue, "Ion implantation in metals and ceramics" *Int Met Rev*, 1986, **31,** (2), 49.

6 J. K. Dennis and D. Jones. "Brush plating", *Surf Technol* 1981, **12,** 57.

7 J. B. Pethica, "Microhardness tests with penetration depths less than ion implanted layer thickness", Ion Implantation into Metals, Ed V. Ashworth, A. Grant and R. P. M. Procter, Pergamon 1982, 147-156.

8 W. C. Oliver, R. Hutchings and J. B. Pethica, "The wear behaviour of nitrogen implanted metals", *Met Trans A*, 1984, **15A,** 2221.

9 J. Y. Robic, J. Piaguet and J. P. Gailliard, "Some measurements of hardness, wear resistance and stresses in ion implanted thin metallic metals", *Nucl Instr & Methods* 1981, **182/183,** 919.

10 R. Hutchings, "The subsurface microstructure of nitrogen implanted metals", *Mat Sci & Eng*, 1985, **69,** 129.

11 I. M. Belii, F. F. Komarov, V. S. Trishkov and V. M. Yankovskii, "Formation of chemical compounds by ion bombardment of thin transition metal films", *Phys Stat Sol*, 1978, **(a) 45,** 343.

12 P. V. Pavlov, D. I. Tetel'baum, A. V. Pavlov and E. I. Zorin, *Sov Phys-Doki*, 1975, **19,** 399.

13 R. Kelly, "On the nature of phases formed when metals are implanted with oxygen or nitrogen", *Radiation Effects*, 1982, **64,** 205.

14 U. Admon, M. P. Dariel and E. Grunbaum, "Microstructure of electrodeposited Co/W thin films", *J Appl Phys*, 1986, **59,** (6), 2002.

15 G. Dearnaley, P. D. Goode, N. E. W. Hartley, G. W. Proctor, J. F. Turner and R. E. J. Watkins, "The ion implantation of steel and cemented carbides", IPAT '79, CEP Consultants Ltd, 243.

16 J. B. Pethica, R. Hutchings and W. C. Oliver, "Composition and hardness profiles", *Nucl Instr & Methods*, 1983, **209/210,** 995.

17 K. Komvopoulos, N. Saka and N. P. Suh, "The mechanism of friction in boundary lubrication", *J Tribology*, 1985, **107,** 452.

18 R. E. J. Watkins, Priv comm, Dept of Atmospheric Physics, Oxford Univ.

19 G. A. Saltzman, "Wet-sand rubber wheel abrasion test for thin coatings", Selection and use of wear tests for coatings, Ed R. G. Bayer, ASTM STP 769, 1982, 71.

20 J. K. Dennis and F. A. Still, "The use of electrodeposited cobalt alloy coatings to enhance the wear resistance of hot forging dies", *Cobalt*, 1975, 17.

21 N. E. W. Hartley, "Friction and wear of ion plated metals – a review", *Thin Solid Films*, 1979, **64,** 177.

22 A. H. Cottrell, "Dislocation and plastic flow in crystals", Clarendon Press, Oxford.

For Conference Discussion – see page 84

Fig 11. Scanning electronmicrograph of worn area of untreated hard chromium, showing microcrack.

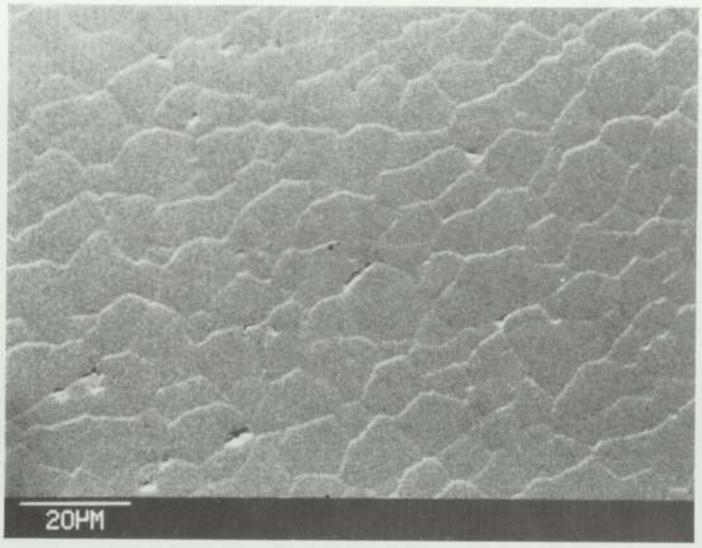

Fig 12a. Scanning electronmicrograph showing worn area of untreated Co-1.5%W Falex test piece after 90 mins wear.

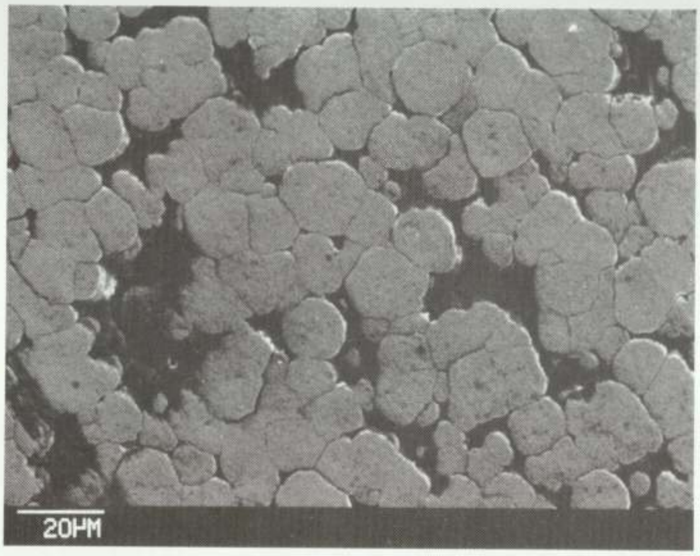

Fig 12b. Scanning electronmicrograph showing worn area of implanted Co-1.5%W Falex test piece after 90 mins wear. Note: less wearing away of nodules than in Fig 12a.

increasing contribution of the ploughing effect. In addition, implantation reduces wear significantly, especially for hard chromium coatings, which is in agreement with other investigations.[8,18]

Final weight losses of the unimplanted hard chromium coatings, although lower than those of the unimplanted Co/W were surprisingly high compared with those of the latter, softer deposits. This effect can be explained as being due to the surface grinding of the chromium and is supported by the findings of Saltzman,[19] who compared the abrasive wear resistance of as-plated and surface ground deposits. Alternatively, the chromium coating might have deteriorated more rapidly due to the severe loading conditions of the test. Co/W deposits have been reported[20] as possessing good high temperature properties and although initial wear rates are higher than those of hard chromium, final wear rates at high loads can be comparable.

In the initial stages of wear, the surface of hard chromium shows some ductile tearing perpendicular to the sliding direction. Wear particles from these zones become detached and if entrapped at the interface cause progressive damage to the surface by ploughing, which accelerates degradation of the coating and can explain the higher wear rates. Fig 10a shows an example of a particle about to be detached. A hard layer of chromium nitrides in the implanted deposit would increase the load bearing capacity of the surface and reduce ploughing by hard particles. The surface is more vulnerable to penetration when this hard layer is worn away.

There is not much evidence to support the mobile interstitial model suggested by Dearnaley *et al*[15,21] which explains the wear resistance improvements by nitrogen implantation of steels beyond the original implanted depth. Once the implanted layer on hard chromium has worn away, the wear mechanism seems to be identical with that of the untreated coating. Chromium nitrides are stable up to high temperatures[11] and therefore would not bring about enhancement of wear properties at greater depths than the implanted layer, by their decomposition through frictional heating. Chromium has a great affinity for nitrogen and even at high concentrations it is unlikely that free nitrogen would be available to diffuse during wear and so block dislocations according to the well reported Cottrell model.[22] Furthermore, this mechanism might not be fully effective in a high dislocation structure such as that of electrodeposited chromium.

Transformation from bcc chromium to Cr_2N involves about a 25% volume expansion, which creates a large compressive stress in the implanted layer, due to constraint of the underlying material. Hutchings[10] has stated that the inherent microcracks in as-plated chromium deposits are preferential sites for the nucleation of wear debris and their closure as a result of the large stresses created by implantation would produce an improvement in wear resistance. In the present work evidence could not be found for this phenomenon. Moreover, microcracks would extend beyond the implanted depth (0.1-0.2μm) and their closure would be marginal. In consequence, its effect on wear resistance would also be minimal, the major role being played by the nitride formation.

APPLICATIONS

Ion implantation of nitrogen into the surface of tools and moulds has been available commercially for over two years and has proved to be a very successful treatment for overcoming abrasive wear problems suffered in production. The process has demonstrated its capability of prolonging the life of punches, progression and press tools, dies and forms, slitting knives and both plastics processing moulds and machine parts.

Tool life extensions have been recorded for all ferrous base materials. The general premise is the better the quality of material, the better the improvement following treatment. However, many tooling applications require the maximum possible performance due to the need for continuous production. In these cases a coating, usually hard chromium, is applied to the substrate material in order to improve both its life expectancy and efficiency. Chromium plated tooling offers industry improved wear performance, better friction characteristics, higher surface hardness and an easier release of product in plastics processing.

Nitrogen implantation following plating serves to further enhance the improvement offered by chromium. The abrasive resistance of the surface is increased by the formation of chromium nitrides, to a point that is greater than the material being processed or the work hardened debris, and hence wear is reduced substantially.

Metal working tools that are often chro-

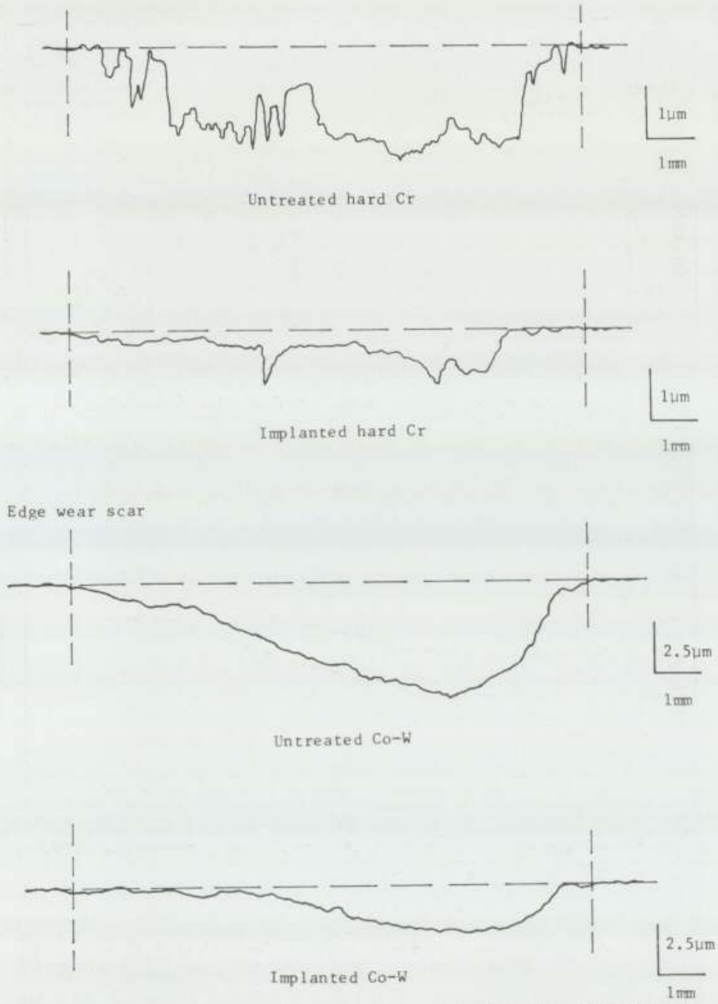

Fig 9. Profilometer traces of worn coatings after 90 minutes Falex wear testing.

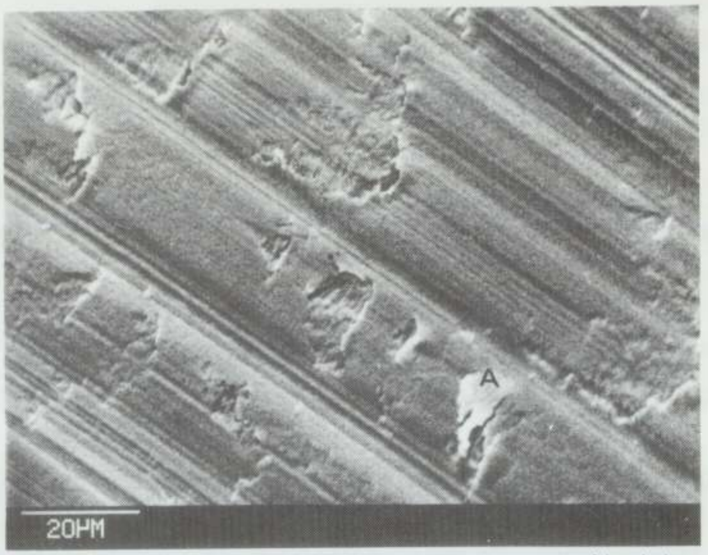

Fig 10a. Scanning electronmicrograph showing worn area of hard chromium Falex test piece after 90 min wear. A: Particle of chromium about to be detached.

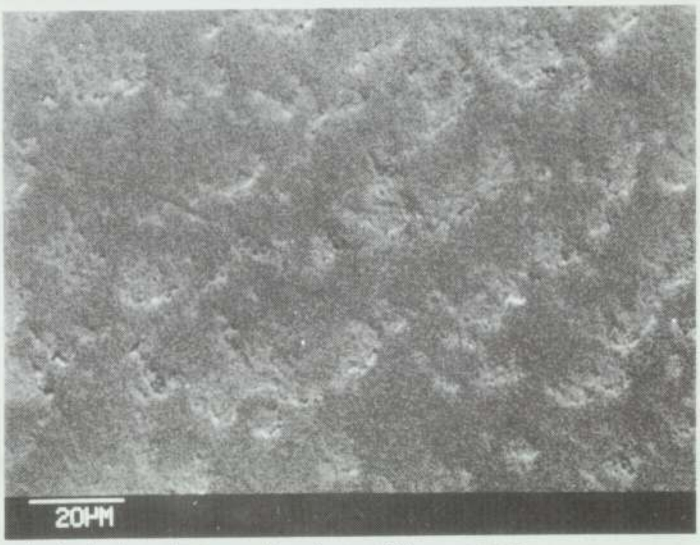

Fig 10b. Scanning electronmicrograph showing worn area of implanted hard chromium Falex test piece, after 90 min wear. ►

for hard chromium. This hardening effect can be explained in terms of residual stress, solid solution hardening and precipitation hardening. The role of residual stress on hardness was studied by Robic *et al*[9] for a number of metal-ion combinations. They concluded that although surface hardness can be increased by ion implantation, no correlation exists between hardness and induced stress.

As-deposited hard chromium coatings have very small grain size and high internal tensile stress which results in bulk hardness of about 1000H$_v$. Therefore little interstitial or solid solution hardening is likely to occur by implantation. Chromium nitrides have hardness of about 1500H$_v$; thus the increase in hardness obtained in the present work seems realistic if the formation of precipitates by the implantation of nitrogen is the major hardening mechanism.

Hutchings[10] has reported the formation of a continuous layer of fine grained Cr_2N when hard chromium was implanted at a dose of 3.5 × 10^{17} ions/cm^2. The work of Belii *et al*[11] revealed the formation, not only of the hcp Cr_2N phase, but also the fcc CrN. A transformation from the first nitride to the latter occurred with increasing ion dose. These studies demonstrated that nitrogen implantation of chromium does produce nitrides. Preliminary unpublished results, obtained by the present authors using transmission electromicroscopy of foils prepared from implanted chromium deposits, suggest that both phases are produced. The precipitation of these nitrides seems to depend on the particular nitrogen dose employed since they are subject to stoichiometric changes resulting from the continuing bombardment.

Implantation above a certain dose (Fig 4) resulted in a slight decrease in the maximum hardness achieved. Maximum nitrogen concentration is likely to be achieved at the optimum dose and sputtering would limit further introduction of nitrogen. Subsequent implantation would only produce an inferior structure by bombardment effects causing coarsening of the nitrides.

Only limited information is available on the effects of the implantation of Co/W alloys other than carbides. The work of Pavlov *et al*,[12] as reviewed by Kelly,[13] suggests that Co_4N can be formed by nitrogen implantation. Results obtained in the present work (Table 2) appear to indicate that implantation of a deposit with higher tungsten content results in a considerable hardening effect, probably by the formation of W_2N.

The microstructure of electrodeposited Co/W films depends on the plating conditions and can be either amorphous or crystalline with a hcp, fcc or mixed lattice.[14] The structure and alloying content of the deposit will influence the properties achieved by nitrogen implantation; a further detailed study is still needed to take full advantage of the process.

Nitrogen implantation produced a light tan colour on the surface of hard chromium. This is thought to result from slight low temperature oxidation induced by the beam,[15] although some carbon contamination from the vacuum system may also contribute to the staining effect. This slight surface contamination during implantation may cause the reduction in the coefficient of friction during the early stages of wear. After longer wear periods, friction coefficients for both implanted and untreated surfaces approached the same values. Pethica *et al*,[16] using XPS, reported the formation of an outer layer of Cr_2O_3 after implantation of hard chromium. Hutchings[10] has confirmed this finding by T.E.M.

In the case of boundary lubricated surfaces, ploughing by wear particles or hard asperities is always the most important mechanism influencing friction,[17] but adhesion between asperities and shearing of the lubricant film make minor contributions. Ploughing did not occur during the first minutes of wear. Moreover adhesion between asperities would be reduced due to the presence of a thin oxide film. This could explain the improvement in frictional behaviour, at least during initial stages of wear. Longer periods result in an increase of the friction coefficient, approaching the value of the unimplanted surface due to removal of the thin oxide layer and to an

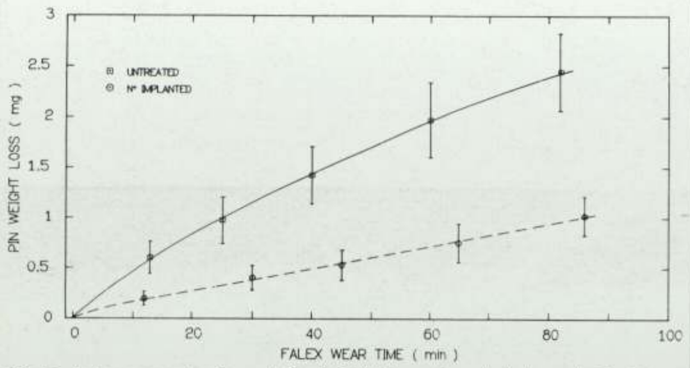

Fig 5. Falex wear testing of Co-1.5%W coating. Lubricated. En 31 steel V-blocks. 710N load.

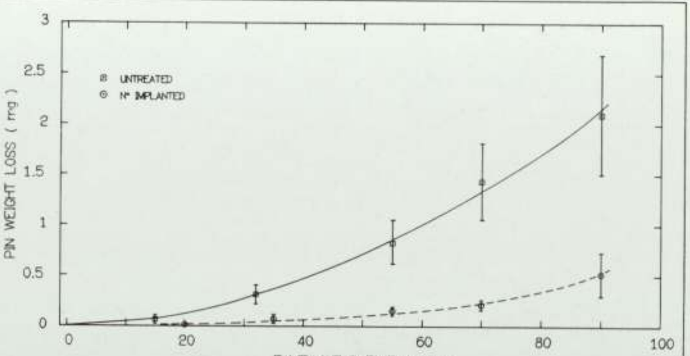

Fig 6. Falex wear testing of hard chromium coating. Lubricated. EN 31 steel V-blocks. 710N load.

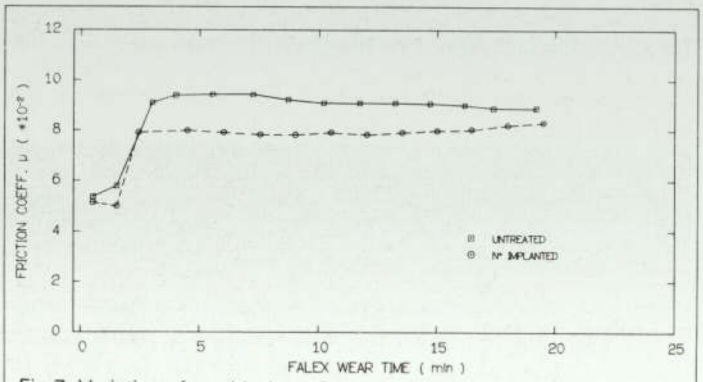

Fig 7. Variation of μ with time. Co-1.5%W coating. Lubricated Falex wear testing. 710N load.

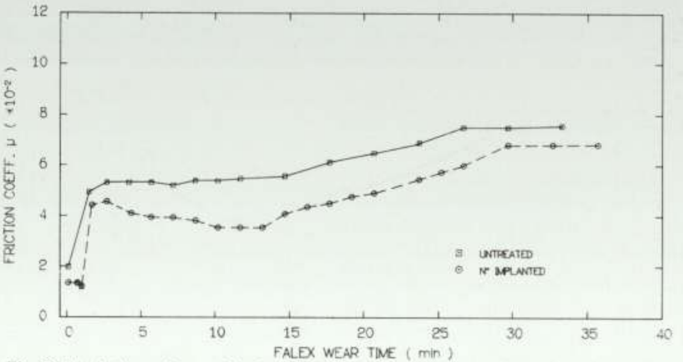

Fig 8. Variation of μ with time. Hard chromium coating. Lubricated Falex wear testing. 710N load.

doses greater than the optimum are employed a slight softening of the deposits occurs due to bombardment induced effects which compete with the hardening effect of the implanted nitrogen (Fig 4).

Tribological Tests

The changes in weight loss with wear time, for the Co/1.5%W alloy and hard chromium, are shown in Figs 5 and 6. Wear data for Co/W and chromium coatings, tested under a load of 710N for 90 minutes are summarized in Tables 3 and 4. Implantation reduced the wear rate of Co/1.5%W coatings by a factor of 2.5 and that of hard chromium by a factor of 4. This improvement in wear rate behaviour was associated with a slight decrease in the coefficient of friction during the first minutes of wear, as illustrated in Figs 7 and 8. After longer test periods, coefficients of friction for both untreated and nitrogen implanted surfaces generally approached the same value, although an improvement in wear resistance still occurred.

Initial wear rates for the hard chromium deposits, either untreated or implanted, were low. Longer test periods showed a logarithmic relation for wear rate, which seems to indicate a degradation of the surface at high loads. Nitrogen implantation reduced this effect, increasing the load bearing capacity of the surface and reducing the amount of abrasive wear.

Examination of worn surfaces

Profilometry traces (Fig 9) showed a significant difference between untreated and implanted coatings. The unimplanted hard chromium deposit exhibited heavy ploughing by wear particles or hard asperites across the wear track after a 90 minute wear period. This was less evident for the surface implanted with the optimum dose. Nitrogen implantation reduced ploughing considerably. As anticipated, the softer Co/W deposits were more ductile and wear occurred more uniformly, and at first more rapidly, than in the case of the chromium coatings. However after 90 minutes the wear rate of Co/W was not much greater than that for hard chromium due to the different wear mechanisms involved.

Examination of wear scars by S.E.M., Figs 10a and 10b, illustrate the differences in wear patterns between untreated and nitrogen implanted hard chromium deposits. Deep grooves and some plastic deformation leading to formation of wear debris are evident on the untreated coating. In contrast, the treated chromium showed much less wear or ploughing effects. Little evidence of cracking was observed in this deposit, probably because fine cracks would be masked by the grinding marks. When cracks were observed, preferential wear did not appear to have occurred at these regions. (Fig 11).

There was little evidence of any serious abrasion by hard asperities or entrapped wear particles on worn surfaces of Co/W coatings. Fig 12a and b show that the surface nodules illustrated in Fig 1 have been worn away during the Falex test. This 'polishing' mechanism was more apparent for the softer untreated deposit, (Fig 12a).

DISCUSSION

Nitrogen implantation produced a significant hardening effect, ie an increase of up to 40% in the case of both types of coatings, when a low load was used to limit penetration of the indenter. These results agree with those obtained by Oliver *et al*[8]

Table 3. Falex wear test results for Co/1.5%W. Operating conditions: 710N, lubricated, 90 minutes wear time.

Pin code	*Untreated*		*Nitrogen Implanted*	
	Weight Loss mg	*Wear Rate $\times 10^{-3}$mg/min*	*Weight Loss mg*	*Wear Rate $\times 10^{-3}$mg/min*
1	3.242	36.025	0.873	9.702
2	2.217	24.639	1.183	13.145
3	2.189	24.327	0.782	8.693
4	3.102	34.465	1.245	13.836
5	2.688	29.865	1.265	14.052
Mean	2.688	29.864	1.070	11.886
Standard Deviation	0.487	5.410	0.225	2.502

Table 4. Falex wear test results for hard chromium. Operating conditions: 710N, lubricated, 90 minutes wear time.

Pin code	*Untreated*		*Nitrogen Implanted*	
	Weight Loss mg	*Wear Rate $\times 10^{-3}$mg/min*	*Weight Loss mg*	*Wear Rate $\times 10^{-3}$mg/min*
1	3.149	34.985	0.361	4.014
2	2.052	22.801	0.779	8.655
3	2.339	25.992	0.458	5.088
4	1.451	16.111	0.771	8.564
5	1.500	16.670	0.243	2.703
Mean	2.098	23.312	0.522	5.805
Standard Deviation	0.697	7.741	0.2429	2.696

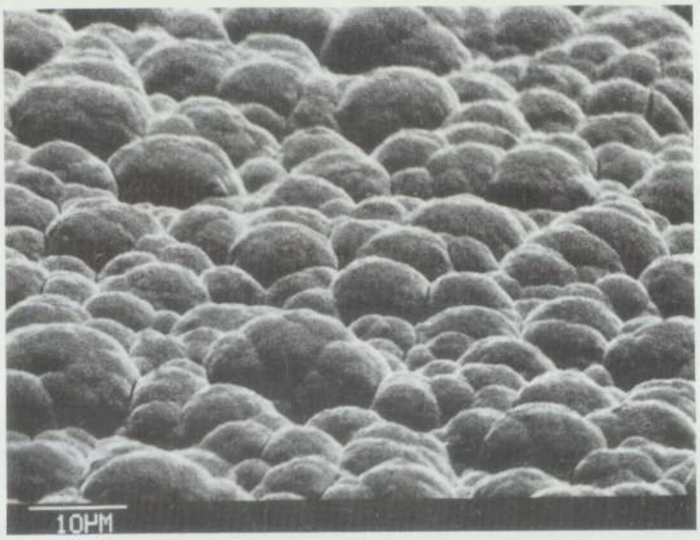

Fig 1. Scanning electronmicrograph showing nodular as plated surface of Co-1.5%W electrodeposit.

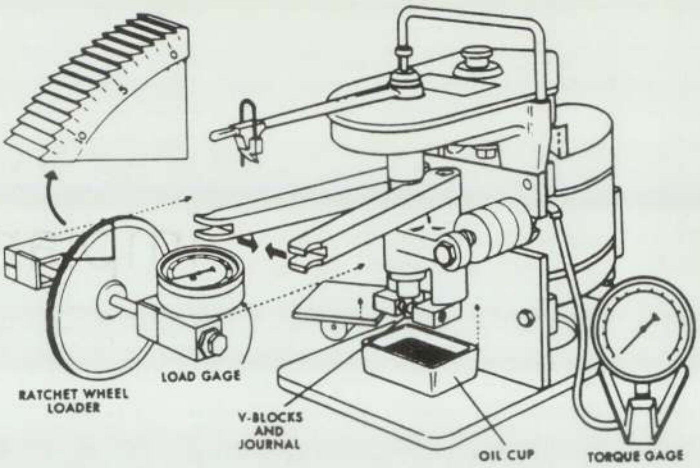

Fig 2. Schematic diagram of Falex wear testing machine.

Implantation was carried out in a commercial unit using a mixed ion beam with approximately 60% singly charged atoms and 40% singly charged nitrogen molecules, with an energy of 90KeV and doses above 10^{17} ions/cm^2. The specimens were mounted on a water cooled device, to avoid excessive heating, and were rotated during implantation to ensure uniform treatment over the significant surface. The beam current density at the target was chosen so as to keep the temperature of the pins below 100°C.

Prior to wear testing, the surface hardness of the coatings was determined with a conventional Vickers microhardness tester. A 5g load was used to limit the depth of penetration of the indentor and so establish a reasonable estimate of the hardness of the implanted layer, typically 0.1 to 0.2μm in depth. Some hardness results have been obtained and reported elsewhere using a special technique which avoids penetration below the implanted layer.[7]

Tribological tests were carried out using a Falex machine, shown schematically in Fig 2. In this test the cylindrical specimen is rotated against two loaded V-blocks, at 290rpm (see Fig 3). The V-blocks were made of EN 31 steel, heat treated to 64-65H_{Rc} (790-850H_v). The load is actuated by means of a ratchet wheel mechanism which squeezes the pin into the vertical grooves of the V-blocks. Wear takes place as the pin rotates under the applied load, causing a decrease in the pin diameter and the formation of vertical wear scars in the blocks.

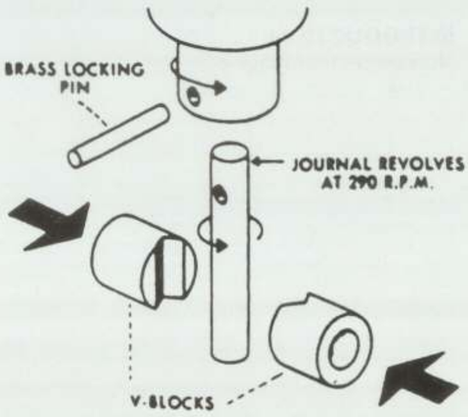

Fig 3. Expanded view of V-blocks and pin arrangement.

As there was no standard Falex wear testing procedure recommended for coatings, the following was used throughout the present work for a total wear period of 90 minutes. The pin and V-blocks were cleaned ultrasonically and placed in position with the oil cup containing 70ml of additive free paraffinic lubricant, (Figs 2 and 3). The motor was activated and the load increased initially to 440N. This value was maintained for a 1 minute run-in period, and then increased slowly to 710N. The test was stopped after periods of either 15 or 30 minutes so that the wear rate of the pins could be monitored by weight loss. This procedure was repeated several times, using fresh oil after each wear period, until the 90 minute total wear period had been completed.

The coefficient of friction was calculated from the torque reading using a formula derived from the geometry of the test pieces:

$$\mu = \frac{2.83 \times \text{Torque (lb in)}}{\text{Load (lb)}}$$

The worn surfaces of the untreated and implanted materials were monitored by scanning electron microscopy (S.E.M.), to investigate whether any change in wear behaviour occurred as a result of nitrogen implantation. These observations were complemented by the use of a Talylin Profilometer, which provided topographical information about the worn surfaces.

RESULTS

Surface Hardness

Micro-hardness results for the coatings in the as-plated and nitrogen implanted condition are presented in Table 2. It can be seen that the increase in hardness for the Co/W deposit depends significantly on the tungsten content. A hardness increase of about 40% was achieved for both the Co/8%W alloy and the hard chromium coating when the optimum implantation dose was used. Since indentation depths are greater than the thickness of the implanted layers, it is only meaningful to consider the relative percentage gains in micro-hardness with respect to the unimplanted coatings. If

Table 2. Effect of optimum nitrogen implantation dose on surface surface hardness (5g load)

Coating	*Micro-hardness, Hv*		*Hardness increase, %*
	Untreated	*Implanted*	
Hard chromium	1160	1660	43
Co/1.5%W	523	560	7
Co/8%W	521	740	42

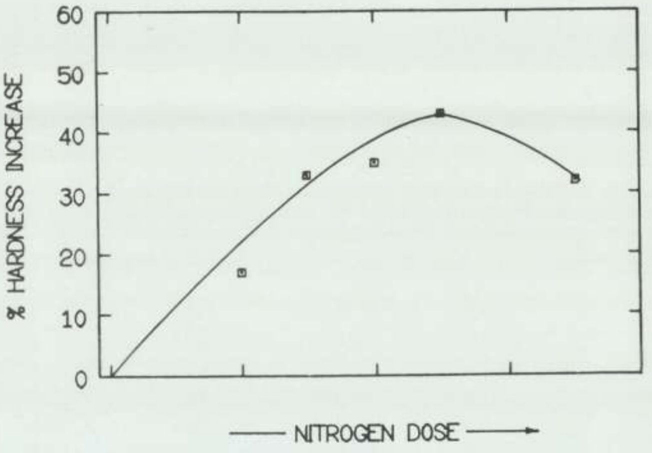

Fig 4. Effect of implantation on hardness of hard Cr coating. Vickers, 5g load.

The effect of nitrogen ion implantation on the properties of coatings

*J. I. Oñate, * J. K. Dennis**
*and S. Hamilton***

*Aston University, Department of Mechanical and Production Engineering
**Tech-Ni-Plant Ltd

Summary – Ion implantation modifies the surface composition and properties of materials by bombardment with high energy ions. The low temperature of the technique ensures the avoidance of distortion or surface degradation of components.

Wear resistance, evaluated by a lubricated Falex test, can be improved by up to four times and the surface hardness of hard chromium and cobalt/tungsten alloys can be increased by up to 40%, when an optimum dose of nitrogen is implanted. These effects are explained in terms of the formation of nitrides, which improve the load bearing capacity of the surface and its abrasion resistance.

Mr Oñate received his first degree in Industrial Engineering at Bilbao University (Spain) in 1981. After an industrial training period at SKF-Spain, he came to Aston University sponsored by the Basque Government to study for an MSc in Metals, Materials and Management, which was awarded in 1984. At present he is carrying out research leading to a PhD degree in the Mechanical and Production Engineering Department at Aston University on the effects of nitrogen implantation on a range of engineering materials.

Dr J. K. Dennis is a senior lecturer in the Department of Mechanical and Production Engineering at Aston University. He has published many papers on metal finishing topics. He is a member of the IMF Council, Publications Committee and Industrial and Technical Committee.

Miss S. Hamilton is the Managing Director of Tech-Ni-Plant Ltd.

J. I. Oñate, J. K. Dennis and S. Hamilton
Trans IMF 1987, **65,** 99

INTRODUCTION

Numerous techniques are now available to provide functional coatings and surface treatments for engineering applications; these have been reviewed in two recent publications.[1,2] However, requirements are becoming more demanding, for example, in terms of the severity of the operating conditions and dimensional accuracy of the surface treated component. Consequently, it is essential that surfaces can withstand the conditions encountered in operations such as the cold forming of metals or the injection moulding of glass filled plastics. In some processes operating conditions are encountered where lubrication becomes marginal and metal-to-metal contact occurs. To meet these demanding requirements, together with restrictions imposed by limitations such as the maximum temperature to which the substrate can be subjected without significant change in its properties, it may be necessary to consider a duplex process. The present paper deals with an example of this technique where first an electrodeposit is layed down but is then subsequently subjected to a surface treatment known as ion implantation.

Ion implantation is a process that upgrades the surface properties and improves the service life of metals or coatings by bombardment with high energy ions. Application of this treatment to enhance the tribological properties of materials is well documented.[3-5] Advantages and limitations of implantation compared with alternative surface treatments are summarized in Table 1.

In this paper the effects of nitrogen implantation on the mechanical properties of hard chromium and cobalt/tungsten alloys have been investigated. Optimum nitrogen doses were implanted so that wear and frictional characteristics could be studied using a cylinder-in-groove geometry test (Falex) under lubricated conditions.

Table 1. Advantages and limitations of nitrogen implantation as a surface treatment.

ADVANTAGES

1. Low temperature process.
2. Negligible dimensional changes.
3. No degradation of surface finish.
4. No sacrifice of bulk properties.
5. No adhesion problems since there is no sharp interface.
6. Solid solubility limit of implanted species can be exceeded.
7. A fine dispersion of precipitates is created providing optimum wear behaviour.
8. Clean vacuum process.
9. Minimum masking costs, ability to treat selective areas.
10. Highly reproducible and controllable process.

LIMITATIONS

1. Line-of-sight process, hence manipulation under vacuum is necessary.
2. Shallow penetration.
3. Relatively expensive equipment.

EXPERIMENTAL PROCEDURE

Cylindrical specimens (6.35mm diameter, 32mm length) were prepared from BH 13 steel bar. These pins were hardened and tempered to a hardness of 52 H_{Rc} (545 H_v) and subsequently coated with either hard chromium or a cobalt/tungsten alloy electrodeposit.

The hard chromium coatings were deposited from a commercially available solution at 55°C and a current density of $50A/dm^2$. The specimens were centreless ground to obtain a uniform deposit 25µm thick.

The cobalt/tungsten alloy coatings were deposited by the brush plating technique from an acid bath of the type described in a previous publication.[6] The deposition conditions were pH 1.5 and voltage 15-17V. Pretreatment was also carried out by a 'brush' procedure. An approximate thickness of 25µm was deposited but since this resulted in a somewhat nodular surface finish (Fig 1), polishing was necessary prior to any further treatment or wear testing. Both the chromium and cobalt alloy coatings had a surface roughness of 0.4µm (C.L.A.) prior to implantation.

phere initially followed the general behaviour of the other tin coatings without a barrier layer. However, on continued storage, a rapid increase in the zinc content of the surface occurred suggesting that a secondary mode of zinc diffusion operates causing this feature. The rupturing of the tin surface by crystallites of Cu_6Sn_5 which then provide a pathway for zinc diffusion is a possibility but no evidence was found for this on the sample having a thinner (5µm) coating of tin on brass.

From the data collected from samples subjected to various storage conditions, it has been clearly demonstrated that zinc will diffuse through a tin coating in the absence of a barrier layer. The diffusion rate of zinc was influenced by the temperature and humidity of the storage environment. The main diffusion path through the tin coating appeared to be along the grain boundaries which are high diffusivity paths due to the atomic mismatch. Grain boundary diffusion/enrichment by low concentration of solute atoms and their effect on wide range of metallurgical properties other than solderability, has been reported in great detail for numerous systems.[20]

Zinc which has a low solubility[21] in tin (0.24at% at room temperature) is not evenly distributed in the coating but concentrated at the grain boundaries at the surface of the coating as indicated by SEM and surface analysis results. The ability of zinc to diffuse to the surface of tin has also been noted by other authors investigating the selective oxidation of dilute Sn-Zn.[22] Work by Farrell[23] using surface analysis to study the effect of heating various copper/zinc alloys in air indicated the enrichment of the alloy surface by zinc and it was noted to be especially prevalent in 70/30 brass. A similar enrichment of the brass surface may also occur on heating, even when coated with tin. The mobility of zinc towards the brass surface is coupled in the case of a tin coating with the removal of copper to form intermetallic thus further enriching the interface in zinc. This phenomenon of surface enrichment is not specific to zinc, a similar effect has been reported to occur for tin coatings containing small amounts of lead.[24]

SUMMARY

1. The major pathway for zinc diffusion in electrodeposited tin coating is along the grain boundaries of the tin and upon diffusing through the coating zinc concentrates at the surface of the coating.
2. The diffusion rate of zinc through a tin coating is increased by raising the temperature and humidity of the storage environment.
3. A 2.5µm thick barrier layer of copper, nickel or iron is adequate to prevent zinc diffusion. The lifetime of the barrier is dependent on the temperature of its environment, the thickness of the barrier and the material used. Both iron and nickel have been shown to have more extended lifetimes than copper at 70°C.
4. The presence of zinc in a tin coating reduces its solderability on storage, whilst the use of a barrier layer has been shown to prevent the deleterious effects on solderability of zinc diffusion.

REFERENCES

1 D. A. Unsworth and C. A. MacKay, *Trans IMF* 1973, **51,** 85.
2 P. J. Kay and C. A. MacKay, *Trans IMF* 1976, **54,** 86.
3 E. W. Brothers, *Western Electric Engineer* 1981, Spring/Summer, 49.
4 C. A. MacKay, *Inst. for Interconnecting & Packaging Electronic Ccts Assembly – Joining Handbook 1984,* April, 1-14.
5 M. E. Warwick and S. J. Muckett, *Circuit World* 1983, **9,** 4.
6 P. E. Davis, S. J. Muckett and M. E. Warwick, *Plating & Surf Fin* 1982, **69,** (9), 72.
7 P. E. Davis, S. J. Muckett and M. E. Warwick, *Plating & Surf Fin* 1983, **70,** (8), 49.
8 S. C. Britton and M. Clarke, *Trans IMF* 1963, **40,** 205.
9 H. F. Hourigan, J. W. Robinson and W. T. Edwards, *J Post Office Elec Eng* 1953, **46,** (3), 1
10 C. J. Thawaites, *Trans IMF,* 1959, **36,** 6.
11 British Standards BS1872, 1984 and BS6137, 1982, International Standard ISO 2093, 1980.
12 P. J. Kay and C.A. MacKay, *Trans IMF* 1979, **57,** 169.
13 B. C. Scott and M. E. Warwick, *Trans IMF* 1983, **61,** 43.
14 The Electrodeposition of Tin, *Pub. No 92,* ITRI, London, 1980.
15 C. J. Thwaites and P.M. Dinsdale, *The Flow Melting of Electrodeposited Tin & Tin Lead Coatings,* Pub No 560, ITRI, London, 1979.
16 *Modern Electroplating,* ed F. A. Lowenheim, John Wiley & Sons, 1974.
17 *Metallogrpahy of Tin and Tin Alloys,* Pub. No 580, ITRI London, 1982.
18 G. Schouten, *Philips Telecommunications Review* 1980, **38,** (8), 3.
19 A. C. Harman, *Proc Internepcon,* Brighton 1978, 42.
20 *Practical Surface Analysis,* ed. D. Briggs and M.P. Seah. John Wiley & Sons, 1983.
21 F. Vauk, M. H. Anisley and R. W. Smith, *J Mat Sci* 1981, **16,** 1171.
22 A. P. Pchelnikov and A. D. Sitnikov, Trans from *Zashita Metallor,* 1980, **15,** 5.
23 T. Farrell, *Met Sci* 1976, **10,** (3), 87.
24 D. W. Bird, T. H. English and W. H. Hill, *Brit Corr J* 1986, **21,** 1.

ACKNOWLEDGEMENTS

The author acknowledges the practical assistance given by Miss A. Chapman, Mr. K. Chaggar, Mr. P. Dodia and Mr. A. Leary and the permission of the International Tin Research Council to publish this work.

The effect of ion (nitrogen) implantation on the properties of martensitic steels.

J.I. Onate, J.K. Dennis and S.A. Hamilton

Paper presented at the 2nd International Conference of Surface Engineering. Stratford-upon-Avon. Great Britain. June 1987. The Welding Institute, 1987, pp.18/1-18/18

The University of Aston in Birmingham
Nitrogen implantation of tool steels and engineering coatings
J.I. Oñate
Doctor of Philosophy
1987

SUMMARY

Ion implantation is a recently developed process for the modification of the surface characteristics of materials by bombardment with high energy ions to improve properties such as wear resistance, hardness, fatigue and friction. The low temperature of this technique ensures the avoidance of distortion and is ideal for the treatment of components and tools finished to a high precision.

Results obtained in the present work illustrate that wear resistance and surface hardness of AISI steels M2, D2 and 420 can be improved by nitrogen implantation at doses in excess of 10^{17} ions/cm^2. Lubricated Falex wear tests carried out using high loads showed an enhancement in wear resistance of up to 43% and a significant decrease in the coefficient of friction. An ultra-microhardness technique shows that the true hardness of implanted surface layers is very much greater than the values reported by conventional microhardness methods which result in penetration below the implanted depth. Applications of the above steels after nitrogen implantation are discussed.

INTRODUCTION

Surface engineering has become an important research and development field aimed at improving the properties of materials so that they are capable of meeting the demanding requirements of numerous technological developments. Surface properties which are usually of most interest to the engineer are wear resistance, corrosion and oxidation behaviour, resistance to chemical attack, frictional characteristics and high temperature performance. Many techniques are now available for providing surface treatments or coatings to achieve these improvements in properties(1). However, one process rarely provides improvements in all the properties listed but ion implantation can meet most, except the high temperature requirement, if the appropriate species are implanted. Some of the advantages and limitations of ion implantation are listed in Table 1. It is a process that upgrades the surface properties of materials by bombarding them with high energy ions. Atoms of the desired elements are ionized and accelerated in an electric field at energies usually in the range of 50 to 200 KeV, under a vacuum of about 10^{-6} Torr. The ions reach the surface of the work-piece with high velocity and penetrate it, coming to rest at a controlled depth following a near Gaussian distribution once they have lost their energy.

Research involving the use of ion implantation as a means of beneficially modifying the chemico-mechanical properties of metals commenced in the 1970's at Harwell(2,3). The early results were so promising that researchers in many establishments around the world were encouraged to investigate the technique and it is now accepted that implantation can improve engineering properties(4,5). Nitrogen implantation of ferrous based materials, tungsten carbides, aluminium, titanium and several hard coatings has proved particularly successful. However, the physico-chemical changes produced and their tribological implications are not always completely understood. The wide spectrum of substrate materials, wear testers and implantation parameters used make it difficult to compare results obtained by different investigators. The effects of implantation are related to the composition and structure of the bulk material and so a study of optimum treatment conditions is necessary for each particular alloy.

The aim of the present work is to investigate the effect of nitrogen implantation at optimum doses on AISI M2, D2 and 420 steels. Their behaviour during wear tests under high loads, a condition commonly encountered in industrial situations such as cutting, forming and plastics moulding will be studied. Nitrogen implantation has already proved successful in these applications.

EXPERIMENTAL PROCEDURE

Cylindrical specimens (6.35 mm diameter, 32 mm in length), for wear testing by the method described below, were prepared from bars of the three steels whose compositions are listed in Table 2. These pins were hardened, tempered and subsequently surface ground to the hardnesses and surface finish indicated in the same Table.

Implantation was carried out in a commercial unit using a mixed ion beam with approximately 60% singly charged atoms and 40% singly charged nitrogen molecules, with an energy of 90 KeV and doses above 10^{17} ions/cm^2. The pins were mounted on a water cooled production tray in order to provide a good thermal sink and were rotated during implantation to ensure uniform treatment over the cylindrical surface. The beam current density at the target was chosen so as to keep the temperature of the pins below 100°C.

Following nitrogen implantation, the surface hardness of the steels was determined using a Vickers microhardness tester. A 5g load was chosen in order to limit the depth of penetration of the indentor, which extends usually beyond the implantation depth (typically 0.1 - 0.2 µm). These measurements yield a hardness value which is a combination of that of the implanted layer plus that of the underlying bulk material. To determine the true hardening effect of nitrogen implantation one of the materials, AISI 420, was tested using an ultra-microhardness technique devised by Pollock and his co-workers(6). This hardness tester, or continuous depth recording technique, uses very small loads of less than 1g, therefore limiting penetration of the indentor to submicrometer dimensions within the implanted surface layer.

Tribological tests were carried out using a Falex machine in the manner reported previously(7). A cylindrical specimen is rotated against two loaded V-blocks, at 290 r.p.m. In this work the V-blocks and pins were made of identical steels. The load is applied by means of a ratchet wheel mechanism which squeezes the pin into the vertical grooves of the V-blocks. Wear takes place as the pin rotates under the applied load, causing a decrease in the pin diameter and the formation of two vertical wear scars in each block. The torque produced when the load is applied is recorded and related to the coefficient of friction by a formula that can be derived from the geometry of the test piece and V-blocks.

$$\mu = \frac{2.83 \times \text{Torque (lb.in)}}{\text{Load (lb)}}$$

All testing was carried out under lubrication, the lubricant being an additive free paraffinic mineral oil. The application of this test for implanted steels has been described previously by several workers(8,9). However, there is no standard Falex wear test procedure recommended for surface treated materials and so the following was employed throughout the present work for a total wear period of 140 minutes. The pins and V-blocks were cleaned ultrasonically and placed in position ready for testing in the oil cup which contained 70 ml of lubricant. The motor was then started and the load increased initially to 440 N by means of the rachet wheel. This value was maintained for a 1 minute preliminary 'run-in' period, and then increased slowly to 900 N. The test was stopped after periods of either 20 or 40 minutes so that the wear rate of the pins could be monitored by weight loss to an accuracy of $\pm$ 10^{-5}g. This procedure was repeated several times, using fresh oil after each wear period, until the 140 minutes total wear period had been completed. Problems of stopping and restarting tests for each pin were minimised since an intimate contact between V-blocks and test pins was generally obtained.

Wear scars were examined by both scanning electronmicroscopy and Talylin profilometry in order to monitor topographical features of worn areas and to investigate whether any change in wear behaviour occurred as a result of nitrogen implantation.

RESULTS

Surface Hardness

The effect of optimum nitrogen implantation dose on surface hardness is shown in Table 3 and the change in hardness with nitrogen dose is illustrated in Fig 1. The low load of 5g limited the penetration of the Vickers pyramid indentor thus minimising the influence of the bulk material below the implanted layer. At such a low load absolute hardness values should be treated with caution but nevertheless they do provide a useful comparison between implanted and unimplanted surfaces. The increase in hardness, as measured by this conventional technique, is limited. A more sophisticated technique was necessary to obtain the true extent of hardening by implantation. This utilised very small loads of less than 1g and thus penetration was restricted to within the implanted layer.

Fig 2 illustrates the indentation depth (d) plotted against the square root of the load (P), for AISI 420 steel. The resulting plot should be linear in the simplest case of constant hardness and ideal plasticity. The same data is re-plotted in Fig 3 in the form of 'normalised' hardness (relative to a silicon standard of known doping) as a function of depth. This graph shows that even at 0.3 um depth the implanted AISI 420 steel is more than twice as hard as the untreated material. Some nitrogen in-diffusion during implantation may have occurred to account for this hardening effect at a depth beyond the theoretical range (0.1 - 0.2 μm)

Tribological Tests

Wear data for the steels, tested under a load of 900 N for a maximum of 140 minutes are summarized in Table 4. Implantation reduced the wear rate of all three steels, the maximum improvement of 43% being achieved for the softest alloy , the martensitic stainless steel AISI 420.

Figures 4 to 6 show the changes in weight loss for the pins as a function of the wear time. The gradients of the lines, or effectively the wear rates, illustrate the beneficial effect of nitrogen implantation even under the severe loading condition employed. Wear reduction was associated with a significant decrease in the coefficient of friction for AISI 420 and AISI D2 steels, especially during the first minutes of wear. Nitrogen implantation did not produce a significant change in friction characteristics for AISI M2 high speed steel. However, a significant effect is observed for AISI D2 and 420 steels, as shown in Fig 7. Both steels have a high chromium content and this effect is thought to be due to the formation of a thin chromium oxide layer during implantation.

Examination of worn surfaces

Profilometry traces of wear scars taken after identical periods of wear are shown in Fig 8 and they illustrate a decrease in wear volume for all the implanted surfaces. In addition, the untreated surfaces appeared to have suffered more ploughing, due to penetration by hard asperities or entrapped wear particles, than the treated ones. This observation was corroborated by examination of the worn surfaces using scanning electronmicroscopy. Figures 9 & 10 show that wear on untreated surfaces occurs by a ploughing or abrasion mechanism. Nitrogen implantation improves the abrasion resistance by increasing the load bearing capacity of the surface thus resulting in a reduction in the ploughing effect observed on the untreated surfaces. Additionally, some means of mild oxidative wear appears to operate in the case of the implanted surfaces, probably initiated by the presence of a thin oxide layer on the surface but which continues throughout the wear period. The fine wear debris generated during wear of AISI M2 steel is shown in Fig 11 together with X-ray analysis of a wear particle.

Fig 12a shows the surface of one of the untreated AISI 420 pins that suffered severe scuffing. Under a high load an entrapped wear particle, combined with inefficient lubrication, causes progressive damage of the surface. This did not occur in the case of the treated surfaces, Fig 12b. Implantation improved not only the load bearing capability of the surface but also the lubricity due to the presence of the thin oxide film.

DISCUSSION

At the doses studied nitrogen implantation resulted in moderate increases in surface hardness (determined by a conventional microhardness technique), for all three steels. Similar or slightly higher hardness increases have been obtained by Iwaki et al(10) and other workers(11). However, conventional microhardness techniques, (Vickers or Knoop), cause indentation to a depth in excess of 1 μm and so the true hardness of the thin implanted layer is not evaluated. The use of an ultra-microhardness technique(6) is more appropriate for the evaluation of this type of surface treatment because it is necessary to determine hardness of very thin layers, eg 0.1 μm thick. An increase in hardness of more than 200% was obtained for nitrogen implanted AISI 420 at 0.1 - 0.2 μm below the surface, (Fig 3), when an ultra-microhardness method was employed.

The increase in hardness by implantation is attributed to ion bombardment effects, compressive stress, formation of solid solution of interstitial elements (eg. nitrogen or carbon) and the creation of a dispersion of hard precipitates. These effects are often inter-related and it is usually difficult to isolate the exact contribution of one particular phenomenon with respect to the hardening mechanism. The role of residual stress has been considered marginal by Robic(12) for a variety of metal/ion combinations.

It has been reported(13) that nitrogen implantation does not provide any significant additional hardening of martensitic structures. This is based mainly on observations on AISI 52100 since by heat treatment most of the available hardening mechanisms have been exploited in this high carbon steel (1%C, 1.5% Cr). The steels investigated in the present work have a high content of nitride forming elements and it is therefore likely that nitride precipitation accounts for the observed hardness improvements.

There have been few attempts to study chemical changes due to implantation of tool steels because their initial structure is complex but the presence of nitrides has been demonstrated in implanted iron and several steels(11,14 - 16). Unpublished work by the present authors, using transmission electronmicroscopy, appears to show the formation of cubic CrN in implanted AISI 420 steel. The work of Dimigen et al (11) also indicates that combination of chromium and nitrogen occurred in a similar steel. Chromium nitrides have also been found after implantation of austenitic stainless steels(17,18).

Nitrogen implantation increased the wear resistance of the three steels, M2, D2 and 420. It is generally agreed that the resistance to deformation of a material is related to its hardness and that the presence of nitrides improves the wear behaviour of surfaces. Nitrogen implantation at low temperature produces a higher density of micro-precititates than that produced by diffusion type treatments(19), and this effect produces optimum results during friction and wear processes.

Implantation improved the load bearing capacity of the surfaces, reducing the ploughing or cutting effect of hard asperities or wear particles that become entrapped between contacting surfaces, Figs 9 & 10, thus decreasing the amount of material removed. There was some evidence that the wear debris resulting from implanted surfaces was finer than that from untreated material, see Fig 11, the latter containing a considerable number of particles that could be identified as carbides. This suggests that the unimplanted martensitic matrix is more easily worn away, primarily by abrasion and plastic deformation, so that carbide particles can be plucked out; ie. the wear mechanism is similar to that for cobalt bonded tungsten carbide. Ion implantation also induces extremely high surface compressive stresses(20) due to a high concentration of interstitials and the creation of hard precipitates which attempt to expand the lattice. These high compressive stresses can close existing micro-cracks or impede their propagation during wear, therefore delaying or preventing the detachment of plate-like particles by tensile stresses induced during sliding contact.

It was observed that some of the untreated AISI 420 specimens when tested under high load in the Falex test suffered both severe adhesive and abrasive wear, combined with a high torque. Wear and friction in boundary lubricated situations occurs mainly by ploughing(21), hence wear particles produced by this mechanism can become entrapped which accelerates degradation. This phenomenon was not observed on the implanted surfaces.

Nitrogen implantation promotes the growth of a thin adherent oxide layer on the surface. This oxide can reduce adhesion between contacting surfaces and deformation of the substrate, which can also lower the coefficient of friction. A significant decrease in the latter was demonstrated for AISI D2 and 420 steels. Both of these contain a high percentage of chromium as an alloying element and chromium oxides or oxynitrides are likely to be formed during implantation thus reducing friction, at least during the ´run in´ period. Moreover, a reduction of the ploughing component of wear would also contribute to the reduction in friction(21,22). This improvement in frictional behaviour has also been reported elsewhere(18,23,24), mainly for high chromium alloyed steels.

One of the most interesting features of nitrogen implanted steels is that improved wear resistance persists at depths below the original implantation depth. Some authors(25,26) explain this phenomenon by the mobile interstitial model which assumes that nitrogen migrates below the wearing surface, driven by the thermal gradient generated at the contacting asperities, and its interaction with defects such as dislocations, impeding their motion. This model is supported by the observations of Lo Russo et al(27), who found 30% of the implanted nitrogen remaining at depths ten times greater than the initial implantation depth. Other authors(11,28) have reported similar results. However, Fischer(29) and Pope(30) have failed to detect any nitrogen below the worn surface. These conflicting results can possibly be explained by a radiation induced diffusion model which could drive the nitrogen beyond the predicted range during implantation or by the use of a wide analysing beam which might have detected nitrogen from unworn adjacent areas(31). Furthermore, the mobile interstitial model is not valid for non-ferrous materials such as aluminium and titanium(13,26).

It has been reported recently(32), that the mechanical effects of implantation are maintained even after any remaining nitrogen is depleted. This suggests that nitrogen could be the initiator of beneficial wear conditions but not the sustainer. Changes in the wear process from adhesive to a mild oxidative wear have been reported after nitrogen implantation(10). These effects have been explained(33) in terms of a modification of the strain hardening processes in the surface and that once ´run in´ has been completed, this effect may become self-propagating.

APPLICATIONS

Many different types of tooling have now been shown commercially to benefit from nitrogen implantation, productive lives having been improved over a range of between two and seven times. A wide area of application relates to steel press tools where both a hard and precise smooth surface is beneficial. One example of a press tool made of M2 steel and implanted with nitrogen ions produced three times more pressings from stainless steel sheet than an unimplanted tool before serious pick up or scoring occurred .

In the non-ferrous industry mill rolls used for the production of rod have had their life extended by a factor of up to four as a result of nitrogen implantation. Results recorded for one mill roll showed that it produced three times more copper rod and, the product was of far higher quality than that obtained using an unimplanted roll. Continuity of production is an important economic benefit in these types of operation as down-time is both costly and time consuming.

As examples of cutting tools, thread cutting dies of M2 high speed steel used to cut threads in cast iron showed a five fold increase in life. Twist drills of similar composition did not show more that double improvement, but this may be due to the high operating temperature (estimated to be about $600^{\circ}C$) causing the nitrogen to out-diffuse from the surface. Gear cutting tools have given an improvement factor of three.

Nitrogen implantation has proved successful in the plastics moulding industry in improving the abrasion resistance of AISI 420 (Stavax) tooling. This is an important advantage when processing heavily filled abrasive thermoplastic or thermoset materials. Implanted Stavax moulding tools have shown improvements of up to four times expected life when processing flame retardant ABS and filled polycarbonate materials for domestic appliances.

The zinc die casting industry sometimes employs tool steels for die casting cavities. In small shot applications improvement from one to three million shots have been obtained with nitrogen implantation.

CONCLUSIONS

Ultra-microhardness techniques are necessary to reveal the true hardness of thin nitrogen implanted layers. Results obtained by conventional methods are influenced by the underlying bulk metal.

Nitrogen implantation does harden significantly martensitic structures, provided that the steel is highly alloyed. Additional hardening is brought about by a fine dispersion of nitrides.

Implantation improves the load bearing capacity of the surface and reduces the ploughing mechanism of abrasive wear even under high loading conditions in the Falex test.

High dose implantation promotes the formation of a thin oxide layer on the surface. This layer reduces the coefficient of friction, at least during the ´run in ´ period and diminishes the tendency for galling in stainless steels.

Nitrogen implantation produces striking improvements in wear resistance of both metal processing and plastics moulding tools. The benefits for metal processors appear to be greater in metal forming or cutting operations in which wear is mainly abrasive. The advantages for plastics moulders are substantial; machine parts, feed areas and cavities can be treated to advantage, especially when subjected to abrasive/erosive wear.

ACKNOWLEDGEMENTS

One of the authors, J.I.Onate, would like to thank the Basque Goverment for its financial support throughout this work.

The authors are also indebted to Mr. G. Cooper (Tech-Ni-Plant Ltd.) for carrying out the implantation treatments and to Dr. Pollock of Lancaster University for the ultra-microhardness results.

REFERENCES

1) Edwards, J. "Wear resistant surfaces in engineering - a guide to their production, properties and selection".
Prepared by the International Research and Development Co. Ltd., Pub. for Dept. of Trade and Industry by HMSO, 1986, ISBN 0 11 513 826 9.

2) Hartley, N.E.W. "The tribology of ion implanted metal surfaces"
Tribology International, 1975,**8**, 65.

3) Dearnaley, G. "Ion implantation in metals"
New Uses of Ion Accelerators, Ed. Ziegler, J.F., Plenum Press, New York, 1975.

4) Hirvonen, J.K. "Ion implantation in tribology and corrosion"
Journal Vac Sci and Technol, 1978, **15 (5)**, 1662.

5) Herman, H. "Surface mechanical properties - effects of ion implantation"
Nuclear Instruments and Methods, 1981, **182/183**, 887.

6) Newey, D., Pollock, H.M. and Wilkins, M.A. "The ultra-microhardness of ion implanted iron and steel at sub-micron depths and its correlation with wear resistance"
Ion Implantation into Metals, eds. Ashworth, V., Grant, W.A. and Proctor, R.P.M., Pergamon, 1982, 157.

7) Onate, J.I., Dennis, J.K. and Hamilton, S. "The effects of ion (nitrogen) implantation on engineering coatings"
Trans Inst Metal Finishing, Proc Annual Conf 1987, Bournemouth.

8) Hale, E.B., Kaiser,T.H., Meng, C.P. and Kohser, R.A. "Effects of nitrogen implantation on the wear properties of steel"
Ion Implantation into Metals, Eds. Ashworth, V., Grant, W.A. and Proctor, R.P.M., Pergamon, 1982, p111.

9) Hartley, N.E.W. and Hirvonen, J.K. "Wear testing under high load conditions"
Nuclear Instruments and Methods, 1983,**209/210**, 933.

10) Iwaki, M., Fujihana, T. and Okitaka, K. "Mechanical and electrochemical properties of various tool steels implanted with nitrogen or NO ions"
Materials Science and Engineering, 1985, **69**, 211.

11) Dimigen, H., Kobs, K., Leutenecker, R., Ryssel, H. and Eichinger, P. "Wear Resistance of nitrogen implanted steels"
Materials Science and Engineering, 1985, **69**, 181.

12) Robic, J.Y., Piaguet, J. and Gailliard J.P. "Some measurements of hardness, wear resistance and stresses in ion implanted thin metallic metals"
Nuclear Instruments and Methods 1981, **182/183**, 919

13) Oliver, W.C., Hutchings, R. and Pethica J.B. "The wear behaviour of nitrogen implanted metals"
Metallurgical Transactions A, 1984, **15A**, 2221

14) Rauschenbach, B. and Kolitsch, A. "Formation of compounds by nitrogen ion implantation in iron"
Phys Status Solidi (2), 1983, **80**, 211.

15) Dos Santos, C.A., Behar, M., de Souza. J.P. and Baumvol, I.J.R. "Composition and thermal evolution of nitrogen implanted steels : a systematic study"
Nuclear Instr and Methods, 1983, **209/210**, 907.

16) Fayeulle, S., Treheux, D. and Esnouf, C. "T.E.M. characterisation of a nitrogen implanted austenitic stainless steel"
Applied Surface Science, 1986, **25**, 288.

17) Baron, M., Chang, A.L., Schreurs, J. and Kossowsky, R. "Nitrogen distribution and nitride precipitation in $^{14}N^+$ ion implanted 304 and 316 steels"
Nuclear Instr and Methods, 1981, **182/183**, 531.

18) Yost, F.G., Picraux, S.T., Follstaedt, D.M., Pope, L.E. and Knapp, J.A. "The effects of nitrogen implantation on the wear and fricton of type 304 and 15-5PH stainless steels"
Thin Solid Films, 1983, **107**, 287.

19) Herman, H., Hu, W.W., Clayton, C.R., Hirvonen, J.K. Kant, R. and MacCrone, R.K. "Modification of mechanical properties through ion implantation"
IPAT ´79, Ion Plating and Allied Techniques (Proc Conf), London, 1979, CEP Consultants Ltd., p255.

20) Hartley, N.E.W., "Surface stresses in ion implanted steel"
Journal Vac Sci Technol, 1975, **12 (1)**, 485.

21) Komvopoulos, K., Saka, N. and Suh, N.P. "The mechanism of friction in boundary lubrication"
Trans ASME. Journal of Tribology, 1985, **107**, 452

22) Sheppard, S.R. and Suh, N.P. "The effects of ion implantation on friction and wear materials"
Journal of Lubrication Technology, 1982, **104**, 29.

23) Bunshah, R.F. and Suri, A.K. "Friction and wear of stainless steels, titanium and aluminium with various surface treatments, ion implantation and overlay hard coatings"
IPAT ´79, Ion Plating and Allied Techniques (proc Conf), London, 1979, CEP Consultants Ltd., p230.

24) Kirk, J.A., Egerton, G.W. and Sartwell, B.D. "Wear and friction of nitrogen ion implanted steel"
Journal of Lubrication Technology, 1983, **105**, 239.

25) Dearnaley, G. "The effects of ion implantation upon the mechanical properties of metals and cemented carbides"
Radiation Effects, 1982, **63**, 1.

26) Hartley, N.E.W. "Friction and wear of ion plated metals - a review".
Thin Solid Films, 1979, **64**, 177

27) Lo Russo, S. Mazzoldi, P., Scotoni, I Tosello, C. and Tosto, S. "Effect of nitrogen ion implantation on the unlubricated sliding wear of steel"
Applied Physics Letters, 1979, **34 (10)**, 627.

28) Cui, F.Z., Li, H.D. and Zhang, X.Z. "Modification of tribological characteristics of metals after nitrogen implantation"
Nuclear Instruments and Methods, 1983, **209/210**, 881.

29) Fischer, T.E., Luton, M.J., Williams, J.M., White, C.W. and Appleton, B.R. "Tribological properties of ion implanted 52100 steel"
ASLE Transactions, 1983, **26 (4)**, 466.

30) Pope, L.E., Yost, F.G., Follstaedt, D.M., Picraux, S.T. and Knapp, J.A. "Friction and wear reduction of 440C stainless steel by ion implantation"
Ion Implantation and Ion Beam Processing of Materials, (Conf Proc), Boston, 1983. North Holland, Elsevier Sc. Pub. Inc, New York 1984. p 661.

31) Singer, I.L. "Tribological properties of ion implanted metals"
ibid, p 585.

32) Sommerer, T.J., Hale, E.B., Burris, K.W. and Kohser, R.A. "Characteristics of wear modes in ion implanted steel from Auger measurements"
Materials Science and Engineering, 1985, **69**, 149.

33) Dearnaley, G. "Adhesive, abrasive and oxidative wear in ion implanted metals"
Materials Science and Engineering, 1985, **69**, 139.

TABLE 1

Advantages and limitations of nitrogen implantation as a surface treatment.

ADVANTAGES

1) Low temperature process.

2) Negligible dimensional changes.

3) No degradation of surface finish.

4) No sacrifice of bulk properties.

5) No adhesion problems since there is no sharp interface.

6) Solid solubility limit of implanted species can be exceeded.

7) A fine dispersion of precipitates is created providing optimum wear behaviour.

8) Clean vacuum process.

9) Minimum masking costs, ability to treat selective areas.

10) Highly reproducible and controllable process.

LIMITATIONS

1) Line of sight proces, hence manipulation under vacuum is necessary.

2) Shallow penetration.

3) Relatively expensive equipment and processing costs.

TABLE 2

Composition of steels

AISI Code	Composition, % by Wt.							Hardness		Surface Roughness µm (CLA)
	C	Si	Mn	Cr	Mo	V	W	Rc	Hv	
M2	0.87	-	-	4.2	5.0	1.9	6.4	62 - 64	750 - 800	0.20
D2	1.55	0.3	0.3	12.0	0.8	0.8	-	58 - 60	650 - 700	0.22
420	0.38	0.8	0.5	13.6	-	0.3	-	52 - 54	540 - 575	0.34

TABLE 3

Effect of optimum* nitrogen implantation dose on surface hardness of steels, (5g load)

Steel	Micro-hardness, Hv		Hardness increase, %
	Untreated	Implanted	
AISI M2	1090 ± 94	1220 ± 105	12
AISI D2	770 ± 35	890 ± 60	16
AISI 420	635 ± 33	714 ± 40	12

* Optimum dose for wear resistance, not for hardness.

TABLE 4

Falex wear test results for steels, Wear rate in gx10^{-6}/min.
Operating conditions : 900 N, lubricated, 140 minutes wear time.

Pin code	AISI M2		AISI D2		AISI 420	
	Untreated	Implanted	Untreated	Implanted	Untreated	Implanted
1	7.320	6.783	13.141	10.000	23.428*	11.070
2	6.233	5.712	18.636	8.496	25.888*	14.289
3	9.379	5.769	15.187	10.550	13.89	15.565
4	7.254	4.728	15.195	9.900	26.712*	8.850
5	6.248	4.693	16.329	12.790	13.73	9.154
Mean	7.287	5.537	15.698	10.347	20.730	11.786
Standard Deviation	1.282	0.867	2.005	1.562	6.431	3.025

* Test stopped due to seizure of the pin.

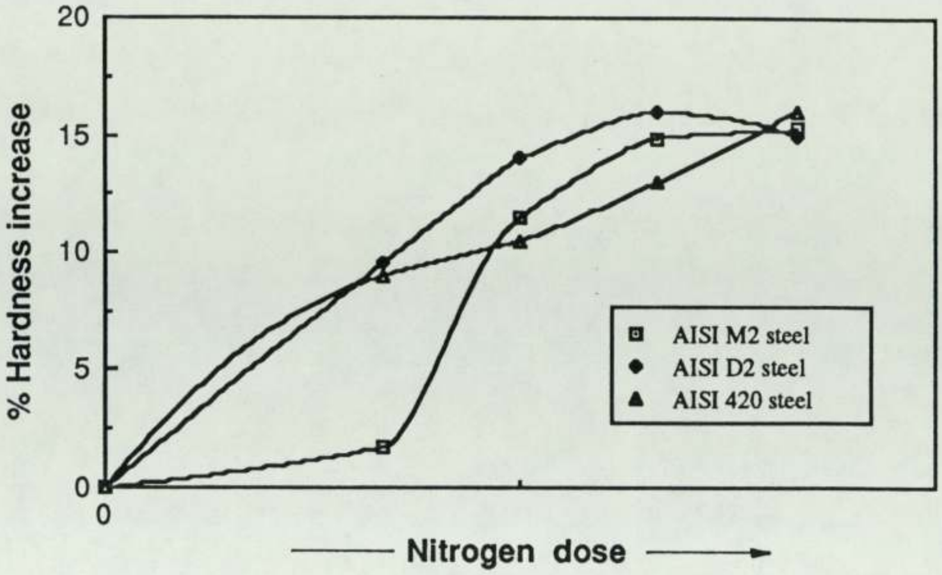

Fig.1: Variation in microhardness (Vickers, 5 g. load) with nitrogen implantation dose.

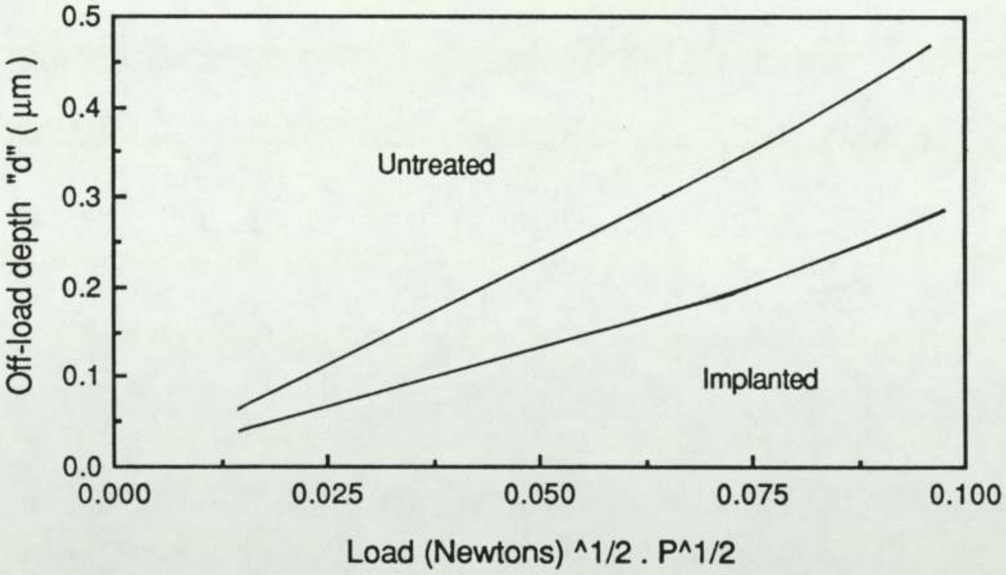

Fig.2: Indentation depth (d) vs. square root of load (P) for AISI 420 steel.

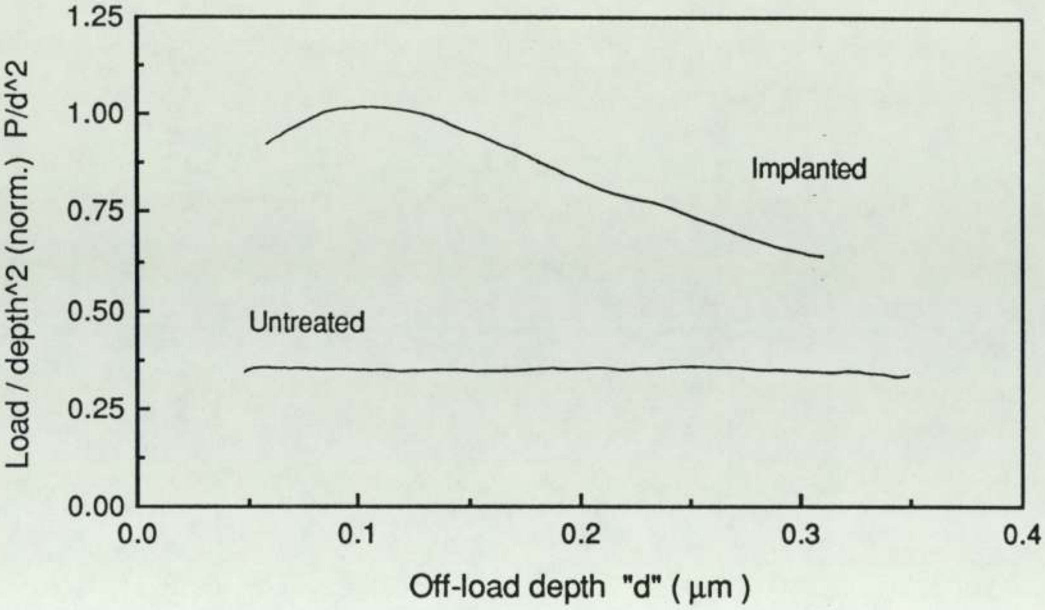

Fig.3: "Normalised" hardness as a function of penetration depth for AISI 420 steel.

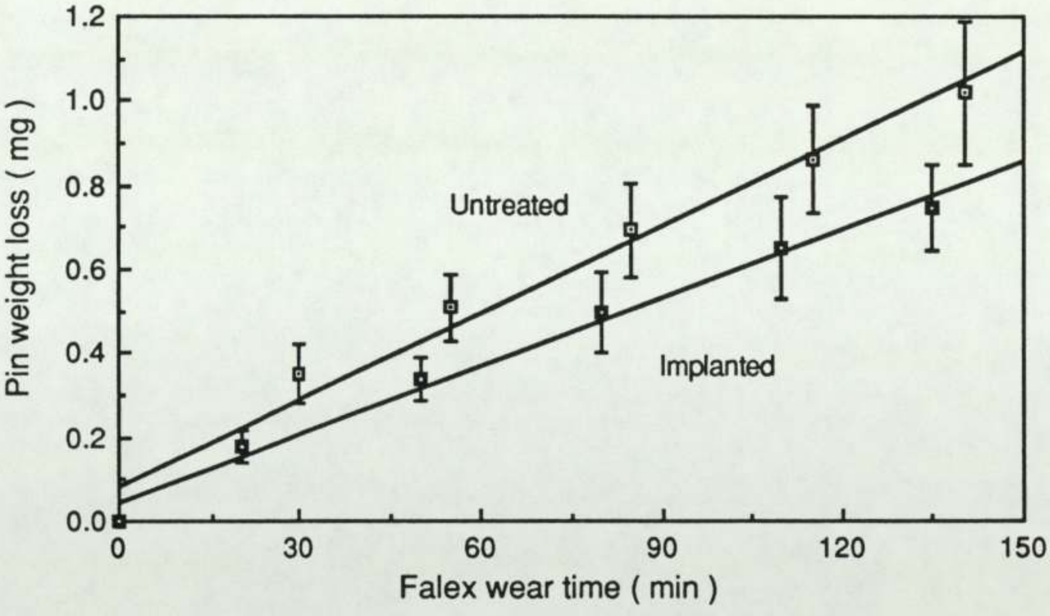

Fig 4 : Falex wear results for AISI M2 steel. AISI M2 V-blocks. 900 N load. Lubricated

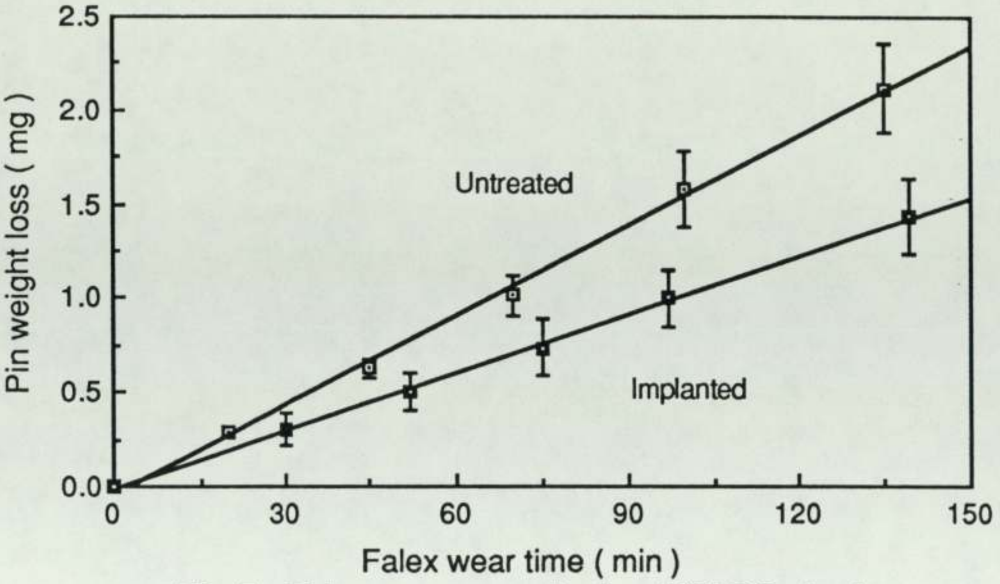

Fig 5 : Falex wear results for AISI D2 steel.
AISI D2 V-blocks. 900 N load. Lubricated.

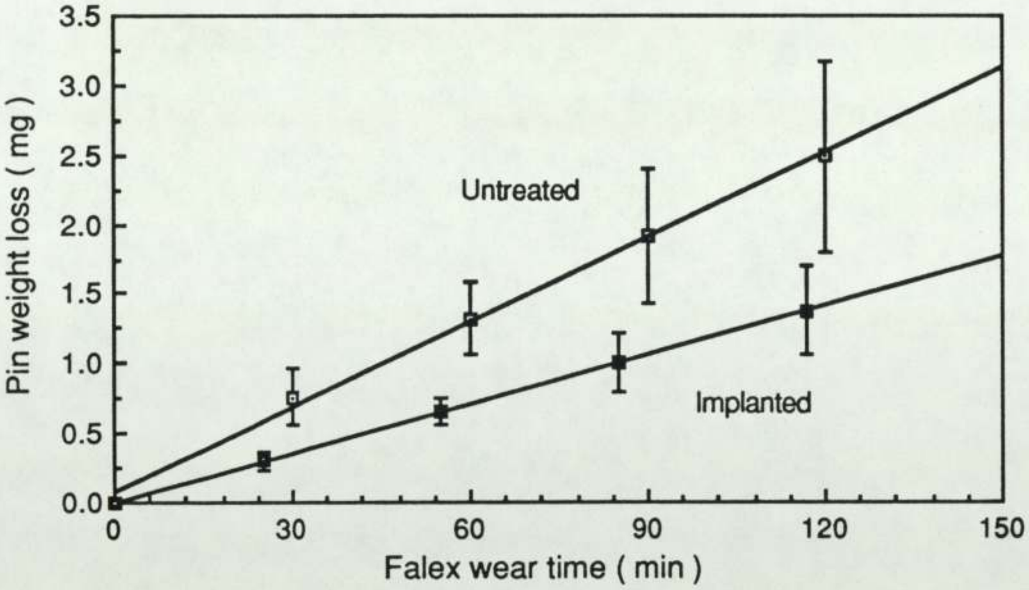

Fig 6 : Falex wear results for AISI 420 steel
AISI 420 V-blocks. 900 N load. Lubricated.

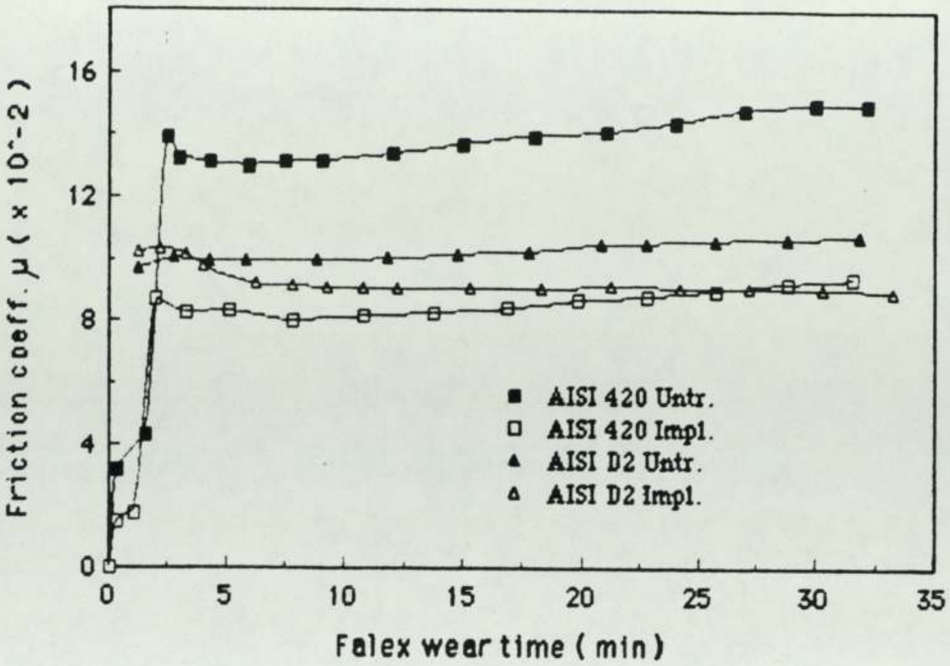

Fig.7: Variation of coeff. of friction with wear time for AISI D2 and 420 steels.

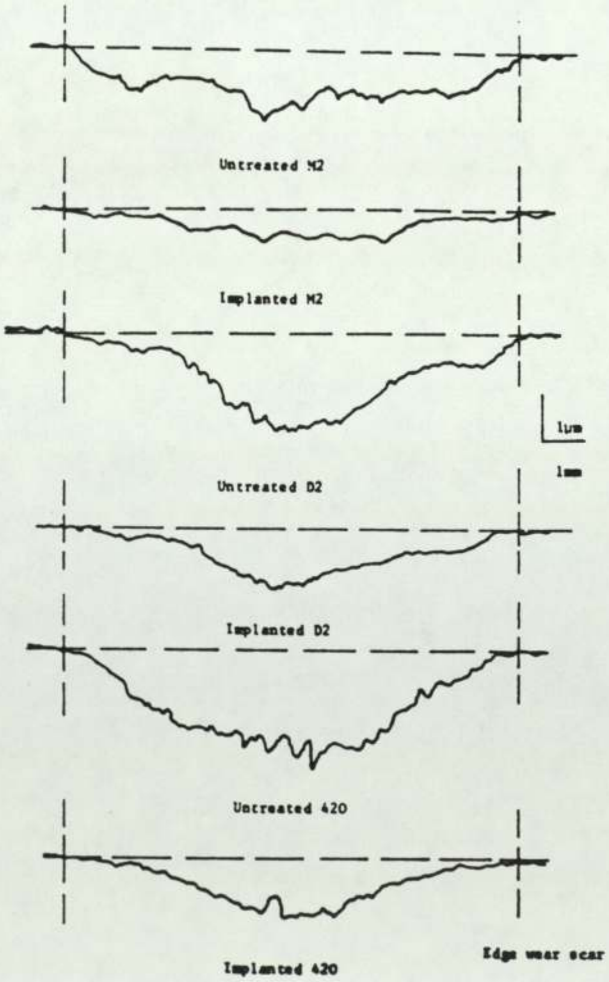

Fig. 8 : Profilometer traces of worn steel surfaces after 140 minutes Falex wear testing.

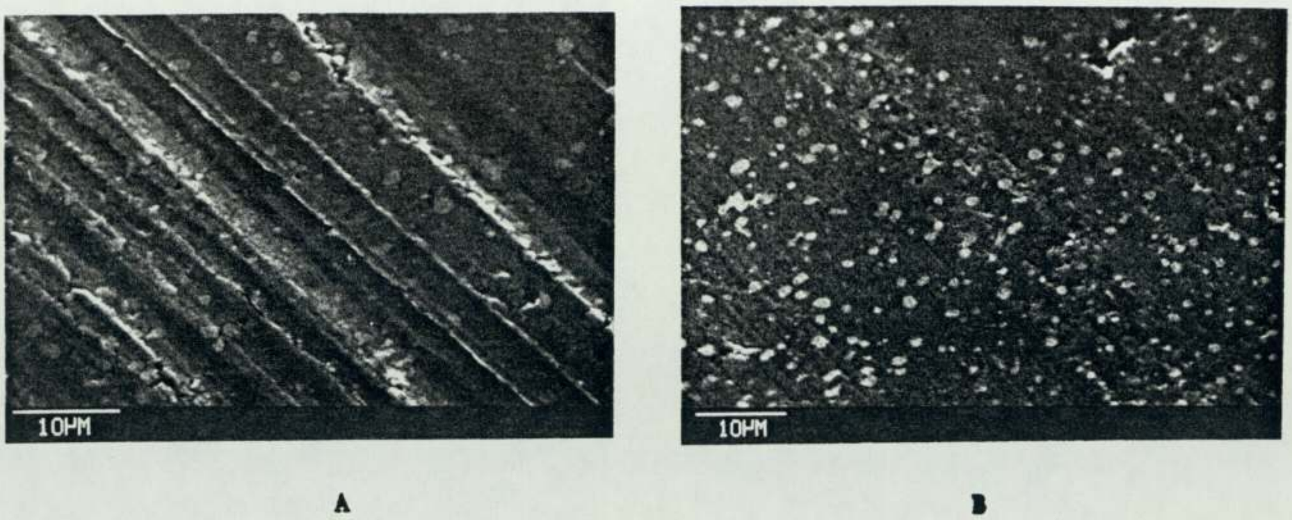

Fig. 9 : Scanning micrographs showing worn surfaces of :
A : untreated AISI M2 steel, ploughing readily visible.
B : Nitrogen implanted AISI M2 steel.

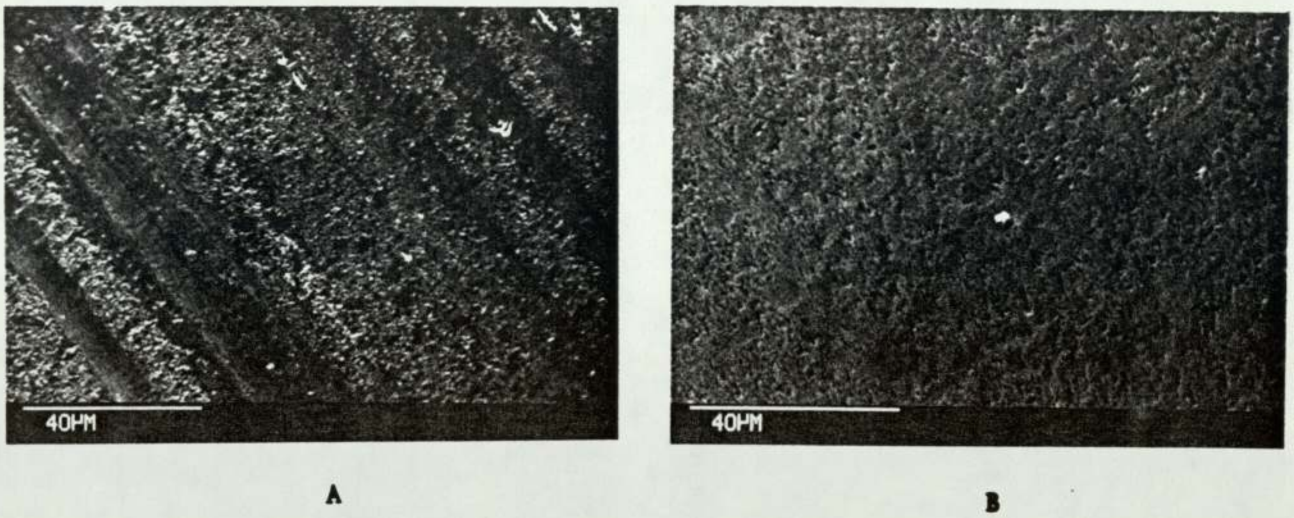

Fig.10 : Scanning micrographs showing worn surfaces of:
A : untreated AISI D2 steel, ploughing readily visible.
B : Nitrogen implated AISI D2 steel.

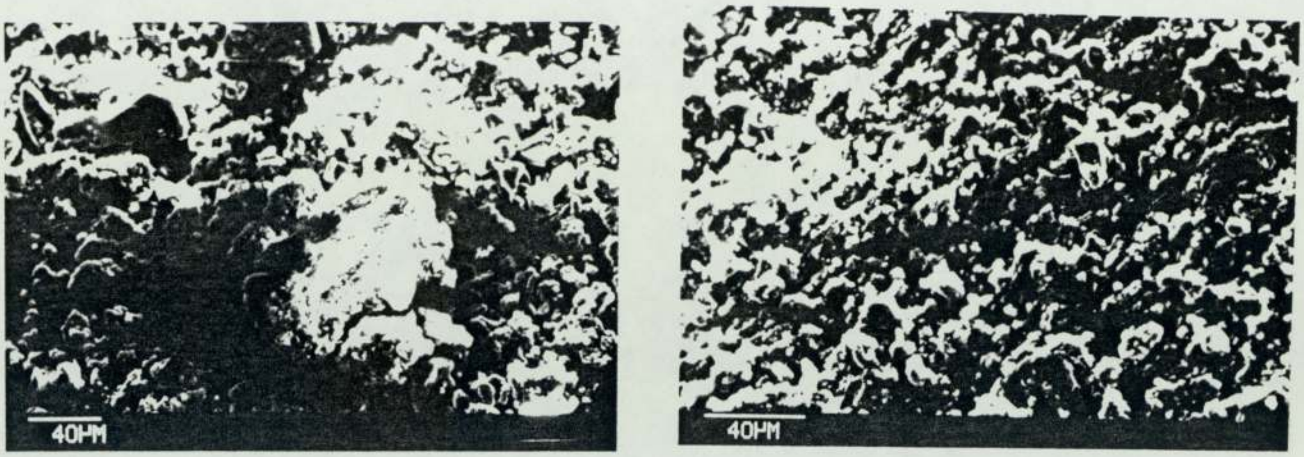

A

B

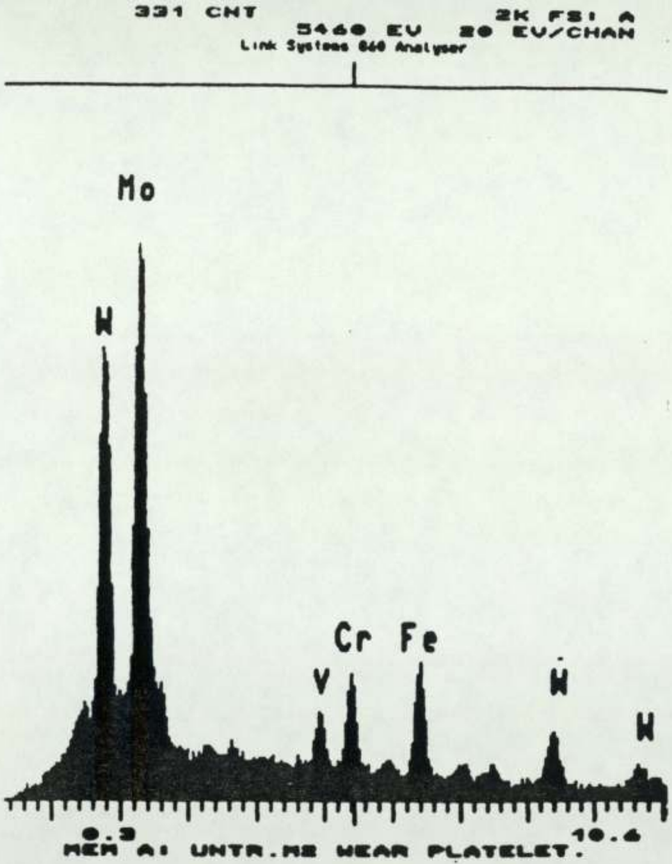

(c)

Fig.11 : Debris generated during wear of A : untreated M2 steel and B : implanted M2 steel. Note the larger size of the wear particles from the untreated surface, with X-ray analysis (c).

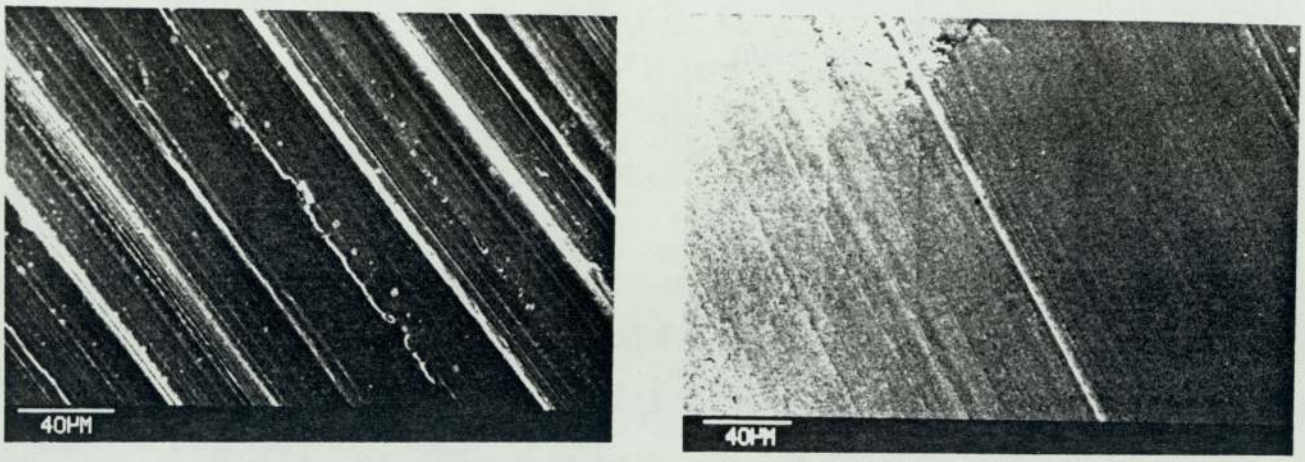

A

B

Fig.12 : A : Scanning micrograph of worn surface of AISI 420, after severe scuffing.
B : Showing worn surface of implanted AISI 420.